University of Venda
Creating Future Leaders



University of Venda
Creating Future Leaders

# Inhibitory effects of Green synthesized *Senna alexandrina* silver nanoparticles (SAAgNPs) on *Escherichia coli* DnaK

**By**

**Seboya Koketso Oscar**

**(19011880)**

**Submitted under the requirements for the degree of**

**Master of Science**

**Biochemistry in the Department of Biochemistry and Microbiology,**

**Faculty of Science, Engineering, and Agriculture**

**University of Venda**

**Supervisor: Dr L.M Mathomu**

February 2025



© University of Venda

## Abstract

Plant extracts have garnered considerable interest in the environmentally friendly and economically viable production of silver nanoparticles (AgNPs) through their application in green synthesis. However, Plant-derived nanoparticles may potentially have unique physicochemical characteristics. This study is significant in that it contributes to the understanding of the effects of AgNPs on the functional and structural integrity of the heat shock protein DnaK. The research presents an improved synthesis process for silver nanoparticles (AgNPs) from the *Senna alexandrina* leaf extract. In addition to evaluating the synthesized AgNP's physicochemical characteristics, the research also examines their effect on the functional activity of *E. coli* DnaK. During synthesis, the color change from light yellow to dark brown was observed within 30 minutes after the addition of 3 ml of *S. alexandrina* leaf extract to 1 mM of silver nitrate. A surface plasmon resonance peak at 420 nm revealed by ultra-violet spectroscopy was used as additional confirmation that AgNP had formed. The synthesized SA-AgNPs were characterized using UV-VIS spectrophotometry, FTIR, and SEM analysis. Furthermore, heat shock proteins (Hsp) are cellular and stress-induced proteins. With respect to this, it is anticipated that the Hsp can also interact with AgNPs transported into cells and/or the circulation system. The present study was intended to investigate the effects of synthesized silver nanoparticles (AgNPs) using locally-sourced leaf extracts of *S. alexandrina* on *E. coli* DnaK. In this study, AgNPs were synthesized using the green synthesizing method by the reduction of silver nitrate into nano-sized silver nanoparticles (AgNPs) inactivated concurrently, which was capped with the phytochemicals of *S. alexandrina* . FTIR, UHPLC-qTOF-MS, investigated the functional groups present in plant extract to identify the compounds responsible for reducing silver ions. Altogether, findings from this study suggest that DnaK is highly involved in *E. coli* cytoprotection against AgNPs. In conclusion, both the effect of AgNPs on DnaK stability to heat stress and function in suppressing MDH aggregation were investigated. More importantly, it was also observed that AgNPs can suppress heat-induced aggregation of MDH and consequently stimulate ATPase activity of DnaK. In silico docking studies revealed promising binding affinities of specific metabolites in relation to key proteins (DnaK and its co-chaperones) involved in bacterial survival.


**Keywords:** AgNPs, *E. coli* DnaK Green synthesis, *Senna alexandrina*, UHPLC-qTOF-MS



© University of Venda

## Table of Contents

Abstract ..... 2
**Declaration** ..... 7
LIST OF SYMBOLS ..... 9
LIST OF FIGURES ..... 12
Introduction and Literature Review ..... 15
CHAPTER 1: INTRODUCTION AND LITERATURE REVIEW ..... 16
1.1. Introduction and literature review ..... 16
1.2. Nanoparticles ..... 18
1.3. Synthesis of metallic nanoparticles ..... 18
1.4. *Senna alexandrina* plant species ..... 19
1.5. Silver nanoparticles ..... 20
1.6. Coating and functionalization of nanoparticles ..... 21
1.7. Green synthesis of silver nanoparticles ..... 24
1.8. Biomedical applications of silver nanoparticles ..... 28
1.9. Applications of silver nanoparticles in drug delivery and gene therapy ..... 28
1.10. Importance of NPs against Antibiotic Resistance ..... 29
1.11. Heat shock proteins (HSP) ..... 29
1.11.1. Heat shock proteins as molecular chaperones ..... 30
1.11.2. Heat shock protein 40 ..... 32
1.11.3. Heat shock protein 70 ..... 32
1.11.4. Hsp40-Hsp70 partnership ..... 36
1.12. Interaction of nanoparticles with proteins ..... 36
1.13. Effects and toxicity of nanoparticles on protein structure and function: ..... 36
1.14. Toxicity of silver nanoparticles, expression of heat shock proteins, and Bacterial cell ..... 37
1.14.1. Critique of literature: ..... 38
1.14.2. Summary: ..... 39
1.14.3. Significance of the study ..... 40
1.15. Problem statement ..... 40
1.16. Research questions ..... 42
1.17. Hypothesis ..... 42
1.18. Specific aim and objectives ..... 43
Chapter 2 ..... 44
Green synthesis of *Senna alexandrina* silver nanoparticles (SAAgNPs) ..... 44



© University of Venda

CHAPTER 2: Green synthesis of *Senna alexandrina* silver nanoparticles (SA-AgNPs) ..... 45
2.2. Experimental procedures ..... 46
2.2.1. Extraction and validation groups of metabolites from *S. Alexandrina* leaves using methanolic extraction and spectrophotometric validation ..... 46
2.2.2. Compound purification using Silica gel column chromatography ..... 46
2.2.3. Compounds separation and identification in *Senna alexandrina* leave extract using Thin Layer Chromatography (TLC) ..... 46
2.2.4. Analysis of metabolites from *Senna alexandrina* through UHPLC-QTOF-MS and Sirius ..... 47
2.2.5. Synthesis of Silver Nanoparticles (Ag-NPs) ..... 47
2.2.6. Characterization and validation of the synthesized of SA-AgNPs through Ultra-violet visible spectroscopy, FTIR, SEM ..... 48
2.2.6.1. Fourier Transform Infrared Spectroscopy (FTIR) ..... 48
2.2.6.2. Scanning Electron Microscopy (SEM) ..... 48
2.3. Results & discussion ..... 48
2.3.1. Visual observation and UV-Vis spectroscopy ..... 48
2.3.2. Absorption Spectra and Visual Appearance of Silver Nanoparticles (AgNPs) at Different Silver Nitrate Concentrations ..... 55
2.3.3. FTIR absorption spectrum of SA-AgNPs and *Senna alexandrina* leaf extract ..... 58
2.3.4. Identification and profiling of phytocompounds from *Senna alexandrina* leaf extract using UHPLC-qTOF-MS ..... 61
Chapter 3 ..... 65
Production of *E. coli* DnaK and Structure-function analysis ..... 65
CHAPTER 3: Production of *E. coli* DnaK and Structure-function analysis ..... 66
3.1. Introduction and experimental procedures ..... 66
3.1.1. Materials ..... 66
3.1.2. Confirmation of *E. coli* DnaK DNA constructs ..... 67
3.1.3. Expression of recombinant protein ..... 67
3.1.4. Purification of recombinant protein ..... 68
3.1.5. Investigation of the secondary structural organization of *E. coli* DnaK ..... 68
3.1.6. Investigation of the tertiary structural organization and temperature-dependent conformational changes of *E. coli* DnaK using tryptophan fluorescence-based analysis ..... 69
3.1.7. Investigation of ATPase activity of *E. coli* DnaK ..... 69
3.2. Results and Discussion ..... 70
3.2.1. Confirmation of the pQE30/DnaK plasmid ..... 70
3.2.2. Overexpression and purification of recombinant *E. coli* DnaK protein ..... 70
3.2.3. Secondary structure analysis of *E. coli* DnaK ..... 70



© University of Venda

University of Venda
Creating Future Leaders

3.2.4. Tertiary structure analysis of *E. coli* DnaK ..... 72
3.2.6. Analysis of enhanced/stimulated ATPase activity of DnaK ..... 74
Biochemical analysis of the functional features of *E. coli* DnaK protein ..... 77
CHAPTER 4: Biochemical analysis of the functional features of *E. coli* DnaK protein ..... 78
4.1. Introduction ..... 78
4.2. Results and Discussion ..... 79
4.2.1. Investigation of the effects of SAAgNPs on the plasmid DNA ..... 79
4.2.2. B. Investigation of SA-AgNPs effects on the secondary structure of *E. coli* DnaK ..... 81
4.2.2 Concentration-Dependent Effects of Silver Nanoparticles (AgNPs) on the Structural Stability of DnaK Monitored by Tryptophan Fluorescence ..... 82
4.2.3. Investigation of *E. coli* DnaK chaperone function using malate dehydrogenase aggregation assay 84
4.2.4. Analysis of the effect of *Senna alexandrina* silver nanoparticles on bacterial growth ..... 87
4.2.5. Effects of SAAgNPs on *E. coli* XL1 Blue cells expressing DnaK as analyzed by SDS-PAGE. ..... 88
4.2.6. Complementation assay ..... 89
Bioinformatics analysis of the structural features of *E. coli* DnaK ..... 92
CHAPTER 5: Bioinformatics analysis of the structural features of *E. coli* DnaK ..... 92
5.2. Multiple sequence alignment ..... 94
5.3. Results and Discussion ..... 94
5.3.1. DnaK predicted biological networks and Alignments ..... 94
5.3.2. Analysis of sequence similarity between *E. coli* DnaK, Arabidopsis thaliana, Thermus thermophilus, Bacillus subtilis, human, yeast and Mycobacterium tuberculosis, Pseudomonas aeruginosa counterparts and homologs, and plasmodium falciparum ..... 99
5.3.3. Phylogenetic analysis of *E. coli* DnaK and its homologs and orthologues ..... 102
5.3.4. Secondary structure analysis of *E.coli* DnaK-like proteins against its homologs and orthologues 103
4.3.5. Biophysiological properties of *E. coli* DnaK and its predicted counterparts and homologs ..... 104
Discussion, Conclusions and Future Perspectives ..... 115
6.2. Conclusion and future perspectives ..... 120
Reference ..... 122
APPENDICES ..... 151
Appendix A: SPECIALISED REAGENTS ..... 151
APPENDIX A-1: The absorption spectrum indicating respective wavelength from ultraviolet, visible and infrared spectrum ..... 152
Appendix B: General Experimental Procedures ..... 153
1.1. Materials: ..... 153
B1. Extraction of plasmid DNA ..... 153
**B2. Conformation of pQE30 vector plasmid and pQE30/DnaK** ..... 153



© University of Venda

B3. Enzymatic restriction digest of Plasmid DNA ..... 153
B4. Agarose gel electrophoresis: ..... 154
B5. Preparation of competent *E. coli* XL1/JM109 Blue cells ..... 154
**B6. Transformation of *E. coli* Competent Cells by pQE30-DnaK** ..... 155
B7. Sodium dodecyl sulfate-polyacrylamide gel electrophoresis (SDS-PAGE) analysis ..... 155
B8. Immunoblotting (Western blot) ..... 156
B9. Determination of protein concentration using Bradford's assay ..... 156
B10. Cell plating complementation assay ..... 157
B11. Determination of molar residue ellipticity in CD spectroscopy ..... 157
B12. Compounds separation and identification (by spots) present in *Senna alexandrina* leave extract using Thin Layer Chromatography (TLC) ..... 157
B14. Protein determination ..... 158
APPENDIX C: Supplementary data ..... 159
C.1 pQE30/DnaK agarose gel ..... 159
C2. SDS-PAGE and western blot analysis of expressed and purified DnaK proteins ..... 159
C3. pQE30 expression gel and Western blot ..... 160
APPENDIX D: Supplementary data ..... 161
D1 Bradford's Assay standard curve ..... 161
D.2. UHPLC-QTOF-MS: ..... 162
Representative densitometric quantification of proteins in the presence of 2.5 µg/mL SA-AgNPs detected by Coomassie staining ..... 164



© University of Venda

# Declaration

I, **Seboya Koketso Oscar**, student number **19011880**, certify that I have read and comprehended the rules and policies of the university pertaining to postgraduate research. I certify that I have, to the best of my knowledge and belief, complied with their requirements. I certify that I am the author of this research and that it is being submitted to The University of Venda in fulfillment of my Master of Science in Biochemistry degree. All sources have been properly cited and acknowledged.

Signature:  Date: 20/08/2025



© University of Venda

**Acknowledgment**

First and foremost, I want to express my gratitude to the Lord Almighty for bringing me thus far since none of this would have been possible without him.

Secondly, I want to express my gratitude to Dr. Lutendo Michael Mathomu, my supervisor, for serving as both my supervisor and a father. Additionally, I am incredibly grateful to my family, Godfrey, Matodzi, and Edna, for their constant support and unwavering belief in me and for giving me the courage and motivation to keep going.

My friends and coworkers, especially Phindulo Mathobo, deserve special recognition for his encouragement and guidance.



© University of Venda

## LIST OF SYMBOLS

| Abbreviations of units | Symbol Interpretation |
|---|---|
| α | Alpha |
| β | Beta |
| bp | base pair |
| °C | degree Celsius |
| A320 | absorbance at 320 nanometres |
| A360 | absorbance at 360 nanometres |
| A595 | absorbance at 595 nanometres |
| A600 | absorbance at 595 nanometres |
| µM | Micromolar |
| g | Gram |
| pM | Picomolar |
| µl | Microlitre |
| ml | Millilitre |
| l | Litres |
| w/v | weight per volume |
| v/v | volume per volume |
| µg | Microgram |
| kDa | Kilodalton |
| % | % percent |
| Ag | Silver |
| ATP | Adenosine Triphosphate |
| CD | Circular dichroism |
| BSA | Bovine serum albumin |
| DLS | Dynamic Light Scattering |
| *E. coli* | Escherichia coli |
| FTIR | Fourier Transform Infrared Spectroscopy |



© University of Venda

| | |
|---|---|
| GRAVY | Grand average of hydropathicity |
| Hsp | Heat shock protein |
| Tm | Melting temperature |
| MDH | Malate Dehydrogenase |
| MIC | Minimum inhibitory concentration |
| MBC | Minimum bactericidal concentration |
| NEFs | Nucleotide Exchange Factors |
| NPs | Nanoparticles |
| NMR | Nuclear Magnetic Resonance |
| NBD | Nucleotide Binding Domain |
| Pf | *Plasmodium falciparum* |
| SAAgNPs | *Senna alexandrina*-silver nanoparticles |
| SBD | Substrate Binding Domain |
| SEM | Scanning Electron Microscopy |
| TEM | Transmission electron Microscopy |
| PBS | Phosphate-Buffered Saline |
| RSMD | Root Mean Square Deviation |
| SDS PAGE | sodium dodecyl sulfate–polyacrylamide gel electrophoresis |
| SPR | Surface plasmon resonance |
| UV | Ultraviolet radiation |
| UHPLC-qTOF-MS | Ultra-high performance liquid chromatography quadrupole time of flight mass spectrometry |
| Vis | Visible light variation |



© University of Venda

## LIST OF TABLES

**Table 1.1. Different surface coatings of nanoparticles** ..... **23**

**Table 1.2. Previous studies that used plant extract to mediate the synthesis of silver nanoparticles** ..... **27**

**Table 1.3. Heat shock proteins (Hsps) families and their functions** ..... **31**

**Table 2.1. Selected compounds involved in reduction, stabilization process of nanoparticle synthesis** ..... **60**

**Table 3.1.1. List of strains and plasmids…** ..... **65**

**Table 3.1. Secondary composition of DnaK…** ..... **70**

**Table 5.1. Secondary structures features…** ..... **100**

**Table 5.2..In-silico prediction of biophysiological properties…** ..... **101**

**Table 5.3…** ..... **105**

**Table 5.4…** ..... **108**

**Table B1. Restriction digestion reaction mixture…** ..... **151**

**Table B2: Preparation of SDS PAGE** ..... **153**

**Table D.3: A master mix was prepared using HKMD buffer** ..... **161**

**Table D.4. Annotated metabolites from *Senna alexandrina* methanol extracts** ..... **164**

**Table D.5. Binding affinities of selected compounds with DnaK clusters…** ..... **183**



© University of Venda

## LIST OF FIGURES

**Figure 1.1.** Surface plasmon resonance (SPR) illustrates what happens on the surface of nanoparticles when interacting with light ..... 17

**Figure 1.2.** *Senna alexandrina* leaves captured at the University of Venda (22.9757° S, 30.4465° E)..... 20

**Figure 1.3.** Schematic representation of AgNP core coated with plant phytochemicals ..... 23

**Figure 1.4.** Biological resources and compounds used for the green synthesis of nanoparticles (Adopted from Rafael and Jesús 2023). ..... 26

**Figure 1.5**.Structural features of the Hsp70..... 34

**Figure 1.6.** The Hsp70/DnaK chaperone cycle. ..... 35

**Figure 1.7.** Ag NPs exhibit antibacterial action through various mechanisms, ..... 38

**Figure 2. 1.** UV-vis of purified *S. alexandrina* metabolites by silica gel chromatography…..... 49

**Figure 2.2.** Comparative TLC profile of *Senna alexandrina* direct methanolic extract…..... 51

**Figure 2. 3.** UV-vis spectroscopy of AgNPs synthesized using different concentrations of *Senna alexandrina* leaves extracts… ..... 53

**Figure 2. 4.** UV/vis spectral of AgNPs synthesized with different volumes of *Senna alexandrina* .....55

**Figure 2.5.** Digital optical images of synthesized silver nanoparticles….....56

**Figure 2.5.** Graph showing time-dependent UV-Vis absorption spectra of green synthesized silver nanoparticles….....56

**Figure 2.7.** FTIR analysis. ..... 58

**Figure 2.6.** Representative SEM images of SA-AgNPs surface features… ..... 59

**Figure 3.1.** CD spectra of DnaK showing secondary structure analysis of DnaK at Apo state ……...….69

**Figure 3.2.** The intrinsic tryptophan fluorescence of recombinant DnaK at Apo state.....70



© University of Venda

**Figure 3.3.** Tertiary structure analysis/tryptophan analysis of temperatures .....72

**Figure 3.4.** SA-AgNPs regulate ATPase activity of recombinant DnaK… .....74

**Figure 4.1**. The effects of SAAgNPs on plasmid DNA integrity ..... 79

**Figure 4.2.** The far-UV CD spectra of the recombinant DnaK in the presence of SA-AgNPs. ... 80

**Figure 4.3.** Tryptophan fluorescence spectra of DnaK in the presence of silver nanoparticles (AgNPs) at varying concentrations… .....82

**Figure 4.4.** Aggregation determination of components of MDH aggregation suppression assay 85

**Figure 4.5.** The growth curves of *E. coli* under SAAgNPs influence at 37 °C .....86

**Figure 4.6.** Comparison of the protein profiles in *E. coli* XL1 Blue cells expressing DnaK… ..... 87

**Figure 4.7.** Complementation assay ..... 88

**Figure 4.8.** Diagram showing a plate of complementation assay at non-permissive temperature 88

**Figure 4.9.** Diagram showing a plate of complementation assay at permissive temperature, and nonpermissive-temperature..... 89

**Figure 5.1.** Interaction prediction of DnaK. Predicted DnaK closely related interactions using string tool .....93

**Figure 5.2.** Sequence analysis of *E. coli* DnaK and its predicted networks .....96

**Figure 5.3.** Sequence analysis of *E. coli* DnaK against Arabidopsis thaliana, Thermus thermophilus, Bacillus subtilis, human, yeast and Mycobacterium tuberculosis, Pseudomonas aeruginosa counterparts and homologs, and plasmodium falciparum.....98

**Figure 5.4.** Evolutional analysis of *E. coli* DnaK against its homologues and counterparts ..... 99

**Figure 5.5..** ATP binding to DnaK.....104

**Figure 5.6.** ATP binding to DnaJ ..... 104

**Figure 5.7.** ATP binding to DnaK-DnaJ .....105

**Figure 5.8.** Competitive binding studies of molecular docking of multiple ligands on DnaK,,,

**Figure S. 1.** Restriction analysis of pQE30/DnaK plasmid. ..... 157

**Figure S. 2.** SDS-PAGE analysis of DnaK. Expression and purification analysis of DnaK ..... 157

**Figure S.3.** Western blot analysis of expressed and purified DnaK… .....158

**Figure S.4.** SDS-PAGE analysis of pQE30 plasmid. ..... 159

**Figure D. 1.** Bradford standard curve.....159

**Figure D.2.** Total Ion Chromatogram of a methanolic extract of *Senna alexandrina* leaves… .....160

**Figure D,3.** Phosphate standard curve.....161

**Figure D.4.** Densitometric analysis.....162

**Figure D.5.** Molecular docking of selected compounds binding to DnaK-DnaJ… ..... 173

**Figure D.6.** Molecular docking of selected compounds binding to DnaK-CBPA..... 174

**Figure D.7.** Molecular docking of selected compounds binding to DnaK-CLPB .....175

**Figure D.8.** Molecular docking of selected compounds binding to DnaK-GROEL .....176

**Figure D.9.** Molecular docking of selected compounds binding to DnaK-GROES .....177

**Figure D.10.** Molecular docking of selected compounds binding to DnaK-GRPE… .....178

**Figure D.11.** Molecular docking of selected compounds binding to DnaK-HSLU .....179

**Figure D.12.** Molecular docking of selected compounds binding to DnaK-HSLV.....180

**Figure D.13.** Molecular docking of selected compounds binding to DnaK-HTPG .....181

**Figure D.14.** Molecular docking of selected compounds binding to DnaK-RPOH .....182



© University of Venda

# Chapter 1

**Introduction and Literature Review**



© University of Venda

# CHAPTER 1: INTRODUCTION AND LITERATURE REVIEW

## 1.1. Introduction and literature review

Nanotechnology is considered among the fastest growing fields, with application in various industrial sectors. With the aid of this technology, larger materials with unique properties can be reduced to nanoparticles (NPs). According to Sengul and Asmatulu (2020), nanotechnology has emerged as a visible tool for the synthesis of nanomaterials, including metal oxides and carbon-based materials, to mention a few. Special material groups of NPs have one dimension of 100 nanometres or less. It has unique features and wide range of applications in different fields (Bali *et al*., 2006; Salam *et al*., 2012). Their importance is based on their small size, high carrier capacity, high reactivity, large surface area-to-volume ratio, and ease of surface property modification (Lal *et al*., 2021).

As a result of advancements in microscopy, nanotechnology allows for manipulation of matter at a nanometric scale, which is exceptionally close to quantum limits. Although the existence of nanoparticles in decorative items has been discovered through the investigation of archaeological objects, the rise in nanotechnology research at the end of the past century addressed concerns around synthesis of nanomaterials. The synthesis, characterization, and uses of nanotechnology in various domains, including geology and medicine, have been covered in various studies (Amina & Guo, 2020; Bromma & Chithrani, 2020).

Due to their production methods, nanoparticles are usually exhibited as colloids, composed of solid and liquid phases, typically water or an organic solvent. Top-down and bottom-up are the primary methods for obtaining nanoparticles (Selmani *et al*., 2022). Due to their inherent qualities, including a high surface-to-volume ratio, promoting interactions, and enhancing nanomaterials' reactivity and functionalization potential, colloids are of great interest in various research areas.

Numerous industrial and medicinal uses exist for the optical properties of metallic nanoparticles resulting from surface plasmon resonance. When illuminated to light, metal particles respond to the light's oscillating electromagnetic field by undergoing a coherent collective oscillation of free electrons. A dipole oscillation aligned with the electric field of light is produced by this electronic oscillation over the particle surface, which causes a charge separation with the ionic lattice (Figure



© University of Venda

1.1). This can favor dipole–dipole electrostatic interactions. A maximal amplitude oscillation at a certain frequency manifest SPR.

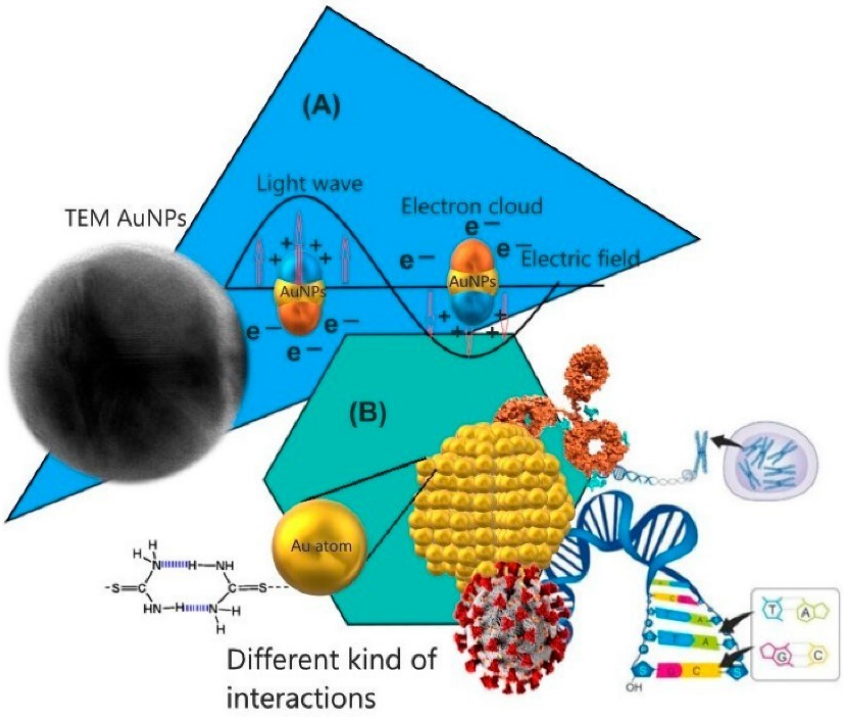



**Figure 1.1. (A)** Surface plasmon resonance (SPR) illustrates what happens on the surface of nanoparticles when interacting with light. (**B**) Types of coating used for medicinal agents, DNA, antibodies, silver nanoparticles, and ligands. They interact through covalent-type ligations or electrostatics, and simultaneously, molecules linked to gold atoms can form interactions such as H-H hydrogen bridges (Rosero *et al*., 2024).

In contrast to other metals, SPR in plasmon nanoparticles, especially those made of noble metals like Au and Ag, notably exhibits a significantly stronger absorption of incident light (Rosero *et al*., 2024). As indicated by Mie's theory, the intensity and wavelength of the SPR band are influenced by the factors affecting electron charge density on the particle surface, which include structure, particle size, metal type, shape, composition, and the dielectric constant of the surrounding medium (Huang & El-Sayed, 2010). Due to their unique optical, photothermal, and electrical properties, metallic nanoparticles such as Au and Ag are considered of great interest (Bali *et al*., 2006; S. Iravani (2011); Mittal *et al*., 2013).



© University of Venda

Although physical and chemical methods can effectively synthesize pure nanoparticles, they are expensive and may be hazardous to the environment (Kumar *et al*., 2009). The green synthesis technique is a quick, easy, affordable, and environmentally friendly method to produce nanoparticles (Mittal *et al*., 2013). Therefore, researchers have become primarily focused on creating innovative green chemical techniques for creating metallic nanoparticles. In addition, previous studies have reported that plants produce more stable nanoparticles and more varied in size and shape (Iravani, 2011).

Due to their comparatively large surface area, nanoparticles have significant adsorption capacities, of which they can bind and/or carry other things such as chemicals, drugs, probes, and proteins that are bound/attached to their surface via covalent bonds or adsorption. By attaching/adding chemical compounds, peptides, or proteins to the surface of nanoparticles, their physiochemical characteristics, such as charge and hydrophobicity, can be changed to design them for biological applications (Bhatia, 2016). There are several potential uses for silver nanoparticles (AgNPs) in the biomedical field, including drug delivery and diagnostic kits (Ghosh et al., 2008).

## 1.2. Nanoparticles

Nanoparticles can be categorized according to their size, shape, and composition. The most common types of nanoparticles are metal oxides, quantum dots, metals, and carbon-based. Owing to their properties, nanoparticles have garnered much interest in several disciplines, including environmental science, electronics, medicine, and energy (Chaudhry *et al*., 2018; Kolahalam *et al*., 2019). Nanoparticles have shown potential for drug delivery, imaging, and cancer therapy, particularly in medicine. By functionalising them with targeting moieties, they can target cancer cells specifically while preserving healthy cells. Additionally, by enhancing drug delivery to the tumour site and decreasing systemic toxicity, nanoparticles can improve the effectiveness of chemotherapy (Zhang *et al*., 2008).

## 1.3. Synthesis of metallic nanoparticles

Due to their unique physicochemical features, which include antibacterial, electronic, optical, and magnetic properties, and catalytic activity, the biosynthesis of metal nanoparticles using extracts from medicinal plants has been thoroughly studied (Begum et al., 2022).



© University of Venda

The previously mentioned effects are associated with their small size and large surface-to-volume ratio (Abdo, 2017; Fardood *et al*., 2017).

### 1.3.1. Dissociation of silver nitrate

When silver nitrate dissolves in water, it dissociates into silver ions ($Ag^+$) and nitrate ions ($NO_3^-$):

$$AgNO3 \rightarrow Ag^+ + NO3^- \ldots\ldots\ldots\ldots\ldots\ldots (1)$$

### 1.3.2. Reduction of Silver Ions by Plant Extract

Plant extracts contain various phytochemicals (such as phenolic compounds, terpenoids, flavonoids, etc.) that act as reducing agents. These reducing agents donate electrons to silver ions ($Ag^+$) to form elemental silver ($Ag^0$ or silver nanoparticles):

$Ag^+$ + Reducing agent (from plant extract) $\rightarrow Ag^0$ + Oxidized product (from plant extract)

### 1.3.3. Overall Reaction

$AgNO3$ +Plant extract$\rightarrow Ag^0 + NO3^-$ + Oxidized plant compounds

## 1.4. *Senna alexandrina* plant species

Medicinal plants contain several natural substances that produce specific physiological actions in the human body, and these bioactive compounds include alkaloids, carbohydrates, glycosides, phytosterols, phenols, tannins, flavonoids, terpenoids, steroids, and quinones (Cantarelli *et al*., 2011; Victor and Obi, 2009). Sennas is a large genus of flowering plants that belong to the Caesalpiniaceae subfamily of the legume family Fabaceae. There are over 260–350 species in this family, and 50 species of senna are known in farming (Edeoga *et al*., 2005; Yagi *et al*., 2013). This medicinal plant is known locally as Sanna Makki in Libya and Middle Eastern countries and has widely been used in folk medicinal in these countries. The anthraquinone glycosides, particularly sennoside A and B, are primarily responsible for the medicinal activities of senna leaves



© University of Venda

(Balasankar *et al*., 2013; Demirezer *et al*., 2011). Senna plants grow in subtropical regions on sandy loam soil and are small shrubs up to 1.5 m high (figure 1.2) (Leelavathi & Udayasri, 2018). The *Senna alexandrina* leaves contain sennosides A, B, C, D, and glycosides (Parivuguna, 2008).



**Figure 1.2.** *Senna alexandrina* leaves collected at the University of Venda (22.9757° S, 30.4465° E).

## 1.5. Silver nanoparticles

Silver nanoparticles (AgNPs) have gained more interest from researchers in recent decades due to their exceptional optical and chemical characteristics, which have been applied in a variety of fields (Dawadi *et al*., 2021; Almatroudi, 2020). Additionally, the high toxicity and large surface area of AgNPs make them a strong candidate for antimicrobial activity since they come into greater contact with microorganisms (Dhand *et al*., 2016). According to research, AgNPs are said to have a strong anti-inflammatory effect (Nadworny *et al*., 2008; Sibbald *et al*., 2007) and quicken up wound healing (Huang *et al*., 2007; Ali *et al*., 2017).

Recent developments in nanoscience and nanotechnology have radically altered the diagnosis, treatment, and prevention of several diseases in various aspects of human life. Silver nanoparticles (AgNPs) are among the most vital and intriguing nanomaterials among the several metallic nanoparticles used in biomedical applications. Although several noble metals have been employed



© University of Venda

for a variety of purposes, AgNPs have drawn attention due to their potential usage in cancer treatment and diagnosis (Zhang *et al*., 2016).

The most significant nanoparticles are silver and gold, and their potential medical applications are growing daily (Sorbiun *et al*., 2018). AgNPs can be synthesized in various methods (Saravanakumar *et al*., 2017; Zia *et al*., 2016). In the field of antimicrobials and medicine, the use of low- cost, non-toxic reducing, stabilizing agents and biodegradable substrates is growing more significant (Fayaz *et al*., 2010; Govindaraju *et al*., 2015; Shameli *et al*., 2012; Rajesh *et al*., 2017). Numerous studies on producing AgNPs using plant extracts have been conducted because chemical methods lead to some toxic substances being adsorbed on AgNPs surface. In a recent study by Kale et al. (2018) Citrus lemon leaves were used as the reducing agent in the recent synthesis of AgNPs by Kale *et al*. They investigated the potential impacts of temperature, pH, and the amount of the reducing agent using response surface methods. As a result, the synthesised AgNPs showed excellent results in terms of particle size. Krishnaraj et al. (2010) used *Acalypha indica* leaf extract to produce AgNPs. The AgNPs (10 µg/ml) showed effective minimal inhibitory activity against water-borne pathogens, *Vibrio cholera and Escherichia coli* (Krishnaraj *et al*., 2010). A study by Ahmed *et al*. reported synthesising AgNPs using an aqueous leaf extract from *Azadirachta indica.* Their results indicated that the leaf extract acts as both capping and reducing agents. Additionally, the AgNPs demonstrated antibacterial activities against both *E. coli, Staphylococcus aureus Bacillus subtilis, Pseudomonas aeruginosa, Salmonella typhimurium* and *Klebsiella pneumoniae* microorganisms (Ahmed *et al*., 2016). UV-visible spectroscopy can be used to confirm the formation of silver nanoparticles, along with several techniques, such as photoluminescence, transmission electron microscopy (TEM), scanning electron microscopy (SEM), dynamic light scattering (DLS), and Fourier transform infrared spectroscopy (FTIR).

### 1.6. Coating and functionalization of nanoparticles

Nanoparticles have been used for disease diagnosis, prevention, and therapies. Their significant advantages in therapeutic safety and efficacy have been the main target of interest, and because of that, they have gained increasing interest in biomedical applications. The effectiveness of engineered nanomaterials depends on their application in immune system prevention, stability in physiological conditions and cell membranes, minimal toxicity, and excellent bio-performances.



© University of Venda

Its unique optical properties make it a great attractor. These NPs have recently been coated using various physical and chemical methods. In NP coatings, biomolecules such as proteins, polysaccharides, peptides, antibodies, DNA, RNA, and biopolymers have all been extensively utilized (especially for silver and gold nanoparticles) for a range of biomedical applications, preserving their biological functions while boosting their biocompatibility (Rosero *et al*., 2024).

Coating involves covering the nanoparticle's surface with a specific material. This primarily aims to provide stability, optimize dispersion in specific media and protect against degradation. As protective barriers, polymers (like PEG), surfactants, and organic materials help nanoparticles integrate harmoniously with the introduced environment. In contrast, functionalization intentionally modifies the NP's surface to provide a desired functionality. Usually, this process is facilitated by the covalent bonding of specific functional groups or molecules to the nanoparticle's surface. Furthermore, these changes allow nanoparticles to react to particular stimuli, attach to specific targets (such as proteins or cells), or act as delivery systems for therapeutic agents. The binding of antibodies to nanoparticles and their selective targeting of tumor cells serves as an example. In practice, coating is initially necessary in many applications to ensure the biocompatibility and stability of nanoparticles. Altogether, these techniques enable the customization of nanoparticles, optimizing their diagnostic capability and therapeutic efficacy (Pinelli *et al*., 2020). NPs comprise a surface modifier and a core substance known as a "capping" or "coating" agent. The surface modifier changes the physicochemical characteristics of the core NP. (De Jong, 2008). NP surfaces can be coated with different materials (Table 1.1), and their surface properties have been reported to play a role in conferring cytotoxicity or cytoprotection. These coatings and functional groups (Figure 1.3) play an important role in determining the characteristics of the NP-protein interface. Smaller NPs are produced when more capping agent is applied to the core of NP. This phenomenon was first discovered by Turkevich in 1957 in a reducing agent gold nanoparticle synthesis method, which was later refined by Frens in the 1970s (Zabetakis *et al*., 2012).



© University of Venda

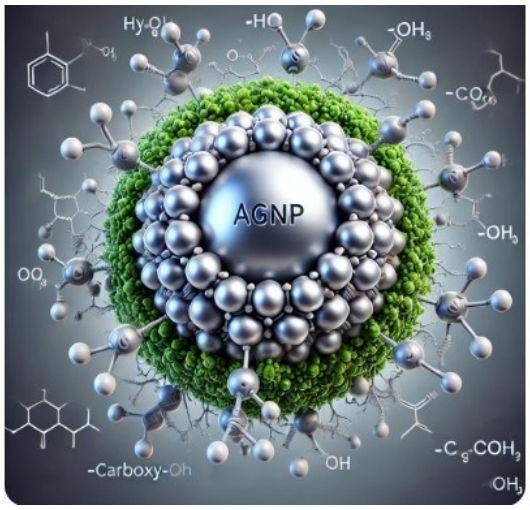



**Figure 1.3.** Schematic representation of AgNP core coated with plant phytochemicals (https://blogs.oregonstate.edu/blenderbio/physical-science/)

**Table 1.1. Different surface coatings of nanoparticles**

| **Surface coatings** | **Acronym** | **Functionalization/ Application** | **Reference source** |
|---|---|---|---|
| Citrate | Cit | Drug delivery, particle stabilization | Ji *et al*., 2007; Lopes-Roudriguez *et al* .,2020 |
| Cysteine | Cys | Biosensing, drug delivery, improving the water solubility and biocompatibility of quantum dots, biolabeling | Luthuli *et al*., 2013; Priyam et al., 2004; Rosen & Gu (2011) |
| 2-(acetoacetoxy) ethyl methacrylate, | AAEM | AAEMA is a polymerizable chelating agent /acetoacetate acrylic monomer used to make acrylic resins for a wide variety of coatings and adhesive applications | Kim *et al*., 2023 |



© University of Venda

| | | | |
|---|---|---|---|
| Bovine serum albumin (BSA)_ | BSA | Targeted Drug Delivery; Biosensing; | Lynch & Dawson (2020) |
| Chitosan | Chi | Targeted Drug Delivery; Biosensing; Electrostatic Adsorption, Facilitates interaction with elements in serum | Gan & Wang (2007); Boyles et al., 2015 |

## 1.7. Green synthesis of silver nanoparticles

In recent years, nanoparticles have garnered interest in biology, medicine, and electronics owing to their remarkable applications (Figure 1.4). Several methods to produce nanoparticles have been developed. However, these methods may require using hazardous substances and high-energy physical processes. Biological methods are an alternative to circumvent these obstacles. Biological resources used for the green synthesis of nanoparticles include plant species, algae, fungi, and Bacteria (Figure 1.4). This approach has provided a method that is straightforward, environmentally beneficial, and reliable (Hebbalalu *et al*., 2013; Velusamy *et al*., 2016); in this study, plant species (*Senna alexandrina*) were used as biological resources for the green synthesis of silver nanoparticles.

Plant extracts are one of the most widely used reducing agents for nanoparticle synthesis because of their environmentally friendly nature, as they avoid using toxic or harmful substances. Because it requires fewer steps overall, it is among the quickest and most cost-effective techniques (Makarov et al., 2014; Hebbalalu et al., 2013). Compared to synthesis utilizing microorganisms, this makes it extremely efficient in producing nanoparticles. Intracellular, extracellular, and phytochemical-mediated techniques can all be used for this synthesis (Dauthal & Mukhopadhyay, 2016).

The synthesis is performed inside the plant cell using the intracellular method, similar to the intracellular approach employing microorganisms. The nanoparticles are retrieved by breaking down the structure. Controlling plant species' growth factors is necessary to prevent them from interfering with synthesis (Saim *et al*., 2021). Extracellular: This approach is the most common due to its simplicity and rapidity.



© University of Venda

The first step in the procedure is to obtain a plant extract, which is commonly water-based, to which a metal salt precursor is added. Reaction conditions, such as pH, temperature, and reaction time, play a crucial role in the size, shape, and yield of the synthesized nanoparticles in many synthesis processes (Agarwal *et al*., 2017; Makarov *et al*., 2014; Hebbalalu *et al*., 2013).

One of the most critical variables is temperature, which affects size, synthesis, and shape (spherical, prismatic, flakes, triangular, octahedral, etc.). Higher yields result from increased nucleation center formation and reaction rate as the temperature rises. Temperatures influence reactant interactions, resulting in different shapes. Higher temperatures increase nanoparticle size (Álvarez *et al*., 2022; Thanh *et al*., 2014). This method uses biologically active substances and natural resources that can serve as capping, stabilizing, or reducing agents in the one-step production of nanoparticles. Overall, green chemistry synthesis of nanoparticles is a viable strategy for efficient and sustainable production (Rafael & Jesús, 2023).

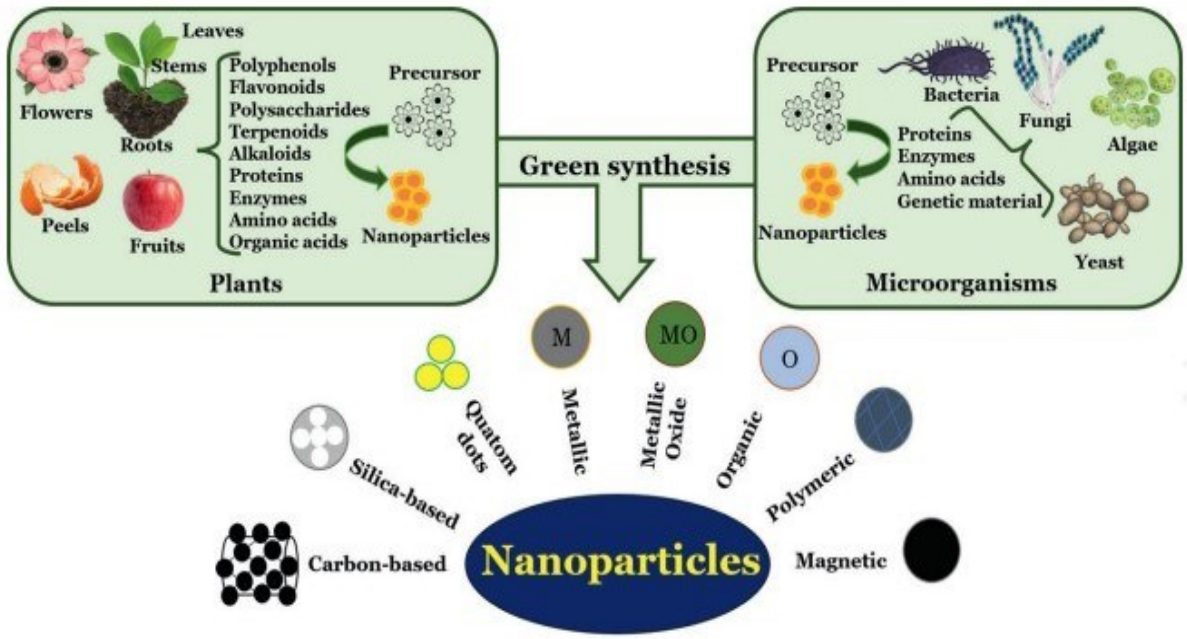



**Figure 1.4.** Biological resources and compounds used for the green synthesis of nanoparticles (Adapted from Rafael & Jesús 2023).



© University of Venda

Two approaches to nanoparticle generation are top-down and bottom-up. Top-down involves physical techniques like grinding or abrasion, while bottom-up uses atoms or molecules as building blocks. The bottom-up approach is preferred due to the use of specialized equipment and the shorter time required to obtain nanoparticles, and green synthesis is gaining more relevance in nanoparticle production within the "bottom-up" approach (Singh *et al*., 2018). Among the most common resources used for this procedure, plant species, algae, or microorganisms like bacteria or fungi are the most used.

By acting together, various compounds from plants or microorganisms, such as terpenes, polyphenols, alkaloids, carbohydrates, proteins, and genetic material, play an essential role in reducing metal ions and stabilizing the resulting nanoparticles in nanoparticle synthesis (Makarov *et al*., 2014; Hebbalalu *et al*., 2013; Carrillo *et al*., 2016). Flavonoids, a broad class of polyphenolic compounds, can actively chelate and reduce metal ions due to their numerous functional groups, which can form these structures. Monosaccharides, like glucose, may serve as reducing agents because they reduce metal ions and produce nanoparticles by oxidizing the sugar's aldehyde group to a carboxyl group by the addition of hydroxyl groups (Makarov *et al*., 2014).

Green nanoparticle synthesis involves polyphenols acting as ligands, forming coordination compounds with metal ions. Aromatic hydroxyl groups bind to metal ions, forming stable complexes. This mechanism undergoes direct decomposition at high temperatures, releasing nanoparticles from the intricate structure (Nava *et al*., 2017). The hydroxyl groups in flavonoids, amino acids, proteins, terpenoids, tannins, and reducing sugars surround the metal ions to form complexes. After this process, the hydroxyl ions undergo oxidation to form carbonyl groups, which in turn stabilizes the nanoparticles. (Carrillo *et al*., 2016, Nava *et al*., 2017). Multiple studies have used different plant extracts for the synthesis of silver nanoparticles, and the results obtained showed different sizes of NPs (Table 1.2).



© University of Venda

**Table 1.2. Previous studies that used plant extract to mediate the synthesis of silver nanoparticles**

| Plant | Size (nm) | Reference |
|---|---|---|
| Pithophora oedogonia | 34.03 | (Sinha *et al*., 2015) |
| Ocimum tenuiflorum | 29 | (Khan *et al*., 2017) |
| Solanum trilobatum | 100 | (Sakthiraj *et al*., 2024) |
| Abutilon indicum | 5-25; 50-100 | (Mata *et al*., 2015; Chandirika & Annadurai, 2018) |
| Potentilla fulgens | 10-15 | (Mittal *et al*., 2015) |
| Banana Peel Extract (BPE) | 23.7 | (Ibrahim, 2015) |
| Hemidemus indicus | 25.24 | (Latha *et al*., 2015) |
| Justicia glauca | 10-20 | (Emmanuel *et al*., 2015) |
| Citrus sinensis | 35 & 10 | (Kaviya *et al*., 2011) |
| Centella asiatica | 30-50 | (Rout *et al*., 2013) |
| Syzygium cumini | 100-160 | (Prasad *et al*., 2012) |
| Artemia salina | 40-60 | (Unal *et al*., 2022) |
| Descurainia sophia | 1-35 | (Khatami *et al*., 2016) |
| Achillea biebersteinii | 12 | (Baharara *et al*., 2014) |
| Rauvolfia serpentina | 7-10 | (Panja *et al*., 2016) |
| Indonesiella echioides | 29-41 | (Yuvarajan *et al*., 2014) |
| Prosopis farcta | 10.8 | (Miri *et al*., 2015; Miri *et al*., 2018) |
| Emblica Officinalis | 10-30 | (Ankamwar *et al*., 2005) |
| Ziziphus jujuba | 28 | (Gavade *et al*., 2015) |
| Pistacia atlantica | 27 | (Sadeghi *et al*., 2015) |

## 1.8. Applications of silver nanoparticles in drug delivery and gene therapy

Over the years, numerous in vitro and in vivo investigations have been conducted on silver nanoparticles to determine their negative effects/toxicity towards biological tissues and organisms. Following this, researchers have demonstrated that AgNPs exhibit a high level of antimicrobial activity against a variety of bacterial species, Neisseria gonorrhoea, Escherichia coli, and Chlamydia trachomatis, including viruses (Marin *et al*., 2015). The limits of conventional cancer



© University of Venda

treatments, such chemotherapy, radiotherapy, or surgery, have been linked to drug toxicity, unpredictable side effects, drug resistance issues, and a lack of specificity in recent years. By reducing side effects and increasing the effectiveness of cancer treatment, AgNPs overcome these limitations. Their capacity to deliver drugs precisely and to penetrate a variety of biological barriers is one of their unique qualities. Specific delivery of anticancer drugs to tumor tissues together with green synthesis of AgNPs offers an innovative approach for improving cancer treatment (Kajani *et al*., 2016).

Due to their unique field properties, such as having a light scattering cross-section that is nearly ten times larger than that of gold nanoparticles of similar size, silver nanoparticles have garnered interest for use as biological label sensors in conjunction with substrates over surface enhanced absorption, fluorescence, and photochemistry (Fawad Ahmad, 2023). Cancer is the second-largest cause of death globally, with lung cancer being the leading cause. Alternative therapies like metallic nanoparticles are needed to replace traditional treatments due to adverse effects and potential resistance. Additionally, current treatments, such as daunorubicin, bleomycin, and cisplatin, are only partially successful but have drawbacks (Jeyaraj *et al*., 2013). Nanoparticles of various sizes and shapes have been created for cancer treatment to decrease the rate of release along with the necessary therapeutic dosage (Fawad Ahmad, 2023).



© University of Venda

## 1.9. Importance of NPs against antibiotic resistance

Green synthesis methods, while environmentally friendly, introduce variability in biological components. Consistency in the choice of precursor materials, reducing agents, stabilizers, and synthesis conditions leads to NPs with reproducible size, shape, and surface properties, allowing reliable comparisons of antibacterial activities (Aguilar-Garay *et al*., 2024). Despite the potential of Ag and Au nanoparticles as antibacterial agents, the emerging bacterial resistance continues to hinder their complete clinical application. This resistance threatens their effectiveness (Aguilar-Garay *et al*., 2024). Previous studies have demonstrated that bacteria can become resistant to silver, and commercial silver-resistant strains exist for laboratory testing. The long-term effectiveness of silver-based antibacterial treatments is threatened by this resistance. In order to combat this, approaches, including using proteins such as Trojan horses to prevent resistance, are being investigated. The delivery and efficacy of silver nanoparticles are enhanced by this protein, ensuring their continued viability in the fight against bacteria resistant to antibiotics. (Hsiao *et al*., 2015). The minimum inhibitory concentration (MIC) and minimum bactericidal concentration (MBC) are critical metrics for evaluating the antibacterial activity of NPs. However, these values are reported using different units and experimental conditions, which in the data leads to significant discrepancies. Training machine learning models to predict NPs' effectiveness against different bacterial strains, optimize synthesis parameters, and discover novel antibacterial drugs requires quantitative data (Aguilar-Garay *et al*., 2024).

## 1.10. Heat shock proteins (HSP)

Heat shock proteins are conserved molecules whose primary function is to facilitate protein folding (Hartl *et al*., 2002). *Escherichia coli* has a particularly well-documented heat shock response. So far, more than 30 proteins have been identified that are associated with the physiological response to heat, which includes DnaK, GroES, and GroEL chaperone proteins involved in the degradation, folding, and repair of proteins. Moreover, the alternative sigma factor controls the expression of the heat shock genes, $\sigma^{32}$ (RpoH) (Fourie & Wilson, 2020).



© University of Venda

According to Bukau and Walker (1989), one of the most prominent heat shock proteins is Hsp70, also known as DnaK in prokaryotes. It recognizes and binds to hydrophobic regions of misfolded proteins, stabilizing them and preventing their aggregation, and it is also capable of reversing protein aggregation (Mayer *et al*., 2000; Shonhai *et al*., 2007). The molecular chaperone machinery (protein folding facilitators) in biological systems is largely composed of Hsps due to their function in protein folding (Ellis, 1987).

Based on their molecular weight, HSPs are categorized into several families, which include HSP27, HSP60, HSP70, HSP90, and HSP110. Although the functions and mechanisms of action of each family of HSPs vary, they are all able to stabilize unfolded proteins and prevent them from aggregating. The HSP70 family has been extensively researched for its role in protein quality control and potential therapeutic implications for various diseases, including neurodegenerative disorders, infectious diseases, and cancer (Mayer & Bukau, 2005).

### 1.10.1. Heat shock proteins as molecular chaperones

Molecular chaperones are a group of proteins that facilitate the folding or unfolding of other proteins to attain the conformational structures necessary for their functions (Kim *et al*., 2013). Molecular chaperones assist other proteins in acquiring their functionally active shape by interacting with and stabilizing them.

Furthermore, molecular chaperones do not contribute to the folded protein's final conformations. Some proteins do not fold to their native state when they fold in vivo (Hoffmann *et al*., 2010). Due to the in vivo environment being too crowded, this results in protein aggregation. Consequently, molecular chaperones are necessarily required to maintain substrates in competent folding form and reduce protein aggregation (Muñoz *et al*., 2015).

Heat shock proteins (Hsp) are molecular chaperones that are upregulated during stress; they were named after their discovery in Drosophila, where they were upregulated during heat stress (Ritosa, 1962). Although HSPs are named in various ways, stress-induced HSPs are usually referred to as Hsp, and cognitively expressed Hsc proteins are called heat shock cognate (Hsc) proteins. They are also named based on their functions, such as holding the substrate in a folding competent state (holdase) or folding it to its native structure (foldase) and unfolding aggregated substrates



© University of Venda

(unfoldase) (Wynn et al., 1994; Saibil, 2013). They are also further classified according to their molecular mass in kilodaltons (kDa) (Table 1.3; Lindquist & Craig, 1988). Furthermore, the major classes are reported to be the Hsp100, Hsp90, Hsp70, Hsp60, Hsp40, and small Hsps (sHsps) (Table 1.3). Hsps ensures cell survival by maintaining proteostasis (Saibil, 2013). Additionally, they regulate protein conformational state, holding proteins in a primed state for ligand binding or post-translational modification (Kim *et al*., 2013), and are implicated in the development and pathogenesis of parasites (Shonhai *et al*., 2011).

**Table 1.3. Heat shock proteins (Hsps) families and their functions**

| **Protein Name** | **Molecular weight (kDa)** | **localization** | **Stress function** | **References** |
|---|---|---|---|---|
| **Hsp100** | 80 – 110 | chloroplast, nucleolus, cytosol, nucleus | Thermo-tolerance, an ATPase(unfoldase) | Squires, (1992); Sanchez *et al.* (1990); Nowicki *et al.* (2012) |
| **Hsp90** | 82 – 96 | Nucleus, cytosol | Thermo-tolerance partners with kinases, Hsp70; ATPase (foldase) | Picard *et al.* (1990); Tai *et al* (1992); Yang *et al*., (2015) |
| **Hsp70** | 67 – 76 | Nucleus, cytosol, mitochondria, Chloroplast, ER | Thermo-tolerance, protein assembly, associates with; Hsp60, Hsp40, Hsp90, GrpE binds unfolded proteins; an ATPase (foldase) | Bukau and Walker (1990); Shonhai *et al* (2005); Kurtz *et a*l (1986) |
| **Hsp60** | 58 – 65 | Chloroplast, mitochondria | ATPase, hydrolysis stimulated by Hsp10 (foldase) | Langer *et* |



© University of Venda

| | | | | |
|---|---|---|---|---|
| | | | | *al* (1992); Sato and Wilson (2004); Martin *et al* (1991) |
| **Hsp40** | 40 – 100 | cytosol, membranes | Co-chaperone of Hsp70, binding to non-native proteins, function with Hsp70 and GrpE (holdase). | Njunge *et al*., 2013 Botha *et al*., 2007 Cheetham and Caplan (1998) |

**Table legend**: ER- endoplasmic reticulum; Hsp- heat-shock protein.

### 1.10.2. Heat shock protein 40

*E. coli* DnaJ (Hsp40 or J-proteins) have recently been named J-domain containing proteins (JDPs) (Kampinga *et al*., 2018). The role of Hsp40s is to speed up the rate of ATP hydrolysis by Hsp70s (Alderson *et al*., 2016; Kampinga et al., 2019). Simultaneously, previous studies suggested that many Hsp40s deliver polypeptide substrates to Hsp70s by directly binding to unfolded or partially folded polypeptides (Craig & Marszalek, 2017; Cyr & Ramos, 2015; Pobre *et al*., 2019).

### 1.10.3. Heat shock protein 70

Hsp70s, a versatile, abundant, and conserved molecular chaperone, is crucial in maintaining intracellular proteostasis in all living organisms. In this role, Hsp70s are linked to various human diseases, including cancers and neurodegenerative disorders, and are recognized as crucial drug targets in developing novel therapeutics for these diseases (Rosenzweig *et al*., 2019). Besides a few archaea, in all species examined, Hsp70 is one of the most common molecular chaperones present in every cellular compartment of eukaryotes (Mayer & Gierasch, 2019). Hsp70 assists in protein folding, disaggregation, and degradation through conformational changes induced by ATP hydrolysis (Zuiderweg *et al*., 2017). In contrast, recent studies have reported that Hsp70s binding prevents client proteins from spontaneous folding.

For instance, the study done by Moràn Luengo et al. (2018) used Malate dehydrogenase (MDH), an Hsp70 substrate, and folding only occurred when Hsp90 knocked off the Hsp70 (Moràn Luengo *et al*., 2018). However, this suggests that Hsp70 is essential at both normal growth and high



© University of Venda

temperatures in different organisms despite its inability to fold proteins at physiological concentrations (reviewed by Yu *et al*., 2015).

Hsp70s are crucial for fundamental housekeeping functions, especially in stressful conditions. It is not surprising that when exposed to a variety of stressful and pathological situations, including high temperatures, Hsp70s are one of the main molecular chaperones that help cells and organisms to survive by providing essential protection to survive these harmful conditions (Hartl & Hayer-Hartl, 2009). Different organisms have varying numbers of genes encoding Hsp70 members; humans have 13 Hsp70 (HSPA) proteins that are present in all cellular compartments (Hageman & Kampinga, 2009) and four related Hsp110 proteins, but *Escherichia coli* only has three members (Vos *et al*., 2008).

Interestingly, Hsp70 chaperones can function as foldases, directing substrate protein folding through molecular dynamics simulations (Lu *et al*., 2021). The exposed hydrophobic residue recognition in non-native protein substrates is initiated by the ATP-dependent binding and release in HSP70 (Imamoglu *et al*., 2020). Hsp70 (DnaK) in bacteria plays a crucial role in protein folding processes, assisting, preventing, and solubilizing aggregates, with approximately 25% of the cytosolic proteome interacting with it (Calloni *et al*., 2012; Mayer, 2021). The Hsp70 protein functions as a holdase and a refoldase (Skowyra et *al*., 1990; Slepenkov & Witt, 2002). Hsp90 and Hsp70 chaperones cooperate to activate and regulate signaling proteins involved in signal transduction by forming multi-chaperone complexes (Genest *et al*., 2019; Morán Luengo *et al*., 2019; Pratt *et al*., 2010).

Additionally, Proteomics studies reveal post-translational modifications on Hsp70 family proteins like phosphorylation, acetylation, and ubiquitination, but understanding their physiological relevance remains a challenge (Nitika *et al*., 2020; Nitika & Truman, 2017). Elucidating the functional roles of Hsp70, such as co-chaperone binding and its allosteric behavior, should enhance therapeutic opportunities, as it is a potential drug target for many diseases (Chiappori *et al*., 2016).

A nucleotide-binding domain (NBD) at N-terminus or a 45 kDa ATPase domain and a 25 kDa C-terminal substrate binding domain (SBD) are the two functional domains of all Hsp70s, with the nucleotide-binding domain (NBD) being the energy component, and to provide energy to empower the chaperone activity it binds and hydrolyzes ATP to ADP. In addition, the C-terminal substrate



© University of Venda

binding domain corresponds to the above two essential intrinsic activities and is the binding site of the protein substrate in which Hsp70s assist them to fold, transport across membranes, assemble, transport across membranes (Swain *et al*., 2007; Rudiger *et al*., 1997). The SBD consists of an 18 kDa ß-sandwich subdomain and 10 kDa α-helical subdomain, and the ß-sandwich subdomain is the substrate-binding domain, while the α-helical subdomain forms a lid structure that covers the peptide-binding domain, respectively (Bertelsen *et al*., 2009; Mayer & Bukau, 2005) (Figure 1.5). These two domains are connected by a highly conserved short linker segment (Figure 1.5) (Mayer *et al*., 2000). The linker motif comprises DVLLLDV residues; this linker is essential for inter-domain communication (Zhuravleva & Gierasch, 2011). Functional impairment of the Hsp70 is reportedly to be caused by mutations on the linker segment (Vogel *et al*., 2006). In cooperation with co-chaperones such as Hsp40, Hsp70 binds to short hydrophobic peptides to promote substrate refolding or degradation (Zhang *et al*., 2014).

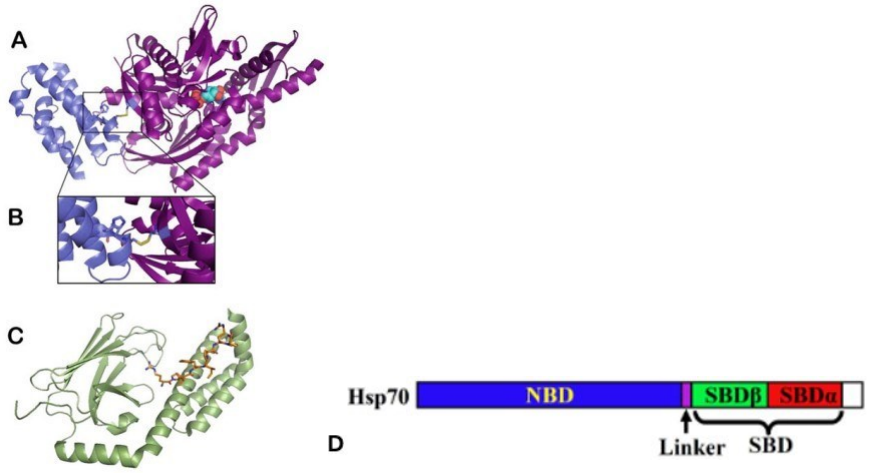



**Figure 1.5**. Structural features of the Hsp70.

The HPD motif directly contacts Hsc70 at a cleft within the ATPase domain of Hsc70. (a) and (b) interaction between the J domain from auxilin (blue) and the ATPase domain of bovine Hsc70 (purple; PDB ID: 2QWP). Nucleotide bound to the ATPase domain of Hsp70 is shown as spheres, and the HPD motif is shown as sticks. (c) The substrate-binding domain with a β-sandwich subdomain and α-helical subdomain. The peptide substrate (orange sticks). (d) The Hsp70 domain organization consists of the NBD (in blue) and the SBD composed of the β- and α-region and the C-terminus lid (in white). A conserved linker (in purple) joins the NBD and SBD and is responsible for interdomain communication. (Adapted from heat shock proteins of Malaria, Second Edition; Liu et al., 2019).



© University of Venda

Hsp70 relies on interaction with co-chaperones and cofactors for regulation of ATP hydrolysis and substrate interaction to cope with the wide variety of different functions in the cell (Mayer, 2010b). Hsp70 has the largest group of co-chaperones comprising the JDP/DnaJ family; to promote protein folding, J domain-containing and Hsp70 proteins work in specific pairs (Hennessy *et al*., 2005). The Hsp70 chaperone cycle switches between the ATP and ADP-bound states through ATP hydrolysis and substrate exchanges (Figure 1.6).

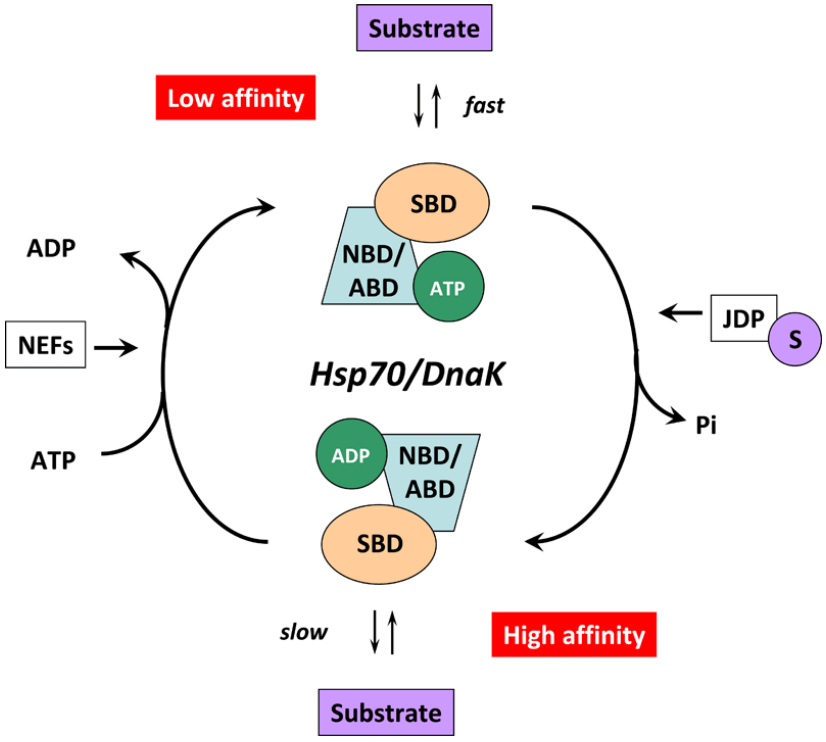



**Figure 1.6.** The Hsp70/DnaK chaperone cycle.

In the ATP-bound state, the NBD/ABD and SBD are docked, the substrate binding grove is open, and the Hsp70/DnaK chaperone exhibits low affinity and fast exchange rates for its substrate. ATP hydrolysis is facilitated by J-domain proteins (JDPs) of the HSP40/DNAJ family and nucleotide exchange factors (NEFs). JDPs with the C-terminally bound substrate (S) interact with Hsp70/DnaK to achieve this. The substrate and JDP interact simultaneously, causing a conformational change in the ATPase domain of Hsp70/DnaK, stimulating ATP hydrolysis and mediating the closure of the substrate binding grove.



© University of Venda

Hsp70/DnaK is ADP-bound; the chaperone exhibits a high affinity and low exchange rates for its substrate because the docking between its two domains is interrupted. The specific interaction of NEFs with the Hsp70/DnaK ATPase domain mediates the release of ADP, followed by a conformational change that results in the release of the substrate and a low-affinity state (www.hsp70.com).

### 1.10.4. Hsp40-Hsp70 partnership

Compared to basal Hsp70 activity, Hsp70's affinity for substrates in its ATP-bound state is lower than that of the synergy of a bound substrate, and Hsp40 results in up-regulation of ATP hydrolysis of up to 1000-fold (Silberg *et al*., 2000; Kampinga & Craig, 2010; Needham *et al*., 2015). Due to its low basal ATPase activity, one Hsp70 protein hydrolyzes one ATP molecule in ~25 minutes at 30 °C (Alderson *et al*., 2014). This somehow slow activity is activated by the binding of a substrate in the $Hsp70_{SBD}$ (Mayer *et al*., 2000).

Interestingly, Hsp40s are also believed to be responsible for attracting Hsp70 to protein aggregation sites. This role is essential concerning the function of Hsp70 as a disaggregase (Torrente & Shorter, 2013). When Hsp70 is recruited to the aggregation site, it subsequently partners with Hsp100 to disentangle aggregated polypeptides, ultimately facilitating their refolding (Mogk *et al*., 2015).

## 1.11. Effects and toxicity of nanoparticles on protein structure and function:

Previous studies conducted suggest that nanoparticles (NPs) exhibit functional features that resemble those of molecular chaperones (Luthuli et al., 2013; De and Rotello, 2008). De and Rotello (2008) demonstrated how metallic nanoparticles prevented aggregation of heat-stressed proteins in vitro. It is conceivable that nanoparticles' ability to prevent protein aggregation makes them attractive candidates for potential application in treating neurodegenerative diseases caused by protein aggregation and stabilizing agents (Triulzi *et al*., 2008).



© University of Venda

## 1.12. Toxicity of silver nanoparticles, expression of heat shock proteins, and Bacterial cell

AgNPs have become a significant class of nanomaterial for a variety of industrial and medicinal uses that could endanger human health. Based on *in vitro* studies, AgNPs caused toxicity that targeted the brain, circulatory system, reproductive organs, liver, and lungs, among other organs. The level of expression of genes involved in cell cycle progression and apoptosis was reported to be induced by AgNPs. With the production of reactive oxygen species (ROS) stimulated by cell uptake of AgNPs, oxidative stress, DNA damage, and apoptosis were found to be the possible pathways of AgNP toxicity (Noga *et al*., 2023; Carlson *et al*., 2008). AgNP toxicity depends on both size and shape; an alveolar macrophage study revealed that the greatest loss in mitochondrial activity was caused by silver nanoparticles with an average size of 15 nm (Ferdous & Nemmar, 2020; Carlson *et al*., 2008).

Furthermore, in vitro research has generally demonstrated that AgNP exposure has an adverse effect on the health of bacteria or cells. Reactive oxygen species (ROS) induction is the main mechanism of AgNP-dependent cytotoxicity in in vitro tests. AgNPs' cytotoxicity and genotoxicity are primarily determined by their size, concentration, and time of exposure (Du *et al*., 2018).

Bacteria's unique cell wall properties, which differ greatly throughout Gram (+/−) strains, affect how susceptible they are to metal nanoparticles (Sánchez-López *et al*., 2020; Duval *et al*., 2019). Research indicates that AgNPs efficiently eradicate Gram (+/−) bacteria; however, 64% of publications show a more significant impact on Gram (−) strains; this could be attributed to structural variations in their cell walls. Gram (−) bacteria are characterised by an outer cell envelope composed of lipoproteins, phospholipids, and lipopolysaccharides, which covers a thin peptidoglycan layer of about 3 nm (Cavassin *et al*., 2015). Of the research analysed, 25% found that Ag NPs had a greater effect on Gram (+) bacteria than on Gram (−) bacteria, whilst 11% reported no significant difference in efficiency against both types of bacteria. According to Acharya *et al*., 2018, physical interactions severely damage the cell walls of Gram (+) bacteria, and the electrostatic affinity between Ag NPs and bacterial surfaces is essential for antibacterial activity. Positively charged Ag ions and negatively charged bacterial cells are observed to be attracted to each other. Gram (+) bacteria contain a high concentration of teichoic and lipoteichoic acids, which have a strong negative charge and may sequester free Ag ions (Khubchandani *et al*., 2022).



© University of Venda

The antibacterial activity of NPs is dependent on the form and composition of the bacteria's membrane, which also affects the region of contact between the bacteria and NPs (Zhan *et al*., 2022; Mutalik *et al*., 2023). Because of their cell wall structure, which facilitates NP entry, some articles propose that NPs may be more effective against Gram-positive bacteria. This is explained by the interaction between NPs and lysine, which is a common amino acid in Gram (+) bacteria, and the ensuing production of ROS (Figure 1.7) (Kumar *et al*., 2020; Katas *et al*., 2019).

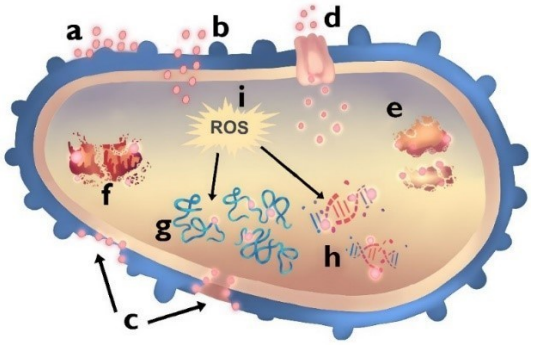



**Figure 1.7.** Ag NPs exhibit antibacterial action through various mechanisms. Including: (**a**) adhesion to the cell wall, (**b**) membrane crossing, (**c**) damage to the cell wall and membrane induced by AgNPs, (**d**) entry of Ag NPs facilitated by porin proteins, (**e**) ribosome disassembly triggered by Ag NPs, (**f**) mitochondrial dysfunction caused by Ag NPs, (**g**) protein denaturation induced by Ag NPs, (**h**) DNA damage caused by Ag NPs, and (**i**) reactive oxygen species (ROS) production and oxidative stress induction resulting from Ag NPs interaction (retrieved from de Lacerda *et al*., 2021; Aguilar-Garay *et al*., 2024).

### 1.12.1. Review & critique of literature

A study by Rai *et al*. (2016) and Mahanty *et al*. (2024) emphasized that AgNPs are potential alternative antibiotics, emphasizing their ability to combat multidrug-resistant bacteria. Another study by Mayer (2005), explored the ATPase activity of DnaK as crucial for its function, suggesting that disruption of this activity could impair bacterial survival. Previous studies have also reported that silver nanoparticles are effective biocides against *E. coli* (Hassanen *et al*., 2021). These theories serve as the basics or foundation for this study on DnaK as a target for SAAgNPs, supporting the idea that inhibiting such critical proteins can effectively impair bacterial stress mechanisms.



© University of Venda

However, a study by Joshi *et al*. (2020) Argued that the strength of AgNPs lies in their broad-spectrum, non-specific mechanisms, such as ROS generation and membrane disruption, which reduce the chance of bacterial resistance. Conversely, Lemire *et al*. (2013) and Jiang *et al*. (2024) suggested that excessive use of AgNPs could promote resistance development, similar to antibiotics, as a result of bacterial adaptation mechanisms. Similarly, Elechiguerra *et al*. (2005) highlighted that inconsistencies in nanoparticle size and shape may influence their antibacterial effectiveness.

Additionally, Narayanan *et al*. (2010) suggested that focusing on a specific bacterial target, which in this study is DnaK, could limit the applicability of AgNPs to specific bacterial strains, further reducing their utility as broad-spectrum agents. Above all, reproducibility, specificity, and resistance concerns may contradict this study. First, this study addresses these challenges by leveraging advanced nanoparticle production for consistent characterization techniques and, second, by demonstrating a targeted mechanism that supports broad-spectrum approaches; lastly, by promoting eco-friendly practices to align with global sustainability goals.



© University of Venda

### 1.12.2. Summary

While heat shock proteins are known to play critical roles in bacterial stress response and survival, their potential as therapeutic targets remains underexplored, especially in the context of nanoparticle-based interventions. Furthermore, existing antibiotics are becoming less effective due to rising AMR (Tang *et al*., 2023), and alternative treatments are urgently needed. Moreover, limited research exists on how nanoparticles interact with specific bacterial proteins at the molecular level.

Although the existing theories state that AgNPs are widely recognized for their strong antibacterial activity due to mechanisms such as the generation of reactive oxygen species (ROS) leading to oxidative stress (Alfei *et al*., 2024). The green synthesis methods using plant extracts are eco-friendly alternatives to chemical synthesis, leveraging natural bioactive compounds as reducing and stabilizing agents (Santhosh *et al*., 2022). Research on medicinal plants such as *Senna alexandrina* for green synthesis is limited, especially in their application to nanoparticle production.

This study emphasizes or highlights DnaK as a novel, essential target for bacterial inhibition by AgNPs. Furthermore, it provides mechanistic insights into how SAAgNPs interact with DnaK, likely disrupting its ATPase activity and protein-folding functions. Above all, this study validates or emphasizes using *S. alexandrina* as a sustainable and cost-effective source for synthesizing AgNPs.



© University of Venda

### 1.12.3. Significance of the study

Like many countries, South Africa faces a growing challenge of antimicrobial resistance (AMR), where traditional antibiotics are losing efficacy against bacterial infections.

Green synthesis of nanoparticles using *Senna alexandrina* aligns with or contributes to Sustainable Development Goal 7 (SDG) 2063 number 7, which emphasizes sustainable practices, reducing reliance on toxic chemicals and energy-intensive methods. Furthermore, encouraging environmentally friendly approaches to drug development supports sustainable healthcare advancements, protecting both human health and the environment.

This study also contributes directly to achieving SDG number 3, by promoting healthy lives and well-being for all ages. It addresses pressing public health challenges such as AMR and foodborne diseases while fostering eco-friendly practices and leveraging South Africa's biodiversity for global health advancements. Particularly in South Africa, contaminated food and water are significant health risks that contribute to the spread of *E. coli*-related infections; by developing effective antibacterial agents such as SAAgNPs could help reduce the prevalence of these diseases, further ensuring safer food and water supplies, which aligns or contributes to SDG number 6, by ensuring availability and sustainable management of water and sanitation for all.

Above all, by targeting DnaK, which is essential for bacterial survival under stress, this approach could provide an alternative mechanism to combat resistant bacterial strains. However, although targeting DnaK is proposed as a promising antibacterial strategy, this approach could raise critical concerns, because DnaK belongs to the Hsp70 family, a group of highly conserved proteins found in all living organisms. Consequently, non-specific inhibition may interfere with host Hsp70 proteins, leading to unintended cytotoxic effects. Furthermore, many commensal bacteria within the human microbiota also rely on DnaK for protein folding and stress adaptation, which suggests that broad inhibition could disrupt beneficial microbial communities and cause dysbiosis. To overcome this challenge, Future studies or therapeutic strategies must ensure high selectivity by identifying unique structural or functional differences between pathogenic DnaK and commensal/host Hsp70 proteins, or focus on infection-site specificity, thus reducing host exposure by employing targeted delivery systems that restrict activity to infection sites.



© University of Venda

## 1.13. Problem statement

The emergence of antibiotic resistance is one of the most pressing challenges in modern medicine, with *Escherichia coli* (*E. coli*), a common bacterial pathogen, as a prime example (Chinemerem-Nwobodo *et al*., 2022). In the WHO African region in 2019, an estimated 1.05 million deaths were associated with bacterial antimicrobial resistance (AMR), and 250,000 deaths were attributable to bacterial AMR (Sartorius *et al*., 2024). The most considerable fatal AMR burden was attributed to lower respiratory, thorax infections, and bloodstream infections. Seven leading pathogens were collectively responsible for these deaths associated with resistance in this region, with four pathogens exceeding 100,000 deaths each: *Streptococcus pneumoniae, Klebsiella pneumoniae, Escherichia coli*, and *Staphylococcus aureus* (Sartorius *et al*., 2024).

DnaK (Hsp70) is a molecular chaperone that assists in the folding, repairing, and degrading of proteins. While its primary function is protection, the negative effects of DnaK can contribute to disease progression (Lu *et al*.,2023). It could promote pathogenic bacteria to survive under stress conditions, especially in bacterial infections (Dalbanjan *et al*., 2024; Chiappori *et al*., 2015). It assists in folding misfolded proteins and protecting cells from damage caused by antibiotics, making the bacteria more resilient to host defenses and the development and persistence of antibiotic resistance. The heat shock protein DnaK, a chaperone involved in protein folding and stress response, plays a crucial role in bacterial survival under adverse conditions (Liu *et al*., 2018). However, traditional antibiotics that target bacterial cell wall synthesis or protein synthesis are becoming less effective due to resistance mechanisms (Ventola, 2015; Baran *et al*., 2023). *Senna alexandrina* belongs to the legume family and is widely used as a traditional medicine for several purposes. All parts of the plant have beneficial pharmacological activities (Oladeji *et al*., 2021). Senna can be found mostly in regions of Africa and Asia (Oladeji *et al*., 2021; Osunga *et al*., 2023). Polyphenol compounds and reducing sugars are the main phytochemical compounds responsible for synthesizing silver nanoparticles (NPs) from Senna sp. AgNPs can be used as antimicrobial substances, catalysts, and drug-delivery carriers (Onitsuka *et al*., 2019). Green synthesis methods, which utilize plant extracts as reducing and stabilizing agents, offer a sustainable alternative to conventional chemical synthesis, potentially reducing the environmental impact and cost (Shafey, 2020; Ying *et al*., 2022). Senna alexandrina (Cassia angustifolia) is a plant known for its medicinal properties and has been explored for nanoparticle synthesis, demonstrating promising results in



© University of Venda

preliminary studies (Albrahim *et al*., 2021; Sharma *et al*., 2017).

Despite the progress in the nanoparticle research field, there remains a gap in understanding the specific mechanisms through which, green-synthesized silver nanoparticles exert their antimicrobial effects, particularly in relation to key bacterial proteins such as DnaK. Previous studies have shown the antibacterial properties of silver nanoparticles but have not thoroughly investigated their interactions with bacterial response proteins (Rodrigues *et al*., 2024; Turbay *et al*., 2021; Gurunathan *et al*., 2014). Furthermore, the impact of Senna Alexandrina-derived silver nanoparticles on bacterial proteins and their potential to inhibit critical functions such as protein folding and stress response is not well-documented.

The burden of AMR in sub-Saharan Africa has largely remained undefined. To address these knowledge gaps, this study presents the effects of SAAgNPs against *E. coli* on DnaK-mediated protein folding or stress response in *E. coli* and predicted sets of binding affinities of SAAgNPs to the active or functional sites of DnaK.

This study aimed to elucidate how these nanoparticles interact with DnaK and assess their antimicrobial efficacy.

## 1.14. Research questions

a) How effective are SAAgNPs in inhibiting the activity of Escherichia coli DnaK protein?

b) What are the physicochemical properties of SAAgNPs synthesized using Senna alexandrina?

c) What is the relationship between the size and morphology of SAAgNPs and their inhibitory effects on *E. coli* DnaK?

d) How does the antimicrobial activity of SAAgNPs against *E. coli* correlate with the inhibition of the DnaK protein?

## 1.15. Hypothesis

SAAgNPs inhibit the activity of *E. coli* DnaK protein, leading to reduced bacterial growth and viability.



© University of Venda

## 1.16. Specific aim and objectives

**Main Aim:** To investigate the inhibitory effects of green-synthesized *Senna alexandrina* silver nanoparticles (SA-AgNPs) on *E. coli* DnaK

### 1.16.1. Objectives

**In order to achieve the aim of this study, the study sought to:**

(a) To extract and validate groups of metabolites from *S. alexandrina* leaves using methanolic extraction and spectrophotometric validation

(b) To validate and analyze metabolites from *S. alexandrina* through UV-VIS, UHPLC-QTOF-MS and computational tools

(c) To synthesize and characterize SA-AgNPs through UV-Visible spectroscopy, FTIR, and SEM

(d) To express and purify recombinant DnaK using Nickel affinity chromatography and biophysically investigate the effects of SA-AgNPs on structural conformations of *E. coli* DnaK

(e) To investigate the effects of SA-AgNPs on ATPase activity of recombinant DnaK aided by co-chaperone DnaJ, and on the ability of recombinant DnaK to suppress aggregation of MDH enzyme *in vitro*

(f) To examine the function of DnaK in protecting the cells (*E. coli* XL1 blue) at different temperatures and the inhibitory effects of SA-AgNPs on cells.

(g) To determine the binding affinity of selected plant compounds on DnaK and DnaK bound to DnaJ using molecular docking



© University of Venda

# Chapter 2

**Green synthesis of *Senna alexandrina* silver nanoparticles (SAAgNPs)**



© University of Venda

# CHAPTER 2: Green synthesis of *Senna alexandrina* silver nanoparticles (SA-AgNPs)

## 2.1. Introduction

This chapter presents a synthesis of silver nanoparticles using senna alexandrina leaf extracts. Plant-based synthesis has drawn significant interest due to its eco-friendly, cost-effective, and biocompatible advantages over traditional chemical and physical processes (Ullah & Lim, 2022). In this study, *Senna alexandrina* (SA) was utilized as a native reducing and stabilizing agent for the green synthesis of silver nanoparticles (SA-AgNPs). To ensure the effective utilization of bioactive compounds from *S. alexandrina*, a multi-step methodology is employed, integrating metabolite extraction, purification, and advanced analytical techniques. The first step of the procedure was the methanolic extraction and validation of crucial metabolites from *S. alexandrina* leaves, which was followed by spectrophotometric analysis to verify the presence of bioactive groups (Demarque *et al*., 2020). Subsequently, compound purification was conducted using silica gel column chromatography to isolate specific phytochemicals. The metabolites present in the extract were further separated and identified using Thin Layer Chromatography (TLC) (Grover *et al*., 2021). In order to obtain a comprehensive metabolomic profile, ultra-high-performance liquid chromatography coupled with quadrupole time-of-flight mass spectrometry (UHPLC-QTOF-MS) was used, together with the Sirius software for structural elucidation of detected compounds (Terrence, 2022). Furthermore, after metabolite identification, purified extracts were further utilized for the synthesis of silver nanoparticles. Moreover, the synthesized SA-AgNPs were characterized using ultraviolet-visible (UV-Vis) spectroscopy to validate nanoparticle formation, and Fourier-transform infrared spectroscopy (FTIR), along with scanning electron microscopy (SEM), was employed to identify functional groups involved in the reduction, stabilization process, and to analyze their morphological and structural properties, respectively (Joudeh & Linke, 2022; Pasieczna-Patkowska *et al*., 2025).



© University of Venda

## 2.2. Experimental procedures

### 2.2.1. Extraction and validation groups of metabolites from *S. Alexandrina* leaves using methanolic extraction and spectrophotometric validation:

In centrifuge tubes, 20 mg of crushed leaves (Figure 1.2) were homogenized with 20 ml 80% (v/v) methanol, then incubated for 48 hours, shaking at 150 rpm, at room temperature. After, samples were centrifuged at 13,000 centrifugal force for 5 minutes using a Multifuge X1 R Pro, 208-240V H-Flex Cell Culture Package centrifuge (ThermoFisher Scientific, USA). The supernatant was filtered using a 0.2 µM nylon syringe filter and stored in the fridge for further use. Samples were diluted 50X with 80% methanol. A methanolic extract sample amount of 40µl was added to 960 µl solvent containing 80% methanol. All tubes containing samples were vortexed before analysis on a 96-well plate multi-reader SpectraMax M3 spectrophotometer (Molecular Devices, USA). The absorbance spectrum was measured at 200-800 nm. Distinctive peaks of the UV-Vis were detected, and their values were recorded (Patle *et al*., 2020).

### 2.2.2. Compound purification using Silica gel column chromatography

The methanol extract was subjected to column chromatography in a silica gel (60-120 mesh) glass column (Silica gel 60 (35-70 µm). The extract was eluted with the solvent (80% methanol) with increasing polarity. In the present study, methanol extract yielded crude extracts that were subjected to column chromatography. The elution was done using the same solvent (80% methanol) with increasing polarity, and the fractions obtained were analyzed using UV-VIS.

### 2.2.3. Compounds separation and identification in *Senna alexandrina* leave extract using Thin Layer Chromatography (TLC)

In order to follow up the compound purification from silica gel chromatography, it was also of interest to ascertain the presence of phytochemicals in *Senna alexandrina* leave extract through separation and identification of compounds of interests from the extract. The separation and identification of leaves extract was carried out according to the method described by Gujjeti and Mamidala (2013) with slightly modifications (Appendix B, section 12).



© University of Venda

### 2.2.4. Analysis of metabolites from *Senna alexandrina* through UHPLC-QTOF-MS and Sirius

The LC-MS analysis was carried out using a Shimadzu LC-MS 9030 system equipped with a Shim Pack Velox C18 column (100 mm × 2.1 mm, 2.7 µm particle size) from Shimadzu Corporation (Kyoto, Japan). The column was maintained at 55 °C in a column oven. The sample was injected with a volume of 3 µL and run with a binary mobile phase gradient composed of solvent A (0.1% formic acid in water) and solvent B (0.1% formic acid in acetonitrile), with a flow rate of 0.3 mL/min for a total runtime of 53 minutes. Sodium iodide (NaI) was used as the calibration solution for monitoring high mass accuracy. The eluents were further analyzed using a high-definition quadrupole time-of-flight (QTOF) mass spectrometer, with MS1 and MS2 data collected simultaneously for ions within an m/z range of 100-1000 and an intensity threshold of 5000, employing data-dependent acquisition. Fragmentation experiments were performed using argon as the collision gas at a collision energy of 30 eV with a spread of 5 eV (Madala & Kabanda, 2021; Ramabulana *et al*., 2021). To further analyze and characterize compounds from this plant, two software tools were used (MS-Dial and SIRIUS).

### 2.2.5. Synthesis of Silver Nanoparticles (Ag-NPs)

This study focused on the specific type of plant used for synthesizing metallic nanoparticles and employed techniques for plant extraction and validating the synthesis of AgNPs. The reducing agents present in the extract play a crucial role in synthesizing metallic nanoparticles using extracts. AgNPs were synthesized using *Senna alexandrina* as a reducing agent, due to the bioactive compounds that it contains, which reduce metal ions to their nanoparticles. 420 µL of 0.05M silver nitrate ($AgNO_3$) was added to 94.6 mL of deionized water, and the solution was heated with stirring until the temperature reached 90 °C. When it reached 90 °C, 5ml of leaf extract was added, stirred, and heated at 100 °C for 30 minutes, the color changed from light yellow to brown indicating the formation of AgNPs, the reaction was allowed to proceed for 2 more hours (Figure 2.5), 1ml of the reaction was aliquoted immediately, 5 minutes after the leaf extract was added, after 30 minutes and 2 hours 1 ml of the reaction was aliquoted for UV-vis analysis (Figure 2.5), the synthesized solution was stored in an airtight, light-protected glass at low temperatures (4°C) to minimize oxidation and photodegradation for further use. Moreover, AgNPs were synthesized using different concentrations (0.4g/10ml – 2.5g/10ml) of leaf extracts for the best synthesis. Furthermore, it was



© University of Venda

also important to evaluate the concentrations of both $AgNO_3$ and plant extracts for the best synthesis of AgNPs, respectively (Figure 2.4).



© University of Venda

### 2.2.6. Characterization and validation of the synthesized of SA-AgNPs through Ultra-violet visible spectroscopy, FTIR, SEM

#### 2.2.6.1. Fourier Transform Infrared Spectroscopy (FTIR)

FTIR measurements were carried out using a single-beam Fourier transform infrared spectrometer (FTIR-430, Jasco, Japan). The FTIR spectra of the samples were obtained in the spectral range from 4000 to 400 cm−1. The FTIR spectra were processed using Jasco Spectra Manager software. The peak areas and the absorbance ratios were obtained accurately by using this software. Fourier transform infrared (FTIR) spectrum was utilized to identify the functional groups present in the synthesized molecule.

#### 2.2.6.2. Scanning Electron Microscopy (SEM)

The emission from the field SEM was utilized to examine the AgNPs' additional structure and validate their size and shape. The *S. alexandrina* extract's structure revealed a mass with a particular form that is characteristic of plant extract (Figure 2.8). The SEM analysis of the synthesized AgNPs revealed their distinct size differences, revealing them to be heterogeneous and small in size, which is agreed with previous studies by Kalakonda *et al*., 2024.

## 2.3. Results & discussion

### 2.3.1. Visual observation and UV-Vis spectroscopy

Absorption peaks indicate the presence of various compounds absorbing light at specific wavelengths (Figure 2.1). Peaks observed at the spectrum (200-400 nm) suggested the potential presence of flavonoids, polyphenolics, alkaloids, and tannins. These secondary metabolite classes in this range are well known for their characteristic absorbance (Patel *et al*., 2020; Maigoda *et al*., 2022). Different peaks suggest that the various elutes consist of these compounds in different concentrations. These results (Figure 2.1) suggest the presence of potential secondary metabolites. The spectra show absorbance peaks for various elutes, which show changes in the composition of the compounds throughout purification.



© University of Venda

The first elute/Blank (Blue Line) exhibits low absorbance, suggesting a lack of significant UV-absorbing compounds. Moreover, this suggested that many of the secondary metabolites were retained on the silica gel; this was further supported by the colorless solution observed in the image attached (Fig 2.1) with a 50 ml tube labeled SW on top; second to Sixth Elutes (Orange to dashed black) indicated a strong absorbance, with peaks around 350 nm and more minor features at 700 nm, which in many studies is an indicative of flavonoids, and the shoulder peak at about 480 nm indicate presence of carotenoids or anthocyanins (Alam *et al*., 2022). However, the observed absorbance patterns in the fractions indicated an increasing compound concentration. A slight peak, around 700 nm (Fig. 2.1), indicates the presence of compounds such as chlorophylls or other pigments (Fernández-Marín *et al*., 2018).

Based on the observed elution pattern, the Silica gel chromatography effectively separated the plant extract into fractions with varying compound compositions. Certain metabolites were preferentially retained on the column, as evidenced by the absorbance intensity and wavelength change across each elute, gradually eluting as the mobile phase progressed. Different elution profiles suggest that the purification has successfully enriched specific secondary metabolites in different fractions, which could be further characterized through additional techniques such as mass spectrometry or NMR. Compounds such as flavonoids, phenolics absorb in the UV range (250–380 nm). These compounds are responsible for reducing $Ag^{+}$ ions to $Ag^{0}$ nanoparticles. After reduction, the same compounds act as capping/stabilizing agents, preventing agglomeration (Demarque *et al*., 2020). The UV–Vis spectral profile provides direct evidence of the role of plant-derived compounds in nanoparticle synthesis. The simultaneous presence of phytochemical peaks and the AgNP SPR band thus demonstrates the dual role of plant metabolites in reducing silver ions and stabilizing the resulting nanoparticles (Khan & Khan, 2023).



© University of Venda

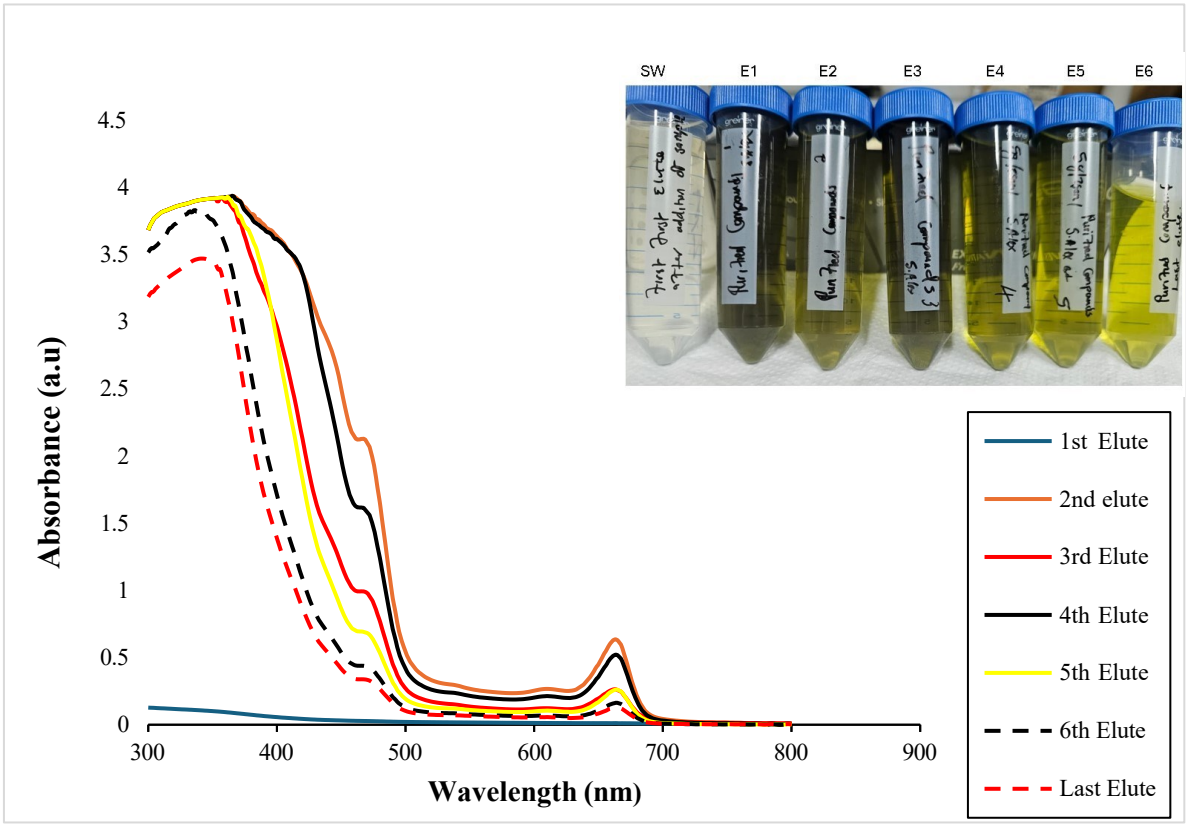



**Figure 2. 1.** UV-vis showing partially purified *S. alexandrina* metabolites by silica gel chromatography.

Blank (SW) – (Solvent) 80% Methanol, 1st – Last Elute, presenting sampled purified metabolites immediately after solvent addition and after elution of plant metabolites. The image at the right corner shows the purification of *Senna alexandrina* extracted compounds by silica gel chromatography. SW- Solvent (80% methanol) wash, E1-E6 (Eluted purified plant compounds), with the lowest concentration showing a light yellowish color (E6) and the highest concentration presenting a dark, concentrated color (E1-E3).



© University of Venda

Senna alexandrina is known to contain bioactive compounds, including flavonoids and phenolics, to name a few; gallic acid and rutin are among the phytochemicals reported in this plant (Omer et al., 2022; Rosmalena et al., 2022). Hence, they were used as controls in this study.

Both Gallic Acid and Rutin controls developed and displayed a yellowish colour. The *p*-anisaldehyde-sulfuric acid on the developing solvent MA (Methanol: Acetone) displayed its potential for spot detection. Two compounds developed, dark in colour, and were spotted and circled together with the developed controls. Under the mobile phase HE (Hexane), both Rutin and gallic acid controls did not migrate; instead, they remained in a stationary phase. Since HE is non-polar, its primary function is to move non-polar molecules up the TLC plate (Figure 2.2).

Due to their high polarity caused by their sugar moieties, hydroxyl (-OH) groups, and carboxyl (-COOH) groups in gallic acid, rutin both interact much more strongly with the polar stationary phase (silica on the TLC plate) than they do with the non-polar hexane solvent (Ibekwe *et al*., 2012). Consequently, the silica tends to stick to them rather than being dissolved and moved up the plate by the non-polar solvent, and these results are supported by the study by Zeb (2021).

A few compounds migrate from the Senna alexandrina extract, while most components stay near the baseline. This could be because the extract contains polar components, like rutin and gallic acid. Under the mobile phase MA (Methanol: Acetone), Consistent with its high polarity, rutin likewise exhibits limited migration, similar to gallic acid (Figure 2.2). The use of four different solvents in TLC ensures comprehensive separation, better resolution of complex mixtures, and confirmation of compound diversity in the extract.

Multiple bands are visible in the extract in both E10 (10 µL) and E5 (5 µL) examples, suggesting that the extract contains various chemical compounds. Both E10 and E5 have spots at the top of the plate, which indicates that some of the extract's constituents are less polar and may migrate up the plate with the MA solvent. In accordance with the behavior of gallic acid and rutin, the chemicals that appear lower on the plate are more polar and interact with the stationary phase more.



© University of Venda

The findings below align with the results observed and discussed by Guo and Gaiki (2011), which confirmed that when non-polar solvents are employed in TLC, highly polar compounds exhibit limited migration. Under the mobile phase TE (Toluene), Rutin has moved from the baseline and appears as a single spot (yellowish spot). This indicates that rutin has moderate polarity and, hence, interacts with the TE solvent so that it moves up the plate some distance (Figure 2.2).

Contrarily, gallic acid, highly polar, elutes lower than rutin, exhibiting greater affinity for the stationary phases. Similarly, movements in E10 and E5 may involve compounds matching gallic acid and rutin polarity. Under the mobile phase EWA (Ethyl-Acetate), the Rutin (R) shows a yellowish spot, which indicates it has traveled significantly up the plate. This implies that rutin and the EWA solvent system interact to render the rutin less polar than gallic acid, enabling it to travel further. Interestingly, the distance traveled by the yellow rutin spot (yellow) and that of the plant extract appear to be almost comparable, which could justify that the constituent of the extracts has a similar polarity or molecular structure analogous to rutin.



© University of Venda

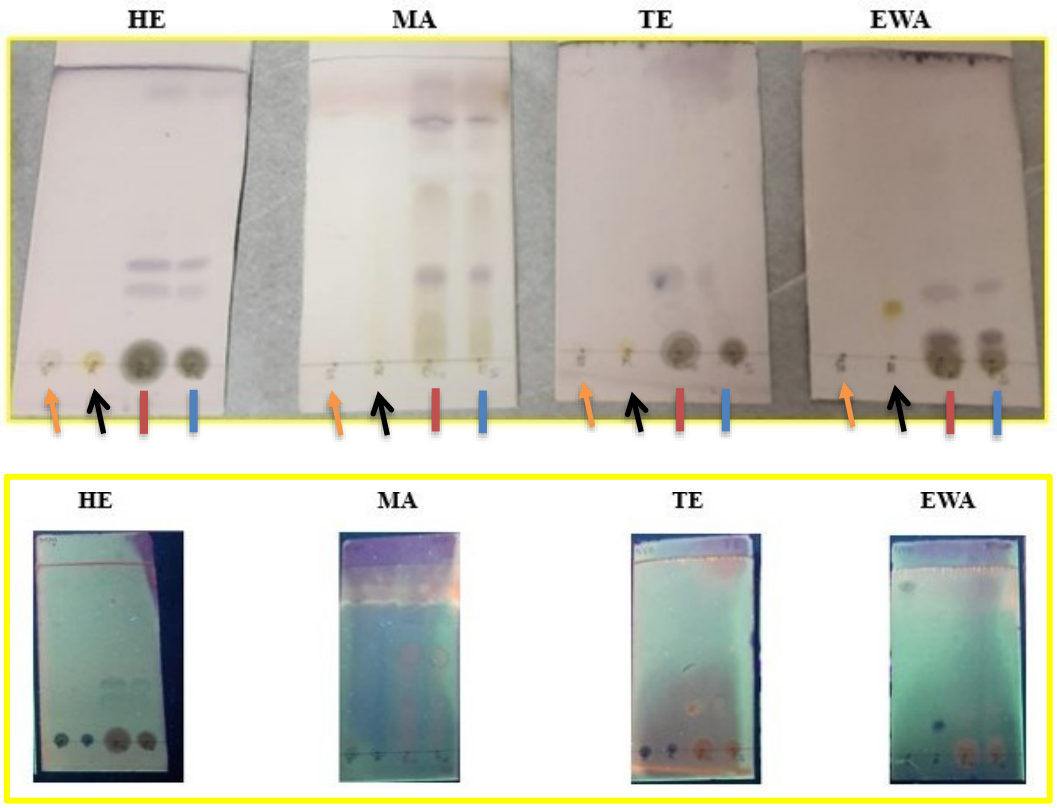



**Figure 2.2.** Comparative TLC profile of *Senna alexandrina* direct methanolic extract, garlic (orange arrow), rutin (black arrow), with E10, E5 represented by red and blue lines, respectively.

Eluted in four solvent systems (HE, MA, TE, and EWA, respectively) of varying polarities that display reactive compounds detected by p-anisaldehyde-sulfuric acid reagent, with G- garlic acid and R- rutin used as controls. The experiment's reliability was confirmed by spotting twice with two different volumes (E10 presenting 10 µL and E5 presenting 5 µL), which, as a result, showed a similar migration pattern of three compounds at the same position for both volumes. The lower panel shows the TLC plate observed under UV light to detect compounds that are not easily visible to the naked eye under normal room lighting conditions.



© University of Venda

The AgNPs synthesized with 2.5g/10 ml plant extract exhibited the highest distinctive absorption peak (0.42) at 446 nm (Red) in the UV-vis spectra, while the SA-AgNPs synthesized with 0.7g/10 ml plant extract showed the lowest peak at 444 nm. The highest peak absorbance (0.42) at about 446 nm is shown in the 2.5g/10ml (red line), suggesting a high concentration of formed AgNPs (Figure 2.3). The concentrations of 1.8g/10ml, which is the black line, 2.1g/10ml, the green line, and 1.4g/10ml, the yellow line, also have prominent peaks but with lower absorbance than the 2.5g/10ml concentration. While lower concentrations, such as 0.4g/10ml, represented in blue, and 0.7 g/10ml, represented in orange, have significantly small peaks, therefore showing a lesser efficiency in nanoparticle formation (Sharma *et al*., 2009). In conclusion, these absorption spectra indicate that the optimal concentration for further experiments was 2.5g/10ml. The highest absorbance indicates that most silver nanoparticles have been synthesized, and the figure below suggests that nanoparticles are polydisperse, irregularly shaped due to a broad SPR peak (Figure 2.3).



© University of Venda

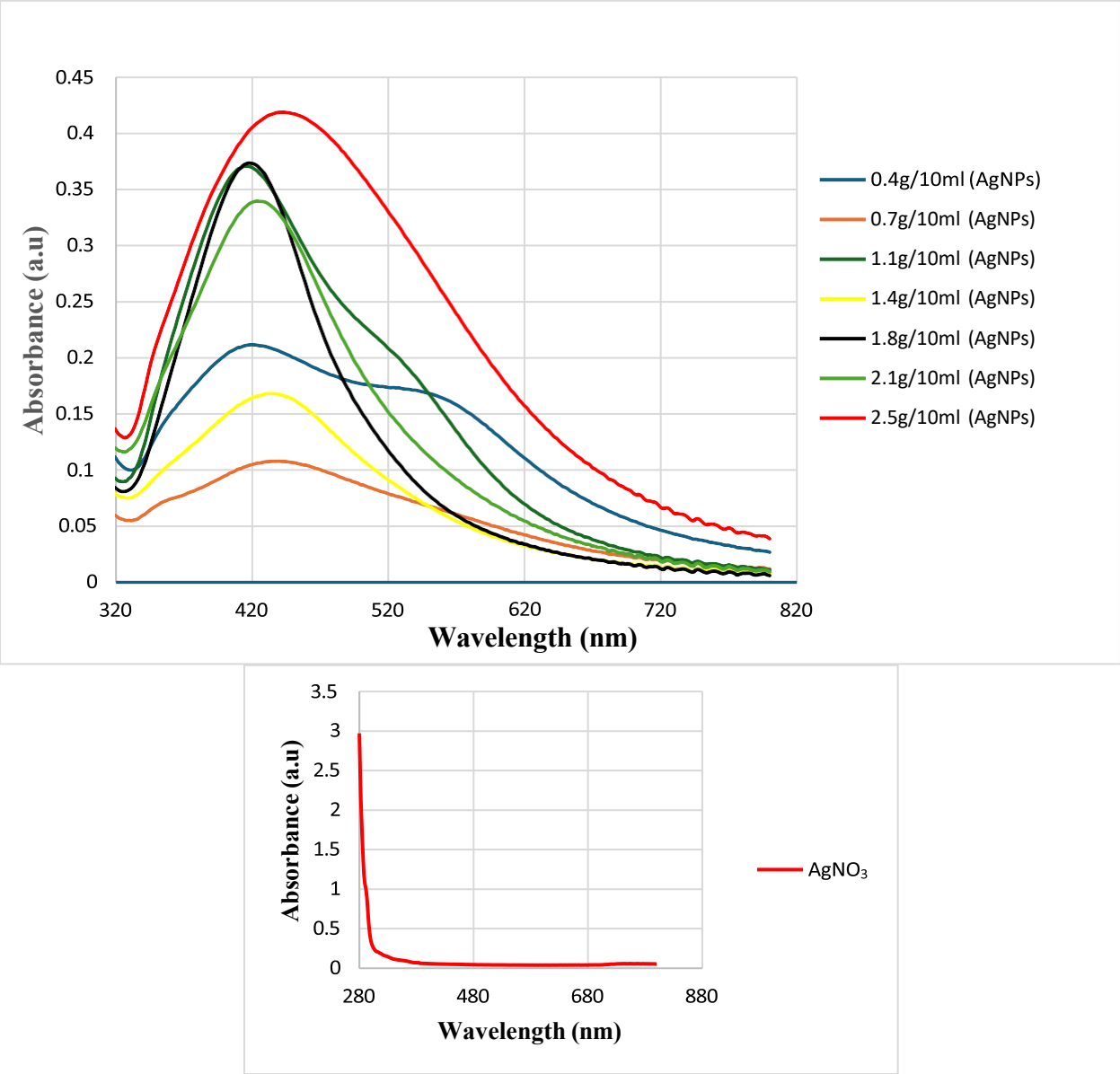



**Figure 2.3.** UV-vis spectroscopy of AgNPs synthesized using different concentrations (0.4g/10ml – 2.5g/10ml) of *Senna alexandrina* leaves extracts (upper spectrum). UV-vis of silver nitrate as negative control (below spectrum)



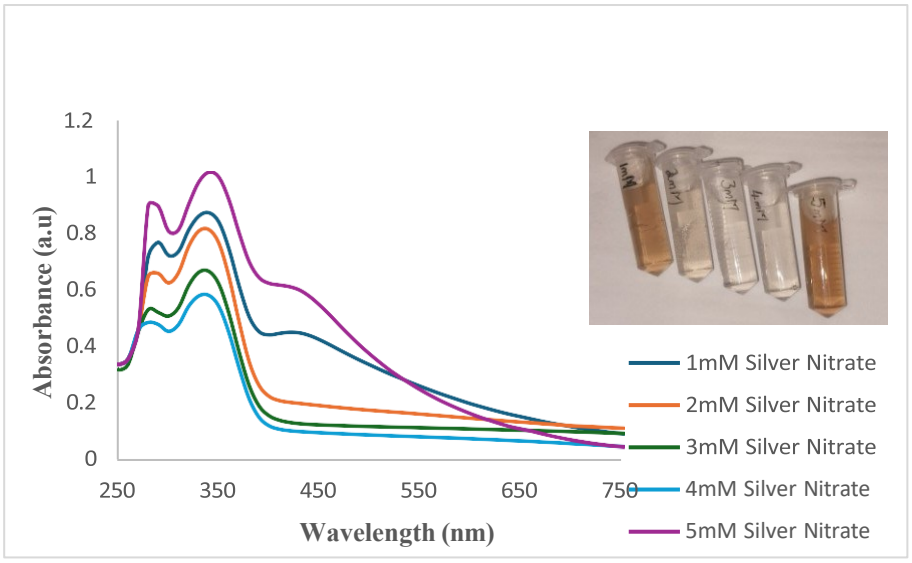
© University of Venda

### 2.3.2. Absorption Spectra and Visual Appearance of Silver Nanoparticles (AgNPs) at Different Silver Nitrate Concentrations

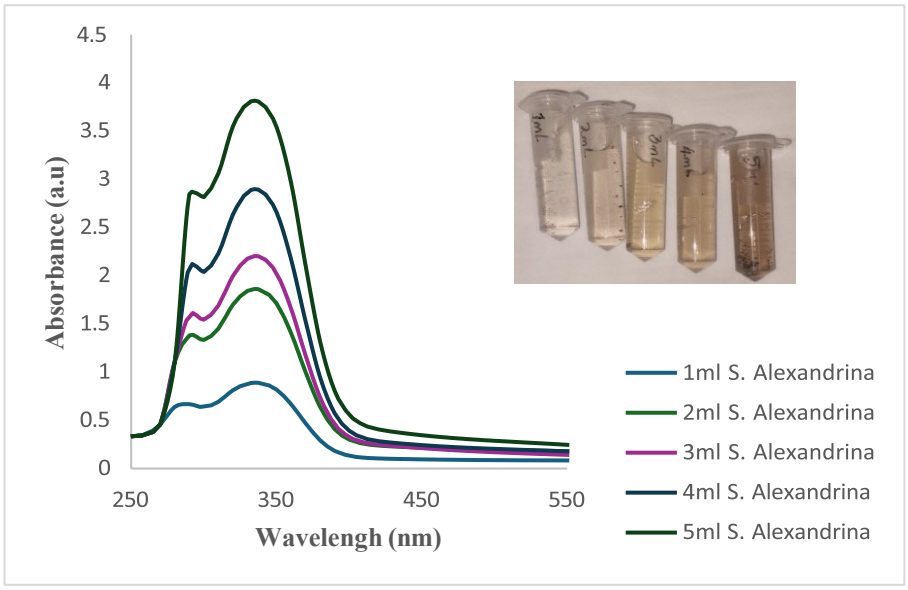
In all experiments, the addition of plant extract of *S. Alexandrina* into the beakers containing aqueous solution of silver nitrate led to the change in the color of the solution to brown (shown in Fig. 2.4) within reaction duration due to excitation of surface plasmon vibrations in silver nanoparticles (Veerasamy et al., 2011). An increase in silver nitrate concentration to 5 mM shows an increase in wavelength up to 448 nm, as presented in Fig. 2.4 A. A peak around 350 nm corresponds to the presence of plant-derived compounds that are used as reducing agents in the extract (Singh et al., 2023), while the absence of the 420–450 nm SPR peak suggests little or no formation of well-defined silver nanoparticles (Fig. 2.4 B) (Sahoo & Hormozi-Nezhad, 2023). The slight variations in absorbance values signify that the changes are the particle size (Tripathy et al., 2010). On increasing the concentration of the extract, there is an increase in absorption intensity. On addition of different volumes (1-5 mL) of leaf extracts to aqueous silver nitrate solution, keeping its concentration 10 mL (1 mM) constant, the color of the solution changed from faint light to yellowish brown and finally to colloidal brown, indicating the formation of silver nanoparticles (Henglein, 1993; Zaheer, 2012), hence it was convenient to use 1 mM due to color change, however this contradicted with the results obtained in Fig. 2.4 A, as there was no well-defined peak observed at this concentration. Different parameters were optimized, including the concentration of silver nitrate, S. Alexandrina leaf extract, and time, which had been identified as factors affecting the yields of silver nanoparticles.



© University of Venda




**(A)**




**(B)**

**Figure 2. 4.** UV/vis spectral of AgNPs synthesized with different volumes of *Senna alexandrina*.

Digital optical images of synthesized silver nanoparticles with different concentrations (A). 1- 5mM of $AgNO_3$ and (B). 1-5ml of extract. It was also interesting to evaluate the best concentrations of $AgNO_3$ and extract for the synthesis of AgNPs, following the results obtained with varying concentrations of plant extracts (Figure 2.3).



© University of Venda

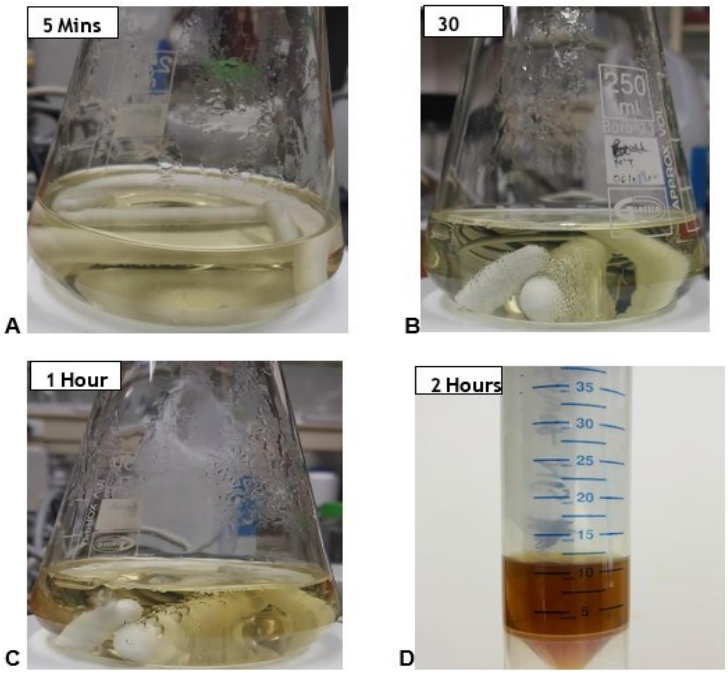



**Figure 2.5.** Digital optical images of synthesized silver nanoparticles,

of green synthesis of Silver Nanoparticles (AgNPs) from Senna alexandrina leaves extract (A). After 5 minutes, (B). After 30 minutes, (C). After 1 hour, (D). After 2 hours, the color changed from light yellow (colorless to brown), indicating the formation of silver nanoparticles. Protocol explained in section 2.2.5.



© University of Venda

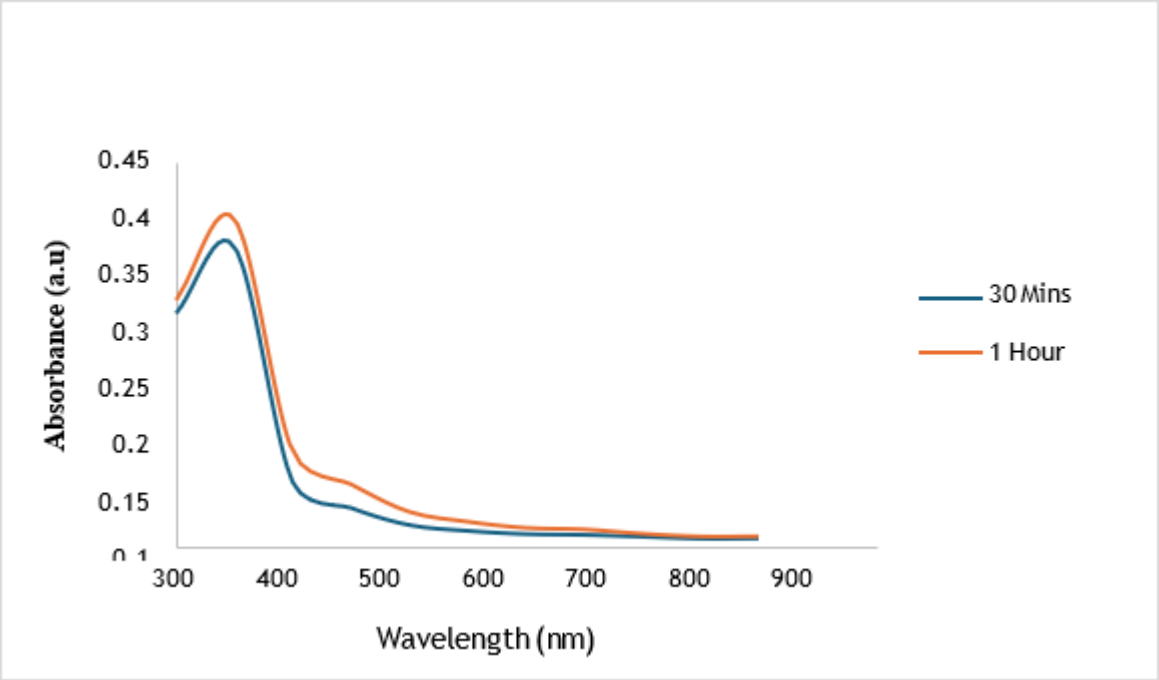



**Figure 2.6.** Graph showing time-dependent UV-Vis absorption spectra of green-synthesized silver nanoparticles. Recorded after 1 hour to confirm the formation of AgNPs. Aliquot samples were taken at time intervals (30 minutes and 1 hour) during bio-reduction.

### 2.3.3. FTIR absorption spectrum of SA-AgNPs and *Senna alexandrina* leaf extract

The ATR-FTIR spectrum indicated different functional groups of synthesized SA-AgNPs. A transmittance spectrum monitored the synthesis of SA-AgNPs from 3500 cm-1 to 500 cm-1 wavenumbers. The spectrum of synthesized SA-AgNPs indicated a pure composition of SA-AgNPs in solution due to the bond stretches probed on ionic carboxylic interactions of hydrogen atoms on silver ions with a silver core. OPUS software (Bruker, Germany) analyzed the distinct functional groups. Figure. 2.7 shows the FTIR spectra of AgNPs fabricated using *S. Alexandrina* extract (Fig. 2.7A) and the functional groups of the *S. Alexandrina* extract (B). Absorption bands at 2946 and 3327 cm −1 are characteristics of the –OH stretching of the phenolic group (Velmurugan *et al*., 2014), which are responsible for reducing Ag+ ions to $Ag^0$.



© University of Venda

Stretching of the C- O related to primary alcohol (phenol) measured at 1016.04 $cm^{-1}$ and of the C=C molecule in relation to the aromatic skeletal mode of the extracts is what causes the peak at 1636.21 $cm^{-1}$. The presence of reducing agents/ stabilizing compounds (functional groups) that are responsible for reducing AgNO3 to $Ag^0$ ions and stabilizing the SA-AgNPs in *Senna alexandrina* leaf extracts are further confirmed through the FTIR (500-4000 $cm^{-1}$), which suggests the phyto-compounds that caused this reduction (Figure 2.7 A). A characteristic band measured at 3313.58 cm-1 corresponds to the stretching vibration of N-H. In addition, the strong peak position at 3300 cm-1 is related to the N-H stretch vibrations, which could be associated with the NH3+ group of the organic cation. The bands of (figure 2.7 B) at 2834.99 $cm^{-1}$ and 2946.74 cm-1 are identified to correspond to C-H stretching. This C-H stretching vibration is associated with a CH3+ group of the organic cation. The results of the FTIR analysis (Fig. 2.7A) demonstrated the presence of N-H stretching-related alkaloids, polyphenols, and flavonoids due to C-H vibrations and terpenes due to OH stretching.

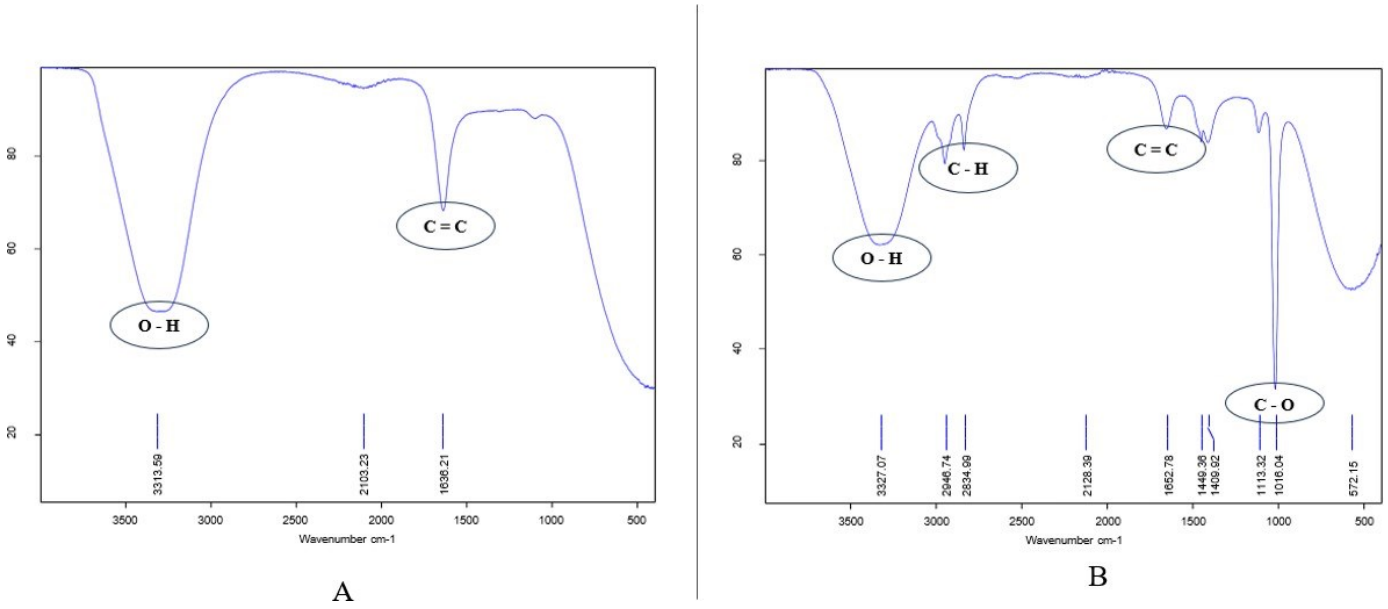



**Figure 2.7.** FTIR analysis (A) FTIR absorption spectrum of AgNPs synthesised by *Senna alexandrina* leaf extract (500-4000 $cm^{-1}$), (B) *Senna alexandrina* leaf extract.



© University of Venda

© University of Venda

SEM was used to further validate the surface morphology associated with the formation of spherical and non-spherical particles, although the complete synthesis of SA-AgNPs had already been confirmed by observing a wavelength spectrum. The surface morphology of SA-AgNPs was determined by drying of SA-AgNPs. AgNPs' antibacterial activity depends more on their size than their shape, with particles less than 20 nm being particularly effective (Figure 2.8, Aguilar-Garay *et al*., 2024). Most of the particles are concentrated. However, some of the particles form small clusters. This may indicate agglomeration due to the van der Waals forces among nanoparticles (Endres *et al*., 2021). Furthermore, Techniques such as dynamic light scattering (DLS) and Transmission electron microscopy (TEM) could further be utilized for SEM analysis to give a better picture of the size distribution and morphology in solution.

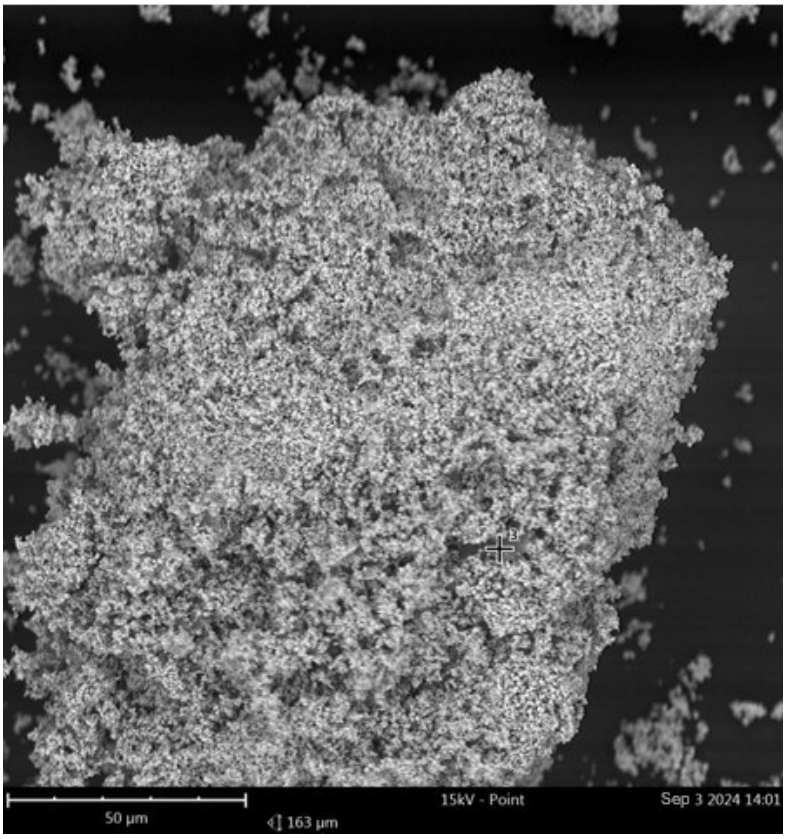



**Figure 2.8.** Representative SEM images of SA-AgNPs surface features.
SEM micrograph of synthesized silver nanoparticles showing aggregated clusters with a rough, granular morphology. The image reveals a significant agglomeration of nanoparticles into larger micro-scale structures, indicating non-uniform particle distribution. The scale bar of 50 µm highlights that while the clusters are large, they are composed of much smaller nano-sized particles.



© University of Venda

### 2.3.4. Identification and profiling of phytocompounds from *Senna alexandrina* leaf extract using UHPLC-qTOF-MS

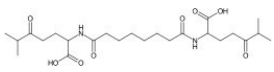
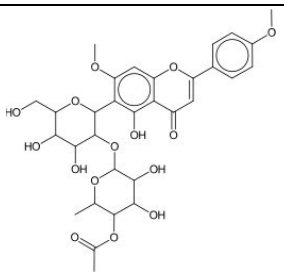
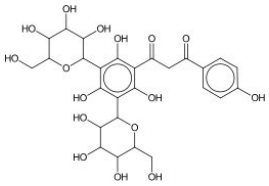
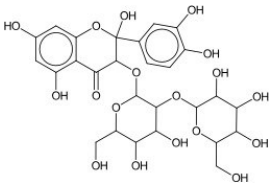
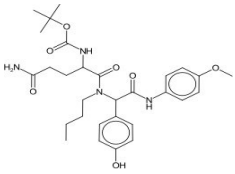
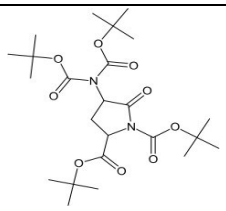
Tools such as MS-Dial and SIRIUS were used to analyze and characterize compounds from *Senna alexandrina* leaf extract. MS-Dial is a program that can perform untargeted metabolomics analysis by integrating multiple data processing algorithms (Tsugawa *et al.,* 2015). SIRIUS is a software that can identify molecular formulas and structures of unknown compounds using mass spectrometry data and machine learning methods (Tian *et al.,*2022). Using these tools, the compounds obtained from the chromatogram (Appendix D.2) were compared with existing databases and annotated with possible identities and functions. The use of MS-Dial and SIRIUS software enabled a comprehensive and detailed characterization of the compounds that were extracted from the plant samples. These tools provided detailed information about the molecular formula, molecular name, compound class, and fragment pattern (Appendix/Table D.4). The above-mentioned table presents a comprehensive list of compounds identified, with their molecular formulas and names, compound classes, and fragmented ions retention times, mass-to-charge ratios (m/z).

FTIR spectra of the extract exhibited a broad O–H stretch (3327 $cm^{-1}$), it is a characteristic of hydroxyl groups in phenolic compounds, which are electron donors capable of reducing $Ag^{+}$ to $Ag^{0}$ (Gallucci *et al*., 2025), phenolic C–O bands (1016.04 $cm^{-1}$) and C=C features (1636.21 $cm^{-1}$), 2834.99 $cm^{-1}$ and 2946.74 cm-1 correspond to C-H bond further support the presence of organic metabolites with hydrophobic moieties, while the C–O stretching band reflects alcohols, esters, and phenolic derivatives known to coordinate metal surfaces and capable of both reducing $Ag^{+}$ and capping nascent AgNPs. Consistently, HPLC identified and quantified high levels of key phenolic/flavonoid constituents (Table 2.1), whose abundance correlated with FTIR results (Figure 2.7). The convergence of FTIR functional group data and HPLC compositional profiling provides strong evidence that these biomolecules act synergistically as reducing and stabilizing agents. On this basis, these compounds were selected as the principal bio-reductants and stabilizers for green synthesis of AgNPs, combining high reducing capacity with reproducible availability in the extract. Moreover, a few compounds involved in the reduction and stabilization process of synthesizing nanoparticles were selected (Table 2.1) and further applied for molecular docking studies (Chapter 5).



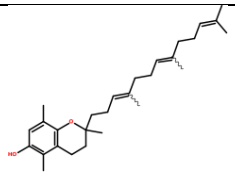
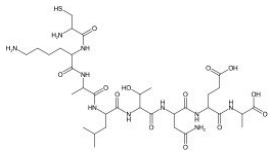
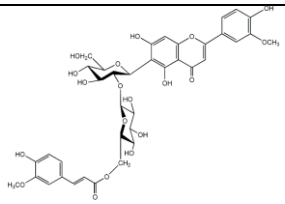
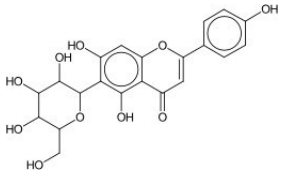
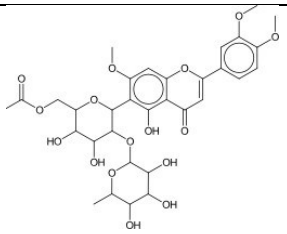
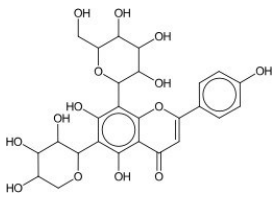
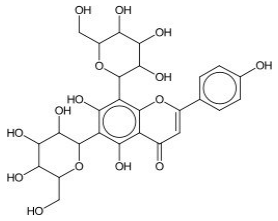
© University of Venda

**Table 2. 1.** Selected compounds involved in the reduction, stabilization process of nanoparticle synthesis

| No | Compound names | Classes | Structures |
|---|---|---|---|
| 1 | (2S)-2-[[8-[[(1S)-1-carboxy-5-methyl-4-oxohexyl]amino]-8-oxooctanoyl]amino]-6-methyl-5-oxoheptanoic acid | Carboxylic acids and derivatives |  |
| 2 | [(2S,3R,4S,5R,6S)-6-[(2S,3R,4S,5S,6R)-4,5-dihydroxy-2-[5-hydroxy-7-methoxy-2-(4-methoxyphenyl)-4-oxochromen-6-yl]-6-(hydroxymethyl)oxan-3-yl]oxy-4,5-dihydroxy-2-methyloxan-3-yl] acetate | Flavanoids |  |
| 3 | 1-(4-hydroxyphenyl)-3-[2,4,6-trihydroxy-3,5-bis[(2S,3R,4R,5S,6R)-3,4,5-trihydroxy-6-(hydroxymethyl)oxan-2-yl]phenyl]propane-1,3-dione | Flavanoids |  |
| 4 | 3-[(2S,3R,4R,6R)-3,4-dihydroxy-6-(hydroxymethyl)-5-[(2S,3R,4S,5R,6R)-3,4,5-trihydroxy-6-(hydroxymethyl)oxan-2-yl]oxyoxan-2-yl]oxy-5,7-dihydroxy-2-(3,4,5-trihydroxyphenyl)-2,3-dihydrochromen-4-one | Flavanoids |  |
| 5 | Boc-DL-Gln-DL-N(Bu)nTyr-NHPh(4-OMe) | Carboxylic acids and derivatives |  |
| 6 | ditert-butyl (2S,4S)-4-[bis[(2-methylpropan-2-yl)oxycarbonyl]amino]-5-oxopyrrolidine-1,2-dicarboxylate | Carboxylic acids and derivatives |  |

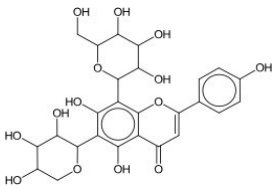


© University of Venda

| | | | |
|---|---|---|---|
| 7 | Gamma-Tocotrienol | Phenols |  |
| 8 | H-DL-Cys-DL-Lys-DL-Ala-DL-Leu-DL-xiThr-DL-Asn-DL-Glu-DL-Ala-OH | Carboxylic acids and derivatives |  |
| 9 | Isoscoparin 2"-(6-(E)-ferulylglucoside) | Flavanoids |  |
| 10 | Isovitexin | Flavanoids |  |
| 11 | Linoside A | Flavanoids |  |
| 12 | Vicenin-1 | Flavanoids |  |
| 13 | Vicenin-2 | Flavanoids |  |



© University of Venda

| | | | |
|---|---|---|---|
| 14 | Vicenin-3 | Flavanoids |  |

## Chapter summary:

In Figure 2.4, the color of the solution changed from faint light to yellowish brown, indicating the formation of silver nanoparticles (Henglein, 1993; Zaheer, 2012), hence it was convenient to use 1 mM due to the color change, however, this contradicts the results obtained in Fig. 2.4 A, as there was no well-defined peak observed at this concentration. Alternatively, 5 mM of silver nitrate was used for further analysis as it demonstrates an SPR peak of AgNPs at 420 to 450 nm. However, this was done to investigate the concentration-dependent effect of silver nitrate on AgNP formation. In conclusion, 0.05M of silver nitrate was used for the synthesis of AgNPs that were further used in this study.
The convergence of FTIR functional group data and HPLC compositional profiling provides strong evidence that these biomolecules act synergistically as reducing and stabilizing agents.



© University of Venda

University of Venda
Creating Future Leaders

# Chapter 3

**Recombinant expression of *E. coli* DnaK and Structure-function analysis**



© University of Venda

# CHAPTER 3: Recombinant expression of *E. coli* DnaK and structure-function analysis

## 3.1. Introduction and experimental procedures

DnaK is essential for protein homeostasis in *Escherichia coli*, facilitating protein folding, preventing aggregation, and regulating stress responses (Fourie & Wilson, 2020). Understanding its structure-function relationship is essential for elucidating its biochemical mechanisms and potential interactions with nanoparticles. This chapter outlines the methodological approach employed in the production and structural-functional characterization of recombinant *E. coli* DnaK

Therefore, to verify the proper insertion and integrity of the DnaK gene, the study starts with plasmid construct confirmation. Followed by the expression of recombinant protein in *E. coli* and subsequently purified using nickel affinity chromatography (Makumire *et al*., 2021).

The protein's secondary structural organization is then examined to determine its folding pattern, into its native conformational state using Far-UV circular dichroism (CD) spectroscopy (Haque *et al*., 2022). Tryptophan fluorescence-based analysis is utilized to assess the tertiary organization of DnaK and its temperature-dependent conformational changes, showing protein's stability and flexibility under varying conditions (Jena *et al*., 2020). Additionally, functional characterization of DnaK and effects of AgNPs on DnaK activity is assessed by measuring ATPase activity in the presence of silver nanoparticles.

### 3.1.1. Materials

The plasmids used in this study are listed in Table 3.1.1. The plasmids constructs were made by genescript (USA) (Table 3.1.1). The pQE30/DnaK plasmid was used to express E. coli DnaK protein. The DnaK insert was cloned between BamHI and HindIII restriction sites. The recombinant protein was expressed attached to N-terminal polyhistidine tag. Anti-DnaK antibodies were used to detect DnaK. Anti-His antibodies were used to confirm E. coli DnaK. Other reagents used in this chapter are listed in (Appendix A).



© University of Venda

**Table 3.1.1. List of strains and plasmids**

| ***E. coli* strains** | **Description** | **Supplier/Reference** |
|---|---|---|
| *E. coli* JM109 | *supE44 relA1 Δ(lac-proAB); e14– (McrA–) ; (F´ traD36 proAB lacIq ZΔM15) ;* | Thermofischer Scientific, USA |
| *E. coli* XL1 Blue | *supE44 relA1 recA1 endA1 gyrA96 thi1 hsdR17 lac (F ṕroAB lacIqZM15 Tn10 (Tetr)* | Thermofischer Scientific, USA |
| | | |
| **Plasmids** | **Description** | **Supplier** |
| pQE30/DnaK | pQE30 encoding *E. coli* DnaK. Ampicillin resistant | Makumire *et al*., 2021 |
| pQE30/DnaJ | pQE30 encoding DnaJ Ampicillin resistant | Makhoba *et al*., 2016 |

### 3.1.2. Confirmation of *E. coli* DnaK DNA constructs

Plasmid constructs expressing *E. coli* DnaK were purified by using the Zymo Research Plasmid Miniprep$^{TM}$ kit (Epigenetics, U.S. A) following the manufacturer's instructions (Appendix B1). The restriction enzymes HindIII and BamHI (Thermo Scientific, U.S.A) were used to digest the plasmid DNA. The restriction digest products were analyzed using 0.8 % agarose gel electrophoresis (Appendix B4).

### 3.1.3. Expression of recombinant protein

Chemically competent *E. coli* JM109 cells were transformed with pQE30/DnaK. The transformed cells were used to express the his-tagged recombinant proteins following a previously described protocol (Zininga *et al*., 2016). A single colony of each transformant was picked and inoculated into fresh 50ml 2 YT broth containing 100 µg/ml ampicillin. Transformants were cultured overnight at 37°C with a shaking incubator at 150 rpm. After overnight incubation, the culture was diluted at a 1:10 ratio and then incubated until OD A600 = 0.6. The culture was then induced with 1 mM isopropyl-β-D-1-thiogalactopyranoside (IPTG) to induce protein expression. A pre-induction sample and post-induction hourly samples were collected until the 6$^{th}$ hour of post-induction for SDS-PAGE analysis. Cells were harvested by centrifuging at 5000 xg for 20 minutes at 4 °C and pellet fractions were suspended in lysis buffer (100 Mm Tris-HCL, pH 7.4, 300 Mm



© University of Venda

NaCl, 10 mM imidazole, 1 mM EDTA, 1 mM PMSF, and 1 mg/mL lysozyme). To allow cell lysis, *E. coli* cells were incubated at room temperature for 1 hour with gentle shaking and then stored at -80°C. The expression of the protein was analyzed using SDS-PAGE analysis (Appendix B.7) and confirmed with Western blot (Appendix B.8).

### 3.1.4. Purification of recombinant protein

Recombinant proteins were purified using sepharose nickel affinity chromatography as previously described (Zininga *et al*., 2015). Cell lysates were centrifuged for 20 minutes at 4°C at 5000 xg (Shonhai *et al*., 2008). The supernatant was added to HisPurTM Nickel-charged nitrilotriacetic acid (Ni-NTA) (Thermo Scientific, USA) immobilized affinity chromatography column and incubated for 1 hour to enhance binding of recombinant protein. Unbound proteins were washed with 2-bed volume of wash buffer I (10 ml Tris-HCl pH 7.5; 300 mM NaCl; 25 mM imidazole; 1 mM PMSF) and wash buffer II (10 ml Tris-HCl pH 7.5; 300 mM NaCl; 80 mM imidazole; 1 mM PMSF). Proteins that were bound to the beads were eluted with elution buffer I (10 ml Tris-HCl pH 7.5; 300 mM NaCl; 250 mM imidazole; 1 mM PMSF) and elution buffer II (10 ml Tris-HCl pH 7.5; 300 mM NaCl; 500 mM imidazole; 1 mM PMSF). Collected wash and elution samples were prepared for analysis with 12% SDS-PAGE (Appendix B.7) and western blot (Appendix B.8).

### 3.1.5. Investigation of the secondary structural organization of *E. coli* DnaK

Far-UV circular dichroism (CD) spectroscopy was used to determine the secondary structure of DnaK as previously described (Zininga *et al*., 2016). Chirascan Plus CD spectrometer (Applied Photophysics, Surrey, UK) instrument that is equipped with a Peltier that controls temperature was used for analysis. A quartz cuvette (Hellma, Singapore) was used during Spectral scans for each protein (2 μM) recorded from 250 and 190 nm. Derived spectra were then deconvoluted using Dichroweb server (http://dichroweb.cryst.bbk.ac.uk) to determine α-helical, β-sheet, β-turn, and unordered regions.



© University of Venda

### 3.1.6. Investigation of the tertiary structural organization and temperature-dependent conformational changes of *E. coli* DnaK using tryptophan fluorescence-based analysis

The organization of the tertiary structure of DnaK was determined by tryptophan fluorescence spectroscopy. The assay was conducted as previously described by (Zininga *et al*., 2016). Purified DnaK protein was diluted to a final concentration of 0.2µM and 4 µM in the buffer (PBS). Protein solution was aliquoted into separate tubes for different temperature points to investigate the stability of DnaK at different temperatures to identify the optimal temperature for its denaturation. The temperature was set at (40°C, 60°C, 70°C, 100°C) for 15 minutes. The required amount of protein of interest was mixed with a desired buffer (PBS), and the tertiary structure of DnaK was analyzed using intrinsic fluorescence spectroscopic analysis at varying temperatures.

### 3.1.7. Investigation of ATPase activity of *E. coli* DnaK

Among the key elements of DnaK chaperone activity is the crucial DnaK-DnaJ interaction. Even while Hsp70s constitute the core of this chaperone machinery, their own activity in protein folding is minimal, and the chaperone's ability to fold proteins depends on the functional Hsp70-Hsp40 interaction. Through the stimulation of ATP hydrolysis and the direct binding of substrates to Hsp70s, Hsp40s primarily help Hsp70s in protein folding. The molecular mechanism of ATPase stimulation can now be partially understood thanks to recent structural and biochemical studies developments. However, the precise molecular mechanism and structural basis of the functional Hsp70-Hsp40 association remain largely unclear. According to the documented function of Hsp40s in promoting the rate at which Hsp70s hydrolyze ATP, Hsp40s Hsp40s interact robustly with Hsp70s only in the ATP state. (Mayer and Bukau 2005; Craig *et al*., 2006; Fan *et al*., 2003). The detailed protocol for evaluating the effects of SA-AgNPs on the ATPase activity of DnaK can be found in Appendix B13.



© University of Venda

## 3.2. Results and Discussion

### 3.2.1. Confirmation of the pQE30/DnaK plasmid

Restriction digest was used to verify the pQE30/DnaK plasmid (Figure S.1). Plasmid pQE30/DnaK expressing DnaK protein was digested with *Bam*HI and *Hind*III. A single digest with either of the enzymes resulted in a linearized plasmid of 5068 bp, corresponding to the size of the pQE30 plasmid. Double digest of pQE30/DnaK with both enzymes resulted in two distinct bands at around 3431 bp and 1906 (Figure S.1).

### 3.2.2. Overexpression and purification of recombinant *E. coli* DnaK protein

SDS-PAGE analysis reveals that recombinant DnaK protein was expressed (Figure S.2) and purified successfully (Figure S.2). The presence of expressed and purified proteins was confirmed by Western blot analysis using an anti-His antibody (Figure S.3). DnaK (Figure S.2) protein migrated to 71 kDa as observed in SDS-PAGE. DnaK was expressed in bulk within the range of 1-6 hours. pQE30 plasmid was used as a control (Figure S.4). Protein concentration was estimated using Bradford assay (Sigma-Aldrich, USA), using bovine serum albumin (BSA) as a protein standard (Figure D. 1).

### 3.2.3. Secondary structure analysis of *E. coli* DnaK:

Determination of the secondary structure and folding properties of recombinant and purified protein were best analyzed using Circular dichroism (CD). *E. coli* DnaK is predominantly α-helical (Mathomu, 2022). The deconvoluted data sets confirmed that DnaK possesses more than 50 % α-helical content. The RMSD shows that the data is reliable as it is less than 1 (Table 3.1.2).

The far-UV CD spectra of DnaK are characterized by a peak at approximately 195 nm and DnaK also displayed a predominantly α-helical structure due to the negative troughs observed at approximately 209 and 222 nm (Figure 3.1), which is consistent with the reported helical nature of the protein (Lebepe et al., 2020). Dichroweb online tool for deconvolution of DnaK structures confirmed that DnaK is α-helical (Fig 3.1; Table 3.1.2). With RMSD values less than 1, all the



© University of Venda

structural values obtained by deconvolution were quality evaluated, indicating confidence in the data's reliability (Table 3.1.2).

The CD spectrum shows a far-UV (190–240 nm), where the signal primarily originated from the DnaK's peptide backbone, which allowed insights into its secondary structure content. The spectrum presents a positive peak near 195 nm and a deep negative trough around 208 nm (Figure 3.1), which indicates the presence of α-helices. These features correspond to the characteristic circular dichroism (CD) spectra of α-helical. Although the trough near 222 nm is weaker, it also suggests α-helical content. Between 210 and 220 nm (figure 3.1), the spectrum showed less distinct troughs, which could suggest less structured regions, potentially representing random coils or loops. The absence of strong negative peaks around 216 nm, primarily associated with β-sheet structures, suggested that DnaK is predominantly α-helical with minimal β-sheet content (Dong, 2008).

The CD spectrum below aligns with previously reported structural composition, as the prominent α-helical content indicates that DnaK retains a highly helical conformation in the measured conditions. Moreover, the changes observed in ellipticity, especially around 208 nm and 222 nm, might reflect conformational flexibility or unfolding transitions of the protein under conditions such as temperature or ligand binding. This CD spectrum strongly supports the presence of a predominantly α-helical secondary structure. This is supported by previous studies of DnaK and its homologs, confirming the importance of α- helices in their functional domains (Zuiderweg, 2004).

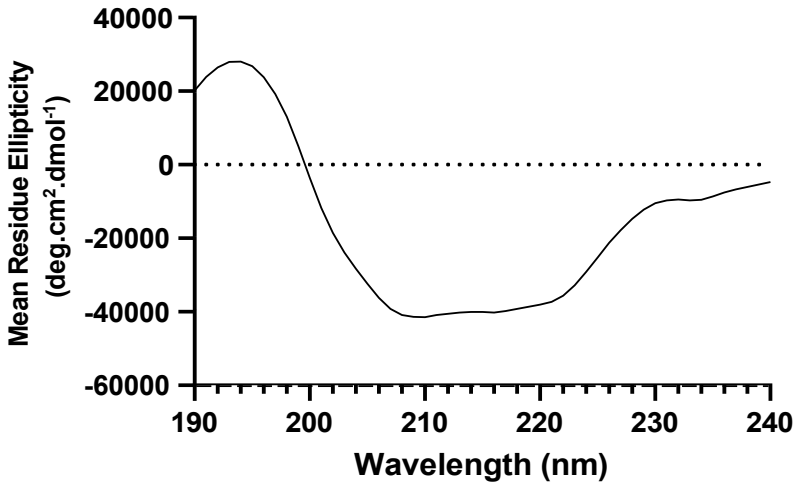



**Figure 3. 1.** CD spectra of DnaK showing secondary structure analysis of DnaK at Apo state. All calculations emanated from the Dichroweb tool.



© University of Venda

**Table 3.1.2. Secondary composition of DnaK.**

| | Combined α-helices | β-sheets | β-turns | Unordered | Total content | RMSD |
|---|---|---|---|---|---|---|
| **DnaK** | 0.89 | 0.039 | 0.0 | 0.071 | 1 | 0.447 |

### 3.2.4. Tertiary structure analysis of *E. coli* DnaK

Tryptophan fluorescence was used to investigate the protein stability and conformational changes. All experiments were carried out in a Jasco J-1500 spectrometer with a Peltier-effect temperature controller. Further analysis, such as thermal denaturation, was performed to further analyze additional insights into the stability and dynamic structural changes of DnaK under different temperature conditions (Figure 3.3).

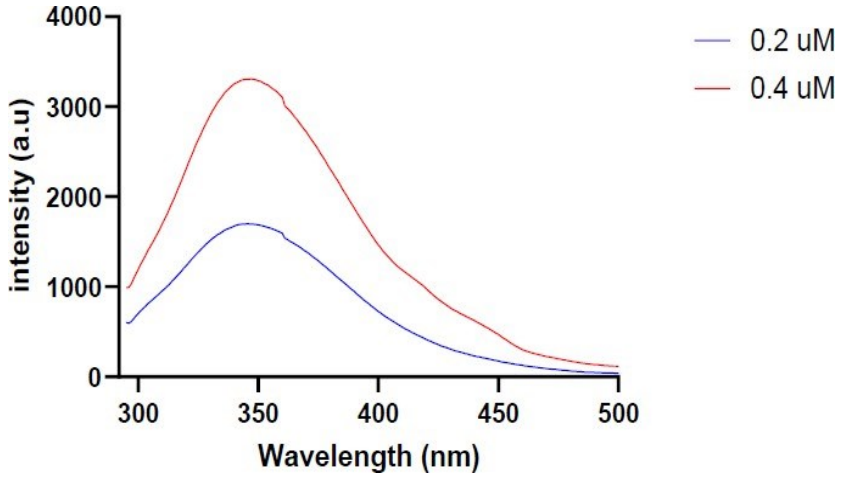



**Figure 3. 2.** The intrinsic tryptophan fluorescence with an initial excitation at 295 nm and emission recorded from 280 nm to 500 nm was used to examine the tertiary structure of recombinant DnaK at Apo state 0.2 µM and 0.4 µM.



© University of Venda

### 3.2.5. Temperature-dependent conformational changes of E. coli DnaK using tryptophan fluorescence-based analysis

Different Colours (Temperature, °C) on the graph show curves at various temperatures (45°C to 100°C), where changes in intensity and peak position reflect the thermal unfolding or structural changes in DnaK (Figure 3.3). At lower temperatures (45°C and 60°C), the intensity is moderate, and the peak is at around 335-340 nm, which is a characteristic of folded proteins where tryptophan is in a more hydrophobic environment (Yang *et al*., 2024). The gradual increase in fluorescence intensity between 45°C and 70°C implies that DnaK undergoes thermal destabilization, most likely starting to unfold (Ricci & Williams, 2008). An increase in fluorescence intensity was observed at 75°C and 90°C, which most likely corresponds to the major unfolding event in DnaK's structure (Rohland *et al*., 2022), where tryptophan residues that were buried inside the protein are now exposed to a more polar environment (Figure 3.3). Aggregation might be suggested due to the drop in intensity at 95°C, leading to a lower fluorescence. As the temperature increases (at 95 °C and above), the intensity increases (as observed with the 70°C and 100°C curves) (Liu *et al*., 2022). This further suggests that the protein partially unfolds, exposing more tryptophan residues to the solvent. At high temperatures (95°C), the fluorescence intensity significantly decreases, indicating that the protein is fully unfolded and may have aggregated, leading to fluorescence loss. The tremendous unfolding occurred between 70°C and 100°C, which suggested that DnaK's melting temperature (Tm) lies within this range, where the protein undergoes significant thermal denaturation (Christensen *et al*., 2022; Stewart, 2024).



© University of Venda

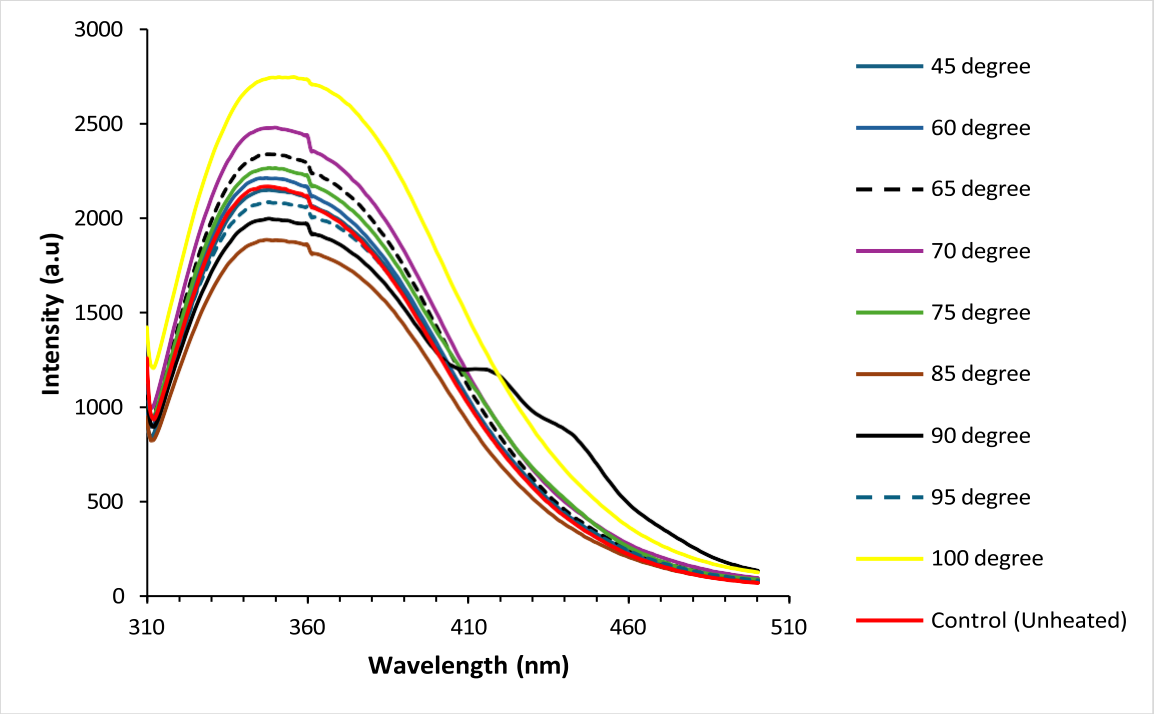



**Figure 3. 3.** Tertiary structure analysis/tryptophan analysis of temperatures (45°C - 95°C).

As the temperature increased, the structure of DnaK unfolded, hence a decrease in fluorescence intensity due to the exposure of aromatic residues, which led to an increase in the emission peak. The x-axis (wavelength, nm) represents the emission wavelength of tryptophan fluorescence, ranging from around 310 nm to 510 nm. Tryptophan emitted fluorescence between 300-400 nm, peaking in the 330-360 nm range under folded conditions. Furthermore, the intensity of fluorescence in arbitrary units (a.u.), reflected how much of tryptophan was exposed to the solvent, which changes depending on whether the protein is folded or unfolded.

### 3.2.6. Analysis of enhanced/stimulated ATPase activity of DnaK

Previous studies have reported that the ATPase activity of DnaK exhibits cooperativity, particularly in conjunction with its co-chaperone DnaJ (Thompson *et al*., 2012). DnaJ significantly enhances DnaK's low intrinsic ATPase activity. Additionally, this is crucial for the chaperone's function in protein folding and prevention of aggregation. Specifically, DnaJ binds to unfolded or misfolded substrates and stimulates DnaK's ATPase activity, facilitating the hydrolysis of ATP and thereby promoting substrate binding and folding (Han & Christen, 2001; Thompson *et al*., 2012).



© University of Venda

In Figure 3.4, as ATP concentration increases, both DnaJ and DnaK (Blue and Black) indicate gradual increases in ATP hydrolysis, which was expected due to higher ATP availability enhancing ATPase activity in these proteins (Rohland *et al*., 2022). Compared to DnaK alone, the cooperativity of DnaJ and DnaK (red) shows a slower increase in ATPase activity until around the concentration of 2 mM. However, it surpasses it at higher concentrations, further suggesting the cooperative interaction between these proteins. Furthermore, the lower ATPase activity across the concentrations exhibited by the boiled DnaK+DnaJ (cyan) indicates that the heat-denatured proteins lose much of their functional capacity to hydrolyze ATP (Amankwah *et al*., 2022). This was used as a control to show the requirement for native, functional protein structure for activity (Zhou *et al*., 2020). It has been previously reported that boiling denatures proteins, which is a common practice that shows loss of activity. The decrease in ATPase activity of boiled DnaJ+DnaK agrees with previous studies that demonstrated that the native structure of chaperone proteins is essential for ATPase activity (Schmid, 1992).

Moreover, as compared to all other conditions, adding silver nanoparticles (green) enhanced the ATPase activity, particularly at higher ATP concentrations. This suggests a synergistic effect, where the SAAgNPs stabilized or otherwise enhanced the ATP hydrolyzing ability of the DnaJ-DnaK chaperone system. The enhanced ATPase activity in the presence of silver nanoparticles is supported and, moreover, agrees with previous studies that nanoparticles can enhance the functional stability of various proteins (Yadav *et al*., 2020),

This interesting observation was not expected but is consistent with other studies where nanoparticles showed enhanced activity of GroEL (Sennuga *et al*., 2012). However, at high concentrations, their nanoparticles acted as an inhibitor of GroEL's ATPase activity, which suggested that the effect of nanoparticles on ATPase activity might be concentration-related because, at lower concentrations, nanoparticles acted as an activator, while at higher concentrations, they acted as an inhibitor. They further stated that an increase in ATPase activity observed could result from particle size (Sennuga *et al*., 2012), which could be further confirmed by TEM in this study.

Above all, no explanation or mechanism was suggested for this increase in activity, and this, along with the suppression of aggregation and folding assay using DnaK nanoparticles, could be the target for future research.



© University of Venda

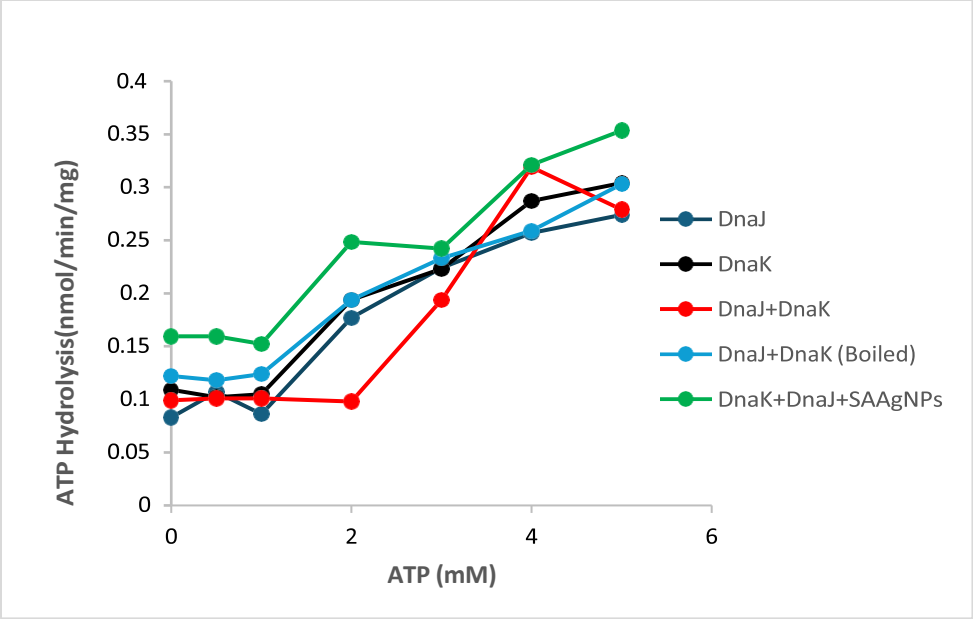



**Figure 3. 4.** SA-AgNPs regulate ATPase activity of recombinant DnaK.

The inorganic phosphate released was monitored by directed calorimetry at 595nm wavelength. The graphs show the stimulated ATPase activity of DnaK. The concentrations of ATP were varied from 0 to 6 mM.

## Chapter summary:

Plasmid pQE30/DnaK expressing DnaK protein was successfully digested with *Bam*HI and *Hind*III; SDS-PAGE analysis revealed that recombinant DnaK protein was expressed (Figure S.2) and purified successfully (Figure S.2). The presence of expressed and purified proteins was confirmed by Western blot analysis (Figure S.3). Secondary structure and folding properties of recombinant and purified protein were best analyzed using Circular dichroism, and data sets confirmed that DnaK possesses more than 50 % α-helical content. Tryptophan fluorescence confirmed the protein stability and conformational changes at varying temperatures. At higher temperatures, the structure of DnaK unfolded. Moreover, the addition of silver nanoparticles enhanced the ATPase activity (Figure 3.4).



© University of Venda

University of Venda
Creating Future Leaders

# Chapter 4

**Biochemical analysis of the functional features of *E. coli* DnaK protein**



© University of Venda

# CHAPTER 4: Biochemical analysis of the functional features of *E. coli* DnaK protein

## 4.1. Introduction

Nanoparticles have been identified as potential modulators of protein structure and function, with critical questions about their interactions with proteins (Park, 2020). Plant derived nanoparticles present a unique chance to explore such interactions, specifically in bacterial systems. This chapter aimed to investigate the biochemical and functional effects of SA-AgNPs on *E. coli* DnaK. This chapter outlines the effects of SA-AgNPs on *E.coli* DnaK investigated at the structural, functional, and cellular levels.

The first study question to be investigated began with assessing the SA-AgNPs effects on plasmid DNA, followed by investigating the impact of SA-AgNPs on the secondary structure of *E. coli* DnaK to evaluate changes in protein folding. Under varying concentrations of AgNPs, the structural stability of DnaK was further analyzed using tryptophan fluorescence spectroscopy.

Furthermore, to evaluate the effects of SA-AgNPs on DnaK structure, the chaperone activity of DnaK was assessed using a malate dehydrogenase (MDH) aggregation assay, this is an assay which determines the ability of DnaK to prevent protein aggregation (Tonui *et al*., 2023). Additionally, the effect of SA-AgNPs on bacterial growth was analyzed to determine antimicrobial properties. The impact of SA-AgNPs on *E. coli* XL1-Blue cells expressing DnaK was further investigated through SDS-PAGE analysis for detecting changes in protein expression. Along with complementation assay to assess the ability of DnaK to protect *E. coli* XL1 Blue cells under stress conditions in the presence of SA-AgNPs.

### 4.1.1. Experimental procedure

a) **Investigation of the Effects of SA-AgNPs on Plasmid DNA**

An amount of 200 ng of plasmid DNA was incubated with varying concentrations of SA-AgNPs (1.8, 2.1, and 2.5 µg/mL) at 37°C for 24 hours. The results were analyzed through agarose gel electrophoresis (Appendix B).

b) **Investigation of SA-AgNPs Effects on the Secondary Structure of *E. coli* DnaK**



© University of Venda

An amount of 5 µM DnaK protein was incubated with different concentrations of SA-AgNPs (0–50 µg/mL) at 25°C for 30 minutes in a buffer (20 mM Tris, pH 7.4; 100 mM NaCl). Secondary structural changes were analyzed using CD spectroscopy.

c) **Investigation of E. coli DnaK Chaperone Function using Malate Dehydrogenase (MDH) Aggregation Assay**

This assay was conducted as previously described (Makumire *et al*., 2015) in the presence and absence of SA-AgNPs. Briefly, 2 µM DnaK was incubated with 0.5 µM MDH (Sigma-Aldrich-Roche, Darmstadt, Germany) in a buffer (20 mM Tris, pH 7.4; 100 mM NaCl). SA-AgNPs were added to each reaction mix to final concentrations ranging from 2.1-2.5 µg/mL. As a positive control, different concentrations of DnaK ranging from 0.2 to 2 µM) were included in place of SA-AgNPs. The mixture was set in triplicate and incubated at 51°C for 1 hour to induce MDH aggregation. BSA was used as control. Aggregation was monitored based on the development of turbidity spectrophotometrically at 360 nm. OD readings were taken every 5 minutes using a SpectraMax M3 spectrometer (Molecular devices, USA). The absorbance units were converted to aggregation percentages relative to MDH aggregation level (set at 100 %).

d) **Analysis of the Effect of SA-AgNPs on Bacterial Growth**

Recombinant *E. coli* was grown overnight at 30°C in LB broth. The culture was diluted to OD600 ~0.1 and treated with SA-AgNPs (0–100 µg/mL) and incubated at 30°C with shaking. OD600 was measured at 2-hour intervals for 6 hours. Effects of SA-AgNPs on *E. coli* XL1 Blue Cells expressing DnaK were further analyzed by SDS-PAGE.



© University of Venda

## 4.2. Results and Discussion

### 4.2.1. Investigation of the effects of SAAgNPs on the plasmid DNA

*Senna alexandrina* silver nanoparticles damage plasmid DNA. Reactions between nanoparticles and biological entities such as proteins and DNA can result in unpredicted and undesirable effects. DNA damage can have major deleterious effects on cells and organisms. This section aimed to investigate the effects of SA-AgNPs on plasmid DNA since these particles were targeted for biological application in *E. coli*. The study on pQE30/DnaK integrity in the presence of nanoparticles revealed the effect of these nanoparticles on DNA structural integrity. The restriction enzyme *Hind*III and *BamH*I was used to confirm the integrity of the purified plasmid. The plasmid is 5342 bp; *BamH*I and *Hind*III cuts at 145 bp and 2068 bp, respectively (Figure S.1). Two fragments migrating at 1906 bp and 3424 bp were observed (Figure S.1). The intact plasmid DNA was exposed to 1.8, 2.1, and 2.5 µg/ml SA-AgNPs and incubated for 24 hours.

The assay was conducted at 37 °C in Tris- HCl buffer that was at pH 7.4. After 24, agarose gel analysis was conducted on the DNA samples using a 1.0 % agarose gel, and the voltage used was 100 V for 1 hour. Two DNA bands were observed in the negative control, marked as supercoiled DNA and relaxed DNA, lane UN (Figure 4.1). This suggests that the untreated plasmid DNA existed in both supercoiled and relaxed conformations under the prevailing conditions, as previously reported (Dunpall *et al*., 2012). The faint smearing at 1.8 µg/ml band may suggest minimal damage or degradation of DNA at this concentration. An apparently higher degree of degradation can be observed at 2.1 µg/ml AgNP concentration, and the smearing pattern in this lane of DNA suggests fragmentation or breakdown, probably due to the interaction with the silver nanoparticles. This indicates that higher concentrations of AgNPs are causing some structural damage to the DNA (figure 4.1). The highest concentration of AgNPs, at 2.5 µg/ml, showed significant band smearing and decreased intensity. This implies significant DNA degradation, most likely due to increased nanoparticle contact that causes DNA fragmentation.



© University of Venda

High concentrations of AgNPs may induce oxidative stress or interact directly with DNA, leading to strand breaks (Ávalos *et al*., 2015). The intensity of the band indicated the degree and extent of linearisation and demonstrated that the damage was concentration-dependent.

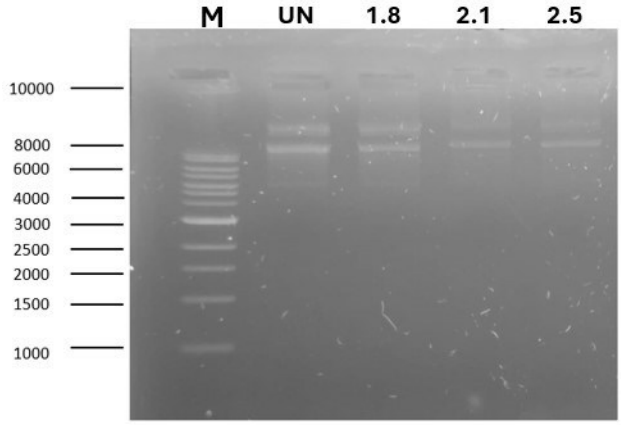



**Figure 4. 1. The effects of SAAgNPs on plasmid DNA integrity.** Plasmid pQE30/DnaK was exposed to varying concentrations from 1.8 - 2.5 µg/ml of SAAgNPs. The untreated (UN) plasmid was used as the negative control. The samples were incubated at 37 °C for 24 hours and were analyzed by agarose gel electrophoresis.



© University of Venda

### 4.2.2. Investigation of SA-AgNPs effects on the secondary structure of *E. coli* DnaK

The investigation of the effects of SA-AgNPs on DnaK secondary structure was investigated by conducting circular dichroism (CD) spectrophotometric analysis. As previously mentioned in (chapter 3; figure 3.1) that *E. coli* DnaK is predominantly alpha helical. DnaK displayed a predominantly α-helical structure due to the negative troughs observed at 209 and 222 nm. The presence of SA-AgNPs (0 – 2.5 µg/ml) from the above observations was found to slightly perturb the secondary structure of DnaK. On the other hand, a study by (Chakraborty & Biswas, 2020), using Hsp18 revealed a protein structure disruption. However, in this study, DnaK showed slight alterations, which may be attributed to its size, as Hsp18 is a small chaperone, whereas DnaK (also known as Hsp70) is a much larger chaperone.

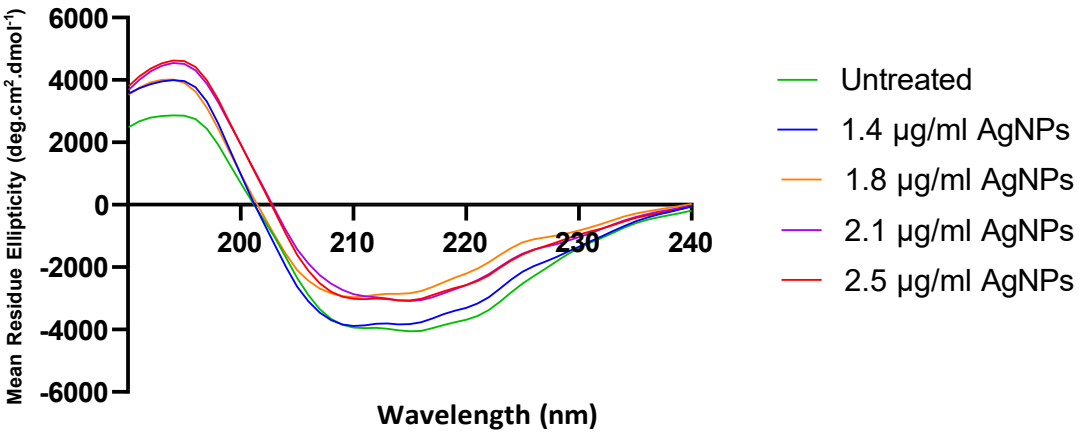



**Figure 4. 2.** The far-UV CD spectra of the recombinant DnaK in the presence of SA-AgNPs. The spectra was presented as molar residue ellipticity and are characterized with minima at 222 nm and 209 nm, and maxima at 194 nm, is consistent with the reported helical nature of the protein (Lebepe *et al*., 2020), The spectra shows the secondary structural analysis of DnaK at 30 oC in the absence and presence of lower and higher order SA-AgNPs concentrations. In conclusion, SA-AgNPs do not disrupt the secondary structure of DnaK.

Following the observation of slightly or nonsignificant effect of SA-AgNPS on DnaK secondary structure. To validate that DnaK structural changes were possible, conformational changes on the



© University of Venda

protein tertiary structure were induced by exposing the DnaK to varying concentrations of SA-AgNPs.

### 4.2.3 Concentration-Dependent Effects of Silver Nanoparticles (AgNPs) on the Structural Stability of DnaK Monitored by Tryptophan Fluorescence

The tertiary structural changes of DnaK were conducted using tryptophan fluorescence spectroscopy by monitoring intrinsic fluorescence analyses. DnaK possesses one tryptophan (TRP-102) residue located in its NBD and seven tyrosine (Tyr) (https://www.uniprot.org/). Tyrosine has a quantum yield like that of TRP. Tryptophan is known to be excited at wavelengths around 280 nm and emits fluorescence in a peak from 300-400 nm, while tyrosine also exhibits fluorescence, with excitation occurring at slightly lower wavelengths than Tryptophan in proteins. The indole group of tryptophan residues is considered the dominant source of absorbance and emission in protein (Yang *et al*., 2017).

Among the twenty naturally occurring amino acids that make all proteins, tryptophan (Trp), tyrosine (Tyr), and phenylalanine (Phe) are intrinsically optically active due to their conjugation with aromatic ring side chains (Yang *et al*., 2017).

Figure 4.3, shows tryptophan fluorescence of DnaK in the presence of varying concentrations of AgNPs (1.4 µg/mL to 2.5 µg/mL). The DnaK peak fluorescence without significant interference was expected to be around 330-350 nm. The observed fluorescence intensity was high at lower concentrations of AgNPs (1.4 µg/mL, blue line, and 1.8 µg/mL, red line), indicating that DnaK is still in a relatively folded state. However, some interactions with nanoparticles may be causing subtle changes. As the AgNP concentration increases (2.1 µg/mL and 2.5 µg/mL), there is a significant drop in fluorescence intensity (purple and light blue lines), implying substantial disruption to DnaK's structure, likely due to the interaction with nanoparticles.

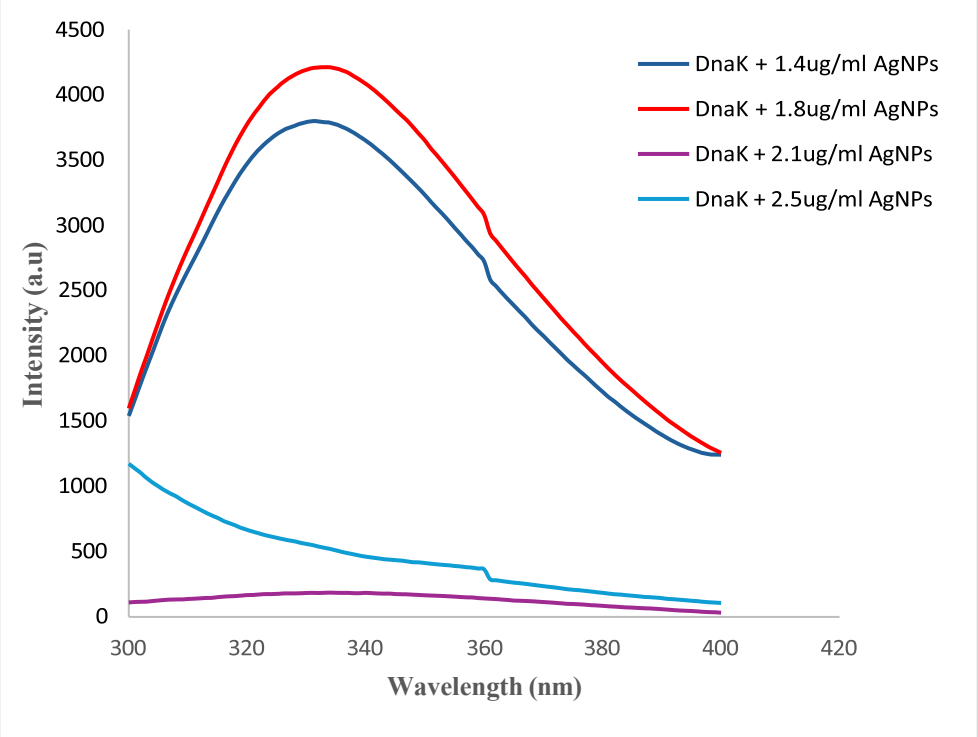
At lower concentrations of AgNPs (1.4 µg/mL (blue) and 1.8 µg/mL (red)), these showed a slight increase in fluorescence intensity, suggesting that the nanoparticles at these concentrations may stabilize DnaK slightly or lead to a slight enhancement of its folded state. In contrast, higher concentrations (2.1 µg/mL (purple) and 2.5 µg/mL (light blue)) of AgNPs caused a tremendous decrease in fluorescence intensity. Moreover, this suggested that higher nanoparticle concentrations result in significant disruption of the DnaK structure, which leads to unfolding or



© University of Venda

aggregation. The exposure of tryptophan residues to a more polar (aqueous) environment due to unfolding would result in reduced fluorescence (Figure 4.3). The steep reduction in fluorescence intensity at AgNP concentrations of 2.1 and 2.5 µg/mL could further suggest that the protein has undergone aggregation following unfolding.

This behavior is consistent with previous research indicating nanoparticle-induced protein aggregation, especially at high concentrations. Bidan and Al-Ali (2024) observed similar effects in their study on AgNPs, where they found that protein unfolding and aggregation are common responses to nanoparticle-induced stress in AgNPs. In these scenarios, protein aggregation results from AgNPs' indiscriminately binding to multiple protein sites, destabilizing the structure. The hydrophobic interactions between nanoparticles and exposed regions of the protein have been reported to accelerate this process (Bidan & Al-Ali, 2024). From the above results, DnaK was found to have maxima in the 340–350 nm range, depending on temperature and salt concentration. This suggest that the proteins assumed a folded state where the tryptophan residue is buried within the hydrophobic region of the protein. A red spectral shift was observed as the fluorescence intensity decreased (Fig 4.3). A tertiary structural conformational change caused due to the presence of different SA-AgNP concentrations was shown by a red spectral shift.






© University of Venda

**Figure 4. 3.** Tryptophan fluorescence spectra of DnaK in the presence of silver nanoparticles (AgNPs) at varying concentrations.

Fluorescence emission spectra of DnaK (excitation at 295 nm) are shown after the addition of AgNPs at concentrations of 1.4 µg/mL (blue line), 1.8 µg/mL (red line), 2.1 µg/mL (purple line), and 2.5 µg/mL (light blue line). The fluorescence intensity peaks around 350 nm, indicating the environment of tryptophan residues. At lower concentrations (1.4 and 1.8 µg/mL), a modest increase in fluorescence suggests stabilization of DnaK. However, the fluorescence intensity decreases significantly at higher concentrations (2.1 and 2.5 µg/mL), indicating protein unfolding and possible aggregation due to interactions with AgNPs.

Complete disruption of DnaK was achieved at 2.1 µg/ml SA-AgNPs. Moreover, at higher concentrations, DnaK fluorescence spectra in the presence of SA-AgNPs indicated changes to the tertiary structure of DnaK in comparison to absence of SA-AgNPs (Chapter 3; Figure 3.2). This may suggest that the tryptophan residues in DnaK were exposed to the environment. Hence, fluorescence intensity is quenched from above 4000 arbitrary units to less than 500 units without red or blue spectral shift. The change or disruption in the tertiary structure of DnaK was further supported by sufficient quenching of the protein as observed in the decrease of the fluorescence intensity (Figure 4.3).

### 4.2.3. Investigation of *E. coli* DnaK chaperone function using malate dehydrogenase aggregation assay

In this study, the ability of SA-AgNPs to suppress heat-induced aggregation of MDH as well as their effect on the activity of *E. coli* DnaK, a well-known Hsp70 homolog, was investigated (Shonhai *et al*., 2005; 2008).

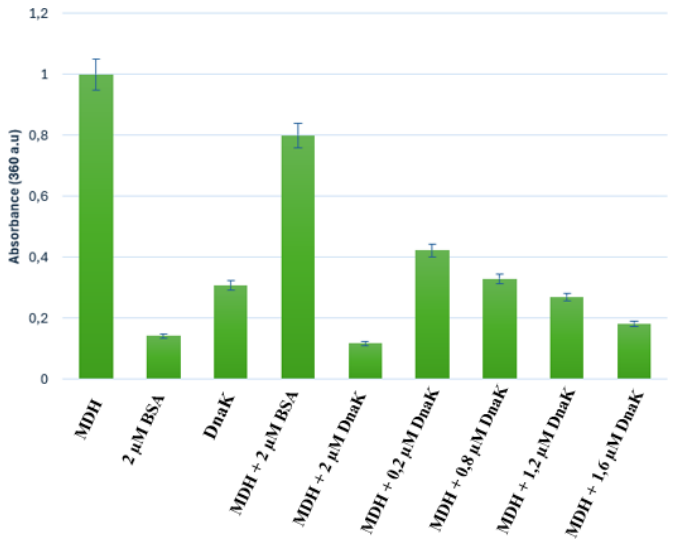
MDH in the presence of AgNPs and the additional presence of DnaK was heated to 51 °C, and aggregation was measured as an increase in turbidity (Figure 4.4). MDH aggregated as indicated by a high absorbance value (Figure 4.4). In the presence of DnaK, MDH aggregation is prevented (bar MDH + DnaK, Figure 4.4). In the presence of lower concentrations of AgNPs (2.1 and 2.5 µg/mL), MDH aggregation was also prevented in a DnaK concentration-dependent



© University of Venda

manner, as shown by low turbidity values (Figure 4.4 A). MDH is an aggregation-prone protein (Shonhai *et al*., 2008) upon exposure to heat stress, as indicated by the increase in turbidity over time.

Surprisingly, the low turbidity values, compared to untreated MDH, confirmed the holdase-like function of these nanoparticles. However, as concentration increased to 2.5 µg/mL, the ability to suppress aggregation by the AgNPs is stimulated or increased (Figure 4.4 B). This would suggest that higher concentrations of the particles were highly effective in suppressing MDH aggregation as compared to low concentrations. The nanoparticles suppress MDH independently by acting in a chaperone-like manner, thereby stabilizing MDH's unfolded or partially folded state. This effect may have risen due to the surface interactions between the nanoparticles and the exposed hydrophobic regions of MDH, which can otherwise contribute to aggregation. At the same time, this function increased at higher nanoparticle concentrations. 2 µM DnaK was incubated with 0.5 µM MDH in figure 4.4 B.




**(A)**



© University of Venda

**(B).**

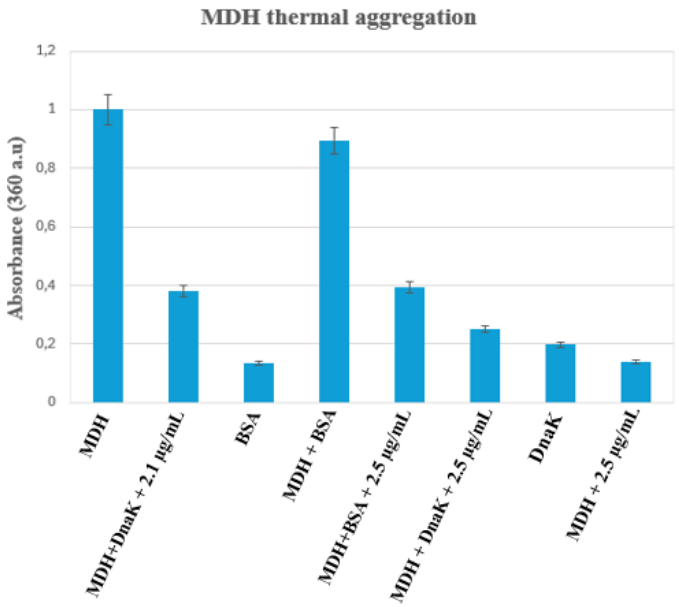



**Figure 4. 4.** Aggregation determination of components of MDH aggregation suppression assay, MDH denaturation was monitored under heating conditions (51 °C for 1 hour 30 minutes) when incubated DnaK in the presence or absence of study nanoparticles (2.1 and 2.5 µg/mL SAAgNPs) MDH alone (positive control), BSA alone (negative control). (A) DnaK was added to MDH and heated to 51 °C to evaluate the suppression activity of DnaK. (B) MDH was also treated with AgNPs of concentrations 2.1 and 2.5 µg/mL in the absence and the presence of DnaK, respectively. Absorbance values were measured in triplicate in a 96-well plate. MDH aggregation level in percentage was regarded as the complete aggregation and used to calculate aggregation level of all other components. Data are presented as mean and standard deviation.



© University of Venda

In the presence of DnaK, MDH aggregation was further suppressed by the NPs in a concentration-dependent manner. This is evident when compared to the untreated MDH control (Figure 4.4 A) and the reaction for MDH exposed to the AgNPs (Figure 4.4 B). Previous studies conducted suggested that nanoparticles (NPs) exhibit functional features that resemble those of molecular chaperones (Luthuli *et al*., 2013) (De and Rotello, 2008). De and Rotello (2008) demonstrated how metallic nanoparticles prevented the aggregation of heat-stressed proteins in vitro (Triulzi *et al*., 2008). Findings from these results are consistent with the above-mentioned reports or are supported by them. Lower turbidity values were observed in the additional presence of the DnaK protein compared to the DnaK positive control. Furthermore, the observed SA-AgNPs interaction may suggest cooperating with DnaK to suppress MDH aggregation (Figure 4.4 B).

### 4.2.4. Analysis of the effect of *Senna alexandrina* silver nanoparticles on bacterial growth

Previous studies have indicated that different kinds of nanoparticles interact with bacterial cells differently, affecting their growth, viability, and physiology. According to reports, biosorption, nanoparticle aggregation or disintegration, and cellular absorption are biophysical interactions between bacteria and nanoparticles that can result in toxicity and membrane damage (Priester *et al*., 2009). To follow up on the *E. coli* XL1 Blue cells' interactions with SA-AgNPs, it was of interest to ascertain whether the nanoparticles had any inhibitory effect on E. coli XL1 Blue bacterial growth, as different classes of bacteria are said to exhibit different susceptibilities to nanoparticles (Fu *et al*., 2005).

*E. coli* XL1 Blue (DnaK transformed) cells suspended in 2YT were exposed to 1.4, 1.8, 2.1, and 2.5 µg/ml SAAgNPs and grown at 37 °C with shaking at 150rpm. Untreated *E. coli* XL1 Blue cells were used as negative control. At hourly intervals, $OD_{600}$ values were monitored from each flask and plotted against time (Figure 4.5 ). Although there is a slight reduction of growth at 37 °C in the presence of nanoparticles, there is, however, dose-dependency in this regard.

The control sample (blue line) displays typical bacterial progression, with an exponential growth phase lasting until around 300 minutes after a lag phase lasting for the first 60 minutes. In the absence of nanoparticles, the OD600 increases to about 1.8, indicating considerable bacterial multiplication. Bacterial growth is seen to be dose-dependently inhibited as SA-AgNP increases. Growth is slower than the control at 1.4 µg/ml (red line), with a maximum OD600 of roughly 1.5



© University of Venda

at 300 minutes. The OD600 peaks at around 1.2 at 1.8 µg/ml (green line), indicating a greater inhibition. The inhibitory impact is considerably more prominent at 2.1 µg/ml (purple line) and 2.5 µg/ml (orange line), with maximal OD600 values of around 1.0 and 0.9, respectively.

Previous studies have shown that nanoparticles tend to aggregate in culture media (Moore *et al*., 2015). The limited cytotoxic effects are caused by the fact that particles in aggregates interact less with bacterial cells. In growth conditions, *E. coli* XL1 Blue cells generally appeared to be able to tolerate the presence of up to 2.5 µg/mL of SA-AgNPs (Figure 4.5).



© University of Venda

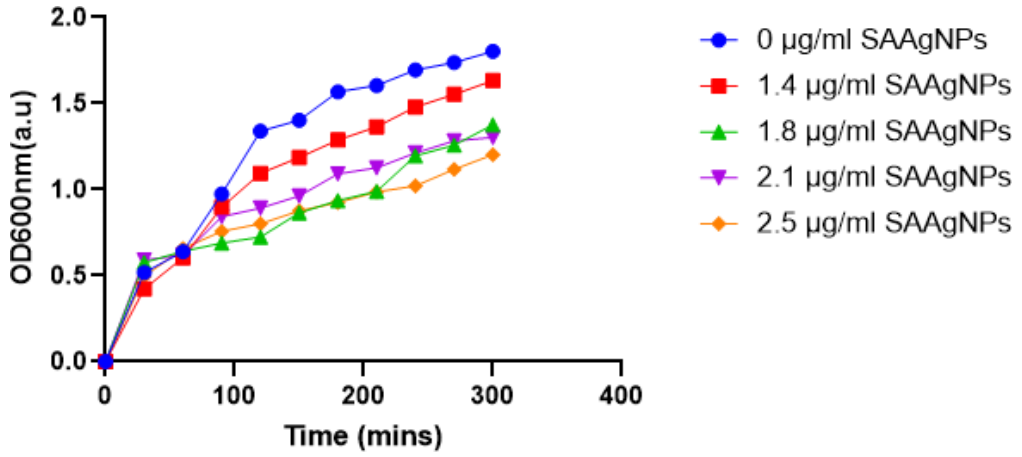



**Figure 4. 5.** The growth curves of *E. coli* under SAAgNPs influence at 37 °C, Cells from an overnight culture were grown to OD600 0.6.

Cells were exposed to SAAgNPs of concentration 1.4, 1.8, 2.1 and 2.5 µg/mL. *E. coli* was set as a negative control without nanoparticles (0 µg/mL AgNPs). These were incubated with shaking at 150rpm. OD values were noted hourly and plotted to evaluate the effects of *Senna alexandrina* silver nanoparticles on bacterial growth.

### 4.2.5. Effects of SAAgNPs on E. coli XL1 Blue cells expressing DnaK as analyzed by SDS-PAGE.

Fernandes *et al*. (2023) representative experiments showed that *E. coli* cells at higher concentrations of Ag-NPs result in more cell death than those at lower concentrations. Previously, Dakal *et al.* demonstrated that the antimicrobial action of AgNPs depends exclusively on the effective concentration of $Ag^{+}$ inside the bacterial cells, deriving from the dissolution of AgNPs (Dakal *et al*., 2016). Higher concentrations of silver nanoparticles resulted in a stronger antibacterial response in the above-mentioned previous studies due to more intense interactions between nanoparticles and bacterial cells; therefore, it was necessary or ideal in this study to continue to carry out experiments with a higher concentration of 2.5 µg/mL as it showed effective or slightly inhibition of cell growth in contrast with lower concentration. DnaK expression was gradual (Figure 4.6 A), as the expression was slightly within the first 2 hours in comparison to the untreated cells (Figure 4.6 B).



© University of Venda

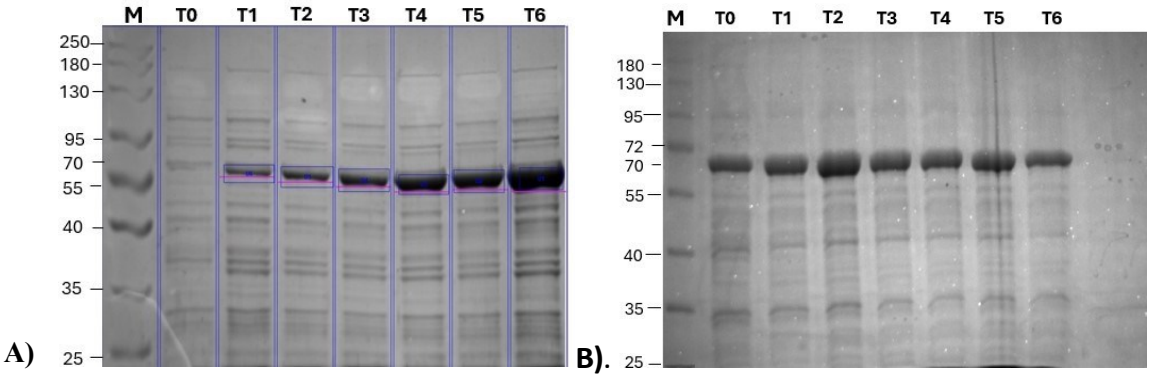
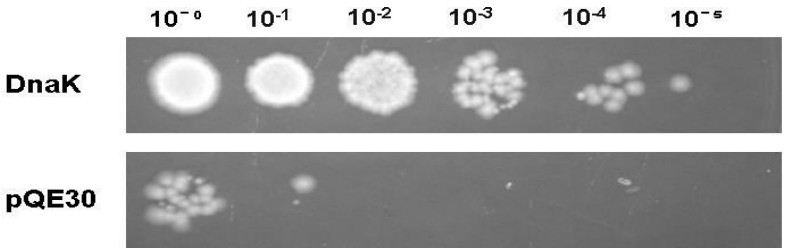



**Figure 4. 6.** Comparison of the protein profiles in *E. coli* XL1 Blue cells expressing DnaK.

(A). Cells were exposed to 2.5 µg/mL SAAgNPs and incubated overnight at 30 °C. (B). Untreated *E. coli* was used as the negative control. The expression was analyzed by SDS PAGE.

### 4.2.6. Complementation assay

In order to follow up the previous bacterial growth curve of *E. coli* XL1 Blue cell's interactions with SA-AgNPs (Figure 4.5), it was also of interest to ascertain whether the nanoparticles had any inhibitory effects on DnaK to protect the *E. coli* XL1 Blue cells at different temperatures. The comparative study (Complementation assay) on the growth of E. coli XL1 Blue cells under the influence of SA-AgNPs at average (37 °C) and non-permissive (43 °C) temperatures was also conducted to investigate the function of DnaK at different temperatures to protect the *E. coli* cells in the presence of nanoparticles (Figure 4.9). The presence of SA-AgNPs reduced bacterial growth insignificantly at 37 °C (Figure 4.9 A). Under optimal growth temperature (37 °C), *E. coli* followed the normal growth colony trend (Figure 4.7); however, no particular trend was noticed in the presence of nanoparticles (Figure 4.9).






© University of Venda

**Figure 4. 7.** Diagram showing a plate of complementation assay at permissive temperature (37°C), with the first spot being undiluted cells and from the 2nd spot to the last representing serial dilutions ($10^{-0}$ to $10^{-5}$).

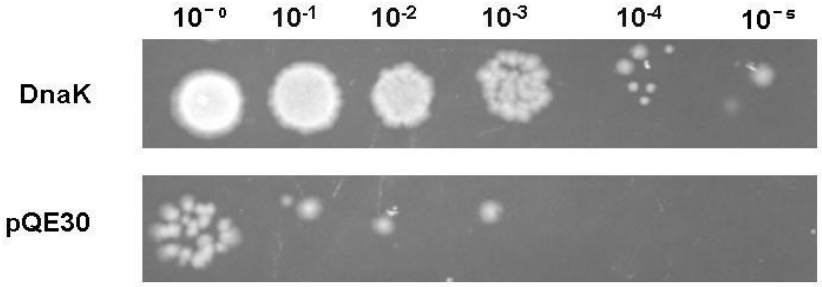
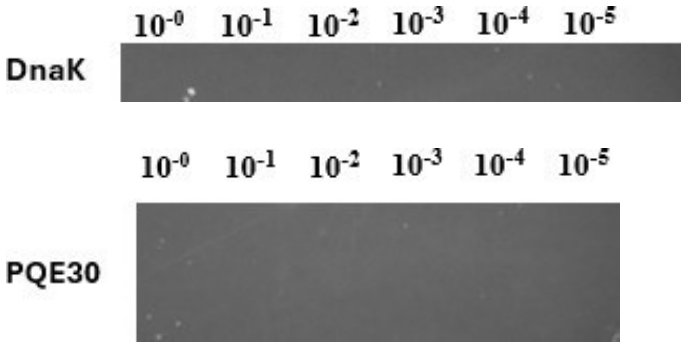



**Figure 4. 8.** Diagram showing a plate of complementation assay at non-permissive temperature (43°C);

The control cells showed no significant difference in growth patterns between the two temperature conditions, suggesting that they were inherently able to tolerate the heat stress (Yadav *et al*., 2022). However, this does not provide conclusive evidence that DnaK was solely responsible for protecting the cells during heat exposure. While DnaK is a well-known molecular chaperone involved in assisting protein folding under stress, other cellular mechanisms and heat-shock proteins may also have contributed to maintaining cell viability and growth.

**(A) Permissive temperature**






© University of Venda

**(B) Nonpermissive temperature**

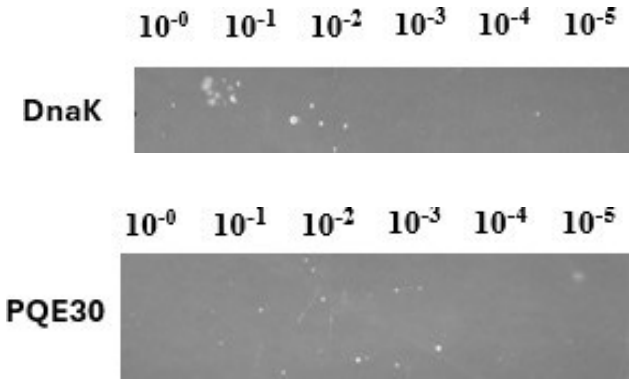



**Figure 4. 9**. Diagram (A), shows a plate of complementation assay at permissive temperature (37°C), and (B). nonpermissive temperature (43,5°C), with the first spot being undiluted cells and the 2nd spot to the last representing serial dilutions ($10^{-0}$ to $10^{-5}$) in the presence of SA-AgNPs. DnaK was unable to protect the cells at both temperatures in the presence of SA-AgNPs, which concludes that silver nanoparticles were able to inhibit the growth of *E. coli* XL1 Blue cells transformed with both pQE30 and DnaK, and PQE30 was used as a control.

## Chapter summary:

In this chapter, the highest concentration of AgNPs, showed significant band smearing and decreased intensity of the DNA, and there was a slightly or nonsignificant effect of SA-AgNPS on DnaK secondary structure. Moreover, at higher concentrations of AgNPs, DnaK fluorescence spectra in the presence of SA-AgNPs indicated changes to the tertiary structure of DnaK in comparison to absence of SA-AgNPs. In the presence of DnaK, MDH aggregation was further suppressed by the NPs in a concentration-dependent manner. Previous studies have shown that nanoparticles tend to aggregate in culture media (Moore *et al*., 2015). The limited cytotoxic effects are caused by the fact that particles in aggregates interact less with bacterial cells. In growth conditions, *E. coli* XL1 Blue cells generally appeared to be able to tolerate the presence of up to 2.5 µg/mL of SA-AgNPs (Figure 4.5). Lastly, SA-AgNPs reduced bacterial growth at both temperatures.



© University of Venda

# Chapter 5

**Bioinformatics analysis of the structural features of *E. coli* DnaK**



© University of Venda

# CHAPTER 5: Bioinformatics analysis of the structural features of *E. coli* DnaK

## 5.1. Introduction

*E. coli* proteins play a crucial role by assisting the organism to tolerate and survive under various stress conditions it encounters throughout its lifecycle, particularly within the human host (Kumar & Tatu, 2003; Pesce *et al*., 2008). Three DnaK-like proteins are present in all malaria parasites, and understanding their characteristics and mechanisms appears to provide insights into their function. The computational analysis of DnaK-like proteins involves examining their primary amino acid sequences to identify conserved motifs and key functional domains; for identification of proteins with established functional biology, protein interaction network prediction offers helpful information (Nibbe *et al*., 2011). For protein network prediction, tools such as STRING(https://string-db.org/) (www.expasy.org) are applicable. According to Protein basics, protein networks in biological systems control cellular processes, modulating an organism's survival ability (Helms, 2018).

A protein's primary amino acid sequence can be used as the basis for predicting its biological activity (Rehman *et al*., 2022). Software such as NCBI, UniProt, and PlasmoDB.org can be used to obtain sequences. Amongst other software, sequence alignment and identification of conserved or similar functional motifs can be done using Clustal W and Bio-edit

7.2.5. Protein's function is determined by their primary, secondary, and tertiary folding patterns. Phyre2 and other secondary structure analysis methods are useful in predicting secondary features' arrangement and percentage contribution. The historical relationships of biological organisms are provided by the phylogenetic tree, and evolutionary traces are useful in identifying origin and classification. Therefore, tools such as Clustal W (genome.jp/tools-bin) are practicable for phylogenetic tree construction.

The affinity of ideal proteins for drug targeting for specific ligands is determined by computational analysis. Understanding how proteins interact with subtle molecules is possible through molecular docking (Stanzione *et al*., 2021). Molecular docking can be practiced by tools such as Biovia Discovery Studio Visualizer v21.1.0 and PyRx virtual screening tool.



© University of Venda

### 5.1.1. Objectives of this chapter:

1. Delineating the *E. coli* DnaK protein with its Plasmodium falciparum, human, yeast, Arabidopsis thaliana, Thermus thermophilus, Bacillus subtilis, Mycobacterium tuberculosis, Pseudomonas aeruginosa counterparts, and homologs.

**Approach:**

- Sequence alignment of *E. coli* DnaK with its predicted biological network
- Sequence alignment of Escherichia coli DnaK protein with its counterparts and homologs
- Phylogenetical analysis of *E. coli* DnaK protein with its counterparts
- Secondary structural prediction of E. coli DnaK protein with counterparts
- Biophysiological properties of *E. coli* DnaK, and its predicted counterparts and homologs Using expasy tool.



© University of Venda

2. In-silico binding analysis of *E. coli* DnaK and DnaJ to Adenosine triphosphate (ATP)

**Approach**

- Molecular docking

3. In-silico binding analysis of *E. coli* DnaK; and DnaK clusters (DnaJ, GROEL, GROES, GRPE, HSLU, HSLV, HTPG, CLPB, CBPA, RPOH) to *Senna alexandrina* compounds.

**Approach**

- Molecular docking

### 5.2. Multiple sequence alignment:

The alignment was conducted to establish the occurrence of similar residues across DnaK homologs/networks. Amino acids were first retrieved from (https://www.ncbi.nlm.nih.gov/protein/). Multiple sequence alignment was then conducted using Bioedit sequence alignment. The conservation percentage of residues is further calculated with the Bioedit tool.

### 5.3. Results and Discussion

#### 5.3.1. DnaK predicted biological networks and alignments

DnaK is a molecular chaperone that plays an essential role in protein folding, stress responses, and heat-shock responses in bacteria. Other proteins in the network include DnaJ, GrpE, GroS, GroL, RpoH, ClpB, HspC, HscA, and HtpG, which are involved in similar functions related to protein quality control and stress response systems (Bukau & Horwich, 1998). DnaK works in conjunction with DnaJ (co-chaperone) and GrpE to fold misfolded proteins, prevent protein aggregation, and assist in stress recovery processes (Sharma *et al*., 2009; Linke, 2005). Proteins such as GroS and GroL (GroEL/ES complex) also act as molecular chaperones, particularly in assisting protein



© University of Venda

refolding after cellular stress (Akgul *et al*., 2018). These are highly interconnected in the network, indicating cooperation among these chaperones in maintaining proteostasis (Figure 5.1).

It was also of interest to inhibit these networks with *Senna alexandrina* phytochemicals which act as the reducing agents in synthesis of silver nanoparticles. NPs can directly interact with *DnaK* and related proteins (DnaJ, GrpE, GroL, GroS, etc.), causing structural changes that impair their chaperone activity. This may block the ATPase activity of *DnaK*, which is critical for its function in protein refolding and stress recovery. As this network is tightly interconnected, nanoparticles could disrupt the interaction between DnaK and its co-chaperones (DnaJ, GrpE). Inhibiting one protein could have a cascading effect on the overall network's functionality, leading to the accumulation of misfolded proteins and bacterial cell death. Furthermore, Green-synthesized nanoparticles, particularly those containing metals such as silver or gold, have been shown to induce oxidative stress in bacterial cells (Das *et al*., 2017). This could further stress the protein quality control machinery, overwhelming the chaperone network (including DnaK) and leading to cell death.



© University of Venda

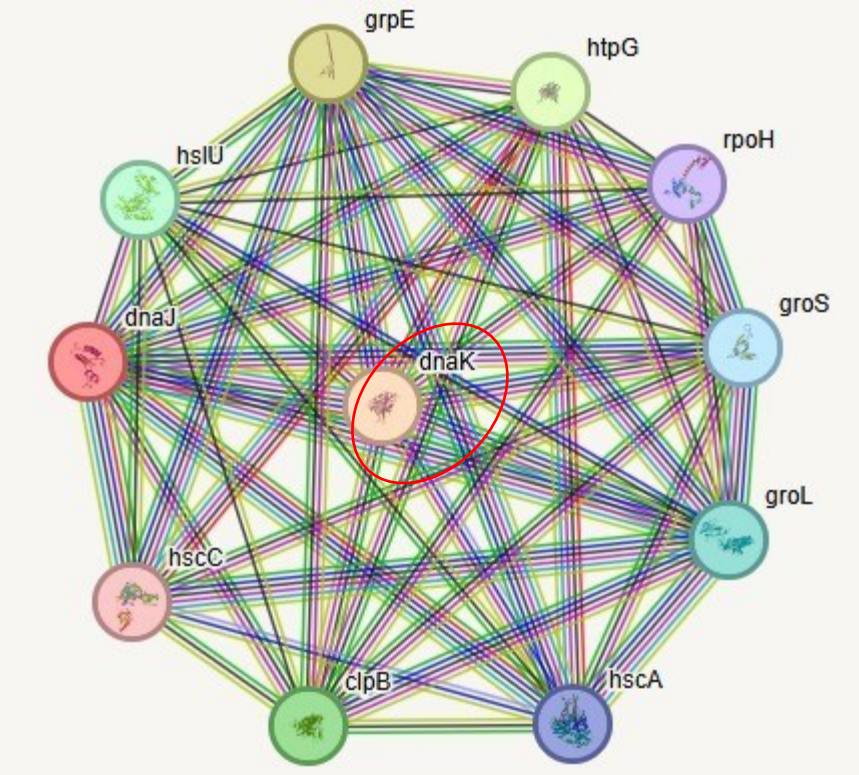
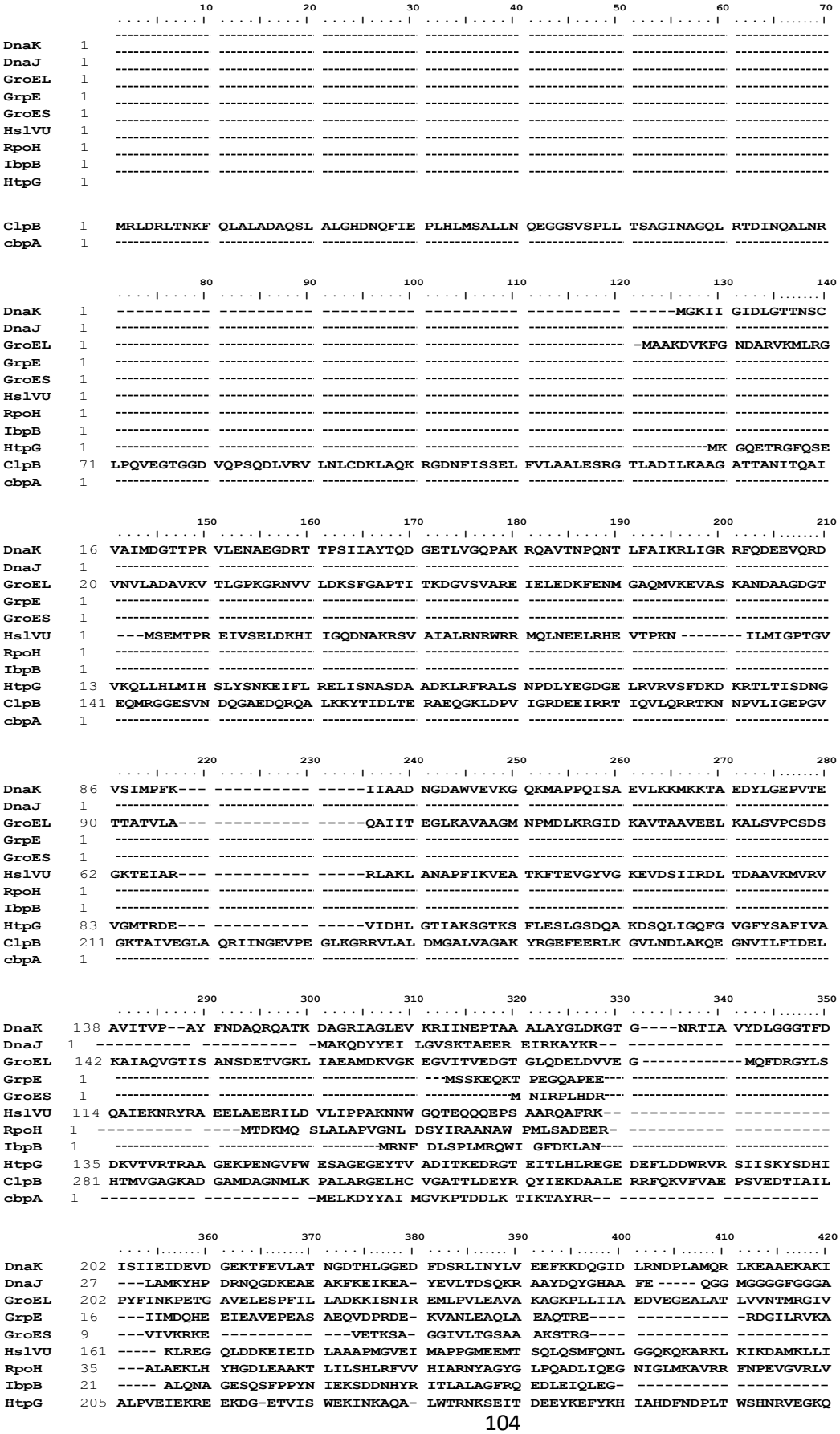



**Figure 5. 1.** Interaction prediction of DnaK. Predicted DnaK closely related interactions using string tool.



© University of Venda





© University of Venda

```
ClpB     351 RGLKERYELH HHVQITDPAI VAAATLSHRY IADRQLPDKA IDLIDEAASS IRMQIDSKPE ELDRLDRRII
```



© University of Venda

```
cbpA    27  ---LARKYHP DVSK-EPDAE ARFKEVAEA- WEVLSDEQRR AEYDQMWQHR NDPQFNRQFH HGDGQSFNAE

                    430         440         450         460         470         480         490
                    ....|....|  ....|....|  ....|....|  ....|....|  ....|....|  ....|....|  ....|.......|
DnaK    272 ELSSAQQTDV NLPYITADAT GPKHMNIKVT RAKLESLVED LVNRSIEPLK VALQDAGLSV SDIDDVILVG
DnaJ     89  DFSDIFGDVF GDIFGGGRGR QRAARGADLR YNMELTLEEA VRGVTKEIRI PTLEECDVCH GSGAKPGTQP
GroEL   272 KVAAVKAPGF GDRRKAMLQD IATLTGGTVI SEEIGMELEK ATLEDLGQAK RVVINKDTTT IIDGVGEEAA
GrpE     68  EMENLR ------ ---------- --RRTELDIE KAHKFALEKF IN---------- ---------- ----------
GroES    38  ---------- ---------- ---------- ---------- ---------- ---------- ----------
HslVU   227 EEEAAKLVNP EELKQDAIDA VEQHGIVFID EIDKICKRGE SSGPDVSRE- ---------- ----------
RpoH    103 SFAVHWIKAE IHEYVLRNWR IVKVATTKAQ RKLFFNLRKT KQRLGWFNQ- ---------- ----------
IbpB     65  ---------- ---------- ---------- ---------- ---------- ---------- ----------
HtpG    273 EYTSLLYIPS QAPWDMWNRD HKHGLKLYVQ RVFIMDDAEQ FMPNYLRFVR GLIDSSDLPL NVSREILQDS
ClpB    421 QLKLEQQALM KESDEASKKR LDMLNEELSD KERQYSELEE EWKAEKASLS GTQTIKAELE QAKIAIEQAR
cbpA     93  DFDDIFSSIF GQHARQSRQR P-ATRGHDIE IEVAVFLEET LTEHKRTI-- ---------- ----------

                    500         510         520         530         540         550         560
                    ....|....|  ....|....|  ....|....|  ....|....|  ....|....|  ....|....|  ....|.......|
DnaK    342 GQTRMPMVQK KVAEFFGKEP RKDVNPDEAV AIGAAVQGGV LTGDVKDVLL LDVTPLSLGI ETMGGVMTTL
DnaJ    159 QTCPTCHGSG QVQMRQGFFA VQQTCPHCQG RG--TLIKDP CNKCHGHGRV ERSKTLSVKI PAGVDTGDRI
GroEL   342 IQGRVAQIRQ QIEEATSDYD REKLQERVAK LAG-------- ---------- -----GVAVI KVGAATEVEM
GrpE     93  ---------- ---------- ---------- ---------- ---------- ----------ELL PVIDSLDRAL
GroES    38  ---------- ---------- ---------- ---------- ---------- ----------EVL AVGNG-----RI
HslVU   275 ---------- ---------- ---------- ---------- ---------- ----GVQRDLL PLVEGCTVST
RpoH    151 ---------- ---------- ---------- ---------- ---------- ---------DEVE MVARELGVTS
IbpB     65  ---------- ---------- ---------- ---------- ---------- ----------TRL SVKGTPEQPK
HtpG    343 TVTRNLRNAL TKRVLQMLEK LAKDDAEKYQ TF--WQQFGL VLKEGPAEDF ANQEAIAKLL RFASTHTDSS
ClpB    491 RVGDLARMSE LQYGKIPELE KQLEAATQLE GKTMRLLRN- ---KVTDAEI AEVLARWTGI PVSRMMESER
cbpA    139 --------SY NLPVYNAFGM IEQEIP---- ---------- ---------- ---KTLNVKI PAGVGNGQRI

                    570         580         590         600         610         620         630
                    ....|....|  ....|....|  ....|....|  ....|....|  ....|....|  ....|....|  ....|.......|
DnaK    412 IAKNTTIPTK HSQVFSTAED NQSAVTIHVL QGERKRAADN KSLGQFNLDG INPAPRGMPQ IEVTFDIDAD
DnaJ    227 RLAGEGEAGE HGAPAGD--- ---------- ---------- ----------------------LYVQVQVKQH
GroEL   390 KEKKARVEDA LHATRAAVEE G--------- ---------- ---------- ---------- ---- VVAGGGV
GrpE    107 EVADKANPDM SAMVEG------- ---------- ---------- ---------- ---------- ------IELTLK
GroES    49  LENGEVKP-- ---------- ---------- ---------- ---------- ---------- ------LDVKVG
HslVU   293 KHGMVKTDHI LFIASG------- ---------- ---------- ---------- ---------- --AFQIAKPS
RpoH    166 KDVREMESRM AAQDMT------- ---------- ---------- ---------- ---------- -------FDLSSD
IbpB     79  EEKKWLHQGL MNQPFS------- ---------- ---------- ---------- ---------- ------LSFTLA
HtpG    411 AQTVSLEDYV SRMKEGQEKI YYITADSYAA AKSSPHLELL RKKGIEVLLL SDRIDEWMMN YLTEFDGKPF
ClpB    557 EKLLRMEQEL HHRVIGQNEA VDAVSNAIRR SRAGLADPNR PIGSFLFLGP TGVGKTELCK ALANFMFDSD
cbpA    175 RLKGQGTPGE NGGPNGD--- ---------- ---------- ----------------------LWLVIHIAPH

                    640         650         660         670         680         690         700
                    ....|....|  ....|....|  ....|....|  ....|....|  ....|....|  ....|....|  ....|.......|
DnaK    482 GILHVSAKDK NSGKEQKITI KASSGLNEDE IQKMVRDAEA NAEADRKFEE LVQTRNQGDH LLHSTRKQVE
DnaJ    254 PIFEREGNNL YCEVPINFAM AALG------ ---------- GEIEVPTLDG RVKLKVPGET QTGKLFRMRG
GroEL   418 ALIRVASKLA DLRGQNEDQN VGIK------ --------VA LRAMEAPLRQ IVLNCGEEPS VVANTVKGGD
GrpE    129 SMLDVVR--- ----KFGVEV IAET------ ---------- NVPLDPNVHQ AIAMVESDDV APGNVLGIMQ
GroES    63  DIV------- ----------I FNDG------ ---------- YGVKSEKIDN EEVLIMSE-- --SDILAIVE
HslVU   317 DLIPELQGRL PIRVELQALT TSDF------ ---------- ERILTEPNAS ITVQYKALMA TEGVNIEFTD
RpoH    188 DDSDSQPMAP VLYLQDKSSN FADG------ ---------- IEDDNWEEQA ANRLTDAMQG LDERSQDIIR
IbpB    101 ENMEVSG--- ---------- ---------- ---------- -ATFVNGLLH IDLIRNEPEP IAAQRIAISE
HtpG    481 QSVSKVDESL EKLADEVDES AKEA------ ---------- EKALTPFIDR VKALLGERVK DVRLTHRLTD
ClpB    627 EAMVRIDMSE FMEKHSVSRL VGAPPGYVG- YEEGGYLTEA VRRRPYSVIL LDEVEKAHPD VFNILLQVLD
cbpA    202 PLFDIVGQDL EIVVPVSPWE AALG------ ---------- AKVTVPTLKE SILLTIPPGS QAGQRLRVKG

                    710         720         730         740         750         760         770
                    ....|....|  ....|....|  ....|....|  ....|....|  ....|....|  ....|....|  ....|.......|
DnaK    552 EAGDKLPADD KTAIESALTA LETALKGEDK AAIEAKMQEL AQVSQKLMEI AQQQHAQQQT AGADASANNA
DnaJ    308 KGVKSVRGGA QGDLLCRVVV ETPVGLNERQ KQLLQELQES FGGPTGEHNS PRSKSFFDGV KKFFDDLTR-
GroEL   474 GNYGYNAATE EYGNMIDMGI LDPTKVTRSA LQYAASVAGL MITTECMVTD LPKNDAADLG AAGGMGGMGG
GrpE    176 KGYTLNG---- -RTIRAAMVT VAKAKA------ ---------- ---------- ---------- ----------
GroES    97  A---------- ---------- ---------- ---------- ---------- ---------- ----------
HslVU   371 SGIKRIAEAA WQVNESTENI GARRLHTVLE RLMEEISYDA SDLSGQNITI DADYVSKHLD ALVADEDLSR
RpoH    242 ARWLDEDNKS TLQELADRYG VSAERVRQLE KNAMKKLRAA IEA------- ---------- ----------
IbpB    137 RPALNS ------ ---------- ---------- ---------- ---------- ---------- ----------
HtpG    535 TPAIVSTDAD EMSTQMAKLF AAAGQKVPEV KYIFELNPDH VLVKRAADTE DEAKFSEWVE LLLDQALLAE
ClpB    696 DGRLTDGQGR TVDFRNTVVI MTSNLGSDLI QERFGELDYA HMKELVLGVV SHNFRPEFIN RIDEVVVFHP
cbpA    256 KGLVSKK--Q TGDLYAVLKI VMPPKPDENT AALWQQLAD- ---------- --AQSSFDPR KDWGKA----

                    780         790         800         810         820         830         840
                    ....|....|  ....|....|  ....|....|  ....|....|  ....|....|  ....|....|  ....|.......|
DnaK    622 KDDDVVDAEF EEVKDKK--- ---------- ---------- ---------- ---------- ----------
DnaJ    376 ---------- ---------- ---------- ---------- ---------- ---------- ----------
GroEL   544 MGGMM------- ---------- ---------- ---------- ---------- ---------- ----------
GrpE    197 ---------- ---------- ---------- ---------- ---------- ---------- ----------
GroES    97  ---------- ---------- ---------- ---------- ---------- ---------- ----------
HslVU   441 FIL---------- ---------- ---------- ---------- ---------- ---------- ----------
RpoH    284 ---------- ---------- ---------- ---------- ---------- ---------- ----------
IbpB    142 ---------- ---------- ---------- ---------- ---------- ---------- ----------
```



© University of Venda

```
HtpG     605 RGTLEDPNLF IRRMNQLLVS ---------- ---------- ---------- ---------- ----------
ClpB     766 LGEQHIASIA QIQLKRLYKR LEERGYEIHI SDEALKLLSE NGYDPVYGAR PLKRAIQQQI ENPLAQQILS
cbpA     306 ---------- ---------- ---------- ---------- ---------- ---------- ----------

                        850           860
                 ....|....|....|....|....|..
DnaK     638 ---------- ---------- ---------- ----
DnaJ     376 ---------- ---------- ---------- ----
GroEL    548 ---------- ---------- ---------- ----
GrpE     197 ---------- ---------- ---------- ----
GroES    97  ---------- ---------- ---------- ----
HslVU    443 ---------- ---------- ---------- ----
RpoH     284 ---------- ---------- ---------- ----
IbpB     142 ---------- ---------- ---------- ----
HtpG     624 ---------- ---------- ---------- ----

ClpB     836 GELVPGKVIR LEVNEDRIVA VQ
cbpA     306 ---------- ---------- ----
```

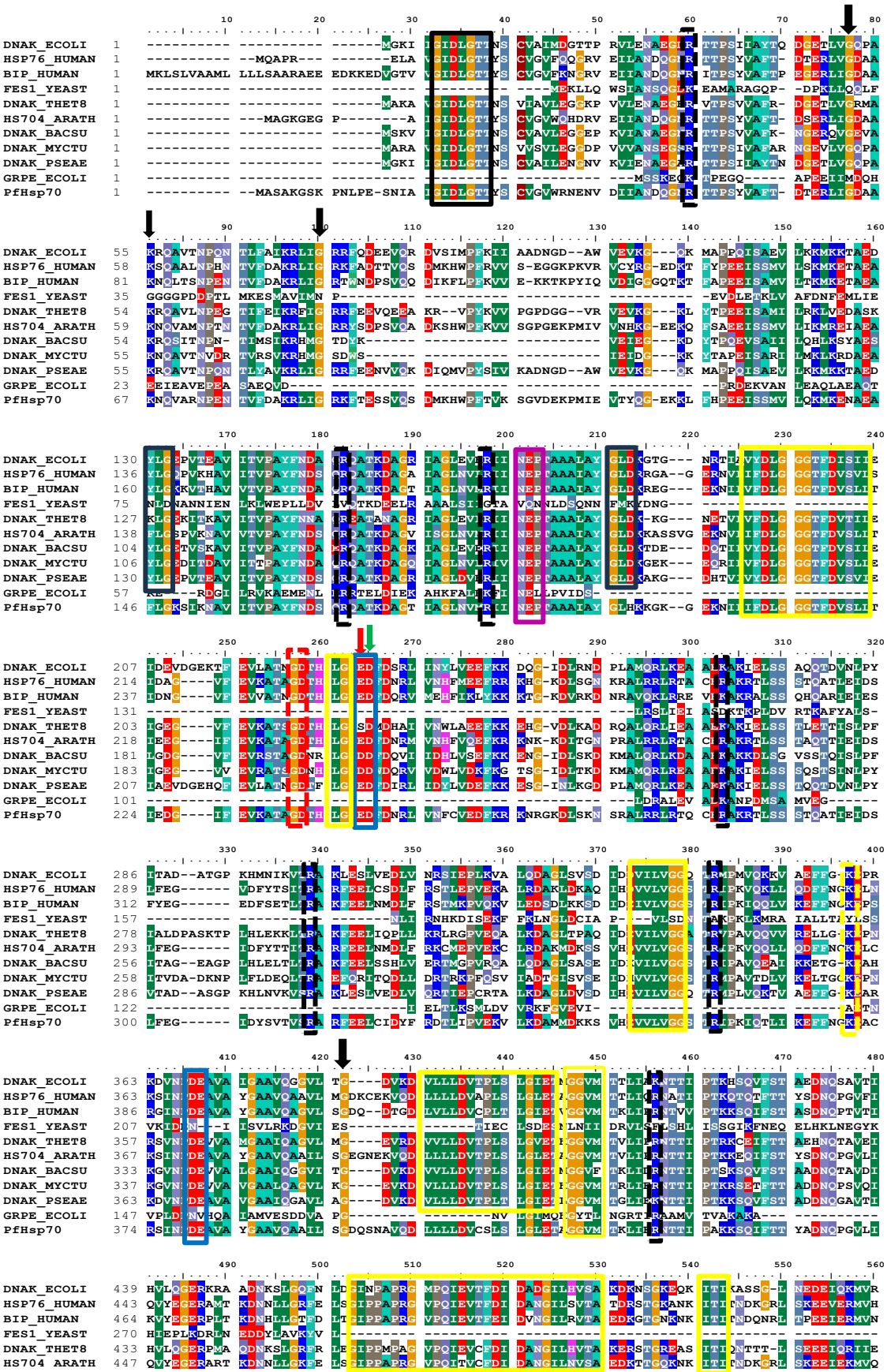
**Figure 5. 2.** Sequence analysis of *E. coli* DnaK and its predicted networks.

The above observed sequence alignment shows no strongly or fully identical or conserved residues in all sequences, which suggest that these networks may be associated with DnaK by their structure and functional behavior (Szklarczyk et al., 2019).

### 5.3.2. Analysis of sequence similarity between *E. coli* DnaK, Arabidopsis thaliana, Thermus thermophilus, Bacillus subtilis, human, yeast and Mycobacterium tuberculosis, Pseudomonas aeruginosa counterparts and homologs, and plasmodium falciparum.



© University of Venda






© University of Venda

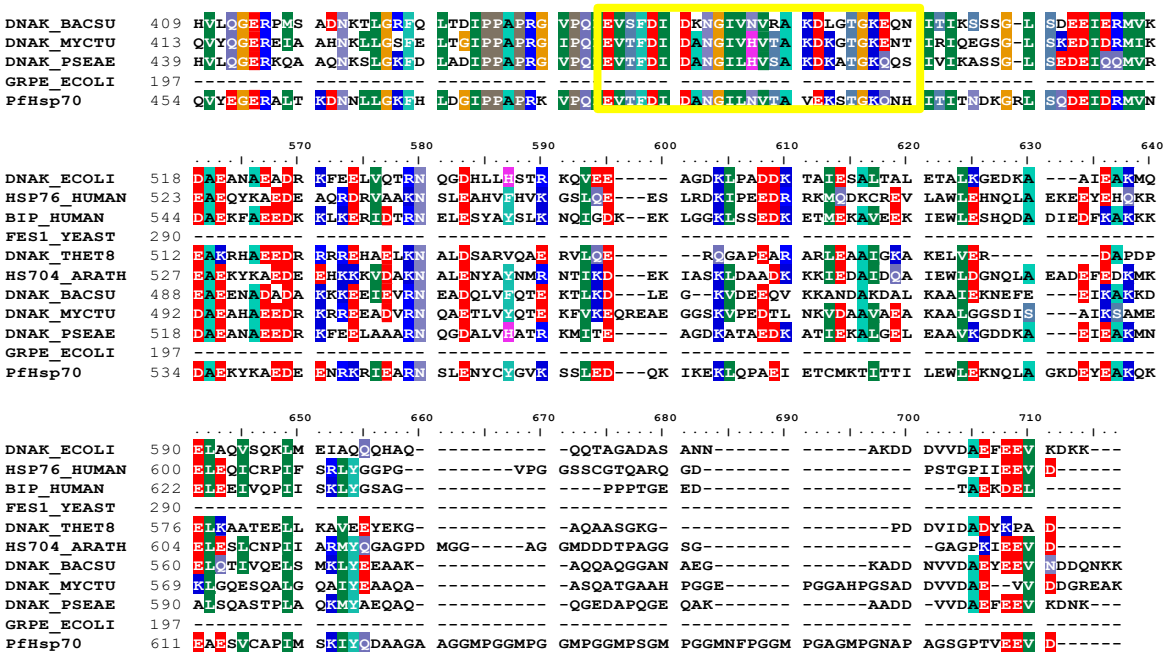



**Figure 5. 3.** Sequence analysis of *E. coli* DnaK against Arabidopsis thaliana, Thermus thermophilus, Bacillus subtilis, human, yeast and Mycobacterium tuberculosis, Pseudomonas aeruginosa counterparts and homologs, and plasmodium falciparum.

DnaK binds and hydrolyses ATP through Switch I and Switch II motifs, Walker A, Walker B motifs, and HPD (His-Pro-Asp) motifs (Mayer, 2013). with highlighted residues presenting (i). Highly conserved; (ii). Strongly conserved; (iii) semi-conserved residues. The residues that are highlighted represent Walker A (outlined in a Black arrow) and Walker B (outlined in a blue box), highly conserved regions (outlined in Black box) which are responsible for adenosine triphosphate (ATP) binding and hydrolysis, respectively (Walker *et al*., 1982; Miller & Enemark, 2016). Arginine Finger (Black dashed box) is used as a protein aggregation, protein-protein interactions suppressor during protein refolding (Arakawa *et al*., 2007). Lysine finger (Yellow dashed box) is also responsible for ATP Binding and hydrolysis, while NEP residues (Purple box) serving as crucial individual residues by stabilizing the substrate-binding domain or facilitating interactions with co-chaperones (Mayer *et al*., 2005). Asp amino acid modulates $Mg^{2+}$, and Gln amino acid is essential for ATP hydrolysis, as shown by a green arrow and red arrow, respectively (Kanade *et al*., 2020). Conserved residues are represented by a (yellow box) and motifs conserved with *E. coli* DnaK (dashed red box).



© University of Venda

The results of the sequence analysis showed similar Walker A and B motifs across all proteins (Figure 5.3). The conserved motifs in certain proteins may indicate or suggest a close relationship in function. The similar functional motifs that these molecules share could defend their similar mechanism of action.

### 5.3.3. Phylogenetic analysis of *E. coli* DnaK and its homologs and orthologues

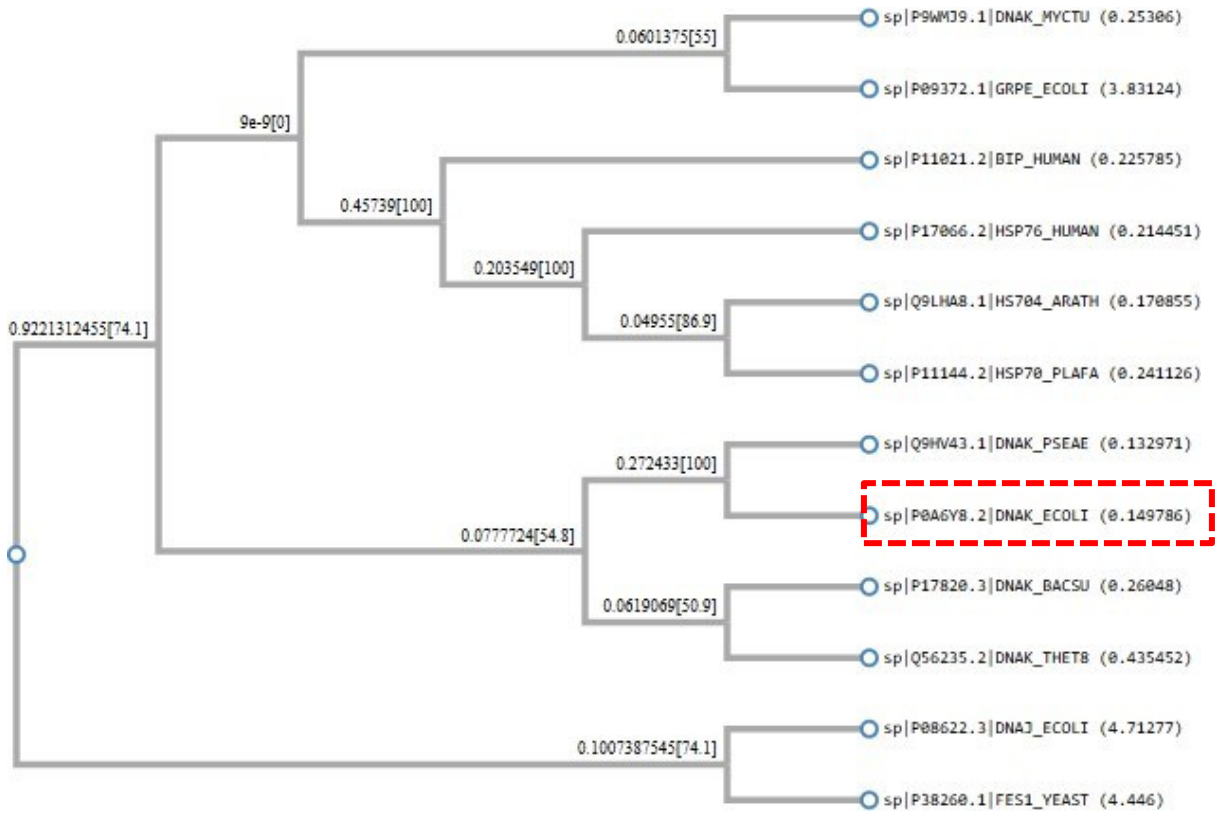



**Figure 5. 4.** Evolutional analysis of *E. coli* DnaK against its homologues and counterparts.

The similarity percentage is shown in the tree square bracket. With protein of interest (DnaK) outlined by Red dashed box. *Escherichia coli* DnaK (P0A6Y8), Homo sapiens HSP76 (P17066), Homo sapiens BiP (P11021), Saccharomyces cerevisiae Ssa1 (P38260), Thermus thermophilus DNAK_THET8 (Q56235), hsp70 (Arabidopsis thaliana) HS704_ARATH (sp|Q9LHA8), Bacillus subtilis DNAK_BACSU (sp|P17820), Mycobacterium tuberculosis DNAK_MYCTU (sp|P9WMJ9), Pseudomonas aeruginosa



© University of Venda

DNAK_PSEAE (sp|Q9HV43), *Escherichia coli* DnaJ (sp|P08622), *Escherichia coli* GrpE _ ECOLI (sp|P09372), HSP70_PLAFA (P11144.2).

Results from the phylogenetic tree show that by origin, DNAK_PSEAE and DNAK_*E. COLI* are closely related to DNAK_MYCTU, HSP70_PLAFA, and DNAK_*E. COLI* and DNAJ_ECOLI are highly divergent, as indicated by the long branch distances (0.25306, 0.241126, and 4.71277 units, respectively). Branches with a support value of 100 (e.i., BIP Human, HSP76 Human, DNAK_PSEAE, and DNAK_E_COLI) show strong evidence for the grouping of these sequences, suggesting these sequences share a relatively recent common ancestor and are closely related. These results support the suggestion by Duncan et al., 2015 that DnaK_MYCTU is closely related to *E. coli* DnaK. Similarly, DNAK_BACSU (from *Bacillus subtilis*) groups separately but is still more closely related to the *E. coli* DNAK proteins than to other distantly related sequences such as FES1_YEAST. Human (HSP76_HUMAN) and plant (*Arabidopsis thaliana*, HS70_ARATH) heat shock proteins are clustered more distantly from the bacterial DnaK proteins, showing greater evolutionary divergence. More interestingly, Hsp70 proteins from humans, plants, and yeast are more distantly related to bacterial DnaK proteins, reflecting the divergence between eukaryotic and prokaryotic lineages. The strong support values indicated confidence in the above evolutionary relationships.

### 5.3.4. Secondary structure analysis of *E.coli* DnaK-like proteins against its homologs and orthologues

**Table 5.1: Secondary structures features**

| Protein | Helix % | B-strand % | Disordered % | Confidence % | Coverage % |
|---|---|---|---|---|---|
| *E. coli* DnaK | 35 | 25 | 14 | 100 | 94 |
| HSP76 | 32 | 26 | 12 | 100 | 84 |
| BIP | 34 | 26 | 12 | 100 | 93 |
| FES1_YEAST(Ssa1) | 66 | 0 | 20 | 99.8 | 96 |
| DNAK_THET8 | 35 | 27 | 11 | 100 | 82 |



© University of Venda

| | | | | | |
|---|---|---|---|---|---|
| HS704_ARATH | 32 | 26 | 14 | 100 | 83 |
| DNAK_BACSU | 35 | 28 | 16 | 100 | 82 |
| DNAK_MYCTU | 35 | 27 | 17 | 100 | 81 |
| DNAK_PSEAE | 36 | 25 | 16 | 100 | 94 |
| DNAJ_ECOLI | 20 | 23 | 35 | 100 | 71 |
| GRPE_ECOLI | 45 | 16 | 29 | 100 | 77 |
| HSP70_PLAFA | 31 | 25 | 17 | 100 | 79 |

Prediction of *E. coli* DnaK protein counterparts and homologs secondary structures. Features predicted using Phyre2 tool.

The secondary structure analyses that were predicted demonstrated a high level of confidence as compared to the prediction of disordered regions. According to the results, there was a slightly difference in the percentage contribution of secondary features (Table 5.1). Conserved regions amongst these proteins from sequence alignment results **(**figure **5.3**) could be justified by the above observed secondary structure analysis (Table 5.1).

### 4.3.5. Biophysiological properties of *E. coli* DnaK and its predicted counterparts and homologs

**Table 5.2: In-silico prediction of biophysiological properties.**

| **Description** | **No. of amino acids** | **Molecular weight** | **Theoretical pI** | **Extinction coefficient** | **Half life** | **Instability index** | **Aliphatic index** | **Gravy** |
|---|---|---|---|---|---|---|---|---|
| DnaK | 638 | 69114.96 | 4.83 | 15930 | 10 hours | 34.15 | 88.57 | -0.409 |
| DNAJ_ECOLI | 376 | 41100.33 | 7.98 | 14900 | 10 hours | 32.81 | 63.80 | -0.634 |
| GRPE_ECOLI | 197 | 21797.83 | 4.68 | 1490 | 10 hours | 40.60 | 94.11 | -0.372 |
| HSP70_PLAFA | 681 | 74287.34 | 5.50 | 39350(Not reduced) 38850(reduced) | 10 hours | 41.09 | 80.09 | -0.409 |
| HSP76 | 643 | 71028.14 | 5.81 | 32360 (not reduced) 31860 (reduced) | 30 hours | 38.39 | 80.86 | -0,460 |



© University of Venda

| | | | | | | | | |
|---|---|---|---|---|---|---|---|---|
| BIP | 654 | 72332.96 | 5.07 | 30495 (not reduced) 30370(reduced) | 10 hours | 32.10 | 85.70 | -0.487 |
| Ssa1(YEAST Hsp70) | 290 | 32604.41 | 4.92 | 20065 (not reduced) 19940 (reduced) | 20 hours | 46.21 | 106.97 | -0.242 |
| DNAK_THET8 | 615 | 66824.41 | 5.32 | 14565 (not reduced) 14440(reduced) | 10 hours | 38.31 | 97.24 | -0.272 |
| HS704_ARATH | 650 | 71101.45 | 5.13 | 36245 (not reduced) 35870 (reduced) | 10 hours | 32.76 | 81.20 | -0.434 |
| DNAK_BACSU | 611 | 66002.12 | 4.76 | 13410 (not reduced) 13410 (reduced) | 10 hours | 34.18 | 89.39 | -0.428 |
| DNAK_MYCTU | 625 | 66830.86 | 4.85 | 28420 | 10 hours | 28.37 | 88.34 | -0.368 |
| DNAK_PSEAE | 637 | 68403.21 | 4.79 | 20525 (not reduced) 20400 (reduced) | 10 hours | 34.05 | 91.00 | -0.326 |

Biophysiological properties of *E. coli* DnaK with HSP76 (Human Hsp70), BIP (HUMAN Endoplasmic reticulum chaperone), Ssa1 (YEAST Hsp70), DNAK_THET8 (Thermus thermophilus DnaK), HS704_ARATH (hsp70 Arabidopsis thaliana), DNAK_BACSU (DnaK Bacillus subtilis), DNAK_MYCTU (Mycobacterium tuberculosis DnaK), DNAK_PSEAE (DnaK Pseudomonas aeruginosa), DNAJ_ECOLI, GRPE_ECOLI, and HSP70_PLAFA (P11144.2) were predicted using expasy tool.

GRPE_ECOLI, HSP70_PLAFA (PfHsp70), and Ssa1(YEAST Hsp70) were both predicted to be unstable while other homologs are stable; this is shown by high aliphatic index and low instability index presenting unstable stable proteins, respectively (Table 5.2).



© University of Venda

### 4.3.6. Molecular Docking

Molecular docking is the most common computational structure-based drug design (SBDD) method and was first described in 1982 (Kuntz *et al*., 1982; Read *et al*., 2011; Berry *et al*., 2015; Zhao *et al*., 2020). It consists of two main jobs, each of which is handled by a distinct algorithm. The several confirmations or poses that the ligand can adopt inside the binding or active pocket are predicted by the sampling algorithm. For each predicted pose, the binding energies between the ligand and receptor are then predicted by a scoring function. Following that, the generated binding poses are classified according to their binding energies, with the top-ranked position representing the ligand's correct confirmation (Phatak *et al*., 2009).

According to Ogura et al. (2004), DnaK proteins are categorized under the ASCE group and are members of the AAA+ class of proteins. Walker A motif is necessary for binding ATP's phosphate to regulate the conformational changes that propel ATP. The Walker A motif regulates conformational changes that drive ATP and is crucial for binding the phosphate of ATP. In contrast, the Walker B motif is critical in ATP hydrolysis and coordinating magnesium ions (Ogura *et al*., 2004).

Following the results observed in ATPase activity (Chapter 3, Figure 3.4), It was also of interest to understand or evaluate the molecular interactions and binding mechanism between ATP and DnaK and its co-chaperone DnaJ. Molecular docking gave an insight into how these proteins bind to ATP by identifying residues involved in the interaction, specific binding sites, and binding energy between the molecules. The results obtained from this investigation support the experimental ATPase activity obtained results.



© University of Venda

**Results: In-silico binding analysis of *E. coli* DnaK and its co-chaperone DnaJ to Adenosine triphosphate (ATP)**

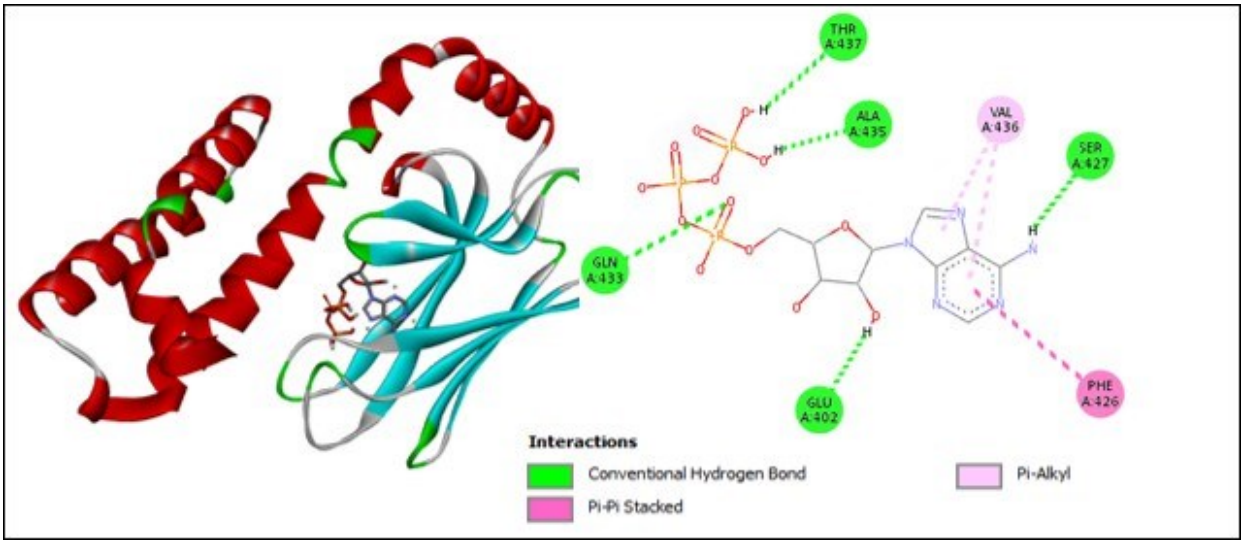



**Figure 5. 5.** ATP binding to DnaK

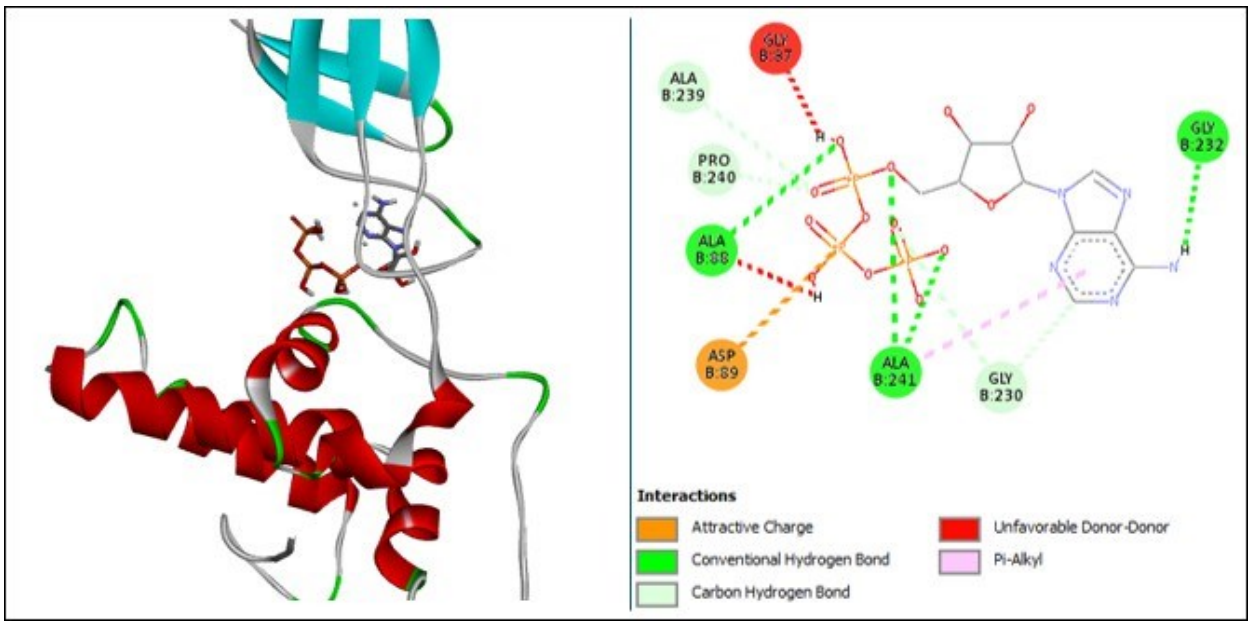



**Figure 5. 6.** ATP binding to DnaJ



© University of Venda

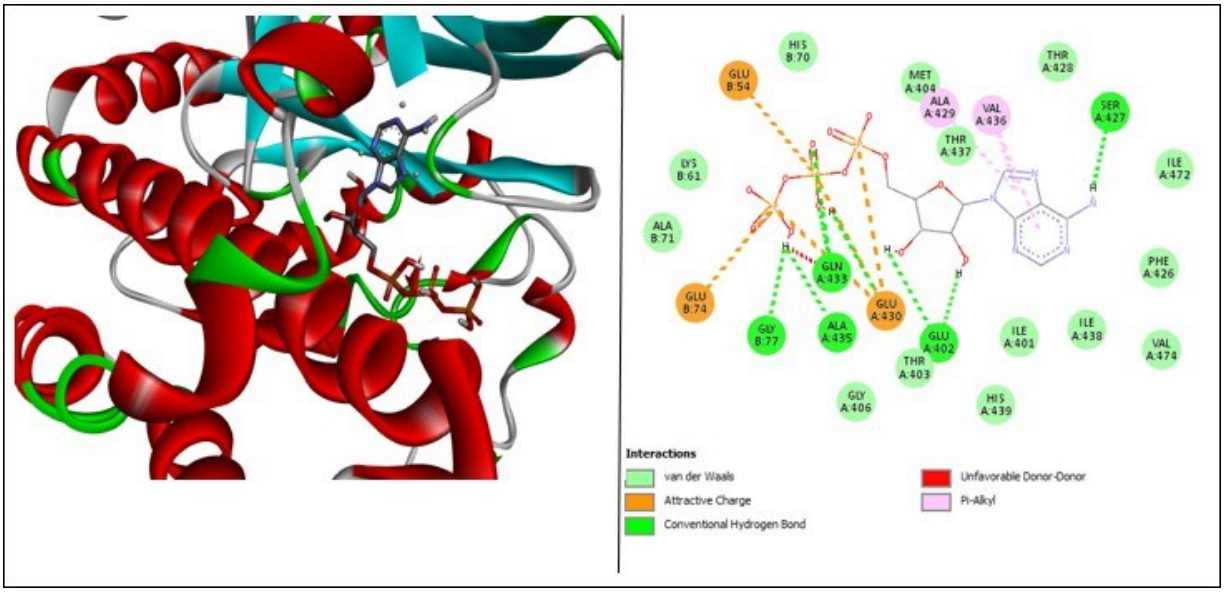



**Figure 5. 7.** ATP binding to DnaK-DnaJ

**Table: 5.3**

| **Macromolecule** | **Ligand** | **Binding affinity (kcal/mol)** | **RMSD/ub** | **RMSD/lb** |
|---|---|---|---|---|
| DnaK | ATP | -7.0 | 0.0 | 0.0 |
| DnaJ | ATP | -6.8 | 0.0 | 0.0 |
| DnaK-DnaJ | ATP | -8.4 | 0.0 | 0.0 |

A low binding affinity was observed between ATP and DnaJ. In comparison with DnaK, DnaJ showed a lower binding affinity for ATP compared to DnaK. However, this has been previously supported by studies such as Liberek *et al*. (1991) and Mayer and Bukau (2005), which confirmed that the role of DnaJ is not primarily dependent on strong ATP binding but, instead, on interacting with DnaK to stimulate its ATPase cycle (Table 5.3). Subsequently, the DnaK-DnaJ complex showed a strong affinity to ATP as compared to DnaK.

Although significantly lower, the individual affinities for DnaK and DnaJ (-7.0 and -6.8 kcal/mol) are close. This aligns with previous findings from studies showing that DnaK's chaperone function depends on its ATPase activity, with DnaJ as a co-chaperone regulating DnaK's ATP binding and hydrolysis (Liberek *et al*., 1991). Previous studies have also evaluated ATP binding affinities for



© University of Venda

DnaK and DnaJ; for instance, their study further supported the idea that DnaJ acts as a co-chaperone that elevates the ATPase activity of DnaK through a direct interaction with Hsp70, which was echoed in the above findings (Table 5.3).

*E. coli* DnaJ and protein substrates synergistically stimulate the rate of ATP hydrolysis by more than 1000-fold (Laufen *et al*., 1999; Karzai & McMacken, 1996; Liberek *et al*., 1991). A study done by Laufen *et al*. (1999) proved that the DnaK-DnaJ complex usually increases stability and functional activity when bound to ATP, thus enhancing protein folding efficiency. Correspondingly, the in-silico binding mechanism from this study supports this synergy by the more negative binding energy observed above for the DnaK-DnaJ complex.

The higher binding affinity for ATP in the DnaK-DnaJ complex, which occurs in the presence of both DnaK and DnaJ, may indicate a functional advantage that enhances protein folding ability in cellular stress responses; this was further recently supported by a study done by (Rosenzweig *et al*., 2019), demonstrating that the presence of a co-chaperone enhances stability and ATP cycling, subsequently increases the efficiency of the chaperone system.



© University of Venda

***In-silico*** **binding analysis of** ***E. coli*** **DnaK and its clusters to** ***Senna alexandrina*** **phytochemicals**

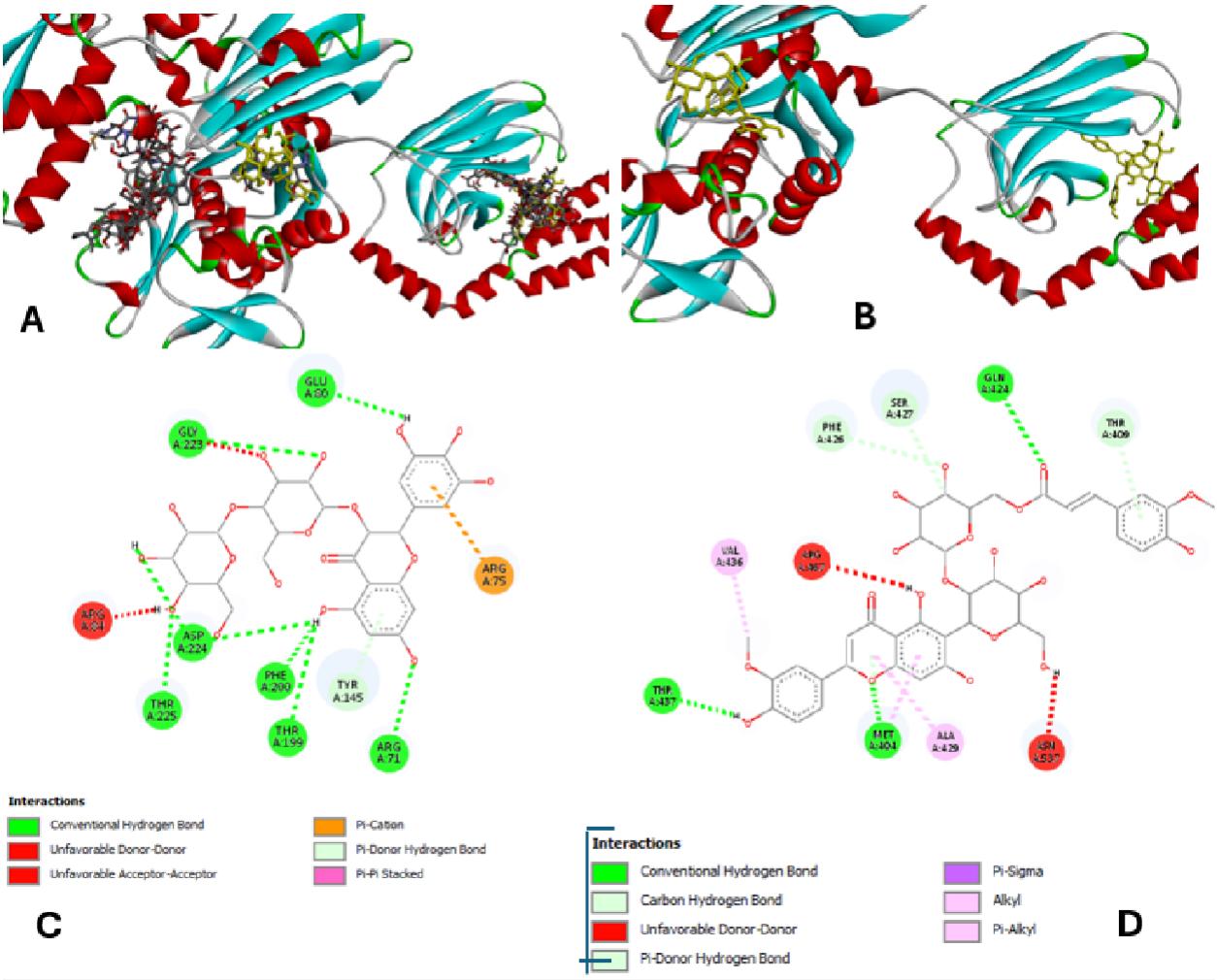



**Figure 5. 8.** Competitive binding studies of molecular docking of multiple ligands on DnaK (A), with two compounds (B), which showed the highest binding affinity (highlighted with yellow) for DnaK compared to 15 other compounds.

2D diagram of the amino acids residues contributing to binding affinity and stability through hydrogen bonding, hydrophobic interactions, pi-stacking, and other interactions are highlighted with different colors (C and D), with (C) representing the compound named: 3-[(2S,3R,4R,6R)-3,4-dihydroxy-6-(hydroxymethyl)-5-[(2S,3R,4S,5R,6R)-3,4,5-trihydroxy-6-(hydroxymethyl)oxan-2-yl]oxyoxan-2-yl]oxy-5,7-dihydroxy-2-(3,4,5-tri hydroxyphenyl)-2,3-dihydrochromen-4-one and (D) representing: Isoscoparin 2''-(6-(E)-ferulylglucoside).



© University of Venda

**Table: 5.4**

| Macro-molecule | Ligand | Binding affinity (kcal/mol) | RMSD/ub | RMSD/lb |
|---|---|---|---|---|
| DnaK | (2S)-2-[[8-[[(1S)-1-carboxy-5-methyl-4-oxohexyl]amino]-8-oxooctanoyl]amino]-6-methyl-5-oxoheptanoic acid | -6.1 | 0.0 | 0.0 |
| DnaK | [(2S,3R,4S,5R,6S)-6-[(2S,3R,4S,5S,6R)-4,5-dihydroxy-2-[5-hydroxy-7-methoxy-2-(4-methoxyphenyl)-4-oxochromen-6-yl]-6-(hydroxymethyl)oxan-3-yl]oxy-4,5-dihydroxy-2-methyloxan-3-yl] acetate | -7.9 | 0.0 | 0.0 |
| DnaK | 1-(4-hydroxyphenyl)-3-[2,4,6-trihydroxy-3,5-bis[(2S,3R,4R,5S,6R)-3,4,5-trihydroxy-6-(hydroxymethyl)oxan-2-yl]phenyl]propane-1,3-dione | -7.3 | 0.0 | 0.0 |
| DnaK | 3-[(2S,3R,4R,6R)-3,4-dihydroxy-6-(hydroxymethyl)-5-[(2S,3R,4S,5R,6R)-3,4,5-trihydroxy-6-(hydroxymethyl)oxan-2-yl]oxyoxan-2-yl]oxy-5,7-dihydroxy-2-(3,4,5-trihydroxyphenyl)-2,3-dihydrochromen-4-one | **-8.1** | 0.0 | 0.0 |
| DnaK | Boc-DL-Gln-DL-N(Bu)nTyr-NHPh(4-OMe) | -6.9 | 0.0 | 0.0 |
| DnaK | ditert-butyl (2S,4S)-4-[bis[(2-methylpropan-2-yl)oxycarbonyl]amino]-5-oxopyrrolidine-1,2-dicarboxylate | -5.9 | 0.0 | 0.0 |
| DnaK | Elatin (flavonoid) | -7.5 | 0.0 | 0.0 |
| DnaK | Gamma-Tocotrienol | -7.1 | 0.0 | 0.0 |
| DnaK | H-DL-Cys-DL-Lys-DL-Ala-DL-Leu-DL-xiThr-DL-Asn-DL-Glu-DL-Ala-OH | -4.9 | 0.0 | 0.0 |
| DnaK | Isoscoparin 2"-(6-(E)-ferulylglucoside) | **-8.3** | 0.0 | 0.0 |
| DnaK | Isovitexin | -7.7 | 0.0 | 0.0 |
| DnaK | Linoside A | -7.9 | 0.0 | 0.0 |
| DnaK | Methyl 4-[2-[N-acetyl-3-methoxy-4-[2-[methoxy(methyl)amino]ethyl-[(2-methyl phenyl)carbamoyl]amino]anilino]ethoxy]benzoate | -6.7 | 0.0 | 0.0 |
| DnaK | Rutin | -7.9 | 0.0 | 0.0 |
| DnaK | Vicenin-1 | -7.3 | 0.0 | 0.0 |
| DnaK | Vicenin-2 | -7.6 | 0.0 | 0.0 |
| DnaK | Vicenin-3 | -7.5 | 0.0 | 0.0 |



© University of Venda

To predict the possible binding, as well as identify possible binding sites of Selected Senna alexandrina compounds on DnaK and its clusters, AutoDock Vina was used. Docking was initiated, and upon completion of the docking, an output file with several binding modes was generated together with a log file scoring the modes in terms of binding affinity (in kcal/mol). The output files (in pdbqt format) were viewed in Discovery Studio Visualizer software and converted to PDB files. The receptor-ligand interactions were then performed in Discovery Studio Visualizer, generating the above images.

Affinity testing for 17 extracted compounds was performed on one protein target (DnaK); as a result, two compounds (Figure 5.8) (highlighted with yellow), namely: Isoscoparin 2''-(6-(E)-ferulylglucoside) and 3-[(2S,3R,4R,6R)-3,4-dihydroxy-6-(hydroxymethyl)-5-[(2S,3R,4S,5R,6R)-3,4,5-trihydroxy-6-(hydroxymethyl)oxan-2-yl]oxyoxan-2-yl]oxy-5,7-dihydroxy-2-(3,4,5-trihydroxyphenyl)-2,3-dihydrochromen-4-one showed the highest binding affinity for DnaK as compared to the other 15 compounds.

These compounds bound to DnaK at notable predicted scores of -8.1 kcal/mol (3-[(2S,3R,4R,6R)-3,4-dihydroxy-6-(hydroxymethyl)-5-[(2S,3R,4S,5R,6R)-3,4,5-trihydroxy-6-(hydroxymethyl)oxan-2-yl]oxyoxan-2-yl]oxy-5,7-dihydroxy-2-(3,4,5-trihydroxyphenyl)-2,3-dihydrochromen-4-one ) and -8.3 kcal/mol (Isoscoparin 2''-(6-(E)-ferulylglucoside)), respectively. Thus, they were of interest in continuing with inhibiting DnaK and its clusters to investigate the mechanisms of their antibacterial activities. These targets were DnaK-DnaJ, DnaK-CPBA, DnaK-CLPB, DnaK-GROEL, DnaK-GROES, DnaK-GRPE, DnaK-HSLU, DnaK-HSLV, DnaK-HTPG, and DnaK-RPOH. Furthermore, all two compounds were again docked simultaneously, and showed different binding affinities for DnaK clusters, with stronger binding affinities than when they were docked DnaK only. DnaK and DnaJ were selected for the docking investigations since they are the most important drug targets for antibacterial activities. Inhibiting DnaK and DnaJ may result in non-functional or misfolded protein accumulation, disrupting crucial cellular functions and activities; the bacteria's inability to defend/protect against protein damage under stress may lead to aggregation and cell death (Hipp & Hartl, 2024). To indicate that the chosen parameters and methodologies were best for selecting the ideal docking pose, the docking technique was validated with RMSD values below 1.0.



© University of Venda

Molecular docking studies were conducted to assess the tendency of selected *Senna alexandrina* phytocompounds to bind to DnaK and its clusters. Upon docking results, two compounds exhibited the highest binding affinity for DnaK, resulting in them being of best interest to continue docking with compared to the remaining 15 phytocompounds. Isoscoparin 2"-(6-(E)-ferulylglucoside) and 3-[(2S,3R,4R,6R)-3,4-dihydroxy-6-(hydroxymethyl)-5-[(2S,3R,4S,5R,6R)-3,4,5-trihydroxy-6-(hydroxymethyl)oxan-2-yl]oxyoxan-2-yl]oxy-5,7-dihydroxy-2-(3,4,5-trihydroxyphenyl)-2,3-dihydrochromen-4-one were the two compounds chosen with highest binding affinity, and they were successfully docked onto DnaK clusters, and the affinities, and molecular docking complexes were determined in each case (Appendix D, Figure D.6 to figure D.14, Table D.5).

In conclusion, the observed results show that Isoscoparin 2"-(6-(E)-ferulylglucoside) had the highest binding affinity for DnaK clusters than 3-[(2S,3R,4R,6R)-3,4-dihydroxy-6-(-(hydroxymethyl)-5-[(2S,3R,4S,5R,6R)-3,4,5-trihydroxy-6-(hydroxymethyl)oxan-2-yl]oxyoxan-2-yl]oxy-5,7-dihydroxy-2-(3,4,5-trihydroxyphenyl)-2,3-dihydrochromen-4-one, the more amino acid interactions between Isoscoparin 2"-(6-(E)-ferulylglucoside) and DnaK clusters further support the stronger binding affinity observed.

However, 3-[(2S,3R,4R,6R)-3,4-dihydroxy-6-(-(hydroxymethyl)-5-[(2S,3R,4S,5R,6R)-3,4,5-trihydroxy-6-(hydroxymethyl)oxan-2-yl]oxyoxan-2-yl]oxy-5,7-dihydroxy-2-(3,4,5-trihydroxyphenyl)-2,3-dihydrochromen-4-one, showed stronger binding affinity than Isoscoparin 2"-(6-(E)-ferulylglucoside) when bound to DnaK-HSLU; DnaK-HSLV and DnaK-RPOH only, which was -9.0; -9.3; -9.2 (Appendix D, Table D.5). In addition, Isoscoparin 2"-(6-(E)-ferulylglucoside) showed stronger binding affinity for DnaK-HTPG (-9.9kca/mol) than other clusters, followed by DnK-DnaJ, DnaK-GROES as compared to other clusters, with a similar affinity of -9.8 and -9.8 kcal/mol, respectively.

Furthermore, findings from this study suggest that Isoscoparin 2"-(6-(E)-ferulylglucoside) can be used as possible drug candidate against diseases and infections associated with E. coli by targeting DnaK. The insights gained in this work can further be used in experimental studies for drug design in the treatment of bacterial infections with novel targets and mechanism of action. These findings suggest that Isoscoparin 2"-(6-(E)-ferulylglucoside) from *Senna alexandrina* and other related



© University of Venda

compounds, prior to those with higher binding affinity that target DnaK and its clusters could serve as possible drug candidates against infectious diseases associated with *E. coli*.



© University of Venda

# Chapter 6

**Discussion, Conclusions, and Future Perspectives**



© University of Venda

# CHAPTER 6: Discussion, Conclusions and Future Perspectives

## 6.1. Discussion

This chapter details the discussion and conclusion of the interpreted results. Furthermore, this chapter aims to discuss the data generated, compare it with findings from other studies, and further align findings from this study with those from other studies that support or contradict it.

*Escherichia coli* (*E. coli*) is a bacterium that is commonly found in the lower intestine of warm-blooded organisms. Most *E. coli* strains are harmless, but some can cause serious food poisoning (Malabadi *et al*., 2024). Infections and diseases caused by *E.coli* include, Bloodstream infections; Prostatitis (prostate infection); Pelvic inflammatory disease (PID); Gallbladder infection (cholecystitis); wound infections (Paitan, 2018).

The current study initially sought, therefore, to determine the effect of SA-AgNPs on functional features and in modulating the tertiary structural conformations of DnaK *in vitro*. FTIR and LC-MS were used in addition to the UV-Vis obtained results for further suitable phytochemical profiling and constituent identification. Compounds from *Senna alexandrina* leaf extract were identified and profiled using UHPLC-qTOF-MS. Several phytochemicals in *Senna alexandrina* extracts found in this study have also been identified in numerous studies (Cantarelli *et al*., 2011; Leelavathi & Udayasri, 2011; El-Morsy, 2013). *S. alexandrina* extract was used successfully as a reducing and capping agent for synthesizing AgNPs. The clear change of color solution due to surface Plasmon vibrations was accomplished during the reaction as the first indication of the formation of silver nanoparticles (Viswanathan & Nallamuthu, 2012; Lu et al., 2009). The color change from light yellow to dark brown was observed within 30 minutes after adding 3 ml of Senna alexandrina leaf extract. Furthermore, it was important to carry out the study using 4 and 5 mM of silver nitrate, as it revealed short peaks at 420 to 450 nm. To further confirm the formation of Ag-NPs, the surface plasmon resonance band at 420 nm (Figure 2.3) revealed by ultra-violet spectroscopy was used as additional confirmation that Ag-NP had formed in relation to the observed color change. Furthermore, Fourier transform infrared spectroscopy (FTIR) confirmed the bioreducing capacity of the *Senna alexandrina* leaf extract. Findings from this study confirmed the green synthesis protocol as an eco-friendly, simple, rapid, and alternative conventional physical/chemical method. Only 30 minutes were required for the conversion of silver ions into silver nanoparticles without the involvement of any hazardous chemicals. FTIR



© University of Venda

was used to identify the compounds responsible for reducing silver ions and identify functional groups present in the plant extract.

Furthermore, circular dichroism and fluorescence spectroscopy established that recombinant DnaK is stable at SA-AgNPs concentrations less than 1.8 µg/ml and the protein was unstable at concentrations beyond 1.8 µg/ml SA-AgNPs. In addition, the ATPase activity of recombinant DnaK increased in the presence of SA-AgNPs at 2.5 µg/ml. Moreover, the ability of DnaK to suppress aggregation of MDH in presence of AgNPs in vitro was less as compared to AgNPs alone, and the presence of >2.5 µg/ml SA-AgNPs with Dnaled to less aggregation. However, one interesting question to ask was how Ag-NPs suppressed MDH aggregation individually and, moreover, enhanced ATPase activity (Figure 4.4 B and Figure 3.4). A previous study by Gould et al. showed that long-term heating of these embedded Ag-NPs causes morphological changes that emphasize the preferential diffusion of Ag atoms away from small-sized NPs, particularly in the presence of surface plane defects. Due to their "perfect" atomic planes, which prevent atoms from detaching, parts of the Ag NPs remain stable at elevated temperatures (Gould *et al*., 2015). Additionally, this question was supported or answered by evidence from a previous study by De and Rotello (2008) which demonstrated how metallic nanoparticles prevented aggregation of heat-stressed proteins in vitro (Triulzi *et al*., 2008).

Certain silver nanoparticle structures maintain stability due to their well-defined atomic planes despite their high reactivity at elevated temperatures. Even under high-temperature conditions, this stability allows them to function effectively (Gould *et al*., 2015). Findings from this study support that silver nanoparticles absorb heat at elevated temperatures. Hence, DnaK is actively functional in suppressing MDH aggregation.

DnaK is known to exhibit ATPase activity as part of its role in the heat shock response, where it binds to unfolded proteins in an ATP-dependent manner. Studies such as Hartl and Hayer-Hartl (2009) discuss the ATPase cycle of Hsp70 proteins (which includes DnaK), highlighting how co-chaperones like DnaJ enhance DnaK's ATPase activity. This study's results are consistent with DnaJ acting as a co-chaperone that stimulates DnaK's ATPase activity. The results from the ATPase and MDH aggregation suppression studies provided insight into how SA-AgNPs and the DnaK chaperone system cooperate functionally. The present study's overall conclusion indicates that, in contrast to altering DnaK's structural conformation, lower concentrations (< 1.8µg/ml) of SA-AgNPs do not induce changes in the structural conformation of DnaK but instead improve its



© University of Venda

functional activity in conjunction with co-chaperone DnaJ (Figure 3.4). AgNPs are also heat tolerant, which explains the slightly increased tenacity of DnaK in the presence of NPs (Iqbal *et al*., 2019).

This study examined the interaction of silver nanoparticles (AgNPs) with DnaK and demonstrated that the effects of AgNPs on protein stability are concentration-dependent. At lower concentrations of AgNPs (1.4–1.8 µg/mL), a modest increase in fluorescence intensity was observed, suggesting a stabilizing effect on DnaK. Moreover, this effect could be attributed to the binding of AgNPs to specific regions on the protein, such as hydrophobic pockets, which enhances the structural integrity of DnaK (Rajan *et al*., 2021). Such stabilizing interactions have been reported in other proteins like bovine serum albumin (BSA), where low concentrations of AgNPs result in enhanced structural rigidity, likely due to specific nanoparticle-protein interactions that preserve the protein's native conformation (Rajan *et al*., 2021; Boutinguiza *et al*., 2015).

Conversely, the fluorescence intensity decreased sharply at higher concentrations (2.1–2.5 µg/mL) of AgNP, suggesting that DnaK's structure was disrupted, possibly resulting in partial or total unfolding. This behavior aligns with the findings of Bidan and Al-Ali (2024), who reported that high concentrations of AgNPs cause protein denaturation and aggregation, which is evidenced by a loss of fluorescence. The decrease in fluorescence can be explained by the exposure of buried tryptophan residues to the solvent due to the unfolding of the protein structure (Rajan *et al*., 2021). In this study, a similar trend was observed with DnaK (Figure 4.3), where the initial increase in fluorescence reflects stabilization. Still, the sharp decline at higher AgNP concentrations suggests that the nanoparticles have disrupted the protein's hydrophobic core, which led to the exposure of tryptophan residues to the aqueous environment.

These findings are further supported by studies on bovine serum albumin (BSA) and human serum albumin (HSA), where fluorescence quenching due to nanoparticle-induced unfolding and aggregation was extensively reported (Rajan *et al*., 2021). According to both studies, protein-nanoparticle interaction causes fluorescence intensity to increase while maintaining protein structure at low nanoparticle concentrations. However, fluorescence decreases as proteins unfold and aggregate at higher nanoparticle concentrations (Rajan *et al*., 2021; Bhattacharjee, 2016).

Tryptophan and other hydrophobic residues are exposed to solvent when nanoparticles interact with the protein's hydrophobic core, thus destabilizing its native conformation. In addition to



© University of Venda

protein destabilization, high AgNP concentrations resulted in protein aggregation in proteins such as lysozyme and hemoglobin, leading to partial unfolding and aggregation. Such effects in understanding the potential cytotoxicity of nanoparticles are crucial, especially in biomedical applications where protein integrity is essential for maintaining cellular homeostasis (Boutinguiza *et al*., 2015).

According to findings from the current study, AgNPs have a biphasic effect on DnaK stability (stabilization at low concentrations and disruption at high concentrations).

Furthermore, based on findings from this study, the effects of nanoparticles on protein stability are concentration-dependent, which further highlights the importance of regulating nanoparticle concentrations in therapeutic applications to prevent critically unintended protein aggregation and denaturation.

The inhibitory effects of SA-AgNPs were investigated on the growth of *E. coli* XL1 Blue cells. As a result, a strong dose-dependent antibacterial effect on *Escherichia coli* growth was significantly revealed by AgNPs' minimum inhibitory concentration (MIC) of 1.8 mg/mL. SA-AgNPs exhibited antibacterial activity against *E. coli* bacteria, demonstrating significant synergistic effects. Moreover, the effects of the SA-AgNPs on the stability of the *E. coli* XL1 blue protein(DnaK) were further investigated, and the observed decrease in band intensity suggested reduced protein expression levels caused by the SA-AgNPs treatment, the band intensity was further validated by densitometry analysis (appendix D, Figure D.5). According to the results of this study, leaf extracts act as reducing and capping agents. Moreover, produced SA-AgNPs indicated an effective minimal inhibitory activity against *E. coli* growth. These findings are supported by findings from study reported using of Azadirachta indica aqueous leaf extract for the synthesis of AgNPs by Ahmed *et al.,* 2016, where the antibacterial activities against both Staphylococcus aureus and *E. coli* microorganisms were shown by the synthesized AgNPs (Ahmed *et al*., 2016).

In order to assess the propensity of ATP to bind to DnaK and its co-chaperones, molecular docking studies were conducted, followed by assessing the ability of *Senna alexandrina*-identified compounds to bind to DnaK clusters. Molecular docking studies were conducted to assess the properties of compounds from *Senna alexandrina* to bind to DnaK and its co-chaperones, and the



© University of Venda

affinity was determined in each case. Findings from this study suggest that among other compounds, Isoscoparin 2"-(6-(E)-ferulylglucoside) interacts more with DnaK and induces structural conformation. *In silico* docking studies revealed promising binding affinities of certain metabolites, which also served as reducing agents in the synthesis of SA-AgNPs concerning key proteins (DnaK and its co-chaperones) involved in maintaining protein homeostasis, especially under stress conditions, in both bacteria and eukaryotic organisms. Their ability to ensure proper protein folding, prevent aggregation, and facilitate cellular recovery from stress makes them vital for cellular survival and functionality. These findings highlight the potential of *S. Alexandrina*-based AgNPs and their associated metabolites as a novel therapeutic method for combating infections caused by *E.coli* aided by DnaK assisting in the folding, repairing, and degrading proteins, at the same time, its primary function is protection; the negative effects of DnaK can contribute to disease progression, which could promote pathogenic bacteria to survive under stress conditions, especially in bacterial infections (Chiappori *et al*., 2015). Its assistance in folding misfolded proteins and protecting cells from damage caused by antibiotics, making the bacteria more resilient to host defenses and the development and persistence of antibiotic resistance, makes it a prime target for further studies and potential therapeutic interventions to disrupt the bacterial arsenal for survival. Their antimicrobial properties warrant further investigation into their potential therapeutic applications, especially in treating resistant bacterial infections. Furthermore, more comparative studies would be essential in thoroughly evaluating the nanoparticles' relative efficacy in contrast to alternative *Senna alexandrina* extract forms and isolated compounds, separately and in conjunction with nanoparticles.

## 6.2. Conclusion and future perspectives:

Findings from this study demonstrated that SAAgNPs are capable of inhibiting DnaK by inducing changes in DnaK confirmational structure and presumably by blocking the protein’s active site, thus preventing DnaK from carrying out its function due to the size, shape, and surface characteristics of NPs affecting protein adsorption. However, AgNPs were found to have anti-aggregation properties by inhibiting MDH aggregation,



© University of Venda

demonstrating their potential stand-alone inhibitory effects. It can be concluded that this study suggests a role for DnaK in alleviating nanoparticle-induced stress in *E. coli.*

Future studies should carry out thorough *in vivo* pharmacological assessments of AgNPs compared to the original extract to evaluate their safety and efficacy before clinical trials; they could also clarify the precise mechanisms that guide the antibacterial activity of the biogenic AgNPs and the *Senna Alexandrina* extract. The effects of *Senna Alexandrina* metabolites on the physicochemical characteristics of the biosynthesized AgNPs would also need to be revealed in order to optimize their biological activities. Overall, SA-AgNPs, produced through biogenetic processes, have shown significant potential in breaking down organic contaminants and possessing excellent antibacterial properties, making them eco-friendly and versatile materials. These findings highlight how they could be used in microbial control. Further toxicity testing, which evaluates the biogenic AgNPs' suitability for biological settings, and stability studies are necessary to provide a more comprehensive understanding of the safety and appropriateness of the silver nanoparticles for potential biomedical applications.



© University of Venda

# Reference

A.B. Sengul, E. Asmatulu, Environ. Chem. Lett. 18 (2020) 1659e1683.

A.K. Mittal, Y. Chisti, U.C. Banerjee, Synthesis of metallic nanoparticles using plant extracts, Biotechnology advances 31 (2013) 346-356.

Abdo, B. M. (2017). Sennosides determination of Ethiopian *Senna alexandrina* Mill accessions. *Nat. Prod. Chem. Res*, *5*(293), 2.

Acharya, D., Singha, K. M., Pandey, P., Mohanta, B., Rajkumari, J., & Singha, L. P. (2018). Shape dependent physical mutilation and lethal effects of silver nanoparticles on bacteria. *Scientific reports*, *8*(1), 201.

Agarwal H, Venkat Kumar S, Rajeshkumar S. (2017). A review on green synthesis of zinc oxide nanoparticles – An eco-friendly approach. Resource-Efficient Technologies, 3(4):406-413. DOI: 10.1016/j.reffit.2017.03.002

Aguilar-Garay, R., Lara-Ortiz, L. F., Campos-López, M., Gonzalez-Rodriguez, D. E., Gamboa-Lugo, M. M., Mendoza-Pérez, J. A., ... & Nicolás-Álvarez, D. E. (2024). A Comprehensive Review of Silver and Gold Nanoparticles as Effective Antibacterial Agents. *Pharmaceuticals*, *17*(9), 1134.

Ahmed, S., Ahmad, M., Swami, B. L., & Ikram, S. (2016). Green synthesis of silver nanoparticles using Azadirachta indica aqueous leaf extract. *Journal of radiation research and applied sciences*, *9*(1), 1-7.

Alam, M. Z., Ramachandran, T., Antony, A., Hamed, F., Ayyash, M., & Kamal-Eldin, A. (2022). Melanin is a plenteous bioactive phenolic compound in date fruits (Phoenix dactylifera L.). *Scientific reports*, *12*(1), 6614.

Alderson, T. R., Kim, J. H., Cai, K., Frederick, R. O., Tonelli, M., Markley, J. L. (2014). The specialized Hsp70 (HscA) interdomain linker binds to its nucleotide-binding domain and stimulates ATP hydrolysis in both cis and trans configurations. Biochemistry, 53: 7148-7159.

Alderson TR, Kim JH, Markley JL. Dynamical structures of Hsp70and Hsp70-Hsp40 complexes. Structure. 2016; 24:1014–1030



© University of Venda

Ali, A., Haq, I. U., Akhtar, J., Sher, M., Ahmed, N., & Zia, M. (2017). Synthesis of Ag-NPs impregnated cellulose composite material: its possible role in wound healing and photocatalysis. *IET nanobiotechnology*, *11*(4), 477-484.

Almatroudi, A. (2020). Silver nanoparticles: synthesis, characterisation and biomedical applications. *Open life sciences*, *15*(1), 819-839.

Álvarez-Chimal R, García-Pérez VI, Álvarez-Pérez MA, Tavera-Hernández R, Reyes-Carmona L, Martínez-Hernández M (2022). Influence of the particle size on the antibacterial activity of green synthesized zinc oxide nanoparticles using Dysphania ambrosioides extract, supported by molecular docking analysis. Arabian Journal of Chemistry, 15(6):103804. DOI: 10.1016/j.arabjc.2022.103804

Amankwah, Y. S., Collins, P., Fleifil, Y., Unruh, E., Márquez, K. J. R., Vitou, K., & Kravats, A. N. (2022). Grp94 works upstream of BiP in protein remodeling under heat stress. *Journal of Molecular Biology*, *434*(19), 167762.

Amina, S. J., & Guo, B. (2020). A review on the synthesis and functionalization of gold nanoparticles as a drug delivery vehicle. *International journal of nanomedicine*, 9823-9857.

Ankamwar, B., Damle, C., Ahmad, A., & Sastry, M. (2005). Biosynthesis of gold and silver nanoparticles using Emblica officinalis fruit extract, their phase transfer and transmetallation in an organic solution. *Journal of nanoscience and nanotechnology*, *5*(10), 1665-1671.

Arakawa, T., Ejima, D., Tsumoto, K., Obeyama, N., Tanaka, Y., Kita, Y., & Timasheff, S. N. (2007). Suppression of protein interactions by arginine: a proposed mechanism of the arginine effects. *Biophysical chemistry*, *127*(1-2), 1-8.

Ávalos, A., Haza, A. I., & Morales, P. (2015). Manufactured silver nanoparticles of different sizes induced DNA strand breaks and oxidative DNA damage in hepatoma and leukaemia cells and in dermal and pulmonary fibroblasts. *Folia Biologica*, *61*(1), 33.

Baharara, J., Namvar, F., Ramezani, T., Hosseini, N., & Mohamad, R. (2014). Green synthesis of silver nanoparticles using Achillea biebersteinii flower extract and its anti-angiogenic properties in the rat aortic ring model. *Molecules*, *19*(4), 4624-4634.



© University of Venda

Balasankar, D., Vanilarasu, K., Preetha, P. S., Rajeswari, S., Umadevi, M., & Bhowmik, D. (2013). Senna–A medical miracle plant. *Journal of Medicinal Plants Studies*, *1*(3), 41-47.

Bertelsen EB, Chang L, Gestwicki JE, Zuiderweg ER (2009) Solution conformation of wild-type *E. coli* Hsp70 (DnaK) chaperone complexed with ADP and substrate. Proc Natl Acad Sci U S A 106(21):8471–8476. https://doi.org/10.1073/pnas.0903503106

Berry, M., Fielding, B., & Gamieldien, J. (2015). Practical considerations in virtual screening and molecular docking. *Emerging trends in computational biology, bioinformatics, and systems biology*, 487.

Bhattacharjee, S. (2016). DLS and zeta potential–what they are and what they are not?. *Journal of controlled release*, *235*, 337-351.

Bidan, A. K., & Al-Ali, Z. S. A. (2024). Evaluation of cytotoxic potential of silver nanoparticles biosynthesized using essential oils of Jasminum sambac against breast cancer and bacterial cells. *3 Biotech*, *14*(10), 227.

Botha M, Pesce ER, Blatch GL (2007) The Hsp40 proteins of Plasmodium falciparum and other apicomplexa: regulating chaperone power in the parasite and the host. Int J Biochem Cell Biol 39(10):1781–1803

Boutinguiza, M., Comesaña, R., Lusquiños, F., Riveiro, A., Del Val, J., & Pou, J. (2015). Production of silver nanoparticles by laser ablation in open air. *Applied Surface Science*, *336*, 108-111.

Boyles, M. S., Kristl, T., Andosch, A., Zimmermann, M., Tran, N., Casals, E., ... & Duschl, A. (2015). Chitosan functionalisation of gold nanoparticles encourages particle uptake and induces cytotoxicity and pro-inflammatory conditions in phagocytic cells, as well as enhancing particle interactions with serum components. *Journal of nanobiotechnology*, *13*, 1-20.

Bracher A, Verghese J. The nucleotide exchange factors ofHsp70 molecular chaperones. Front Mol Biosci. 2015; 2:10.

Bromma, K., & Chithrani, D. B. (2020). Advances in gold nanoparticle-based combined cancer therapy. *Nanomaterials*, *10*(9), 1671.

Bukau B, Walker G. Cellular defects caused by deletion of *Escherichia coli* DnaK gene indicate roles for heat shock protein in normal metabolism. J Bacteriol. 1989; 171: 2337–2346. PMID: 2651398



© University of Venda

Bukau, B., Walker, G. C. (1990). Mutations altering heat shock specific subunit of RNA polymerase suppress major cellular defects of *E. coli* mutants lacking the DnaK chaperone. EMBO J, 9: 4027-4036.

Calloni G, Chen T, Schermann SM, Chang HC, Genevaux P, Agostini F, Tartaglia GG, HayerHartl M, Hartl FU (2012) DnaK functions as a central hub in the *E. coli* chaperone network. Cell Rep 1(3):251–264. https://doi.org/10.1016/j.celrep.2011.12.007

Carlson, C., Hussain, S. M., Schrand, A. M., K. Braydich-Stolle, L., Hess, K. L., Jones, R. L., & Schlager, J. J. (2008). Unique cellular interaction of silver nanoparticles: size-dependent generation of reactive oxygen species. *The journal of physical chemistry B*, *112*(43), 13608-13619.

Carrillo-López LM, SotoHernández RM, Zavaleta-Mancera HA, Vilchis-Néstor AR. (2016). Study of the performance of the organic extracts of Chenopodium ambrosioides for Ag nanoparticle synthesis. Journal of Nanomaterials,1-13. DOI: 10.1155/2016/4714162

Cantarelli, M. A., Pellerano, R. G., Marchevsky, E. J., & Camiña, J. M. (2011). Simultaneous determination of amoxicillin and diclofenac in pharmaceutical formulations using UV spectral data and the PLS chemometric method. *Analytical Sciences*, *27*(1), 73-78.

Cavassin, E. D., de Figueiredo, L. F. P., Otoch, J. P., Seckler, M. M., de Oliveira, R. A., Franco, F. F., ... & Costa, S. F. (2015). Comparison of methods to detect the in vitro activity of silver nanoparticles (AgNP) against multidrug resistant bacteria. *Journal of nanobiotechnology*, *13*, 1-16.

Chakraborty, A., & Biswas, A. (2020). Structure, stability and chaperone function of Mycobacterium leprae Heat Shock Protein 18 are differentially affected upon interaction with gold and silver nanoparticles. International Journal of Biological Macromolecules, 152, 250–260. https://doi.org/10.1016/j.ijbiomac.2020.02.182.

Chandirika, J. U., & Annadurai, G. (2018). Biosynthesis and characterization of silver nanoparticles using leaf extract Abutilon indicum. *Glob. J. Biotechnol. Biochem*, *13*, 7-11.

Chaudhry N, Dwivedi S, Chaudhry V, Singh A, Saquib Q, Azam A. (2018). Bioinspired nanomaterials in agriculture and food: Current status, foreseen applications and challenges. Microbial Pathogenesis, 123:196-200. DOI: 10.1016/j.micpath.2018.07.013



© University of Venda

Cheetham ME, Caplan AJ (1998) Structure, function and evolution of DnaJ: conservation and adaptation of chaperone function. Cell Stress Chaperones 3(1):28–36

Chiappori F, Fumian M, Milanesi L, Merelli I. DnaK as Antibiotic Target: Hot Spot Residues Analysis for Differential Inhibition of the Bacterial Protein in Comparison with the Human HSP70. PLoS One. 2015 Apr 23;10(4):e0124563.

Chiappori F, Merelli I, Milanesi L, Colombo G, Morra G (2016) An atomistic view of Hsp70 allosteric crosstalk: from the nucleotide to the substrate binding domain and back. Sci Rep 6:23474. https://doi.org/10.1038/srep23474

Christensen, S., Rämisch, S., & André, I. (2022). DnaK response to expression of protein mutants is dependent on translation rate and stability. Communications Biology, 5(1), 597.

Craig EA, Huang P, Aron R, Andrew A. The diverse roles ofJ-proteins, the obligate Hsp70 co-chaperone. Rev Physiol Bio-chem Pharmacol. 2006; 156:1–21.19.

Craig EA, Marszalek J. How do J-proteins get Hsp70 to do so many different things? Trends Biochem Sci. 2017; 42:355–368.24.

Cyr DM, Ramos CH. Specification of Hsp70 function by type Iand type II Hsp40. Subcell Biochem. 2015; 78:91–102.25.

D. Balasankar, K. Vanilarasu, P.S. Preetha, S.R.M. Umadevi and D. Bhowmik, J. Med. Plants Stud.,1, 41 (2013)2.

Dhand, V., Soumya, L., Bharadwaj, S., Chakra, S., Bhatt, D., & Sreedhar, B. J. M. S. (2016). Green synthesis of silver nanoparticles using Coffea arabica seed extract and its antibacterial activity. *Materials Science and Engineering: C*, *58*, 36-43.

Dakal, T. C., Kumar, A., Majumdar, R. S., & Yadav, V. (2016). Mechanistic basis of antimicrobial actions of silver nanoparticles. *Frontiers in microbiology*, *7*, 1831.



© University of Venda

Dawadi, S., Katuwal, S., Gupta, A., Lamichhane, U., Thapa, R., Jaisi, S., ... & Parajuli, N. (2021). Current research on silver nanoparticles: synthesis, characterization, and applications. *Journal of nanomaterials*, *2021*(1), 6687290.

Das, B., Dash, S. K., Mandal, D., Ghosh, T., Chattopadhyay, S., Tripathy, S., ... & Roy, S. (2017). Green synthesized silver nanoparticles destroy multidrug resistant bacteria via reactive oxygen species mediated membrane damage. *Arabian Journal of Chemistry*, *10*(6), 862-876.

Dauthal P, Mukhopadhyay M. (2016). Noble metal nanoparticles: Plant-mediated synthesis, mechanistic aspects of synthesis, and applications. Industrial and Engineering Chemistry Research, 55(36):9557-9577. DOI: 10.1021/acs. iecr.6b0086

De Lacerda Coriolano, D., de Souza, J. B., Bueno, E. V., Medeiros, S. M. D. F. R. D. S., Cavalcanti, I. D. L., & Cavalcanti, I. M. F. (2021). Antibacterial and antibiofilm potential of silver nanoparticles against antibiotic-sensitive and multidrug-resistant Pseudomonas aeruginosa strains. *Brazilian Journal of Microbiology*, *52*, 267-278.

De Jong. (2008). Drug delivery and nanoparticles: Applications and hazards. International Journal of Nanomedicine, 133. https://doi.org/10.2147/ijn.s596

De M, Rotello V. Synthetic "chaperones": nanoparticle mediated refolding of thermally denatured proteins. Chem Commun (Camb). 2008; 3504–3506.

Demarque, D. P., Dusi, R. G., de Sousa, F. D., Grossi, S. M., Silvério, M. R., Lopes, N. P., & Espindola, L. S. (2020). Mass spectrometry-based metabolomics approach in the isolation of bioactive natural products. *Scientific Reports*, *10*(1), 1051.

Demirezer, L. O., Karahan, N., Ucakturk, E., Kuruuzum-Uz, A., Guvenalp, Z., & Kazaz, C. (2011). HPLC fingerprinting of sennosides in laxative drugs with isolation of standard substances from some senna leaves. *Rec. Nat. Prod*, *5*(4), 261-270.

Dong, H. (2008). *Self-assembly of alpha-helical and beta-sheet nanofibers*. Rice University.



© University of Venda

Du, J., Tang, J., Xu, S., Ge, J., Dong, Y., Li, H., & Jin, M. (2018). A review on silver nanoparticles-induced ecotoxicity and the underlying toxicity mechanisms. *Regulatory Toxicology and Pharmacology*, *98*, 231-239.

Duval, R. E., Gouyau, J., & Lamouroux, E. (2019). Limitations of recent studies dealing with the antibacterial properties of silver nanoparticles: Fact and opinion. *Nanomaterials*, *9*(12), 1775.

Duncan, E. J., Cheetham, M. E., Chapple, J. P., & van der Spuy, J. (2015). The role of HSP70 and its co-chaperones in protein misfolding, aggregation and disease. *The Networking of Chaperones by Co-chaperones: Control of Cellular Protein Homeostasis*, 243-273.

Edeoga, H. O., Okwu, D. E., & Mbaebie, B. O. (2005). Phytochemical constituents of some Nigerian medicinal plants. *African journal of biotechnology*, *4*(7), 685-688.

El-Morsy, T. H. (2013). Antibiotic properties of leaf extracts of Sennaalexandrina (L). *J Am Sci*, *9*(1), 288-92.

Ellis J. (1987). Proteins as molecular chaperones. Nature, 328: 378–379. PMID: 3112578

Emmanuel, R., Palanisamy, S., Chen, S. M., Chelladurai, K., Padmavathy, S., Saravanan, M., ... & Al-Hemaid, F. M. (2015). Antimicrobial efficacy of green synthesized drug blended silver nanoparticles against dental caries and periodontal disease causing microorganisms. *Materials Science and Engineering: C*, *56*, 374-379.

Endres, S. C., Ciacchi, L. C., & Mädler, L. (2021). A review of contact force models between nanoparticles in agglomerates, aggregates, and films. *Journal of Aerosol Science*, *153*, 105719.

Fan CY, Lee S, Cyr DM. (2003). Mechanisms for regulation of Hsp70function by Hsp40. Cell Stress Chaperones, 8:309–316

Fardood, S. T., Ramazani, A., & Moradi, S. (2017). Green synthesis of Ni–Cu–Mg ferrite nanoparticles using tragacanth gum and their use as an efficient catalyst for the synthesis of polyhydroquinoline derivatives. *Journal of Sol-Gel Science and Technology*, *82*, 432-439.



© University of Venda

Fawad Ahmad, A. (2023). Brief review on applications of gold and silver nanoparticles in drug delivery and DNA interaction. *World Journal of Physics*, *1*(1), 5.

Fayaz, A. M., Balaji, K., Girilal, M., Yadav, R., Kalaichelvan, P. T., & Venketesan, R. (2010). Biogenic synthesis of silver nanoparticles and their synergistic effect with antibiotics: a study against gram-positive and gram-negative bacteria. *Nanomedicine: Nanotechnology, Biology and Medicine*, *6*(1), 103-109.

Ferdous, Z., & Nemmar, A. (2020). Health impact of silver nanoparticles: a review of the biodistribution and toxicity following various routes of exposure. *International journal of molecular sciences*, *21*(7), 2375.

Fernández-Fernández MR, Valpuesta JM (2018) Hsp70 chaperone: a master player in protein homeostasis. F1000Research 7:1497.

Fernandes, M., González-Ballesteros, N., da Costa, A., Machado, R., Gomes, A. C., & Rodríguez-Argüelles, M. C. (2023). Antimicrobial and anti-biofilm activity of silver nanoparticles biosynthesized with Cystoseira algae extracts. *JBIC Journal of Biological Inorganic Chemistry*, *28*(4), 439-450.

Fernández-Marín, B., García-Plazaola, J. I., Hernández, A., & Esteban, R. (2018). Plant photosynthetic pigments: methods and tricks for correct quantification and identification. *Advances in plant ecophysiology techniques*, 29-50.

Fourie, K. R., & Wilson, H. L. (2020). Understanding GroEL and DnaK stress response proteins as antigens for bacterial diseases. *Vaccines*, *8*(4), 773.

Fu, G., Vary, P.S., & Lin, C.T. (2005). Anatase TiO2 composites for antimicrobial coatings. J. Phys. Chem. B. 109: 8889-8898.

Gallucci, M. N., Cisneros, A. B., Loto, A. M., Maillard, A. F., Hollmann, A., & Borsarelli, C. D. (2025). Antibacterial activity modulation of silver nanoparticles prepared by green synthesis with aqueous extracts from different organs of native Argentinean trees. *Biochemical Engineering Journal*, *215*, 109612.

Gan, Q., & Wang, T. (2007). Chitosan nanoparticle as protein delivery carrier—systematic examination of fabrication conditions for efficient loading and release. *Colloids and Surfaces B: Biointerfaces*, *59*(1), 24-34.



© University of Venda

Gavade, N. L., Kadam, A. N., Suwarnkar, M. B., Ghodake, V. P., & Garadkar, K. M. (2015). Biogenic synthesis of multi-applicative silver nanoparticles by using Ziziphus Jujuba leaf extract. *Spectrochimica Acta Part A: Molecular and Biomolecular Spectroscopy*, *136*, 953-960.

Genest O, Wickner S, Doyle SM (2019) Hsp90 and Hsp70 chaperones: collaborators in protein remodeling. J Biol Chem 294(6):2109–2120. https://doi.org/10.1074/jbc.REV118.002806

Georgopoulos C, Welch WJ (1993) Role of the major heat shock proteins as molecular chaperones. Ann Rev Cell Biol 9:601–634. https://doi.org/10.1146/annurev.cb.09.110193.003125

Ghosh, P., Han, G., De, M., Kim, C. K., & Rotello, V. M. (2008). Gold nanoparticles in delivery applications. Adv. Drug. Deliv. Rev. 60, 1307–1315.

Gou, Y., Zhou, R., Ye, X., Gao, S., & Li, X. (2015). Highly efficient in vitro biosynthesis of silver nanoparticles using Lysinibacillus sphaericus MR-1 and their characterization. *Science and technology of advanced materials*.

Grover, M., Behl, T., Sehgal, A., Singh, S., Sharma, N., Virmani, T., ... & Bungau, S. (2021). In vitro phytochemical screening, cytotoxicity studies of Curcuma longa extracts with isolation and characterisation of their isolated compounds. *Molecules*, *26*(24), 7509.

Guo, Y., & Gaiki, S. (2011). Retention and selectivity of stationary phases for hydrophilic interaction chromatography. *Journal of Chromatography A*, *1218*(35), 5920-5938.

Gould, A. L., Kadkhodazadeh, S., Wagner, J. B., Catlow, C. R. A., Logsdail, A. J., & Di Vece, M. (2015). Understanding the thermal stability of silver nanoparticles embedded in a-Si. *The Journal of Physical Chemistry C*, *119*(41), 23767-23773.

Govindaraju, K., Krishnamoorthy, K., Alsagaby, S. A., Singaravelu, G., & Premanathan, M. (2015). Green synthesis of silver nanoparticles for selective toxicity towards cancer cells. *IET nanobiotechnology*, *9*(6), 325-330.

Gurunathan, S., Park, J. H., & Kim, J. H. (2014). "Silver nanoparticles: Green synthesis, antimicrobial efficacy, and potential applications." *International Journal of Molecular Sciences*, 15(4), 7989-8026.



© University of Venda

H.A. Salam, P. Rajiv, M. Kamaraj, P. Jagadeeswaran, S. Gunalan, R. Sivaraj, Plants: Green route for nanoparticle synthesis, Int. Res. J. Biol. Sci. 1 (2012) 85-90.

Hageman J, Kampinga HH (2009) Computational analysis of the human HSPH/HSPA/DNAJ family and cloning of a human HSPH/HSPA/DNAJ expression library. Cell Stress Chaperones 14(1):1–21. https://doi.org/10.1007/s12192-008-0060-2

Han, W., & Christen, P. (2001). Mutations in the interdomain linker region of DnaK abolish the chaperone action of the DnaK/DnaJ/GrpE system. *FEBS letters*, *497*(1), 55-58.

Haque, M. A., Kaur, P., Islam, A., & Hassan, M. I. (2022). Application of circular dichroism spectroscopy in studying protein folding, stability, and interaction. In *Advances in Protein Molecular and Structural Biology Methods* (pp. 213-224). Academic Press.

Hartl FU, Hayer-Hartl M. (2002). Molecular chaperones in the cytosol: from nascent chain to folded protein. Science, 295: 1852–1858. PMID: 11884745

Hartl FU, Hayer-Hartl M. (2009). Converging concepts of protein folding in vitro and in vivo. Nat Struct Mol Biol, 16:574–581

Hassanen, E. I., Morsy, E. A., Hussien, A. M., Farroh, K. Y., & Ali, M. E. (2021). Comparative assessment of the bactericidal effect of nanoparticles of copper oxide, silver, and chitosan-silver against Escherichia coli infection in broilers. *Bioscience Reports*, *41*(4).

Hebbalalu D, Lalley J, Nadagouda MN, Varma RS. (2013). Greener techniques for the synthesis of silver nanoparticles using plant extracts, enzymes, bacteria, biodegradable polymers, and microwaves. ACS Sustainable Chemistry & Engineering;1(7):703-712. DOI: 10.1021/sc4000362

A. Henglein, J. Phys. Chem. 97 (1993) 5457.

Helms, V. (2018). *Principles of computational cell biology: from protein complexes to cellular networks*. John Wiley & Sons.

Hendrickson WA, Liu Q. Exchange we can believe in. Structure.2008;16:1153–1155.27.

Hennessy F, Boshoff A, Blatch GL (2005) Rational mutagenesis of a 40 kDa heat shock protein from Agrobacterium tumefaciens identifies amino acid residues critical to its in vivo function. Int J Biochem Cell Biol 37(1):177–191.



© University of Venda

Hipp, M. S., & Hartl, F. U. (2024). Interplay of Proteostasis Capacity and Protein Aggregation: Implications for Cellular Function and Disease. *Journal of Molecular Biology*, 168615.

Hoffmann, A., Bukau, B., Kramer, G. (2010). Structure and function of the molecular chaperone Trigger Factor. Biochim Biophys Acta Mol Cell Res. 1803:650-661.

Huang, Y., Li, X., Liao, Z., Zhang, G., Liu, Q., Tang, J., ... & Luo, Q. (2007). A randomized comparative trial between Acticoat and SD-Ag in the treatment of residual burn wounds, including safety analysis. *Burns*, *33*(2), 161-166.

Huang, X., & El-Sayed, M. A. (2010). Gold nanoparticles: Optical properties and implementations in cancer diagnosis and photothermal therapy. *Journal of advanced research*, *1*(1), 13-28.

Hsiao, I. L., Hsieh, Y. K., Wang, C. F., Chen, I. C., & Huang, Y. J. (2015). Trojan-horse mechanism in the cellular uptake of silver nanoparticles verified by direct intra-and extracellular silver speciation analysis. *Environmental science & technology*, *49*(6), 3813-3821.

IBEKWE, N. N. (2012). *PHYTOCHEMISTRY AND ANTIMYCOBACTERIAL ACTIVITIES OF THE LEAF EXTRACTS OF PAVETTA CRASSIPES K. SCHUM* (Doctoral dissertation).

Ibrahim, H. M. (2015). Green synthesis and characterization of silver nanoparticles using banana peel extract and their antimicrobial activity against representative microorganisms. *Journal of radiation research and applied sciences*, *8*(3), 265-275.

Imamoglu R, Balchin D, Hayer-Hartl M, Hartl FU (2020) Bacterial Hsp70 resolves misfolded states and accelerates productive folding of a multi-domain protein. Nat Commun 11:365. https://doi.org/10.1038/s41467-019-14245-4

Iqbal, M., Raja, N. I., Mashwani, Z. U. R., Hussain, M., Ejaz, M., & Yasmeen, F. (2019). Effect of silver nanoparticles on growth of wheat under heat stress. *Iranian Journal of Science and Technology, Transactions A: Science*, *43*, 387-395.

Iravani, S. (2011). Green synthesis of metal nanoparticles using plants. *Green chemistry*, *13*(10), 2638-2650.

Jena, R., Garg, D. K., Achary, M. M. V., Singh, J., Tomar, R., Choudhury, L., ... & Kundu, B. (2020). Application of a protein domain as chaperone for enhancing biological activity and stability of other



© University of Venda

proteins. *Journal of biotechnology*, *310*, 68-79.

Jeyaraj, M., Sathishkumar, G., Sivanandhan, G., MubarakAli, D., Rajesh, M., Arun, R., ... & Ganapathi, A. (2013). Biogenic silver nanoparticles for cancer treatment: an experimental report. *Colloids and surfaces B: Biointerfaces*, *106*, 86-92.

Joudeh, N., & Linke, D. (2022). Nanoparticle classification, physicochemical properties, characterization, and applications: a comprehensive review for biologists. *Journal of Nanobiotechnology*, *20*(1), 262.

Kajani, A. A., Zarkesh-Esfahani, S. H., Bordbar, A. K., Khosropour, A. R., Razmjou, A., & Kardi, M. (2016). Anticancer effects of silver nanoparticles encapsulated by Taxus baccata extracts. *Journal of Molecular Liquids*, *223*, 549-556.

Kalakonda, P., Thodeti, M., Ganneboina, C., Ankathi, K., Kathri, S., Begari, K., ... & Podila, B. B. (2024). Eco-Friendly Fabrication of Silver Nanoparticles for Sustainable Water Purification and Antibacterial Synergy. *Plasmonics*, 1-13.

Kale, R. D., & Jagtap, P. (2018). Biogenic synthesis of silver nanoparticles using citrus limon leaves and its structural investigation. In *Advances in Health and Environment Safety: Select Proceedings of HSFEA 2016* (pp. 11-20). Springer Singapore.

Kampinga HH, Hageman J, Vos MJ, Kubota H, Tanguay RM, Bruford EA, Cheetham ME, Chen B, Hightower LE (2009) Guidelines for the nomenclature of the human heat shock proteins. Cell Stress Chaperones 14(1):105–111. https://doi.org/10.1007/s12192-008-0068-7

Kampinga, H. H., Craig, E. (2010). The Hsp70 chaperone machinery: J proteins as drivers of functional specificity. Nat Rev Mol Cell Biol, 11: 579–592.

Kampinga HH, Andreasson C, Barducci A, Cheetham ME, Cyr D, Emanuelsson C, Genevaux P, Gestwicki JE, Goloubinoff P, Huerta-Cepas J, Kirstein J, Liberek K, Mayer MP, Nagata K, Nillegoda NB, Pulido P, Ramos C, De Los RP, Rospert S, Rosenzweig R, Sahi C, Taipale M, Tomiczek B, Ushioda R, Young JC, Zimmermann R, Zylicz A, Zylicz M, Craig EA, Marszalek J (2019) Function, evolution, and structure of J-domain proteins. Cell Stress Chaperones 24 (1):7–15. https://doi.org/10.1007/s12192-018-0948-4

Kanade, M., Chakraborty, S., Shelke, S. S., & Gayathri, P. (2020). A distinct motif in a prokaryotic small Ras-Like GTPase highlights unifying features of walker B motifs in P-Loop NTPases. *Journal of molecular biology*, *432*(20), 5544-5564.

Karzai, A. W., & McMacken, R. (1996). A Bipartite Signaling Mechanism Involved in DnaJ-mediated Activation of the *Escherichia coli* DnaK Protein (∗). *Journal of Biological Chemistry*, *271*(19), 11236-11246.



© University of Venda

Katas, H., Lim, C. S., Azlan, A. Y. H. N., Buang, F., & Busra, M. F. M. (2019). Antibacterial activity of biosynthesized gold nanoparticles using biomolecules from Lignosus rhinocerotis and chitosan. *Saudi Pharmaceutical Journal*, *27*(2), 283-292.

Kaviya, S., Santhanalakshmi, J., Viswanathan, B., Muthumary, J., & Srinivasan, K. (2011). Biosynthesis of silver nanoparticles using Citrus sinensis peel extract and its antibacterial activity. *Spectrochimica Acta Part A: Molecular and Biomolecular Spectroscopy*, *79*(3), 594-598.

Kelly KL, Coronado E, Zhao LL, Schatz GC. (2003). The optical properties of metal nanoparticles: The influence of size, shape, and dielectric environment. The Journal of Physical Chemistry. B, 107(3):668-677. DOI: 10.1021/ jp026731y

Khan, M. Z. H., Tarek, F. K., Nuzat, M., Momin, M. A., & Hasan, M. R. (2017). Rapid biological synthesis of silver nanoparticles from Ocimum sanctum and their characterization. *Journal of Nanoscience*, *2017*(1), 1693416.

Khan, M. F., & Khan, M. A. (2023). Plant-derived metal nanoparticles (PDMNPs): synthesis, characterization, and oxidative stress-mediated therapeutic actions. *Future Pharmacology*, *3*(1), 252-295.

Khatami, M., Mehnipor, R., Poor, M. H. S., & Jouzani, G. S. (2016). Facile biosynthesis of silver nanoparticles using Descurainia sophia and evaluation of their antibacterial and antifungal properties. *Journal of Cluster Science*, *27*, 1601-1612.

Khubchandani, M., Thosar, N. R., Dangore-Khasbage, S., & Srivastava, R. (2022). Applications of silver nanoparticles in pediatric dentistry: An overview. *Cureus*, *14*(7).

Kim, Y. E, Hipp, M. S, Bracher, A, Haye-Hartl, M and Hartl, F. U. (2013) Molecular chaperone functions in protein folding and proteostasis. Annu Rev Biochem, 82: 323-355.

Kim, N., Kim, Y., Yun, J. M., Jeong, S. K., Lee, S., Lee, B. Z., & Shim, J. (2023). Surface Coating of titanium dioxide nanoparticles with a polymerizable chelating agent and its physicochemical property. *ACS omega*, *8*(21), 18743-18750.

Kolahalam LA, Kasi Viswanath IV, Diwakar BS, Govindh B, Reddy V, Murthy YLN. (2019). Review on nanomaterials: Synthesis and applications. Materials Today: Proceedings, 18:2182-2190. DOI: 10.1016/j.matpr.2019.07.371.

Krishnaraj, C., Jagan, E. G., Rajasekar, S., Selvakumar, P., Kalaichelvan, P. T., & Mohan, N. J. C. S. B. B. (2010). Synthesis of silver nanoparticles using *Acalypha indica* leaf extracts and its antibacterial activity against water borne pathogens. *Colloids and Surfaces B: Biointerfaces*, *76*(1), 50-56.



© University of Venda

Kumar, H., Bhardwaj, K., Kuča, K., Kalia, A., Nepovimova, E., Verma, R., & Kumar, D. (2020). Flower-based green synthesis of metallic nanoparticles: Applications beyond fragrance. *Nanomaterials*, *10*(4), 766.

Kuntz, I. D., Blaney, J. M., Oatley, S. J., Langridge, R., & Ferrin, T. E. (1982). A geometric approach to macromolecule-ligand interactions. *Journal of molecular biology*, *161*(2), 269-288.

Kurtz, S., Rossl, J., Petko, L., Lindquist, S. (1986). An ancient developmental induction: Heat- shock proteins induced in sporulation and oogenesis. Science 231: 1154-1157.

Lal, H. M., Thomas, S., Li, T., & Maria, H. J. (2021). *Polymer Nanocomposites Based on Silver Nanoparticles* (pp. 247-265). Springer.

Langer T, Lu C, Echols H, Flanagan J, Hayer MK, Hartl FU (1992) Successive action of DnaK, DnaJ and GroEL along the pathway of chaperone-mediated protein folding. Nature 356 (6371):683–689

Latha, M., Sumathi, M., Manikandan, R., Arumugam, A., & Prabhu, N. M. (2015). Biocatalytic and antibacterial visualization of green synthesized silver nanoparticles using Hemidesmus indicus. *Microbial pathogenesis*, *82*, 43-49.

Laufen, T., Mayer, M. P., Beisel, C., Klostermeier, D., Mogk, A., Reinstein, J., & Bukau, B. (1999). Mechanism of regulation of hsp70 chaperones by DnaJ cochaperones. *Proceedings of the National Academy of Sciences*, *96*(10), 5452-5457.

Lebepe, C. M., Matambanadzo, P. R., Makhoba, X. H., Achilonu, I., Zininga, T., & Shonhai, A. (2020). Comparative characterization of Plasmodium falciparum Hsp70-1 relative to *E. coli* DnaK reveals the functional specificity of the parasite chaperone. *Biomolecules*, *10*(6), 856.

Leelavathi, V., & Udayasri, P. (2018). Qualitative and quantitative analytical studies for the screening of phytochemicals from the leaf extracts of *Senna alexandrina* Mill. *J. Pharm. Clin. Res*, *10*, 210-215.

Liberek, K., Marszalek, J., Ang, D., Georgopoulos, C., & Zylicz, M. (1991). *Escherichia coli* DnaJ and GrpE heat shock proteins jointly stimulate ATPase activity of DnaK. *Proceedings of the National Academy of Sciences*, *88*(7), 2874-2878.

Lindquist, S., Craig, E.A. (1988). The heat-shock proteins. Annu Rev Genet, 22: 631– 677.

Linke, K. (2005). *Characterization of the DnaK-DnaJ-GrpE system under oxidative heat stress* (Doctoral dissertation, Technische Universität München).

Liu Qinglian, Ce Liang, Lei Zhou (2019) Structural and functional analysis of the Hsp70/Hsp40 chaperone



© University of Venda

system. DOI: 10.1002/pro.3725378 The Protein Society Protein Science. 2020(29):378–390.

Liu, Y., Chen, J., & Zeng, W. (2018). "The role of heat shock protein DnaK in bacterial stress responses and its potential as a target for antimicrobial therapy." *Journal of Microbiology Research*, 10(4), 453-468.

Liu, J., Varghese, B. M., Hansen, A., Zhang, Y., Driscoll, T., Morgan, G., ... & Bi, P. (2022). Heat exposure and cardiovascular health outcomes: a systematic review and meta-analysis. *The Lancet Planetary Health*, *6*(6), e484-e495.

Lu J, Zhang X, Wu Y, Sheng Y, Li W, Wang W (2021) Energy landscape remodeling mechanism of Hsp70-chaperone-accelerated protein folding. Biophys J 120:1971–1983. https://doi.org/10.1016/j.bpj.2021.03.013

Lu, X., Rycenga, M., Skrabalak, S. E., Wiley, B., & Xia, Y. (2009). Chemical synthesis of novel plasmonic nanoparticles. *Annual review of physical chemistry*, *60*, 167-192.

Luthuli SD, Chili MM, Revaprasadu N, Shonhai A. Cysteine-capped gold nanoparticles suppress aggregation of proteins exposed to heat stress. IUBMB Life. 2013; 65: 454–461. doi: 10.1002/iub.1146 PMID: 23436466

Lynch, I., & Dawson, K. A. (2020). Protein–nanoparticle interactions. *Nano-enabled medical applications*, 231-250.

Madala, N. E., & Kabanda, M. M. (2021). LC-MS based validation and DFT investigation on the antioxidant properties of clovamide:• OH and• OOH scavenging and Cu (II) chelation mechanisms. *Journal of Molecular Structure*, *1236*, 130349.

Maigoda, T. C., Judiono, J., Purkon, D. B., Haerussana, A. N. E. M., & Mulyo, G. P. E. (2022). Evaluation of Peronema canescens leaves extract: Fourier transform infrared analysis, total phenolic and flavonoid content, antioxidant capacity, and radical scavenger activity. *Open Access Macedonian Journal of Medical Sciences*, *10*(A), 117-124.

Majdalawieh, A., Kanan, M. C., El-Kadri, O., & Kanan, S. M. (2014). Recent advances in gold and silver nanoparticles: synthesis and applications. *Journal of nanoscience and nanotechnology*, *14*(7), 4757-4780.

Makarov VV, Love AJ, Sinitsyna OV, Makarova SS, Yaminsky IV, Taliansky ME, et al. "Green" nanotechnologies: Synthesis of metal nanoparticles using plants. Acta Naturae. 2014;6(1):35-44. DOI: 10.32607/20758251-2014-6-1-35-44

Makumire, S., Dongola, T. H., Chakafana, G., Tshikonwane, L., Chauke, C. T., Maharaj, T., ... & Shonhai,



© University of Venda

A. (2021). Mutation of GGMP repeat segments of Plasmodium falciparum Hsp70-1 compromises chaperone function and Hop co-chaperone binding. *International Journal of Molecular Sciences*, *22*(4), 2226.

Malabadi, R. B., Sadiya, M. R., Kolkar, K. P., & Chalannavar, R. K. (2024). Pathogenic *Escherichia coli* (*E. coli*) food borne outbreak: Detection methods and controlling measures. *Magna Scientia Advanced Research and Reviews*, *10*(1), 052-085.

Marin, S., Mihail Vlasceanu, G., Elena Tiplea, R., Raluca Bucur, I., Lemnaru, M., Minodora Marin, M., & Mihai Grumezescu, A. (2015). Applications and toxicity of silver nanoparticles: a recent review. *Current topics in medicinal chemistry*, *15*(16), 1596-1604.

Martin, J., Langer, T., Boteva, R., Schramel, A., Horw1cha, L., Hartl, F. U. (1991). Chaperonin-mediated protein folding at the surface of GroEL through a 'Molten Globule'-like Intermediate. Nature, 352: 36-42.

Martínez-Mera I, Espinosa Pesqueira ME, Pérez-Hernández R, Arenas-Alatorre J. (2007). Synthesis of magnetite (Fe3O4) nanoparticles without surfactants at room temperature. Materials Letters, 61(23-24):4447- 4451. DOI: 10.1016/j.matlet.2007.02.018

Mata, R., Nakkala, J. R., & Sadras, S. R. (2015). Biogenic silver nanoparticles from Abutilon indicum: Their antioxidant, antibacterial and cytotoxic effects in vitro. *Colloids and Surfaces B: Biointerfaces*, *128*, 276-286.

Mathomu, L. M. (2022). *The role of molecular chaperones in Escherichia coli cells subjected to gold nanoparticles induced stress* (Doctoral dissertation).

Mayer, M. P., Rüdiger, S., & Bukau, B. (2000). Molecular basis for interactions of the DnaK chaperone with substrates.

Mayer, M. P., Schröder, H., Rüdiger, S., Paal, K., Laufen, T., Bukau, B. (2000). Multistep mechanism of substrate binding determines chaperone activity of Hsp70. Nat Struct Biol, 7: 586-593.

Mayer, M. P. (2013). Hsp70 chaperone dynamics and molecular mechanism. *Trends in biochemical sciences*, *38*(10), 507-514.

Mayer MP, Bukau B (2005) Hsp70 chaperones: cellular functions and molecular mechanism. Cell Mol Life Sci 62(6):670–684. https://doi.org/10.1007/s00018-004-4464-6



© University of Venda

Mayer MP (2010b) Phosphotyrosine confers client specificity to Hsp90. Mol Cell 37(3):295–296. https://doi.org/10.1016/j.molcel.2010.01.028

Mayer MP, Gierasch LM. Recent advances in the structural andmechanistic aspects of Hsp70 molecular chaperones. J BiolChem. 2019;294:2085–2097.

Mayer MP (2021) The Hsp70-chaperone machines in bacteria. Front Mol Biosci 8:694012. https://doi.org/10.3389/fmolb.2021.694012

Miller, J. M., & Enemark, E. J. (2016). Fundamental characteristics of AAA+ protein family structure and function. *Archaea*, *2016*(1), 9294307.

Min SH, Lee TH, Lee S, Song JH, Lee GY, Zontar D. (2019). Simulation of electrical conductivity for nanoparticles and nanotubes composite sensor according to geometrical properties of nanomaterials. Composites Part B: Engineering. 174:107003. DOI: 10.1016/j.compositesb.2019.107003

Miri, A., Sarani, M., Bazaz, M. R., & Darroudi, M. (2015). Plant-mediated biosynthesis of silver nanoparticles using Prosopis farcta extract and its antibacterial properties. *Spectrochimica acta part a: molecular and biomolecular spectroscopy*, *141*, 287-291.

Miri, A., & Sarani, M. (2018). Biological studies of synthesized silver nanoparticles using Prosopis farcta. *Molecular biology reports*, *45*, 1621-1626.

Mittal, A. K., Tripathy, D., Choudhary, A., Aili, P. K., Chatterjee, A., Singh, I. P., & Banerjee, U. C. (2015). Bio-synthesis of silver nanoparticles using Potentilla fulgens Wall. ex Hook. and its therapeutic evaluation as anticancer and antimicrobial agent. *Materials Science and Engineering: C*, *53*, 120-127.

Mogk, A., Kummer, E., Bukau, B. (2015). Cooperation of Hsp70 and Hsp100 chaperone machines in protein disaggregation. Front Mol Biosci, 2: 22.

Morán Luengo, T., Kityk, R., Mayer, M.P., Rudiger, S.D.G. (2018). Hsp90 breaks the deadlock of the Hsp70 chaperone system. Molecular Cell, 70: 1-8. doi: 10.1016/j.molcel.2018.03.028.

Moore, T. L., Rodriguez-Lorenzo, L., Hirsch, V., Balog, S., Urban, D., Jud, C., ... & Petri-Fink, A. (2015). Nanoparticle colloidal stability in cell culture media and impact on cellular interactions. *Chemical Society Reviews*, *44*(17), 6287-6305.

Morán Luengo T, Mayer MP, Rüdiger SGD (2019) The Hsp70-Hsp90 chaperone cascade in protein folding. Trends Cell Biol 29(2):164–177. https://doi.org/10.1016/j.tcb.2018.10.004

Mount, D. W. (2004). Bioinformatics-sequence and genome analysis.



© University of Venda

Muñoz, P.L.A., Minchaca, Z.A., Mares, R.E., Ramos, M.A. (2015). Protein folding and molecular chaperones of protozoa. Nova Science Publishers, Inc, ISBN: 978-1-63483-543-5

Mutalik, C., Saukani, M., Khafid, M., Krisnawati, D. I., Widodo, Darmayanti, R., ... & Kuo, T. R. (2023). Gold-based nanostructures for antibacterial application. *International journal of molecular sciences*, *24*(12), 10006.

Nadworny, P. L., Wang, J., Tredget, E. E., & Burrell, R. E. (2008). Anti-inflammatory activity of nanocrystalline silver in a porcine contact dermatitis model. *Nanomedicine: nanotechnology, biology and medicine*, *4*(3), 241-251.

Naganthran, A., Verasoundarapandian, G., Khalid, F. E., Masarudin, M. J., Zulkharnain, A., Nawawi, N. M., Karim, M., Che Abdullah, C. A., & Ahmad, S. A. (2022). Synthesis, Characterization and Biomedical Application of Silver Nanoparticles. *Materials (Basel, Switzerland)*, *15*(2), 427. https://doi.org/10.3390/ma15020427

Nava OJ, Luque PA, Gómez-Gutiérrez CM, Vilchis-Nestor AR, Castro-Beltrán A, Mota-González ML. (2017). Influence of Camellia sinensis extract on zinc oxide nanoparticle green synthesis. Journal of Molecular Structure, 1134:121-125

Needham, P. G., Patel, H. J., Chiosis, G., Thibodeau, P. H., Brodsky, J. L. (2015). Mutations in the Yeast Hsp70, Ssa1, at P417 Alter ATP Cycling, interdomain coupling, and specific chaperone functions. J Mol Biol, 427: 2948-65.

Nibbe, R. K., Chowdhury, S. A., Koyutürk, M., Ewing, R., & Chance, M. R. (2011). Protein–protein interaction networks and subnetworks in the biology of disease. *Wiley Interdisciplinary Reviews: Systems Biology and Medicine*, *3*(3), 357-367.



© University of Venda

Nitika, Truman AW (2017) Cracking the Chaperone Code: Cellular Roles for Hsp70 Phosphorylation. Trends Biochem Sci 42(12):932–935.https://doi.org/10.1016/j.tibs.2017.10.002

Nitika, Porter CM, Truman AW, Truttmann MC (2020) Post-translational modifications of Hsp70 family proteins: Expanding the chaperone code. J Biol Chem 295(31):10689–10708. https://doi.org/10.1074/jbc.REV120.011666

Njunge, J.M, Ludewig, M.H, Boshoff, A., Pesce, E., Blatch, G.L. (2013). Hsp70s and J proteins of Plasmodium parasites infecting rodents and primates: structure, function, clinical relevance, and drug targets. Curr Pharm Des, 19: 387-403.

Noga, M., Milan, J., Frydrych, A., & Jurowski, K. (2023). Toxicological aspects, safety assessment, and green toxicology of silver nanoparticles (AgNPs)—critical review: state of the art. *International Journal of Molecular Sciences*, *24*(6), 5133.

Nowicki, Ł., Leźnicki, P., Morawiec, E., Litwińczuk, N., Liberek, K. (2012). Role of a conserved aspartic acid in nucleotide binding domain 1 (NBD1) of Hsp100 chaperones in their activities. Cell Stress Chaperones, 17: 361–373.

Obaid, A. Y., Al-Thabaiti, S. A., Al-Harbi, L. M., & Khan, Z. (2015). Extracellular biosynthesis of silver nanoparticles. Global Advanced Research Journal of Microbiology, 3(8), 119e126.

Omer, H. A., Caprioli, G., Abouelenein, D., Mustafa, A. M., Uba, A. I., Ak, G., ... & Yagi, S. (2022). Phenolic profile, antioxidant and enzyme inhibitory activities of leaves from two Cassia and two Senna species. *Molecules*, *27*(17), 5590.

Onitsuka S., Hamada T., Okamura H. Preparation of Antimicrobial Gold and Silver Nanoparticles from Tea Leaf Extracts. Colloids Surf. B Biointerfaces. 2019; 173:242–248

Paitan, Y. (2018). Current trends in antimicrobial resistance of Escherichia coli. *Escherichia coli, a versatile pathogen*, 181-211.

Parivuguna, V. (2008). Antimicrobial Properties and Phytochemical Constituents of Rheo discolor Hance. *Ethnobotanical Leaflets*, *2008*(1), 114.



© University of Venda

Patel, S. R. (2021). *Studies for developing shoot cultures of Leptadenia reticulata (Retz.) wight and arn and Tylophora indica (Burm. F.) Merrill with phytochemical analysis* (Doctoral dissertation, Maharaja Sayajirao University of Baroda (India)).

Panja, S., Chaudhuri, I., Khanra, K., & Bhattacharyya, N. (2016). Biological application of green silver nanoparticle synthesized from leaf extract of Rauvolfia serpentina Benth. *Asian Pacific Journal of Tropical Disease*, *6*(7), 549-556.

Park, S. J. (2020). Protein–nanoparticle interaction: corona formation and conformational changes in proteins on nanoparticles. *International journal of nanomedicine*, 5783-5802.

Patle, T. K., Shrivas, K., Kurrey, R., Upadhyay, S., Jangde, R., & Chauhan, R. (2020). Phytochemical screening and determination of phenolics and flavonoids in Dillenia pentagyna using UV–vis and FTIR spectroscopy. *Spectrochimica Acta Part A: Molecular and Biomolecular Spectroscopy*, *242*, 118717.

Phatak, S. S., Stephan, C. C., & Cavasotto, C. N. (2009). High-throughput and in silico screenings in drug discovery. *Expert Opinion on Drug Discovery*, *4*(9), 947-959.

Picard, D., Khursheed, B., Garabedian, M. J., Fortin, M.G., Lindquist S, Yamamoto K. R. (1990). Reduced levels of Hsp90 compromise steroid receptor action in vivo. Nature, 348: 166-168.

Pinelli, F., Perale, G., & Rossi, F. (2020). Coating and functionalization strategies for nanogels and nanoparticles for selective drug delivery. *Gels*, *6*(1), 6.

Pobre KFR, Poet GJ, Hendershot LM. The endoplasmic reticulum (ER) chaperone BiP is a master regulator of ER functions: Getting by with a little help from ERdj friends. J Biol Chem.2019; 294:2098–2108

Polier S, Dragovic Z, Hartl FU, Bracher A (2008b) Structural basis for the cooperation of Hsp70 and Hsp110 chaperones in protein folding. Cell 133(6):1068–1079. https://doi.org/10.1016/j. cell.2008.05.022

Prasad, R., Swamy, V. S., & Varma, A. (2012). Biogenic synthesis of silver nanoparticles from the leaf extract of Syzygium cumini (L.) and its antibacterial activity. *Int J Pharma Bio Sci*, *3*(4), 745-752.

Pratt WB, Morishima Y, Peng HM, Osawa Y (2010) Proposal for a role of the Hsp90/Hsp70-based chaperone machinery in making triage decisions when proteins undergo oxidative and toxic damage. Exp Biol Med (Maywood) 235(3):278–289. https://doi.org/10.1258/ebm.2009.009250

Priester, J., Stoimenov, P., Mielke, R., Webb, S., Ehrhardt, C., Zhang J., Stucky, G., & Holden, P. (2009). Effects of soluble cadmium salts versus CdSe quantum dots on the growth of planktonic Pseudomonas aureginosa. Environ. Sci. Technol. 43: 2589-2594



© University of Venda

R. Bali, N. Razak, A. Lumb, A.T. Harris, The synthesis of metallic nanoparticles inside live plants, in: International Conference on Nanoscience and Nanotechnology, IEEE, 2006.

Rafael Á. C., Jesús Á. A.A (2023). Green Synthesis of Nanoparticles: A Biological Approach. DOI: http://dx.doi.org/10.5772/intechopen.1002203.

Rajan, R., Ahmed, S., Sharma, N., Kumar, N., Debas, A., & Matsumura, K. (2021). Review of the current state of protein aggregation inhibition from a materials chemistry perspective: Special focus on polymeric materials. *Materials Advances*, *2*(4), 1139-1176.

Rajesh, V., Sophiya, J., Jacob, S., Arumugam, P., & Jayaraman, P. (2017). Biosynthesis of silver nanoparticles using Diospyros ferrea (Willd.) bakh. leaves and evaluation of its antioxidant, anti-inflammatory, antimicrobial and anticancer activity. *Journal of Bionanoscience*, *11*(1), 24-33.

Raviol H, Sadlish H, Rodriguez F, Mayer MP, Bukau B (2006) Chaperone network in the yeast cytosol: Hsp110 is revealed as an Hsp70 nucleotide exchange factor. EMBO J 25 (11):2510–2518. https://doi.org/10.1038/sj.emboj.7601139

Read, R. J., Adams, P. D., Arendall, W. B., Brunger, A. T., Emsley, P., Joosten, R. P., ... & Zwart, P. H. (2011). A new generation of crystallographic validation tools for the protein data bank. *Structure*, *19*(10), 1395-1412.

Rehman, A., Nazir, G., Rhee, K. Y., & Park, S. J. (2022). Valorization of orange peel waste to tunable heteroatom-doped hydrochar-derived microporous carbons for selective CO2 adsorption and separation. *Science of the Total Environment*, *849*, 157805.

Ricci, L., & Williams, K. P. (2008). Development of fluorescence polarization assays for the molecular chaperone Hsp70 family members: Hsp72 and DnaK. *Current chemical genomics*, *2*, 90.

Ritossa, F. (1996). Discovery of the heat shock response. Cell Stress Chaperones, 1:97-8.

Rohland, L., Kityk, R., Smalinskaitė, L., & Mayer, M. P. (2022). Conformational dynamics of the Hsp70 chaperone throughout key steps of its ATPase cycle. *Proceedings of the National Academy of Sciences*, *119*(48), e2123238119.



© University of Venda

Rohland, L., Kityk, R., Smalinskaitė, L., & Mayer, M. P. (2022). Conformational dynamics of the Hsp70 chaperone throughout key steps of its ATPase cycle. *Proceedings of the National Academy of Sciences*, *119*(48), e2123238119.

Roncarati D, Scarlato V (2017) Regulation of heat-shock genes in bacteria: from signal sensing to gene expression output. FEMS Microbiol Rev 41:49–574. https://doi.org/10.1093/femsre/fux015

Rosenzweig, R., Nillegoda, N. B., Mayer, M. P., & Bukau, B. (2019). The Hsp70 chaperone network. *Nature reviews molecular cell biology*, *20*(11), 665-680.

Rosen, J. E., & Gu, F. X. (2011). Surface functionalization of silica nanoparticles with cysteine: a low-fouling zwitterionic surface. *Langmuir*, *27*(17), 10507-10513.

Rosero, W. A. A., Barbezan, A. B., de Souza, C. D., & Rostelato, M. E. C. M. (2024). Review of advances in coating and functionalization of gold nanoparticles: from theory to biomedical application. *Pharmaceutics*, *16*(2), 255.

Rosmalena, R., Senlia, A. O., Hanafi, M., Artanti, N., Eldafira, E., Handayani, S. I., ... & Prasasty, V. D. (2022). Phytochemical, Antioxidant and Antidiabetic properties of *Senna alexandrina* Leaf Extract. *Research Journal of Pharmacy and Technology*, *15*(12), 5835-5840.

Rosenzweig R, Nillegoda NB, Mayer MP, Bukau B (2019) The Hsp70 chaperone network. Nat Rev Mol Cell Biol 20(11):665–680. https://doi.org/10.1038/s41580-019-0133-3

Rosero, W. A. A., Barbezan, A. B., de Souza, C. D., & Rostelato, M. E. C. M. (2024). Review of advances in coating and functionalization of gold nanoparticles: from theory to biomedical application. *Pharmaceutics*, *16*(2), 255.

Rout, A. N. A. N. D. I. N. I., Jena, P. K., Parida, U. K., & Bindhani, B. K. (2013). Green synthesis of silver nanoparticles using leaves extract of Centella asiatica L. For studies against human pathogens. *Int J Pharm Biol Sci*, *4*(4), 661-74.

Rudiger S, Buchberger A, Bukau B. Interaction of Hsp70 chaper-ones with substrates. Nat Struct Biol. 1997;4:342–349

Sadeghi, B., Rostami, A., & Momeni, S. S. (2015). Facile green synthesis of silver nanoparticles using seed aqueous extract of Pistacia atlantica and its antibacterial activity. *Spectrochimica Acta Part A: Molecular and Biomolecular Spectroscopy*, *134*, 326-332.

Sahoo, S. K., & Hormozi-Nezhad, M. R. (Eds.). (2023). *Gold and silver nanoparticles: synthesis and applications*. Elsevier.



© University of Venda

Saibil, H. (2013) Chaperone machines for protein folding, unfolding and disaggregation. Nat Rev Mol Cell Biol, 14: 630–642.

Saim AK, Kumah FN, Oppong MN. (2021). Extracellular and intracellular synthesis of gold and silver nanoparticles by living plants: A review. Nanotechnology for Environmental Engineering, 6(1):1. DOI: 10.1007/s41204-020-00095-9

Sanchez, Y., Taulien, J., Borkovich, K., Lindquist, S. L. (1990). Hsp104 is required for tolerance to many forms of stress. Science, 248: 1112-1115.

Sánchez-López, E., Gomes, D., Esteruelas, G., Bonilla, L., Lopez-Machado, A. L., Galindo, R., ... & Souto, E. B. (2020). Metal-based nanoparticles as antimicrobial agents: an overview. *Nanomaterials*, *10*(2), 292.

Saravanakumar, A., Peng, M. M., Ganesh, M., Jayaprakash, J., Mohankumar, M., & Jang, H. T. (2017). Low-cost and eco-friendly green synthesis of silver nanoparticles using Prunus japonica (Rosaceae) leaf extract and their antibacterial, antioxidant properties. *Artificial cells, nanomedicine, and biotechnology*, *45*(6), 1165-1171.

Sastry, M., Mayya, K. S. & Bandyopadhyay, K. pH Dependent changes in the optical properties of carboxylic acid derivatized silver colloidal particles. Colloids Surf. A: Physicochem. & Engi. Aspects 127, 221–228 (1997).

Sato, S., Wilson, R.J. (2004). The use of DsRED in single- and dual-color fluorescence labeling of mitochondrial and plastid organelles in Plasmodium falciparum. Mol Biochem Parasitol, 134:175-9.

Schmid, F. X. (1992). *Protein folding* (pp. 197-241).

Selmani, A., Kovačević, D., & Bohinc, K. (2022). Nanoparticles: From synthesis to applications and beyond. *Advances in colloid and interface science*, *303*, 102640.

Sennuga, A., van Marwijk, J., Boshoff, A., & Whiteley, C. G. (2012). Enhanced activity of chaperonin GroEL in the presence of platinum nanoparticles. *Journal of Nanoparticle Research*, *14*, 1-11.

Shameli, K., Ahmad, M. B., Jazayeri, S. D., Sedaghat, S., Shabanzadeh, P., Jahangirian, H., ... & Abdollahi, Y. (2012). Synthesis and characterization of polyethylene glycol mediated silver nanoparticles by the green method. *International journal of molecular sciences*, *13*(6), 6639-6650.

Shaner L, Sousa R, Morano KA (2006) Characterization of Hsp70 binding and nucleotide exchange by the yeast Hsp110 chaperone Sse1. Biochemistry 45(50):15075–15084. https://doi.org/10. 1021/bi061279k

Sharma, V. K., Yngard, R. A., & Lin, Y. (2009). Silver nanoparticles: green synthesis and their antimicrobial



© University of Venda

activities. *Advances in colloid and interface science*, *145*(1-2), 83-96.

Sharma, S. K., Christen, P., & Goloubinoff, P. (2009). Disaggregating chaperones: an unfolding story. *Current Protein and Peptide Science*, *10*(5), 432-446.

Sharma, S., Yadav, M., & Bhardwaj, N. (2017). "*Senna alexandrina*-mediated green synthesis of silver nanoparticles: Synthesis, characterization, and antimicrobial activity." *International Journal of Nanotechnology*, 14(3), 128-139.

Shonhai A, Boshoff A, Blatch GL. The structural and functional diversity of Hsp70 proteins from Plasmodium falciparum. Protein Sci. 2007; 16: 1803–1818. PMID: 17766381

Shonhai, A., Maier, A.G., Przyborski, J., and Blatch, G.L. (2011). Intracellular protozoan parasites of humans: the role of molecular chaperones in development and pathogenesis. Protein Pept Lett, 18: 143-157 doi: 10.2174/092986611794475002.

Shonhai, A., Boshoff, A., Blatch, G. L. (2005). Plasmodium falciparum heat shock protein 70 is able to suppress the thermosensitivity of an *Escherichia coli* DnaK mutant strain. Mol Genet Genomics, 274: 70–78.

Shonhai, A., Botha, M., Beer. T.A.P., Boshoff, A., and Blatch, G.L. (2008). Structure-function analysis of Plasmodium falciparum heat shock protein 70 using three dimensional modelling and in vitro analysis. Protein Pept. Lett. 15: 1117-1125.

Sibbald, R. G., Contreras-Ruiz, J., Coutts, P., Fierheller, M., Rothman, A., & Woo, K. (2007). Bacteriology, inflammation, and healing: a study of nanocrystalline silver dressings in chronic venous leg ulcers. *Advances in skin & wound care*, *20*(10), 549-558.

Silberg, J. J., Vickery, L. E. (2000) Kinetic characterization of the ATPase cycle of the molecular chaperone Hsc66 from Escherichia coli. J Biol Chem, 275: 7779−7786.

Singh R, Altaee A, Gautam S. (2020). Nanomaterials in the advancement of hydrogen energy storage. Heliyon, 6(7):e04487. DOI: 10.1016/j. heliyon. 2020.e0448

Singh J, Dutta T, Kim KH, Rawat M, Samddar P, Kumar P.(2018). 'Green' synthesis of metals and their oxide nanoparticles: Applications for environmental remediation. Journal of Nanbiotechnology, 16(1):84. DOI: 10.1186/s12951-018-0408-4



© University of Venda

Singh, H., Desimone, M. F., Pandya, S., Jasani, S., George, N., Adnan, M., ... & Alderhami, S. A. (2023). Revisiting the green synthesis of nanoparticles: uncovering influences of plant extracts as reducing agents for enhanced synthesis efficiency and its biomedical applications. *International journal of nanomedicine*, 4727-4750.

Sinha, S. N., Paul, D., Halder, N., Sengupta, D., & Patra, S. K. (2015). Green synthesis of silver nanoparticles using fresh water green alga Pithophora oedogonia (Mont.) Wittrock and evaluation of their antibacterial activity. *Applied Nanoscience*, *5*, 703-709.

Skowyra D, Georgopoulos C, Zylicz M (1990) The *E. coli* dnaK gene product, the hsp70 homolog, can reactivate heat-inactivated RNA polymerase in an ATP hydrolysis-dependent manner. Cell 62(5):939–944. https://doi.org/10.1016/0092-8674(90)90268-j

Slepenkov SV, Witt SN (2002) The unfolding story of the *Escherichia coli* Hsp70 DnaK: is DnaK a holdase or an unfoldase? Mol Microbiol 45(5):1197–1206. https://doi.org/10.1046/j.1365-2958. 2002.03093.x

Sondi, I., & Salopek-Sondi, B. (2004). "Silver nanoparticles as antimicrobial agents: A case study." *Journal of Colloid and Interface Science*, 275(1), 177-182.

Sorbiun, M., Shayegan Mehr, E., Ramazani, A., & Mashhadi Malekzadeh, A. (2018). Biosynthesis of metallic nanoparticles using plant extracts and evaluation of their antibacterial properties. *Nanochemistry Research*, *3*(1), 1-16.

Squires, C. (1992). The Clp proteins: proteolysis regulators or molecular chaperones. J Bacteriol, 174: 1081-1085.

Stewart, A. L. (2024). CRISPR systems-molecular mechanisms of the interaction between Cas1 and DnaK (Doctoral dissertation, University of Nottingham).

Swain, J.F, Dinler, G, Sivendran, R, Montgomery, D. L, Stotz, M, and Gierasch, L. M. (2007) Hsp70 chaperone ligands control domain association via an allosteric mechanism mediated by the interdomain linker. Mol Cell, 26: 27–39.

Szklarczyk, D., Gable, A. L., Lyon, D., Junge, A., Wyder, S., Huerta-Cepas, J., ... & Mering, C. V. (2019). STRING v11: protein–protein association networks with increased coverage, supporting functional discovery in genome-wide experimental datasets. *Nucleic acids research*, *47*(D1), D607-D613.

Tai, P. K.K., Albers, M. W., Chang, H., Faber, L.E, Schreiber, S.L. (1992). Association of a 50-kilodalton immunophilin with the glucocorticoid receptor complex. Science, 256: 1315-1318.



© University of Venda

Terrence, M. D. (2022). *Development of Liquid Chromatography Mass Spectrometry technique for evaluation and differentiation of plant derived isomers* (Doctoral dissertation, University of Johannesburg).

Thanh NTK, Maclean N, Mahiddine S. (2014). Mechanisms of nucleation and growth of nanoparticles in solution. Chemical Reviews, 114(15):7610- 7630. DOI: 10.1021/cr400544s

Thompson, A. D., Bernard, S. M., Skiniotis, G., & Gestwicki, J. E. (2012). Visualization and functional analysis of the oligomeric states of *Escherichia coli* heat shock protein 70 (Hsp70/DnaK). *Cell Stress and Chaperones*, *17*(3), 313-327.

Tonui, R., John, R. O., & Edkins, A. L. (2023). Optimized Microscale Protein Aggregation Suppression Assay: A Method for Evaluating the Holdase Activity of Chaperones. In *Chaperones: Methods and Protocols* (pp. 113-123). New York, NY: Springer US.

Torrente M. P., Shorter J. (2013). The metazoan protein disaggregase and amyloid depolymerase system: Hsp110, Hsp70, Hsp40, and small heat shock proteins. Prion, 7: 457–463.

Tripathy, A., Raichur, A. M., Chandrasekaran, N., Prathna, T. C., & Mukherjee, A. (2010). Process variables in biomimetic synthesis of silver nanoparticles by aqueous extract of Azadirachta indica (Neem)

Triulzi RC, Dai Q, Zou J, Leblanc RM, Gu Q, Orbulesu J et al. Photothermal ablation of amyloid aggregates by gold nanoparticles. Colloids Surf B Biointerfaces. 2008; 63: 200–208. doi: 10.1016/j.colsurfb.2007.12.006 PMID: 18262396

Tsugawa, H., Cajka, T., Kind, T., Ma, Y., Higgins, B., Ikeda, K., ... & Arita, M. (2015). MS-DIAL: data-independent MS/MS deconvolution for comprehensive metabolome analysis. *Nature methods*, *12*(6), 523-526.

Ullah, A., & Lim, S. I. (2022). Plant extract-based synthesis of metallic nanomaterials, their applications, and safety concerns. *Biotechnology and Bioengineering*, *119*(9), 2273-2304.

V. Kumar, S.K. Yadav, Plant-mediated synthesis of silver and gold nanoparticles and their applications, Journal of Chemical Technology & Biotechnology 84 (2009) 151-157.

Veerasamy, R., Xin, T. Z., Gunasagaran, S., Xiang, T. F. W., Yang, E. F. C., Jeyakumar, N., et al. (2011). Biosynthesis of silver nanoparticles using mangosteen leaf extract and evaluation of their antimicrobial activities. Journal of Saudi Chemical Society, 15, 113e120.

Velmurugan, P., Anbalagan, K., Manosathyadevan, M., Lee, K. J., Cho, M., Lee, S. M., ... & Oh, B. T.



© University of Venda

(2014). Green synthesis of silver and gold nanoparticles using Zingiber officinale root extract and antibacterial activity of silver nanoparticles against food pathogens. *Bioprocess and biosystems engineering*, *37*, 1935-1943.

Velusamy P, Kumar GV, Jeyanthi V, Das J, Pachaiappan R. (2016). Bio-inspired green nanoparticles: Synthesis, mechanism, and antibacterial application. Toxicological Research, 32(2):95- 102. DOI: 10.5487/TR.2016.32.2.095

Ventola, C. L. (2015). "The antibiotic resistance crisis: Part 1: Causes and threats." *Pharmacy and Therapeutics*, 40(4), 277-283.

Viswanathan, S., & Nallamuthu, T. (2012). Phytochemical screening and antimicrobial activity of leaf extracts of *Senna alexandrina* Mill. against human pathogens. *International Journal of Current Science*, *2*, 51-56.

Vogel, M, Mayer, M. P, Bukau, B. (2006) Allosteric regulation of Hsp70 chaperones involves a conserved interdomain linker. J Biol Chem, 281: 38705–38711.

Vos MJ, Hageman J, Carra S, Kampinga HH (2008) Structural and functional diversities between members of the human HSPB, HSPH, HSPA, and DNAJ chaperone families. Biochemistry 47 (27):7001–7011

Walker, J. E., Saraste, M., Runswick, M. J., & Gay, N. J. (1982). Distantly related sequences in the alpha- and beta-subunits of ATP synthase, myosin, kinases, and other ATP-requiring enzymes and a common nucleotide binding fold. *The EMBO journal*, *1*(8), 945–951.

Wang, H. C., Spencer, M., Susko, E., & Roger, A. J. (2007). Testing for covarion-like evolution in protein sequences. *Molecular biology and evolution*, *24*(1), 294-305..

Wu Q , Shou MW, Du ZY, Jun GH, Hui D. (2020). Mechanical properties of nanomaterials: A review. Nanotechnology Reviews, 9(1): 259-273. DOI: 10.1515/ntrev-2020-0021

Wynn, R. M., Davie, J. R., Cox, R. P., Chuang, D. T. (1994). Molecular chaperones: heat-shock proteins, foldases, and matchmakers. J Lab Clin Med, 124: 31–36.

Yadav, V. K., Khan, S. H., Malik, P., Thappa, A., Suriyaprabha, R., Ravi, R. K., ... & Gnanamoorthy, G. (2020). Microbial synthesis of nanoparticles and their applications for wastewater treatment. *Microbial biotechnology: basic research and applications*, 147-187.



© University of Venda

Yadav, M. R., Choudhary, M., Singh, J., Lal, M. K., Jha, P. K., Udawat, P., ... & Prasad, P. V. (2022). Impacts, tolerance, adaptation, and mitigation of heat stress on wheat under changing climates. *International Journal of Molecular Sciences*, *23*(5), 2838.

Yagi, S., El Tigani, S., Ali, M., Elkhidir, I., & Mohammed, A. M. (2013). Chemical constituents and insecticidal activity of Senna italica Mill. from the Sudan. *International letters of chemistry, Physics and Astronomy*, *9*, 146-151.

Yang, C., Wang, H., Zhu, D., Hong, C.S., Dmitriev, P., Zhang, C., Li, Y., Ikejiri, B., Brady, R.O., Zhuang, Z. (2015). Mutant glucocerebrosidase in Gaucher disease recruits Hsp27 to the Hsp90 chaperone complex for proteasomal degradation. Proc Natl Acad Sci U S A, 112: 1137-42.

Yang, H., Xiao, X., Zhao, X., & Wu, Y. (2017, March). Intrinsic fluorescence spectra of tryptophan, tyrosine and phenyloalanine. In *Selected papers of the Chinese society for optical engineering conferences held october and november 2016* (Vol. 10255, pp. 1199-1206). SPIE.

Yang, L., Dong, H., Wang, J., Dadmohammadi, Y., Zhou, Y., Lin, T., ... & Abbaspourrad, A. (2024). Fabrication and characterization of whey protein isolate-tryptophan nanoparticles by pH-shifting combined with heat treatment. *Food Research International*, *196*, 115031.

Yu, A., Li, P., Tang, T., Wang, J., Chen, Y., Liu, L. (2015). Roles of Hsp70s in stress responses of microorganisms, plants, and animals. BioMed Research International, 2015. doi: 10.1155/2015/510319.

Yuvarajan, R., Natarajan, D., & Jayavel, R. (2014). Green synthesized silver nanoparticles from Indoneesiella echioides and its antibacterial potential. *Indo Am. J. Pharm. Res*, *4*, 5121-5128.

Zabetakis, K., Ghann, W. E., Kumar, S., & Daniel, M.-C. (2012). Effect of high gold salt concentrations on the size and polydispersity of gold nanoparticles prepared by an extended Turkevich–Frens method. Gold Bulletin, 45(4), 203–211. https://doi.org/10.1007/s13404-012 0069-2

Zaheer, Z. (2012). Silver nanoparticles to self-assembled films: green synthesis and characterization. Colloids and surfaces B: Biointerfaces, 90, 48-52.

Zeb, A. (2021). Chromatography of Phenolic Antioxidants. In: Phenolic Antioxidants in Foods: Chemistry, Biochemistry and Analysis. Springer, Cham. https://doi.org/10.1007/978-3-030-74768-8_16

Zhan, X., Yan, J., Tang, H., Xia, D., & Lin, H. (2022). Antibacterial properties of gold nanoparticles in the modification of medical implants: a systematic review. *Pharmaceutics*, *14*(12), 2654.

Zhang, P, Leu, J. I.-J, Murphy, M. E, George, D. L, Marmorstein, R. (2014) Crystal structure of the stress-inducible human heat shock protein 70 substrate-binding domain in complex with a peptide substrate. PloS



© University of Venda

ONE, 9: e103518.

Zhang L, Gu F, Chan J, Wang A, Langer R, Farokhzad O. (2008). Nanoparticles in medicine: Therapeutic applications and developments. Clinical Pharmacology and Therapeutics. 2008;83(5):761-769. DOI: 10.1038/sj.clpt.6100400

Zhao, J., Cao, Y., & Zhang, L. (2020). Exploring the computational methods for protein-ligand binding site prediction. *Computational and structural biotechnology journal*, *18*, 417-426.

Zhao L, Vecchi G, Vendruscolo M, Korner R, Hayer-Hartl M, Hartl FU (2019) The Hsp70 chaperone system stabilizes a thermo-sensitive subproteome in *E. coli*. Cell Rep 28 (5):1335–1345. e1336. https://doi.org/10.1016/j.celrep.2019.06.081

Zhou, J., Panaitiu, A. E., & Grigoryan, G. (2020). A general-purpose protein design framework based on mining sequence–structure relationships in known protein structures. *Proceedings of the National Academy of Sciences*, *117*(2), 1059-1068.

Zhuravleva, A, and Gierasch, L.M. (2011) Allosteric signal transmission in the nucleotide -binding domain of 70-kDa heat shock protein (Hsp70) molecular chaperones. Proc Natl Acad Sci U S A, 108: 6987–6992.

Zia, M., Gul, S., Akhtar, J., Haq, I. U., Abbasi, B. H., Hussain, A., ... & Chaudhary, M. F. (2017). Green synthesis of silver nanoparticles from grape and tomato juices and evaluation of biological activities. *IET nanobiotechnology*, *11*(2), 193-199.

Zininga, T., Achilonu, I., Hoppe, H., Prinsloo, E., Dirr, H.W., Shonhai, A. (2015). Overexpression, purification and characterization of the Plasmodium falciparum Hsp70-z (PfHsp70-z) Protein, PLoS ONE 10: e0129445

Zininga, T., Achilonu, I., Hoppe, H., Prinsloo, E., Dirr, H., Shonhai, A. (2016). Plasmodium falciparum Hsp70-z, an Hsp110 homolog, exhibits independent chaperone activity and interacts with Hsp70–1 in a nucleotide-dependent fashion. Cell Stress Chaperones. 21:499-513

Zuiderweg, E.R.P. (2004). The structure of the chaperone protein DnaK reveals its intricate working mechanism. *Trends in Biochemical Sciences*, 29(2), 148-153

Zuiderweg ER, Hightower LE, Gestwicki JE (2017) The remarkable multivalency of the Hsp70 chaperones. Cell Stress Chaperones 22:173–189. https://doi.org/10.1007/s12192-017-0776-y



© University of Venda

# APPENDICES

## Appendix A: SPECIALISED REAGENTS & EQUIPMENT

### Table A: Special chemical reagents & equipment

| Name of reagents | Supplier |
|---|---|
| Agarose | Merck |
| Ammonium persulphate | Sigma-Aldrich |
| Ampicillin | Calbiochem |
| Chemiluminescence Western blotting kit | Amersham |
| 2-mercaptoethanol | Merck |
| Bovine serum albumin | Melford |
| Bromophenol blue | Merck |
| Calcium chloride | Merck |
| Multifuge X1 R Pro, 208-240V H-Flex Cell Culture Package | ThermoFisher Scientific, USA |
| Coomassie brilliant blue R250 | Merck |
| Ethidium bromide | Merck |
| Glacial acetic acid | Merck |
| Glycerol | Merck |
| Glycine | Merck |
| Imidazole | Merck |
| Lambda DNA Fermantas | Life sciences |
| Lysozyme | Merck |
| Methanol | Merck |
| L-Malate dehydrogenase | Glentham |
| Magnesium chloride | Merck |
| Monoclonal mouse anti-His antibody | Merck |
| Phenylmethylsulfonyl fluoride (PMSF) | Merck |
| Polyacrylamide | Merck |
| Restriction enzymes | ThermoFisher Scientific, USA |
| Sodium chloride | Merck |
| Sodium dodecyl sulphate | Merck |
| Sodium hydroxide | Merck |



© University of Venda

| | |
|---|---|
| TEMED | Sigma-Aldrich |

| | |
|---|---|
| Tris | Merck |
| Tryptone | Oxoid, England |
| Tween 20 | Radchem |
| Yeast | Merck |
| Broth | Merck |
| Nutrient agar | Merck |
| Glucose | Merck |
| Protein ladder | New England Biolabs; ThermoFisher Scientific, USA |



© University of Venda

# Appendix B: General Experimental Procedures

## 1.1. Materials:

The *E. coli* JM109 cells and *E. coli* XL1 Blue cells were obtained from Prof Addmore Shonhai's Probiom lab at the University of Venda. Other reagents used in this study are listed in Appendix A-1.

### B1. Extraction of plasmid DNA:

Plasmid DNA extraction was performed using Zyppy$^{TM}$ Plasmid Miniprep Kit following the manufacturer's protocol.

### B2. Conformation of pQE30 vector plasmid and pQE30/DnaK:

Agarose gel electrophoresis and restriction digest were used to verify the integrity of the plasmid pQE30 vector and the DNA segment encoding for DnaK (pQE30-DnaK) (Appendix C-1, Figure S.1). A pQE30-DnaK plasmid is an IPTG inducible expression fused to an N-terminal 6xHis tag. It was obtained from Addgene (USA) in stab culture format. Upon arrival, it was verified using restriction digestion.

### B3. Enzymatic restriction digest of Plasmid DNA:

Plasmid DNA was digested according to the protocol outlined below (Table B1) using the appropriate diagnostic restriction enzymes. Restriction enzymes, *Hind* III and *Bam*H1 were used to fast digest the Plasmid DNA. The reaction was incubated for 1 hour at 37 °C. A 2 µl DNA sample contained approximately (1 µg DNA). A 4 µl loading dye (0.25% bromophenol blue and 30% glycerol) was added to stop the digestion reaction. The resulting product was analyzed through agarose gel electrophoresis, as described in (Appendix B4).



© University of Venda

**Table B1: Restriction digestion reaction mixture**

| Constituents | Tube A<br><br>Uncut (Control) | Tube B<br><br>*Bam*H1 | Tube C<br><br>*Hind*III | Tube D<br><br>*Bam*H1 & *Hind*III |
|---|---|---|---|---|
| Nuclease free $H_2O$ | 16 µl | 15 | 14 µl | 13 µl |
| 10X fast digest buffer | 2 µl | 2 µl | 2 µl | 2 µl |
| DNA | 2 µl | 2 µl | 2 µl | 2 µl |
| *Bam*H1 | -- | 1 µl | -- | 1 µl |
| *Hind*III | -- | -- | 2 µl | 2 µl |
| **Total vol (µl))** | 20 µl | 20 µl | 20 µl | 20 µl |

**B4. Agarose gel electrophoresis:**

To prepare a 0.8% (w/v) agarose gel, the required amount of agarose was thoroughly dissolved in 1x TAE buffer (40 mM, 20 mM acetic acid, and 1 mM EDTA) by heating with frequent agitation. After cooling to 55°C, ethidium bromide (0.5 µg/ml) was added to the agarose. At room temperature, the agarose gel was allowed to polymerize for 15 to 30 minutes. The gel was placed in the electrophoresis chamber and covered with 1x TAE buffer. After adding 20 µl of sample to 4 µl of 10x DNA loading buffer (0.25% bromophenol blue + 30% glycerol), the samples were loaded into the wells. Electrophoresis was conducted at 100 volts for one hour. The gel was then visualized using Chemidoc imager (Biorad, USA).

**B5. Preparation of competent *E. coli* XL1/JM109 Blue cells:**

From a 2YT (2x yeast-tryptone) agar plate (1.6g tryptone, 0.5g yeast, 1g yeast, and 1.5g agar per 100 ml distilled water), a colony of E. coli XL1 blue cells/JM109 cells was picked, and it was then inoculated into 5ml of 2x YT broth which contained 1.6g tryptone, 0.5 yeast, and 1g yeast. The culture was incubated overnight at 37°C, shaking at 160 rpm. The overnight culture was transferred to 45ml 2 YT broth, grown to OD 0.3-0.6 at 600 nm, and then centrifuged at 5000 xg for 20 minutes at 4°C. For 30 minutes, the pellet was placed in ice after being resuspended in 10 ml of 0.1M MgCl2. Following a 10-minute centrifugation at 5000 xg and 4°C, the cells were resuspended in 5 ml of 0.1M CaCl2 and gently shaken for four hours in an ice-filled incubator. The cells were resuspended in 5 ml CaCl2 and ice-cold 30% glycerol after being



© University of Venda

centrifuged for 10 minutes at 5000 xg and 4°C. Additionally, competent cells were aliquoted into 2 ml tubes and then stored at -80°C refrigerator for future use.

**B6. Transformation of *E. coli* Competent Cells by pQE30-DnaK:**

The pQE30-DnaK plasmid was transformed in *E. coli* XL1 blue cells. 5 µL of plasmid DNA was added into a 1.5 mL tube on ice, followed by 50 µl of *E. coli* XL1 blue ells. Before the tube was placed on ice for 30 minutes, the content was mixed by flicking the tube. The mixture was then heat-shocked by placing the tubes immediately from ice to a heating block at 42°C for 10 seconds for cells to take in the pQE30-DnaK clone. Following heat shock, the tube was placed on ice for five minutes. In the tubes containing cells transformed with a pQE30-DnaK clone, 900 and 50 µl of room temperature Super Optimal broth with Catabolite suppression (SOC) media was added. Following that, the reaction mixture was incubated while shaking at 250 rpm for an hour at 37°C. After incubation, 20 µL of each transformed culture was plated into LB agar plates that contained 100 µg/mL of ampicillin. The plates were then incubated at 37°C overnight.

**B7. Sodium dodecyl sulfate-polyacrylamide gel electrophoresis (SDS-PAGE) analysis**

Prior to boiling at 100 °C on a heating block for 10 minutes for the purpose of denaturing, the protein was mixed with SDS sample buffer (0.25 % coomassie brilliant blue (R250); 2 % SDS; 10 % glycerol (v/v); 100 mM Tris;1 % β-mercaptoethanol) in a ratio of 4:1 respectively. Following the denaturing step, the samples were resolved on a 12 % SDS-PAGE gel prepared as shown in (table B2). The gel was then transferred into the electrophoresis tank containing electrophoresis buffer (25 mM Tris, 250 mM glycine and 0.1 % (w/v) SDS, pH 8.3). The boiled samples were loaded in respective wells and pre-stained protein molecular weight markers (ThermoFisher Scientific, USA) were also loaded. The gel was run at 120 volts for 90 minutes utilizing the Bio-Rad Mini protein electrophoresis system (Biorad, U.S.A).

**Table B2: Preparation of SDS PAGE:**

| **Reagent (ml)** | **5 % Stacking gel** | **12 % Separating gel** |
|---|---|---|
| 30 % Bis/acrylamide | 0.235 | 2.08 |
| 1.0 M Tris (pH 6.8) | 0.437 | - |
| 1.5 M Tris (pH 8.8) | - | 1.25 |
| 10 % SDS | 0.0175 | 0.05 |



© University of Venda

| | | |
|---|---|---|
| Distilled water | 1.05 | 1.58 |
| 10% Ammonium persulphate | 0.00875 | 0.025 |
| TEMED | 0.0020 | 0.0020 |

**B8. Immunoblotting (Western blot):**

Proteins were initially resolved by SDS-PAGE analysis (Appendix B7) and the unstained gel, and the nitrocellulose membrane was incubated in Western transfer buffer (25 mM Tris, 192 mM and 20 % methanol) for 15 minutes. One of the pre-wetted Whatman filter papers were then put on the positive plate of the trans-blotter. The pre-wetted nitrocellulose membrane was then placed on the filter paper, followed by placement of the gel on the nitrocellulose membrane and lastly covering with another pre-wetted filter paper. The negative plate was placed on top of the filter to make a sandwich. The trans-blotter was run at 100 V, 3 A, for 10 minutes. After transfer, the blots were blocked with 5 % milk in TBS (20 mM Tris, pH 7.5, 500 mM NaCl) for an hour. Anti-DnaK primary antibodies (1:1000) were used to incubate the blot for 1hr with gentle shaking. Washing was done thrice with TBS-Tween for 10 minutes each time. Incubation was done with secondary rabbit raised antibodies (1:2,500) for 1hour with gentle shaking. Proceeding washing as done with primary antibody visualization was done with chemiluminescence substrates (Thermoscientific) using ChemidocTM MP Imaging System was used (BioRad, USA) to visualize the image.

**B9. Determination of protein concentration using Bradford's assay**

Protein concentration was determined using Bradford's reagent (Sigma-Aldrich, USA). The principle of this process is based on the formation of a complex between the dye, Brilliant Blue G, and proteins in solution. The absorption of the solution at 595 nm is proportional to the amount of proteins present. Standards in the range 0.1- 1.4 mg/ml of bovine serum albumin (BSA) were prepared. The Bradford reagent in the bottle was mixed and brought to room temperature. 5ul of the buffer (PBS) (137 mM NaCl, 27 mM KCl, 4.3 mM Na2HPO4 and 1.4 mM KH2PO4) was added to the wells assigned as blanks. The addition of 5 µl of the protein standards to separate wells in the 96 well plates was done. The unknown sample(s) were prepared with an approximate concentration between 0.1 –1.4 mg/ml. To each well being used, 250 µl of the Bradford reagent was added and mixed on a shaker for approximately 30 seconds. Incubation was done at room temperature for 5 – 45 minutes. The absorbance was measured at 595 nm using a UV-Vis spectrophotometer. The concentrations of the proteins were determined by comparing the net absorbance at wavelength 595 nm values against the standard curve obtained (Figure D.1).



© University of Venda

**B10. Cell plating complementation assay:**

2x10ml 2xYT broth was prepared for inoculation of the colonies (1). PQE30 and (2). DnaK that were grown overnight. 100ml agar was also prepared to plate the cultures. The cells were inoculated and grown overnight in the YT broth containing 10 µl/ml of ampicillin at a 30 °C incubator. The overnight culture OD was reduced to be standardized to 0.2 OD. Serial dilution from $10^{-0}$ to $10^{-5}$ was done using 6 microcentrifuge tubes for each that were labeled DnaK, and pQE30. Spotting was then done on the agar plates together with AgNPs (2 µL was spotted) containing, 100 µg/ml ampicillin and 0.5 mM of IPTG, which was used to check the growth rate & sensitivity of the cells.

**B11. Determination of molar residue ellipticity in CD spectroscopy:**

For the analysis of CD spectroscopy data CD spectrum ellipticity units from the CD spectrometer was converted to molar residue ellipticity using the following formulae:

$[\theta] = (100 \times \theta) / CMR \times l$ _____ Equation 1

$CMR = c \times N$_____ Equation 2

Where [θ]: molar residue ellipticity (deg.cm2 / dmol)
100: constant converting path length in meters
θ: ellipticity (mdeg)
l: cuvette path length
CMR: mean residue concentration
Protein concentration (mol)

**B12. Compounds separation and identification (by spots) present in *Senna alexandrina* leave extract using Thin Layer Chromatography (TLC):**

The TLC of leaves extract was carried out according to the method described by Gujjeti & Mamidala (2013). The ethanol and ethyl acetate extract of *Senna alexandrina* leaves was subjected to TLC studies. For the TLC analysis, the dimensional ascending method (Gujjeti & Mamidala, 2013) was used. A 20×20 cm TLC silica gel 60 F254 plates (Germany) were cut with a scissor 10 cm long and 5 cm wide. The plates



© University of Venda

were marked with the pencil softly 1 cm from the bottom. 10 µL and 5 µLof the plant extracts were spotted on the TLC plates using a micropipette on the pencil-marked bottom line. 5ul of gallic acid and rutin were used as positive standards. Four mobile phases of different polarities, HE (Hexane), EWA (ethyl acetate), TE (toluene), and MA (Methanol: Acetone), were used to develop the compounds spotted on the TLC plate. After developing the compounds, the plates were removed to air dry for about 15 minutes. Furthermore, phytochemical antioxidant compounds in the TLC plates were visualized by spraying the developed TLC plates with p-anisaldehyde-sulfuric acid reagent. The fume hood was utilized when spraying the plates with the spray reagents

**B13. ATPase activity:**

5 reactions were prepared, (i) reaction with just DnaJ which served as control, (ii) reaction with just DnaK, (iii) reaction with DnaJ and DnaK. (iv) reaction with DnaK and DnaJ that has been boiled for 15 minutes and lastly (v) reaction with DnaK, DnaJ and SA-AgNPs. ATP was added into HKMD buffer 160µL aliquots and incubated for 4 hours at 37°C with agitation on 96 well plate. 50µL of each reaction was pipetted into wells in triplicate. 50µL of 10% SDS was added to stop the reaction, then 50µL of 1,25 % Ammonium molybdate and 50µL of Ascorbic acid. The solution was then incubated at room temperature for 30 minutes

**B14. Protein determination**

The protein concentration for all experiments was routinely determined in triplicate, according to Bradford's method (1976). In each prepared standard, 1 ml of Bradford reagent was added, followed by reading absorbance using a 96-well titer plate. The mixture was incubated (room temperature, 30 min), the absorbance of the solution was measured at 595 nm, and the concentration of the unknown sample was determined using a BSA standard curve (Figure D.1).



© University of Venda

## APPENDIX C: Supplementary data

### C.1 pQE30/DnaK agarose gel

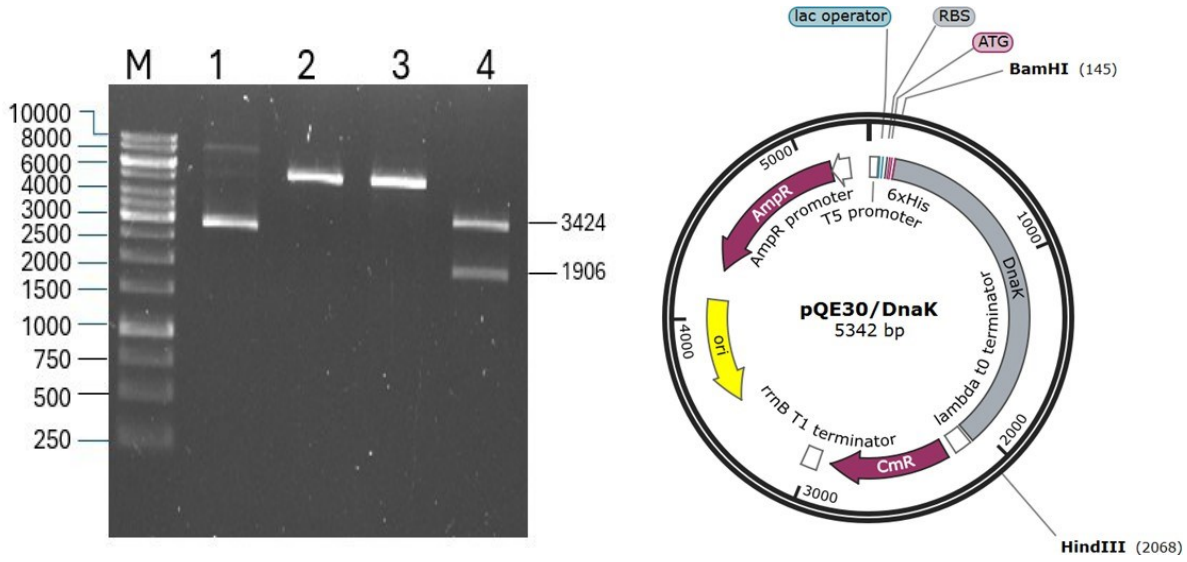
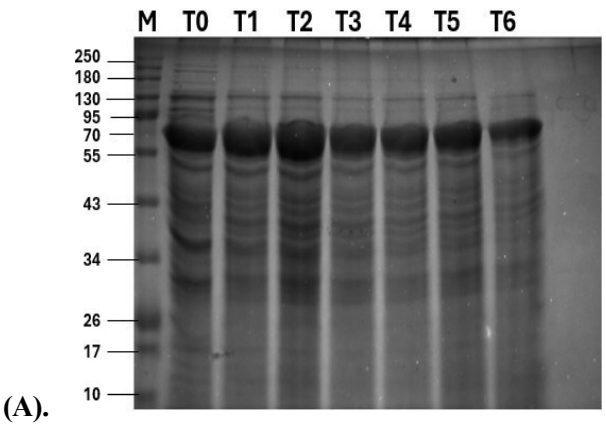


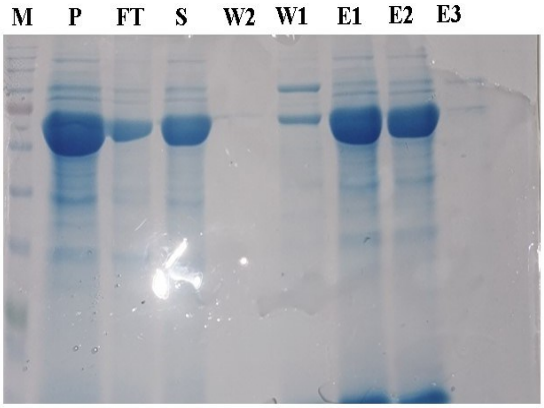

**Figure S. 1.** Restriction analysis of pQE30/DnaK plasmid.

(A) Agarose gel electrophoresis of pQE30/DnaK. (B) Plasmid map of pQE30/DnaK showing the BamHI and HindIII restriction sites: Lane M, DNA molecular weight maker in bp; Lane 1 represents both linear and circular forms of undigested pQE30/DnaK plasmid; Lane 2, pQE30/DnaK digested with BamHI; Lane 3, pQE30/DnaK digested with HindIII; Lane 4, pQE30/DnaK digested with both BamHI and HindIII.

### C2. SDS-PAGE and western blot analysis of expressed and purified DnaK proteins




(A).




(B).



© University of Venda

**Figure S. 2.** SDS-PAGE analysis of DnaK. Expression and purification analysis of DnaK.
Lane M – Protein ladder, T0-0 hour, T1-T6 (hours from 1 to 6). **(A).** Protein expression gel, **(B).** Purification gel.

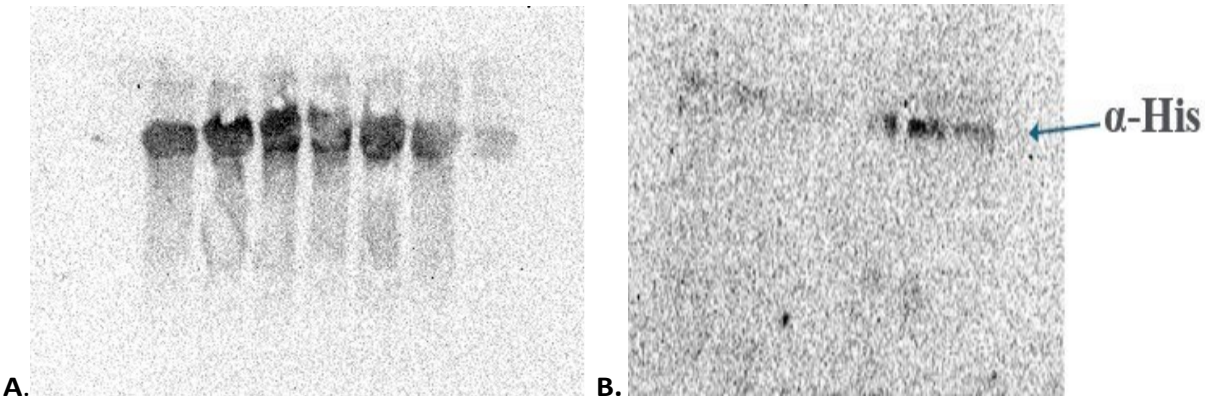
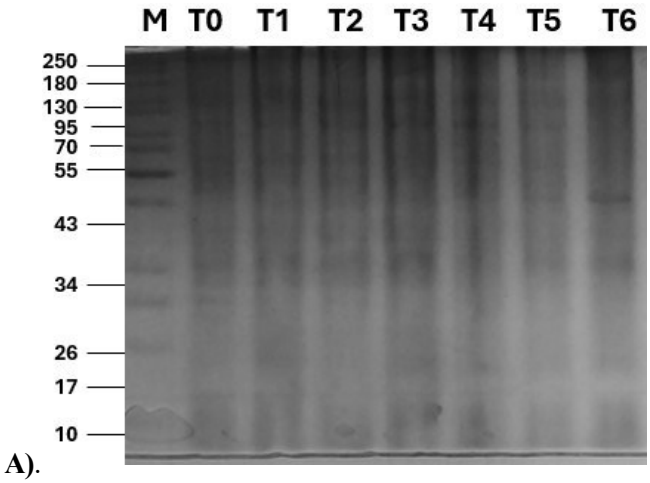


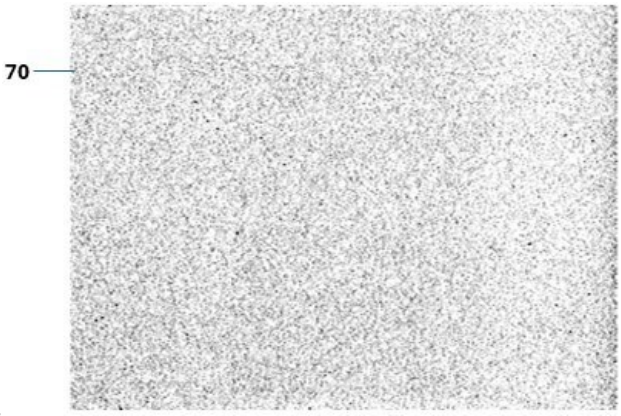

**Figure S. 3.** Western blot analysis of the above (Figure S.2), **(A).** expressed and **(B).** purified DnaK to confirm DnaK expression and purification.

**C3. pQE30 expression gel and Western blot:**






© University of Venda



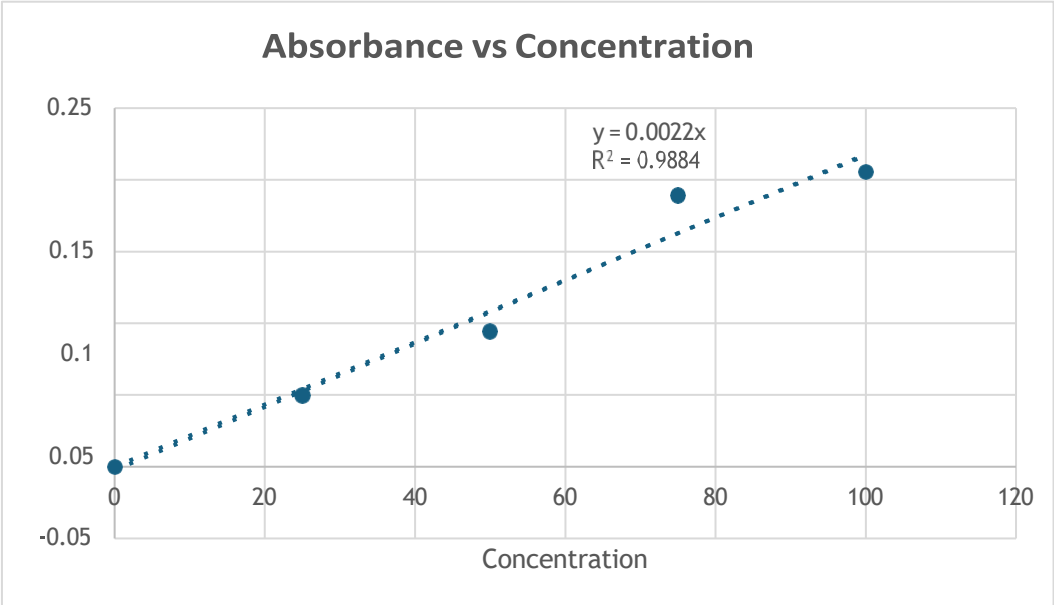

B).

**Figure S. 6.** SDS-PAGE analysis of pQE30 plasmid.

The expression of the pQE30 plasmid was examined using SDS-PAGE. The lanes represent: Lane M contains the protein marker (kDa), Lane 0 represents the pre-induction sample, and Lanes 1-6 correspond to hourly samples taken after induction.

**APPENDIX D: Supplementary data**

**D1 Bradford's Assay standard curve**






© University of Venda

**Figure D. 1. Bradford standard curve**.

Bovine serum albumin (BSA) standards of concentration varying from 0 to 0.9mg/ml were prepared, and absorbance was read at 595 nm using a Spectramax M3 spectrometer. The linear equation: $y = 0.0022x + 0.0044$, $R^2 = 0.9884$ was used to calculate protein concentration

## D.2. UHPLC-QTOF-MS:

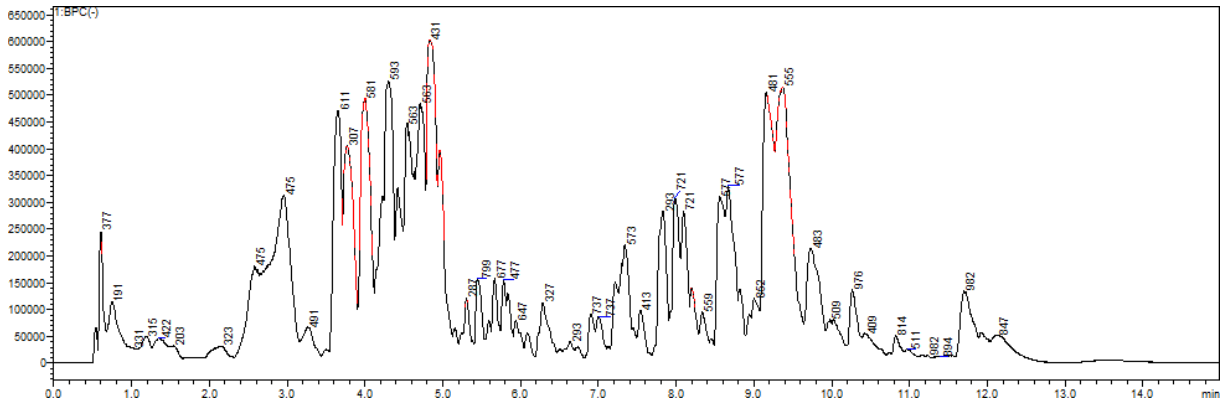



**Figure D. 2.** Total Ion Chromatogram of a methanolic extract of *Senna alexandrina* leaves, analysed by liquid chromatography-mass spectrometry (LC-MS).

The x-axis represents the retention period (in minutes), while signal strength is displayed on the y-axis. Peaks at specific retention times correspond to individual compounds/ fragments detected in the sample. Prominent peaks around 4–5 minutes and 8–10 minutes indicate major constituents, with notable signal intensities likely representing high-abundance compounds.



© University of Venda

**D.3: Phosphate standard curve for ATPase assay.**

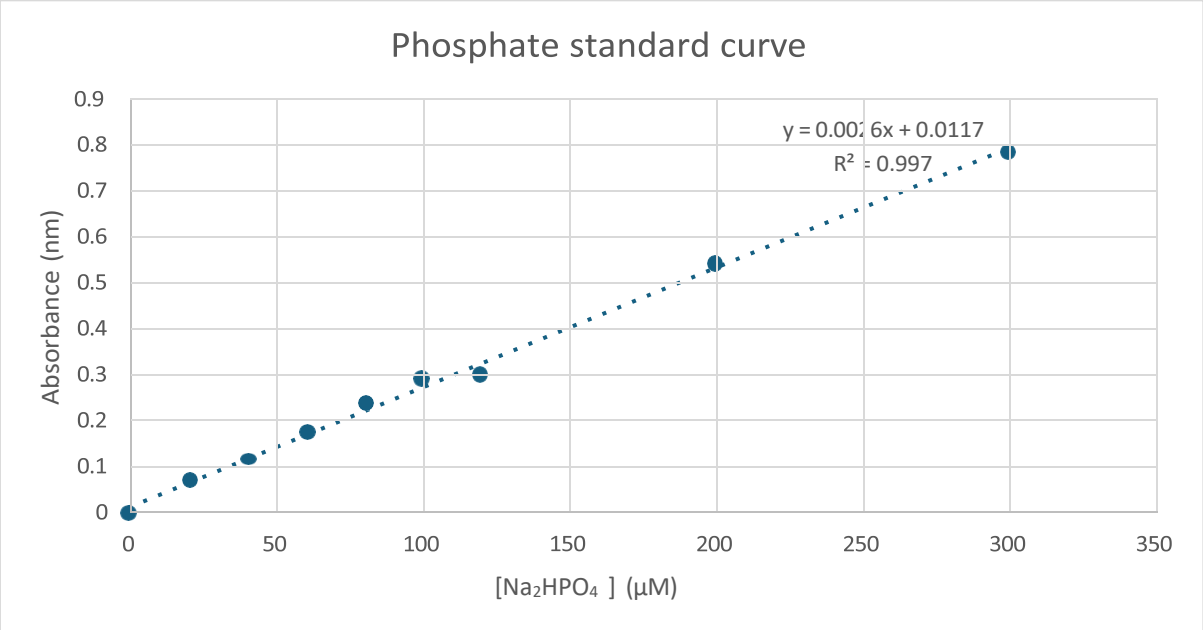



**Figure D. 4.** Phosphate standard curve showing [$Na_2HPO_4$] ranging from 0 to 300 µM and absorbance read at 660 nm. The linear equation was used to calculate the inorganic phosphate released during ATP hydrolysis.

**Table D.3:** A master mix was prepared using HKMD buffer (100mM HEPES, 1M KCl, 100mM MgCl2, and 100mM DTT), Protein components (DnaJ and DnaK); SA-AgNPs and varying concentrations of ATP.

| | **1** | **2** | **3** | **4** | **5** | **6** | **7** | **8** | **9** |
|---|---|---|---|---|---|---|---|---|---|
| Na2HPO4(µl) | - | 2 | 4 | 6 | 8 | 10 | 12 | 20 | 30 |
| [conc](µm) | 0 | 20 | 40 | 60 | 80 | 100 | 120 | 200 | 300 |
| H20(µL) | 100 | 98 | 96 | 94 | 92 | 90 | 88 | 80 | 70 |
| 1,25% Ammonium molybdate (µl) | 50 | 50 | 50 | 50 | 50 | 50 | 50 | 50 | 50 |



© University of Venda

| | | | | | | | | | |
|---|---|---|---|---|---|---|---|---|---|
| 9% Ascorbic acid (µL) | 50 | 50 | 50 | 50 | 50 | 50 | 50 | 50 | 50 |

**Representative densitometric quantification of proteins in the presence of 2.5 µg/mL SA-AgNPs detected by Coomassie staining**

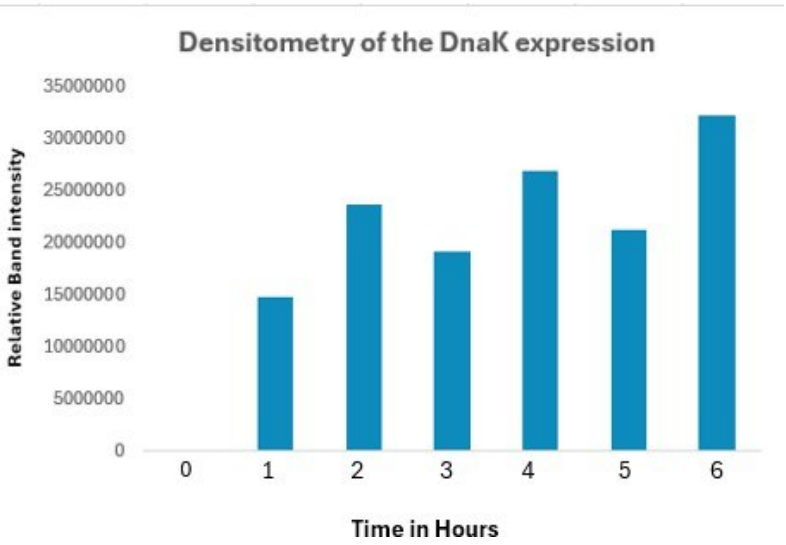


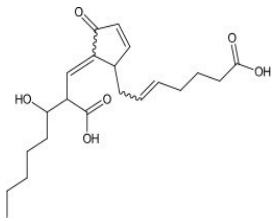
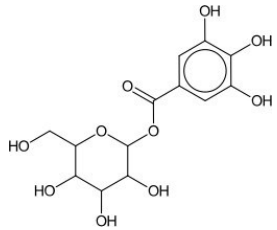
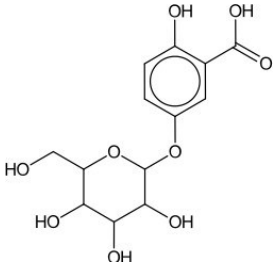
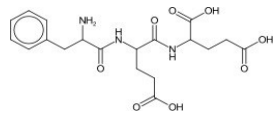

**Figure D. 5.** Densitometric analysis of DnaK expression in the presence of 2.5 µg/mL SA-AgNPs over 6 hours.

The graph displays relative band intensity of the hourly-measured DnaK protein levels. An initial stress response to SAAgNP exposure is indicated by a significant increase in DnaK expression from 1 to 2 hours. DnaK expression increased significantly from 1 to 2 hours, indicating an initial stress response to SAAgNP exposure. Between hours 2 and 5, DnaK expression shows variability. The ban intensity increases at hour 2, decreases at hour 3, and increases again at hour 4, followed by a decrease at hour 5. This variation might indicate that DnaK levels are adjusting to control cellular stress in response to the cells' attempts to adapt to the continuous presence of SA-AgNPs accordingly. At hour 6, band intensity increases, which may suggest or indicate a sustained cellular stress that is likely caused by prolonged exposure. This trend indicates that DnaK is essential for controlling the long-term *Senna alexandrina* silver nanoparticle-related proteotoxicity and emphasises the dynamic cellular response to SAAgNP-induced stress (Singh *et al*., 2009)



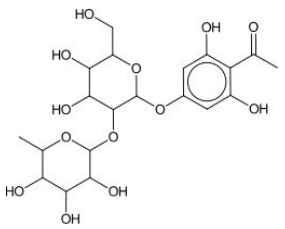
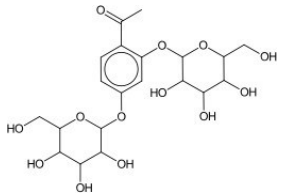
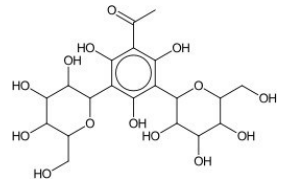
© University of Venda

## Table D.4. Annotated metabolites from Senna alexandrina methanol extracts

| No. | M/Z | RT(Min) | Fragmentations | Molecular Formulas | Classes | Subclasses | Compound names | Structures |
|---|---|---|---|---|---|---|---|---|
| **1** | 377.19 | 7.25 | 377.1938 | C21H30O6 | Diarylheptanoids | Linear Diarylheptanoids | [(1R,5R,8R,9S)-1-[(1E)-2,6-dimethylhepta-1,5-dienyl]-8-methoxy-3,6-dioxo-2-oxaspiro[4.5]decan-9-yl] acetate |  |
| **2** | 331.07 | 1.02 | 331.0663 | C13H16O10 | Benzene and substituted derivatives | Benzoic acids and substituted derivatives | 1-O-galloyl-d-glucopyranose |  |
| **3** | 315.07 | 1.20 | 315.0712 | C13H16O9 | Organooxygen compounds | Carbohydrates and carbohydrate conjugates | 2,5-dihydroxybenzoic acid 5-O-beta-D-glucoside |  |
| **4** | 422.16 | 1.34 | 422.1591 | C19H25N3O8 | Carboxylic acids and derivatives | Amino acids, peptides and analogues | 2-[[2-[(2-Amino-3-phenylpropanoyl)amino]-5-hydroxy-5-oxopentanoyl]amino]pentanedioic acid |  |

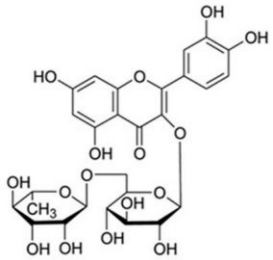
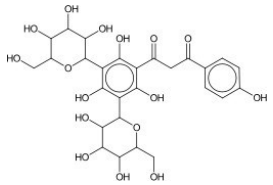
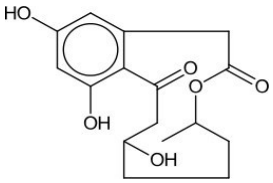
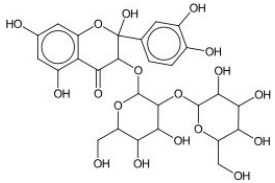


© University of Venda

| | | | | | | | | |
|---|---|---|---|---|---|---|---|---|
| **5** | 475.14 | 2.57 | 475.1447 | C20H28O13 | Organooxygen compounds | Carbohydrates and carbohydrate conjugates | 1-[4-[(2R,3R,4R,5S,6S)-4,5-dihydroxy-6-(hydroxymethyl)-3-[(2S,3S,4S,5R,6R)-3,4,5-trihydroxy-6-methyloxan-2-yl]oxyoxan-2-yl]oxy-2,6-dihydroxyphenyl]ethanone |  |
| **6** | 475.14 | 3.47 | 475.1449 | C20H28O13 | Organooxygen compounds | Carbohydrates and carbohydrate conjugates | 1-[4-[(2R,3R,4R,5S,6S)-4,5-dihydroxy-6-(hydroxymethyl)-3-[(2S,3S,4S,5S,6R)-3,4,5-trihydroxy-6-methyloxan-2-yl]oxyoxan-2-yl]oxy-2,6-dihydroxyphenyl]ethanone |  |
| **7** | 491.14 | 3.26 | 491.1395 | C20H28O14 | Organooxygen compounds | Carbohydrates and carbohydrate conjugates | 1-[2,4,6-trihydroxy-3,5-bis[(2S,3R,4R,5S,6R)-3,4,5-trihydroxy-6-(hydroxymethyl)oxan-2-yl]phenyl]ethanone |  |

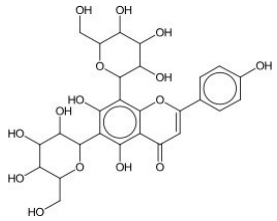
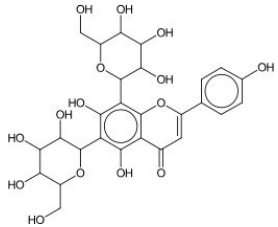
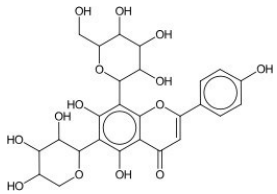


© University of Venda

| | | | | | | | | |
|---|---|---|---|---|---|---|---|---|
| **8** | 555.17 | 9.45 | 555.1687 | C27H30O16 | Flavonoids | Flavonoid glycosides | 2-(3,4-dihydroxyphenyl)-5,7-dihydroxy-3-[(2*S*,3*R*,4*S*,5*S*,6*R*)-3,4,5-trihydroxy-6-[[(2*R*,3*R*,4*R*,5*R*,6*S*)-3,4,5-trihydroxy-6-methyloxan-2-yl]oxymethyl]oxan-2-yl]oxychromen-4-one |  |
| **9** | 611.16 | 3.65 | 611.1611 | C27H32O16 | Flavonoids | Flavonoid glycosides | 1-(4-hydroxyphenyl)-3-[2,4,6-trihydroxy-3,5-bis[(2S,3R,4R,5S,6R)-3,4,5-trihydroxy-6-(hydroxymethyl)oxan-2-yl]phenyl]propane-1,3-dione |  |
| **10** | 307.12 | 3.77 | 307.1216 | C16H20O6 | Macrolides and analogues | Zearalenones | 11-Hydroxycurvularin |  |
| **11** | 581.15 | 4.01 | 643.1516 | C27H32O18 | Flavonoids | Flavonoid glycosides | 3-[(2S,3R,4R,6R)-3,4-dihydroxy-6-(hydroxymethyl)-5-[(2S,3R,4S,5R,6R)-3,4,5- |  |

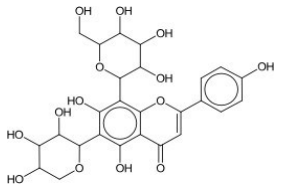
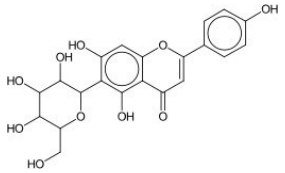
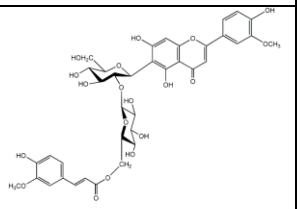
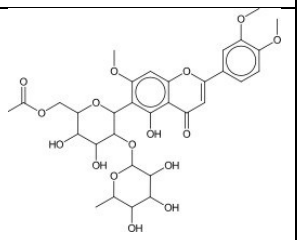
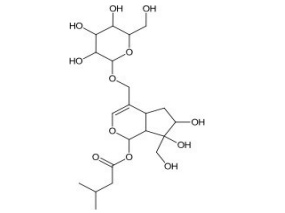


© University of Venda

| | | | | | | | | |
|---|---|---|---|---|---|---|---|---|
| | | | | | | | trihydroxy-6-(hydroxymethyl)oxan-2-yl]oxyoxan-2-yl]oxy-5,7-dihydroxy-2-(3,4,5-trihydroxyphenyl)-2,3-dihydrochromen-4-one | |
| **12** | 593.15 | 4.30 | 593.1506 | C27H30O15 | Flavonoids | Flavonoid glycosides | Vicenin-2 |  |
| **13** | 593.15 | 4.93 | 593.1504 | C27H30O15 | Flavonoids | Flavonoid glycosides | Elatin |  |
| **14** | 563.14 | 4.55 | 563.1400 | C26H28O14 | Flavonoids | Flavonoid glycosides | Vicenin-1 |  |

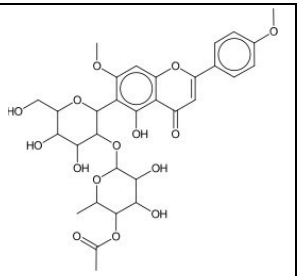
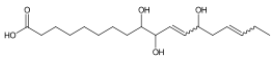
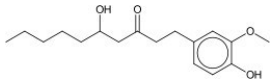
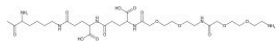


© University of Venda

| | | | | | | | | |
|---|---|---|---|---|---|---|---|---|
| **15** | 563.16 | 4.81 | 563.1602 | C26H28O14 | Flavonoids | Flavonoid glycosides | Vicenin-3 |  |
| **16** | 431.10 | 4.83 | 431.0981 | C21H20O10 | Flavonoids | Flavonoid glycosides | Isovitexin |  |
| **17** | 799.21 | 5.34 | 799.2072 | C38H40O19 | Flavonoids | Flavonoid glycosides | Isoscoparin 2"-(6-(E)-ferulylglucoside) |  |
| **18** | 677.21 | 5.67 | 677.2078 | C32H38O16 | Flavonoids | Flavonoid glycosides | Linoside A |  |
| **19** | 477.20 | 5.65 | 477.1970 | C21H34O12 | Hydroxy acids and derivatives | Beta Hydroxy acids and derivatives | Kanokoside B |  |



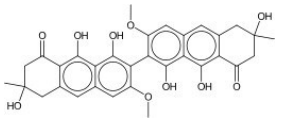
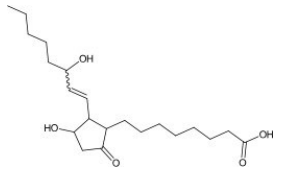
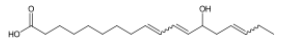
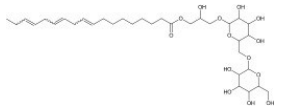
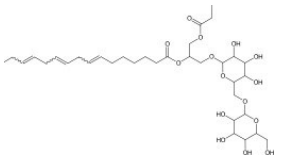
© University of Venda

| | | | | | | | | |
|---|---|---|---|---|---|---|---|---|
| **20** | 647.20 | 5.85 | 647.1973 | C31H36O15 | Flavonoids | Flavonoid glycosides | [(2S,3R,4S,5R,6S)-6-[(2S,3R,4S,5S,6R)-4,5-dihydroxy-2-[5-hydroxy-7-methoxy-2-(4-methoxyphenyl)-4-oxochromen-6-yl]-6-(hydroxymethyl)oxan-3-yl]oxy-4,5-dihydroxy-2-methyloxan-3-yl] acetate |  |
| **21** | 327.22 | 6.29 | 327.2169 | C18H32O5 | Fatty Acyls | Lineolic acids and derivatives | (9R,10S,11E,13S,15Z)-9,10,13-trihydroxyoctadeca-11,15-dienoic acid |  |
| **22** | 293.17 | 6.73 | 293.1751 | C17H26O4 | Benzene and substituted derivatives | Benzenoids | Gingerol |  |
| **23** | 737.36 | 6.90 | 737.3590 | C19H52N6O13 | Fatty Acyls | Fatty Acyl glycosides | (2S)-2-[[(4S)-4-[[2-[2-[2-[[2-[2-(2-aminoethoxy)ethoxy]acetyl]amino]ethoxy]ethoxy]acetyl]amino]-4-carboxybutanoyl]amino]-5-[[(5S)-5-amino-6- |  |



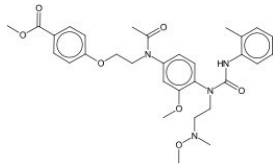
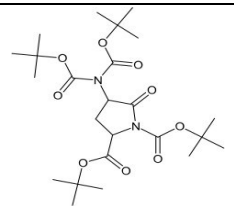
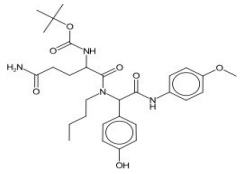
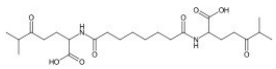
© University of Venda

University of Venda
Creating Future Leaders

| | | | | | | | | |
|---|---|---|---|---|---|---|---|---|
| | | | | | | | oxoheptyl]amino]-5-oxopentanoic acid | |
| **24** | 573.18 | 7.35 | 573.1759 | C32H30O10 | Perylenequinones | Benzenoids | 3,8,9-Trihydroxy-6-methoxy-3-methyl-7-(1,6,9-trihydroxy-3-methoxy-6-methyl-8-oxo-5,7-dihydroanthracen-2-yl)-2,4-dihydroanthracen-1-one |  |
| **25** | 413.25 | 7.54 | 413.2538 | C21H36O5 | Fatty Acyls | Fatty acids and conjugates | 8-[(1S,2S,3S)-3-hydroxy-2-(3-hydroxyoct-1-enyl)-5-oxocyclopentyl] octanoic acid |  |
| **26** | 293.21 | 8.84 | 293.2117 | C18H30O3 | Fatty Acyls | Lineolic acids and derivatives | (9E,11Z,13R,15Z)-13-hydroxyoctadeca-9,11,15-trienoic acid |  |
| **27** | 721.36 | 8.10 | 721.3647 | C33H56O14 | Glycerolipids | Glycosylglycerols | Gingerglycolipid A |  |
| **28** | 721.36 | 8.19 | 721.3641 | C34H56O15 | Glycerolipids | Glycosylglycerols | [1-propanoyloxy-3-[3,4,5-trihydroxy-6-[[3,4,5-trihydroxy-6-(hydroxymethyl)oxan-2-yl]oxymethyl]oxan-2- |  |

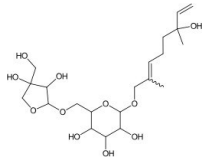
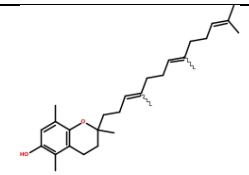
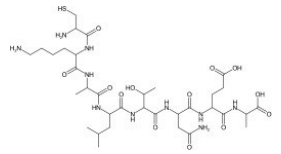
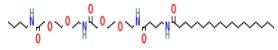


© University of Venda

| | | | | | | | | |
|---|---|---|---|---|---|---|---|---|
| | | | | | | | yl]oxypropan-2-yl] (7Z,10Z,13Z)-hexadeca-7,10,13-trienoate | |
| **29** | 577.27 | 8.56 | 577.2682 | C31H38N4O7 | Carboxylic acids and derivatives | Amino acids, peptides, analogues | methyl 4-[2-[N-acetyl-3-methoxy-4-[2-[methoxy(methyl)amino]ethyl-[(2-methylphenyl)carbamoyl]amino]anilino]ethoxy]benzoate |  |
| **30** | 481.26 | 9.16 | 499.2661 | C24H40N2O9 | Carboxylic acids and derivatives | Amino acids, peptides, analogues | ditert-butyl (2S,4S)-4-[bis[(2-methylpropan-2-yl)oxycarbonyl]amino]-5-oxopyrrolidine-1,2-dicarboxylate |  |
| **31** | 555.28 | 9.22 | 555.2838 | C29H40N4O7 | Carboxylic acids and derivatives | Amino acids, peptides, analogues | Boc-DL-Gln-DL-N(Bu)nTyr-NHPh(4-OMe) |  |
| **32** | 483.27 | 9.49 | 483.2715 | C24H40N2O8 | Carboxylic acids and derivatives | Amino acids, peptides, analogues | (2S)-2-[[8-[[(1S)-1-carboxy-5-methyl-4-oxohexyl]amino]-8-oxooctanoyl]amino]-6-methyl-5-oxoheptanoic acid |  |



© University of Venda

| | | | | | | | | |
|---|---|---|---|---|---|---|---|---|
| **33** | 509.12 | 9.76 | 509.2234 | C21H36O11 | Fatty acyls | Fatty acyl glycosides | Distyloside B |  |
| **34** | 409.31 | 10.46 | 409.3102 | C28H42O2 | Phenols | Benzenoids | Gamma-Tocotrienol |  |
| **35** | 847.40 | 12.20 | 847.3970 | C34H60N10O13S | Carboxylic acids and derivatives | Amino acids, peptides, analogues | H-DL-Cys-DL-Lys-DL-Ala-DL-Leu-DL-xiThr-DL-Asn-DL-Glu-DL-Ala-OH |  |
| **36** | 759.54 | 11.92 | 759.5440 | C38H74N4O8 | Sphingolipids | Glycosphingolipids | N-[4-[2-[2-[2-[2-[2-[2-(butylamino)-2-oxoethoxy]ethoxy]ethylamino]-2-oxoethoxy]ethoxy]ethylamino]-4-oxobutyl]octadecanamide |  |



© University of Venda

**Two selected compounds binding to DnaK-DnaJ**

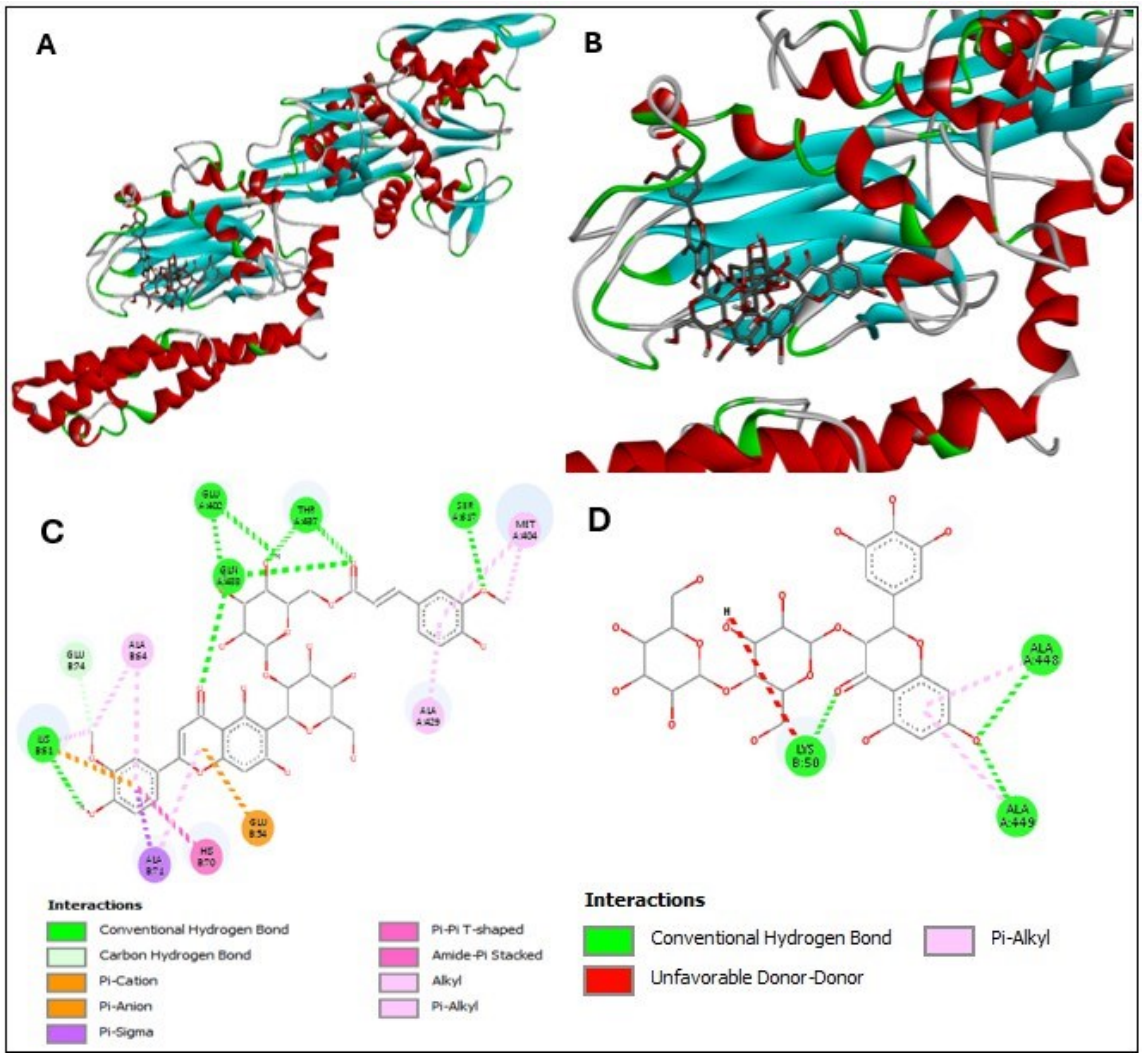



**Figure D. 6.** Molecular docking of **(A)** Isoscoparin 2"-(6-(E)-ferulylglucoside) and **(B)** 3-[(2S,3R,4R,6R)-3,4-dihydroxy-6-(hydroxymethyl)-5-[(2S,3R,4S,5R,6R)-3,4,5-trihydroxy-6-(hydroxymethyl)oxan-2-yl]oxyoxan-2-yl]oxy-5,7-dihydroxy-2-(3,4,5-trihydroxyphenyl)-2,3-dihydrochromen-4-one with DnaK-DnaJ. Letters (C) and (D) represent a 2D diagram of the compound in letters A and B, respectively. With the DnaK-DnaJ amino acid residues contributing to binding affinity and stability. Ligand or compound (Isoscoparin 2"-(6-(E)-ferulylglucoside) (C) showed the highest binding affinity (-9.8 kcal/mol) and more amino acid interactions for DnaK-DnaJ complex compared to compound (D) (-8.2 kcal/mol) (Appendix D, Table D.5).



© University of Venda

**Two selected compounds binding to DnaK-CBPA:**

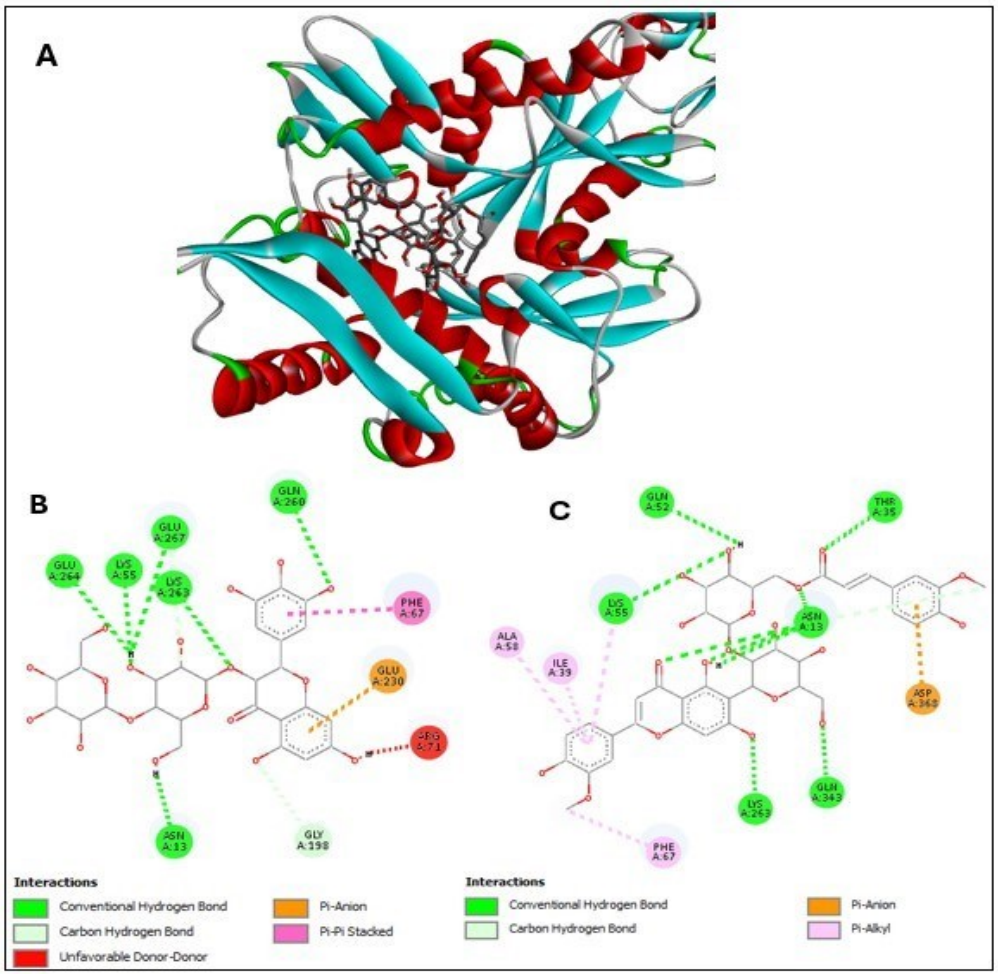



**Figure D. 7.** Molecular docking of **(A)** Isoscoparin 2"-(6-(E)-ferulylglucoside) and 3-[(2S,3R,4R,6R)-3,4-dihydroxy-6-(hydroxymethyl)-5-[(2S,3R,4S,5R,6R)-3,4,5-trihydroxy-6-(hydroxymethyl)oxan-2-yl]oxyoxan-2-yl]oxy-5,7-dihydroxy-2-(3,4,5-trihydroxyphenyl)-2,3-dihydrochromen-4-one with DnaK-CBPA. Letter **(B)** and **(C)** represent a 2D diagram of compounds docked in letter A.

Compound in letter **(C)** showed the highest binding affinity (-8.9 kcal/mol) for DnaK-CBPA complex compared to compound **(B)** (-7.5 kcal/mol) (Appendix D, Table D.5).



© University of Venda

**Two selected compounds binding to DnaK-CLPB:**

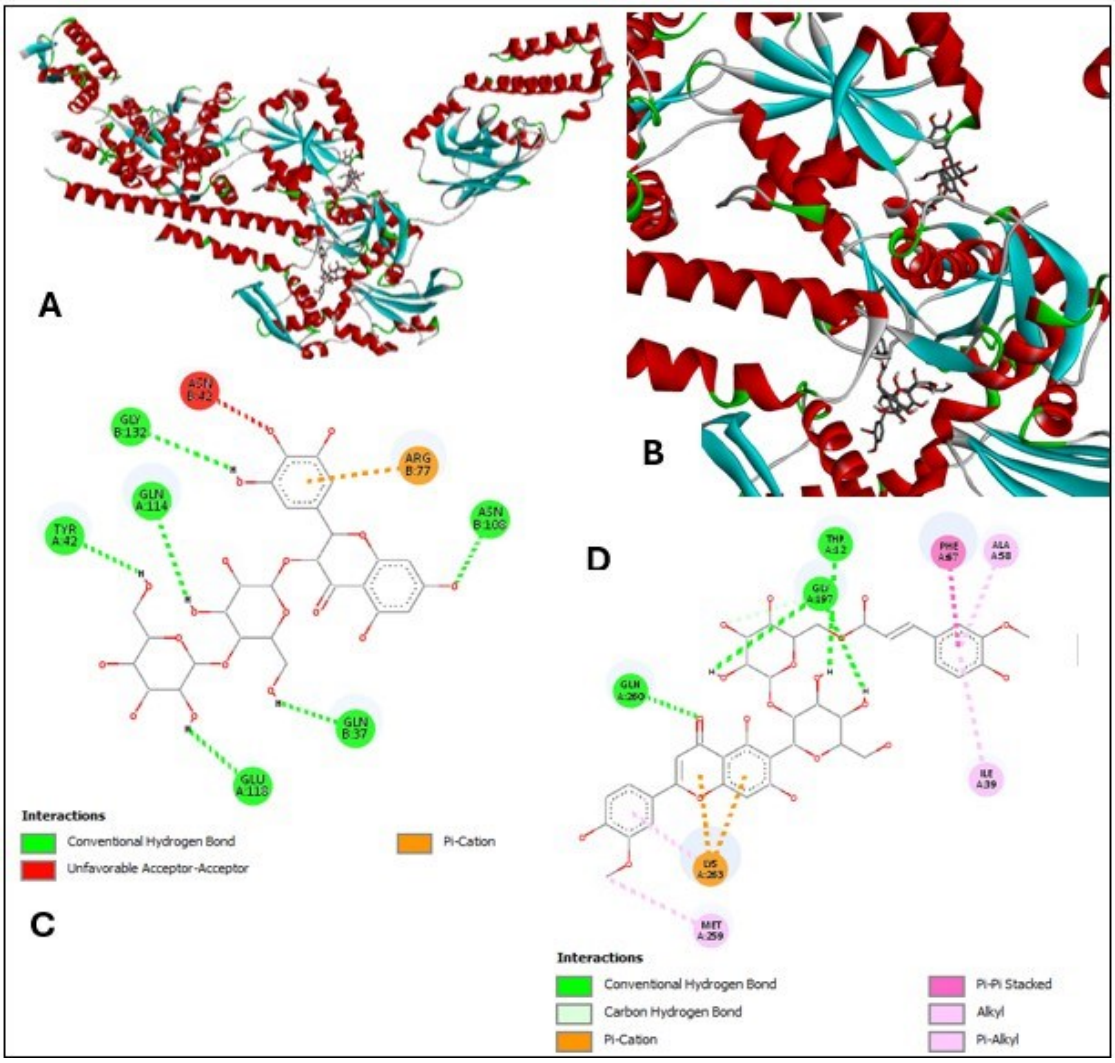



**Figure D. 8.** Molecular docking of **(A)** Isoscoparin 2''-(6-(E)-ferulylglucoside) and 3-[(2S,3R,4R,6R)-3,4-dihydroxy-6-(hydroxymethyl)-5-[(2S,3R,4S,5R,6R)-3,4,5-trihydroxy-6-(hydroxymethyl)oxan-2-yl]oxyoxan-2-yl]oxy-5,7-dihydroxy-2-(3,4,5-trihydroxyphenyl)-2,3-dihydrochromen-4-one with DnaK-CLPB. Letter (B), shows a zoomed in ligand interaction, while Letter **(C)** and **(D)** represent a 2D diagram of compounds docked in letter A and B.

Compound, Isoscoparin 2''-(6-(E)-ferulylglucoside) **(D), s**howed the highest binding affinity (-9.5 kcal/mol) and more amino acid interactions for DnaK-CLPB complex compared to compound **(C)** (-7.9 kcal/mol) (Appendix D, Table D.5).



© University of Venda

**Two selected compounds binding to DnaK-GROEL:**

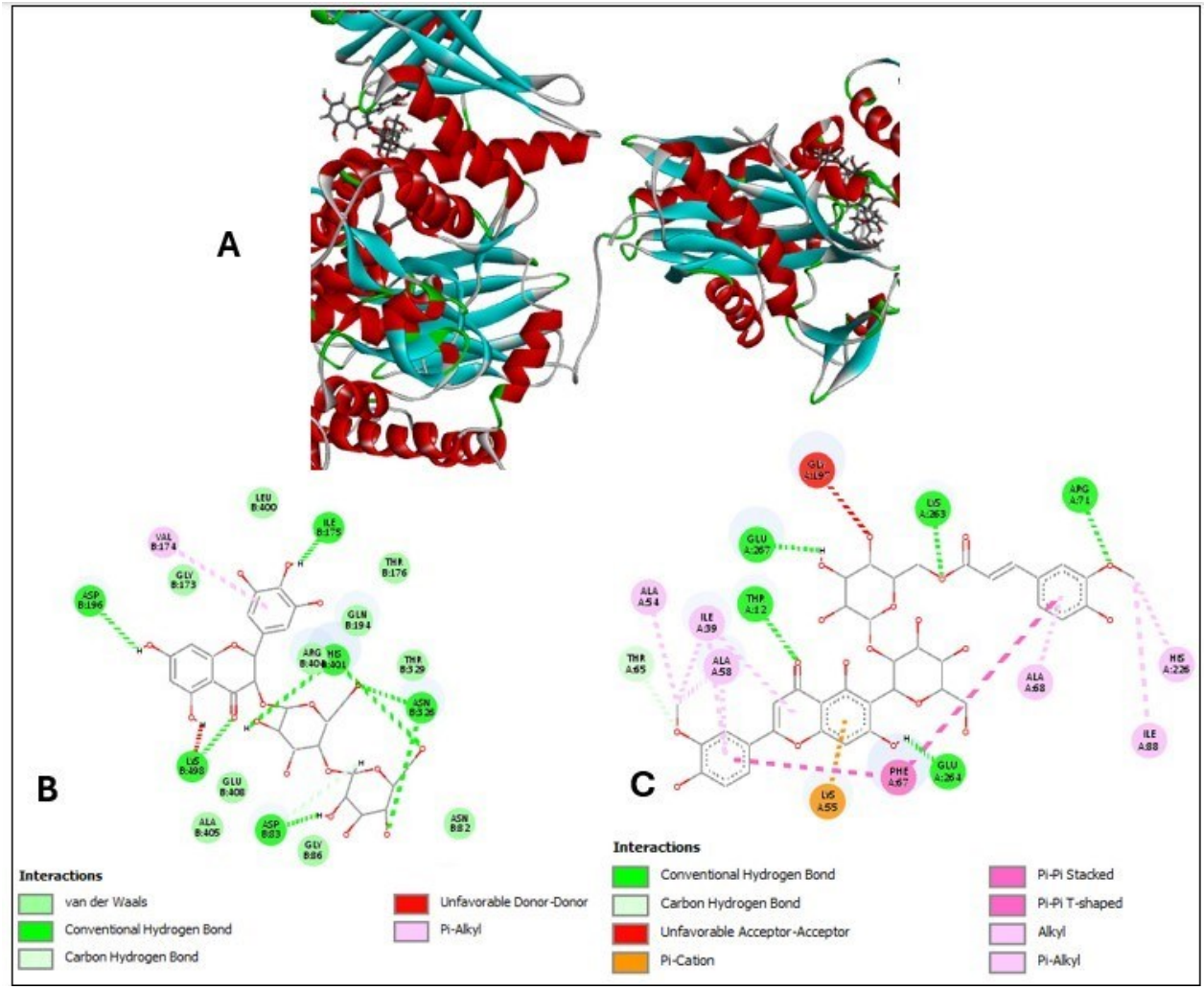



**Figure D. 9.** Molecular docking of **(A)** Isoscoparin 2"-(6-(E)-ferulylglucoside) and 3-[(2S,3R,4R,6R)-3,4-dihydroxy-6-(hydroxymethyl)-5-[(2S,3R,4S,5R,6R)-3,4,5-trihydroxy-6-(hydroxymethyl)oxan-2-yl]oxyoxan-2-yl]oxy-5,7-dihydroxy-2-(3,4,5-trihydroxyphenyl)-2,3-dihydrochromen-4-one with DnaK-GROEL. Letter **(B)** and **(C)** show a 2D diagram of compounds docked in letter A.

Compound, Isoscoparin 2"-(6-(E)-ferulylglucoside) **(C), s**howed the highest binding affinity (-9.4 kcal/mol) and more amino acid interactions for DnaK-GROEL complex as compared to compound **(D)** (-8.2 kcal/mol) (Appendix D, Table D.5).



© University of Venda

**Two selected compounds binding to DnaK-GROES:**

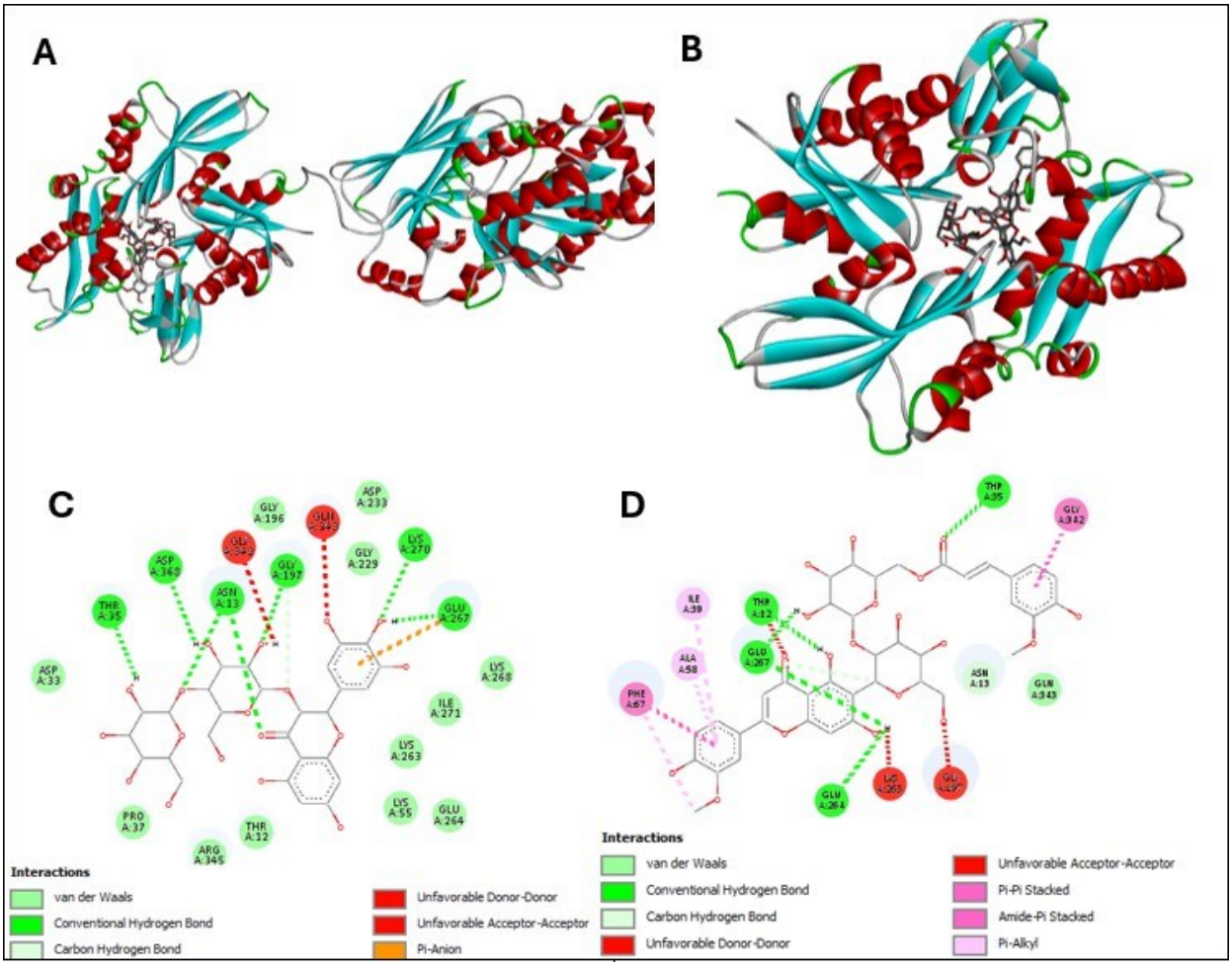



**Figure D. 10.** Molecular docking of **(A)** Isoscoparin 2''-(6-(E)-ferulylglucoside) and 3-[(2S,3R,4R,6R)-3,4-dihydroxy-6-(hydroxymethyl)-5-[(2S,3R,4S,5R,6R)-3,4,5-trihydroxy-6-(hydroxymethyl)oxan-2-yl]oxyoxan-2-yl]oxy-5,7-dihydroxy-2-(3,4,5-trihydroxyphenyl)-2,3-dihydrochromen-4-one with DnaK-GROES. Letter **(B),** shows a zoomed in ligand interaction, while Letter **(C)** and **(D)** represent a 2D diagram of compounds docked in letter A and B.

Compound, Isoscoparin 2''-(6-(E)-ferulylglucoside) **(D), s**howed the highest binding affinity (-9.8 kcal/mol) and more amino acid interactions for DnaK-GROES complex as compared to compound **(C)** (-7.6 kcal/mol) (Appendix D, Table D.5).



© University of Venda

**Two selected compounds binding to DnaK-GRPE:**

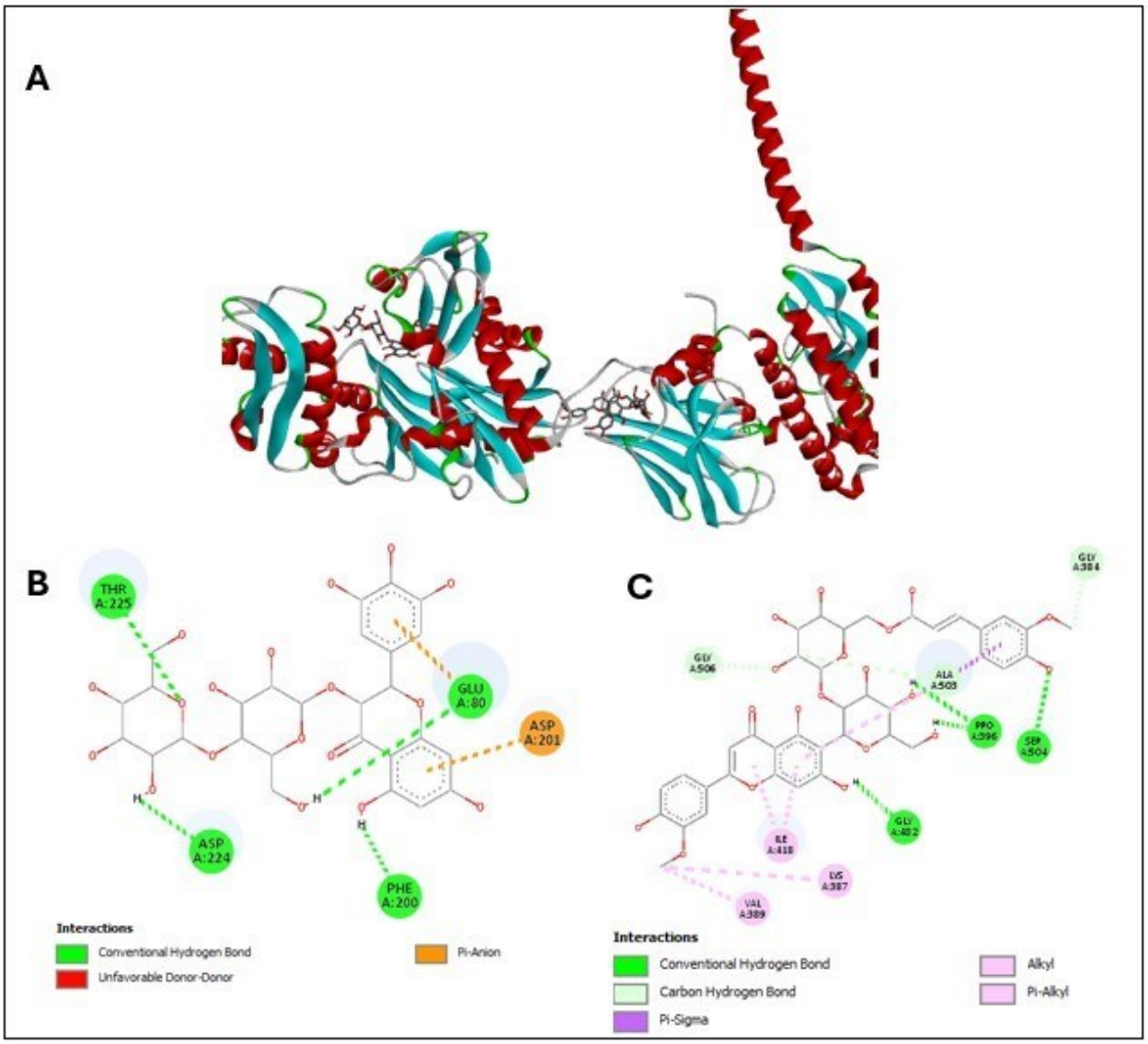



**Figure D. 11.** Molecular docking of **(A)** Isoscoparin 2''-(6-(E)-ferulylglucoside) and 3-[(2S,3R,4R,6R)-3,4-dihydroxy-6-(hydroxymethyl)-5-[(2S,3R,4S,5R,6R)-3,4,5-trihydroxy-6-(hydroxymethyl)oxan-2-yl]oxyoxan-2-yl]oxy-5,7-dihydroxy-2-(3,4,5-trihydroxyphenyl)-2,3-dihydrochromen-4-one with DnaK-GRPE. Letter **(B)** and **(C)** show a 2D diagram of compounds docked in letter A.



© University of Venda

Compound, Isoscoparin 2"-(6-(E)-ferulylglucoside) **(C), s**howed the highest binding affinity (-8.1 kcal/mol) and more amino acid interactions for DnaK-GRPE complex as compared to compound **(B)** (-7.3 kcal/mol) (Appendix D, Table D.5).

**Two selected compounds binding to DnaK-HSLU:**

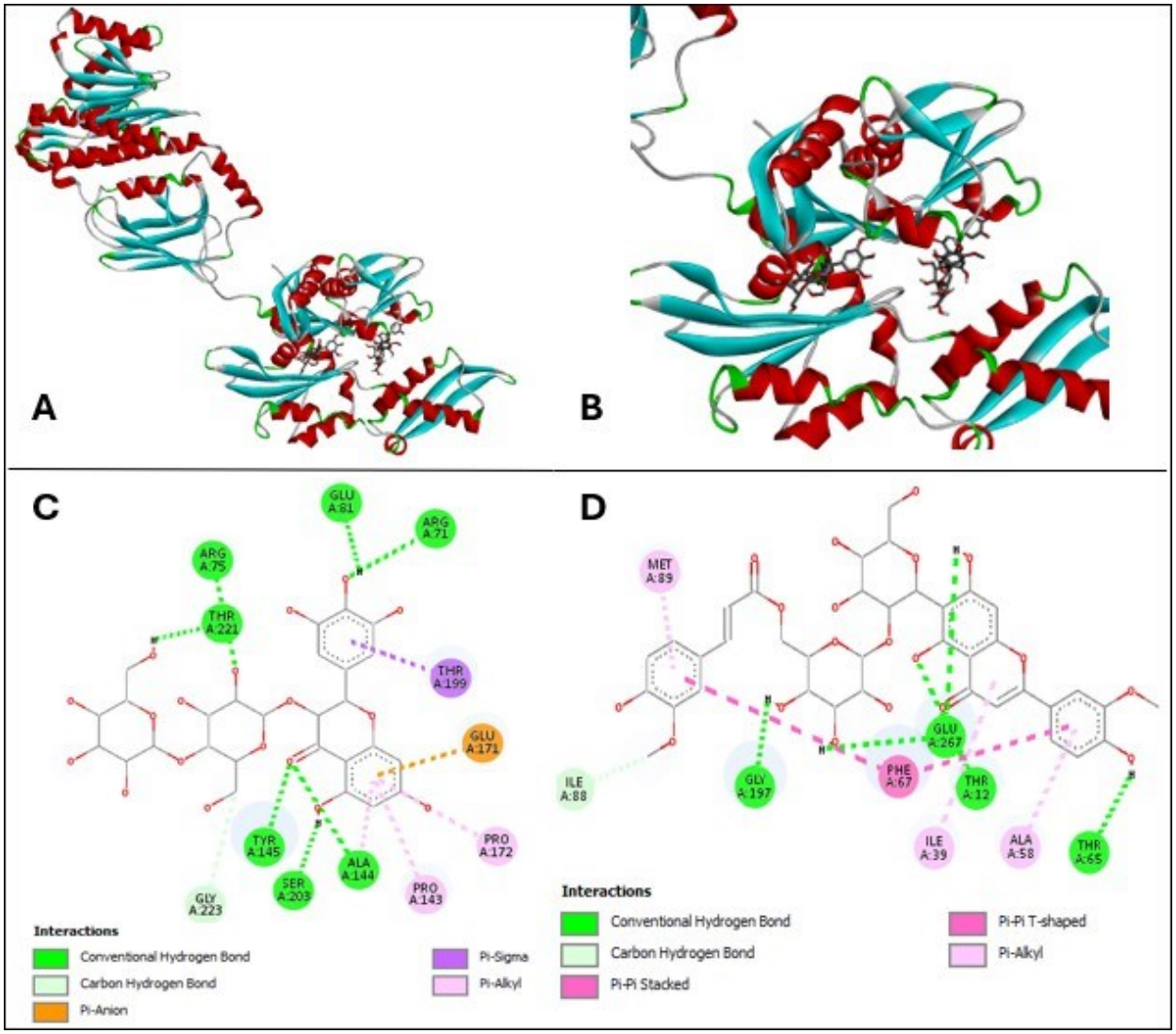



**Figure D. 12.** Molecular docking of **(A)** Isoscoparin 2"-(6-(E)-ferulylglucoside) and 3-[(2S,3R,4R,6R)-3,4-dihydroxy-6-(hydroxymethyl)-5-[(2S,3R,4S,5R,6R)-3,4,5-trihydroxy-6-(hydroxymethyl)oxan-2-yl]oxyoxan-2-yl]oxy-5,7-dihydroxy-2-(3,4,5-trihydroxyphenyl)-2,3-



© University of Venda

dihydrochromen-4-one with DnaK-HSLU. Letter **(B),** shows a zoomed in ligand interaction, while Letter **(C)** and **(D)** represent a 2D diagram of compounds docked in letter A and B.

Compound **(C),** 3-[(2S,3R,4R,6R)-3,4-dihydroxy-6-(hydroxymethyl)-5-[(2S,3R,4S,5R,6R)-3,4,5-trihydroxy-6-(hydroxymethyl)oxan-2-yl]oxyoxan-2-yl]oxy-5,7-dihydroxy-2-(3,4,5-trihydroxyphenyl)-2,3-dihydrochromen-4-one **s**howed the highest binding affinity (-9.0 kcal/mol) for DnaK-HSLU complex as compared to compound **(D)** (-8.9 kcal/mol) (Appendix D, Table D.5).

**Two selected compounds binding to DnaK-HSLV:**

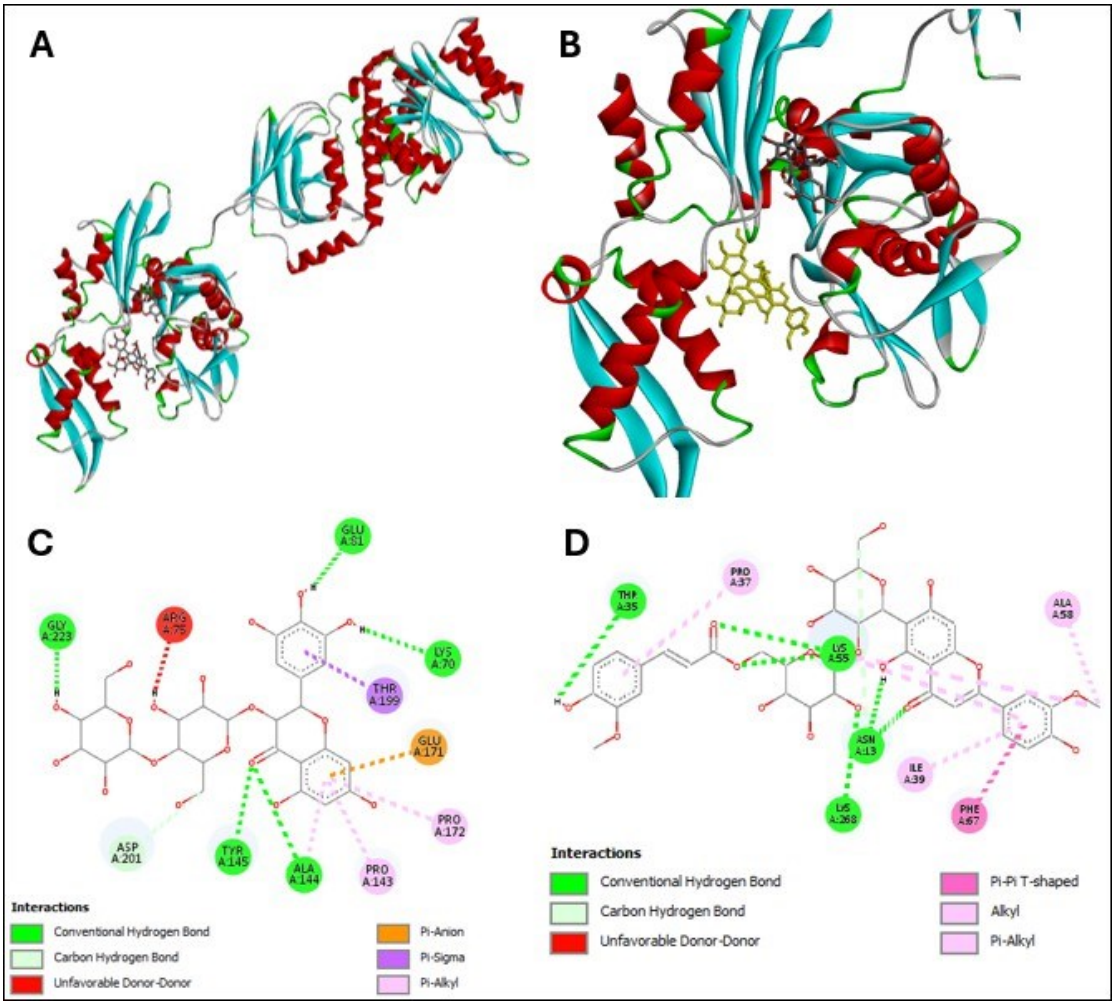



**Figure D. 13.** Molecular docking of **(A)** Isoscoparin 2"-(6-(E)-ferulylglucoside) and 3-[(2S,3R,4R,6R)-3,4-dihydroxy-6-(hydroxymethyl)-5-[(2S,3R,4S,5R,6R)-3,4,5-trihydroxy-6-(hydroxymethyl)oxan-2-

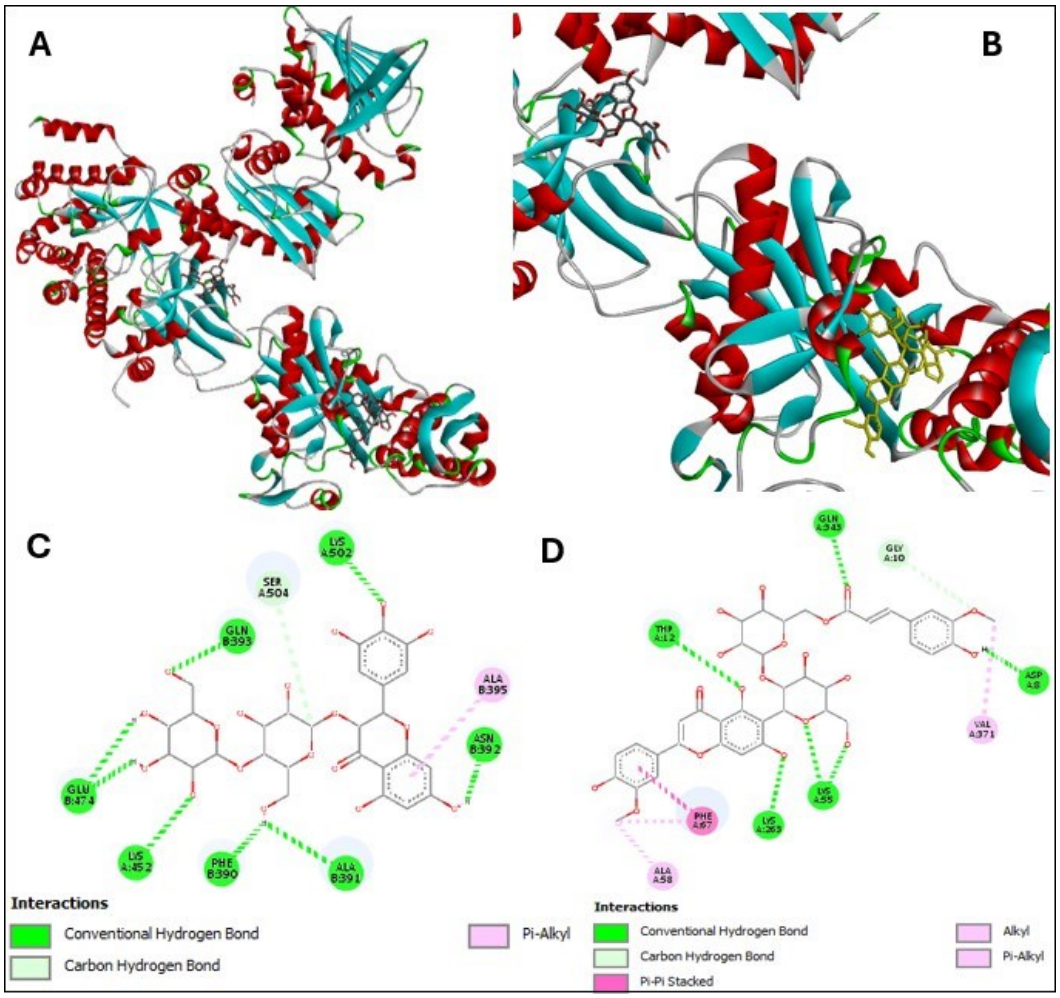


© University of Venda

yl]oxyoxan-2-yl]oxy-5,7-dihydroxy-2-(3,4,5-trihydroxyphenyl)-2,3-dihydrochromen-4-one with DnaK-HSLV. Letter **(B),** shows a zoomed in ligand interaction, the ligand with highest binding affinity is highlighted in (yellow); while Letter **(C)** and **(D)** represent a 2D diagram of compounds docked in letter A and B.

Compound **(C),** 3-[(2S,3R,4R,6R)-3,4-dihydroxy-6-(hydroxymethyl)-5-[(2S,3R,4S,5R,6R)-3,4,5-trihydroxy-6-(hydroxymethyl)oxan-2-yl]oxyoxan-2-yl]oxy-5,7-dihydroxy-2-(3,4,5-trihydroxyphenyl)-2,3-dihydrochromen-4-one **s**howed the highest binding affinity (-9.3 kcal/mol) for DnaK-HSLV complex as compared to compound **(D)** (-9.1 kcal/mol) (Appendix D, Table D.5).

**Two selected compounds binding to DnaK-HTPG:**



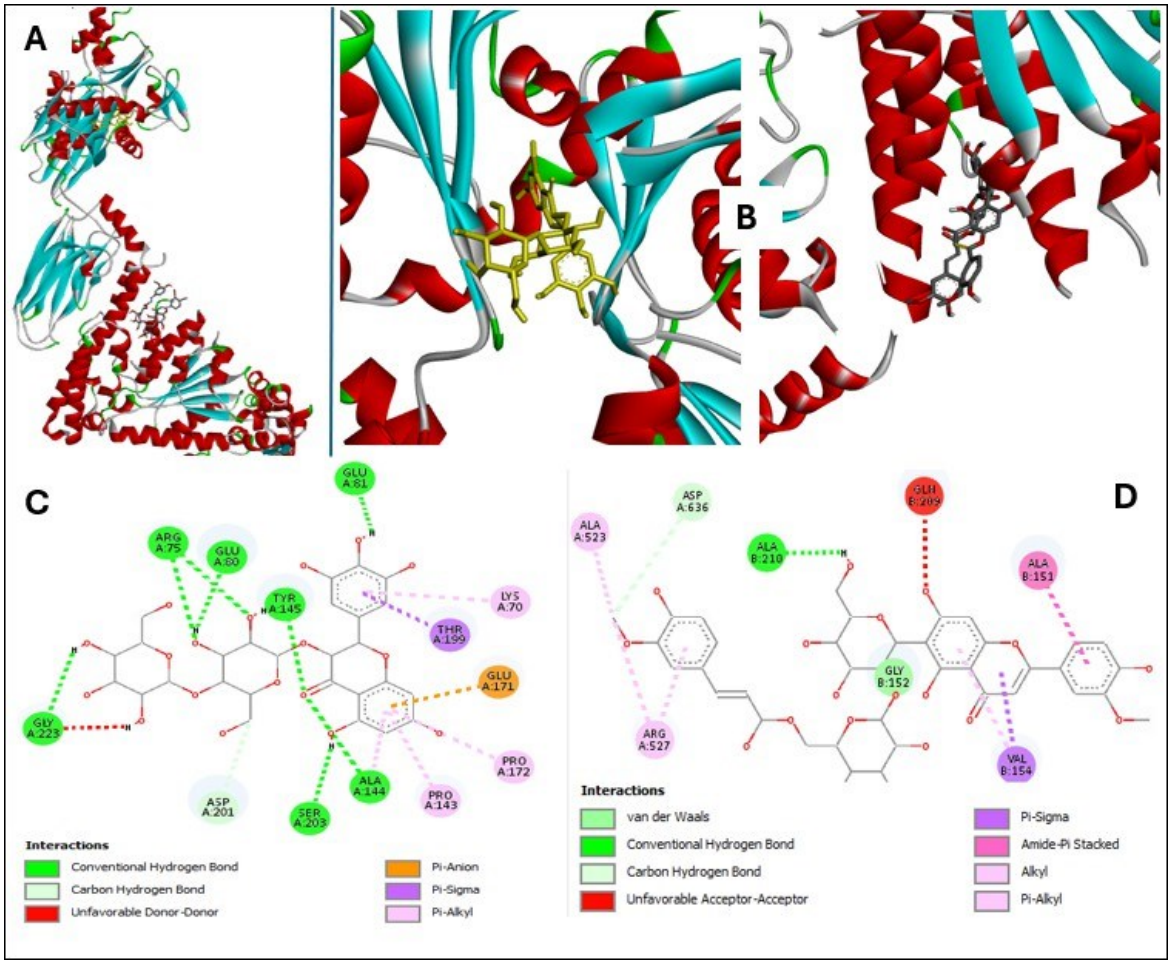



© University of Venda

**Figure D. 14.** Molecular docking of **(A)** Isoscoparin 2''-(6-(E)-ferulylglucoside) and 3-[(2S,3R,4R,6R)-3,4-dihydroxy-6-(hydroxymethyl)-5-[(2S,3R,4S,5R,6R)-3,4,5-trihydroxy-6-(hydroxymethyl)oxan-2-yl]oxyoxan-2-yl]oxy-5,7-dihydroxy-2-(3,4,5-trihydroxyphenyl)-2,3-dihydrochromen-4-one with DnaK-HTPG. Letter **(B),** shows a zoomed in ligand interaction, the ligand which exhibited highest binding affinity is highlighted in (yellow); while Letter **(C)** and **(D)** represent a 2D diagram of compounds docked in letter A and B.

Compound **(D),** Isoscoparin 2''-(6-(E)-ferulylglucoside) showed the highest binding affinity (-9.9 kcal/mol) for DnaK-HTPG complex as compared to compound **(C)** (-7.9 kcal/mol) (Appendix D, Table D.5).

**Two selected compounds binding to DnaK-RPOH:**






© University of Venda

**Figure D. 15.** Molecular docking of **(A)** Isoscoparin 2"-(6-(E)-ferulylglucoside) and 3-[(2S,3R,4R,6R)-3,4-dihydroxy-6-(hydroxymethyl)-5-[(2S,3R,4S,5R,6R)-3,4,5-trihydroxy-6-(hydroxymethyl)oxan-2-yl]oxyoxan-2-yl]oxy-5,7-dihydroxy-2-(3,4,5-trihydroxyphenyl)-2,3-dihydrochromen-4-one, with DnaK-RPOH. Letter **(B),** shows a zoomed in ligand interaction, the ligand with highest binding affinity is highlighted in (yellow); while Letter **(C)** and **(D)** represent a 2D diagram of compounds docked in letter A and B.

Compound **(C),** 3-[(2S,3R,4R,6R)-3,4-dihydroxy-6-(hydroxymethyl)-5-[(2S,3R,4S,5R,6R)-3,4,5-trihydroxy-6-(hydroxymethyl)oxan-2-yl]oxyoxan-2-yl]oxy-5,7-dihydroxy-2-(3,4,5-trihydroxyphenyl)-2,3-dihydrochromen-4-one, **s**howed the highest binding affinity (-9.2 kcal/mol) for DnaK-RPOH complex as compared to compound **(D)** (-8.2 kcal/mol) (Appendix D, Table D.5).

**Table D.5. Binding affinities of selected compounds with DnaK clusters**

| **Macromolecule** | **Ligand** | **Binding affinity (kcal/mol)** | **RMSD/ub** | **RMSD/lb** |
|---|---|---|---|---|
| DnaK-DnaJ | 3-[(2S,3R,4R,6R)-3,4-dihydroxy-6-(hydroxymethyl)-5-[(2S,3R,4S,5R,6R)-3,4,5-trihydroxy-6-(hydroxymethyl)oxan-2-yl]oxyoxan-2-yl]oxy-5,7-dihydroxy-2-(3,4,5-trihydroxyphenyl)-2,3-dihydrochromen-4-one | -8.2 | 0.0 | 0.0 |
| | Isoscoparin 2"-(6-(E)-ferulylglucoside) | -9.8 | 0.0 | 0.0 |
| DnaK-CBPA | 3-[(2S,3R,4R,6R)-3,4-dihydroxy-6-(hydroxymethyl)-5-[(2S,3R,4S,5R,6R)-3,4,5-trihydroxy-6-(hydroxymethyl)oxan-2- | -7.5 | 0.0 | 0.0 |



© University of Venda

| | | | | |
|---|---|---|---|---|
| | yl]oxyoxan-2-yl]oxy-5,7-dihydroxy-2-(3,4,5-trihydroxyphenyl)-2,3-dihydrochromen-4-one | | | |
| | Isoscoparin 2"-(6-(E)-ferulylglucoside) | -8.9 | 0.0 | 0.0 |
| DnaK-CLPB | 3-[(2S,3R,4R,6R)-3,4-dihydroxy-6-(hydroxymethyl)-5-[(2S,3R,4S,5R,6R)-3,4,5-trihydroxy-6-(hydroxymethyl)oxan-2-yl]oxyoxan-2-yl]oxy-5,7-dihydroxy-2-(3,4,5-trihydroxyphenyl)-2,3-dihydrochromen-4-one | -7.9 | 0.0 | 0.0 |
| | Isoscoparin 2"-(6-(E)-ferulylglucoside) | -9.5 | 0.0 | 0.0 |
| DnaK-GROEL | 3-[(2S,3R,4R,6R)-3,4-dihydroxy-6-(hydroxymethyl)-5-[(2S,3R,4S,5R,6R)-3,4,5-trihydroxy-6-(hydroxymethyl)oxan-2-yl]oxyoxan-2-yl]oxy-5,7-dihydroxy-2-(3,4,5-trihydroxyphenyl)-2,3-dihydrochromen-4-one | -8.2 | | |
| | Isoscoparin 2"-(6-(E)-ferulylglucoside) | -9.4 | 0.0 | 0.0 |
| DnaK-GROES | 3-[(2S,3R,4R,6R)-3,4-dihydroxy-6-(hydroxymethyl)-5-[(2S,3R,4S,5R,6R)-3,4,5-trihydroxy-6-(hydroxymethyl)oxan-2- | -7.6 | 0.0 | 0.0 |



© University of Venda

| | | | | |
|---|---|---|---|---|
| | yl]oxyoxan-2-yl]oxy-5,7-dihydroxy-2-(3,4,5-trihydroxyphenyl)-2,3-dihydrochromen-4-one | | | |
| | Isoscoparin 2"-(6-(E)-ferulylglucoside) | -9.8 | 0.0 | 0.0 |
| DnaK-GRPE | 3-[(2S,3R,4R,6R)-3,4-dihydroxy-6-(hydroxymethyl)-5-[(2S,3R,4S,5R,6R)-3,4,5-trihydroxy-6-(hydroxymethyl)oxan-2-yl]oxyoxan-2-yl]oxy-5,7-dihydroxy-2-(3,4,5-trihydroxyphenyl)-2,3-dihydrochromen-4-one | -7.3 | 0.0 | 0.0 |
| | Isoscoparin 2"-(6-(E)-ferulylglucoside) | -8.1 | 0.0 | 0.0 |
| DnaK-HSLU | 3-[(2S,3R,4R,6R)-3,4-dihydroxy-6-(hydroxymethyl)-5-[(2S,3R,4S,5R,6R)-3,4,5-trihydroxy-6-(hydroxymethyl)oxan-2-yl]oxyoxan-2-yl]oxy-5,7-dihydroxy-2-(3,4,5-trihydroxyphenyl)-2,3-dihydrochromen-4-one | -9.0 | 0.0 | 0.0 |
| | Isoscoparin 2"-(6-(E)-ferulylglucoside) | -8.9 | 0.0 | 0.0 |
| DnaK-HSLV | 3-[(2S,3R,4R,6R)-3,4-dihydroxy-6-(hydroxymethyl)-5-[(2S,3R,4S,5R,6R)-3,4,5-trihydroxy-6-(hydroxymethyl)oxan-2- | -9.3 | 0.0 | 0.0 |



© University of Venda

| | | | | |
|---|---|---|---|---|
| | yl]oxyoxan-2-yl]oxy-5,7-dihydroxy-2-(3,4,5-trihydroxyphenyl)-2,3-dihydrochromen-4-one | | | |
| | Isoscoparin 2"-(6-(E)-ferulylglucoside) | -9.1 | 0.0 | 0.0 |
| DnaK-HTPG | 3-[(2S,3R,4R,6R)-3,4-dihydroxy-6-(hydroxymethyl)-5-[(2S,3R,4S,5R,6R)-3,4,5-trihydroxy-6-(hydroxymethyl)oxan-2-yl]oxyoxan-2-yl]oxy-5,7-dihydroxy-2-(3,4,5-trihydroxyphenyl)-2,3-dihydrochromen-4-one | -7.9 | 0.0 | 0.0 |
| | Isoscoparin 2"-(6-(E)-ferulylglucoside) | -9.9 | 0.0 | 0.0 |
| DnaK-RPOH | 3-[(2S,3R,4R,6R)-3,4-dihydroxy-6-(hydroxymethyl)-5-[(2S,3R,4S,5R,6R)-3,4,5-trihydroxy-6-(hydroxymethyl)oxan-2-yl]oxyoxan-2-yl]oxy-5,7-dihydroxy-2-(3,4,5-trihydroxyphenyl)-2,3-dihydrochromen-4-one | -9.2 | 0.0 | 0.0 |
| | Isoscoparin 2"-(6-(E)-ferulylglucoside) | -8.2 | 0.0 | 0.0 |



© University of Venda